Smithsonian

Contributions to Astrophysics

VOLUME 6

RESEARCH IN SPACE SCIENCE

SMITHSONIAN INSTITUTION

Washington, D.C.

1963

Publications of the Astrophysical Observatory

This series, *Smithsonian Contributions to Astrophysics*, was inaugurated in 1956 to provide a proper communication for the results of research conducted at the Astrophysical Observatory of the Smithsonian Institution. Its purpose is the "increase and diffusion of knowledge" in the field of astrophysics, with particular emphasis on problems of the sun, the earth, and the solar system. Its pages are open to a limited number of papers by other investigators with whom we have common interests.

Another series is *Annals of the Astrophysical Observatory*. It was started in 1900 by the Observatory's first director, Samuel P. Langley, and has been published about every 10 years since that date. These quarto volumes, some of which are still available, record the history of the Observatory's researches and activities.

Many technical papers and volumes emanating from the Astrophysical Observatory have appeared in the *Smithsonian Miscellaneous Collections*. Among these are *Smithsonian Physical Tables*, *Smithsonian Meteorological Tables*, and *World Weather Records*.

Additional information concerning these publications may be secured from the Editorial and Publications Division, Smithsonian Institution, Washton, D.C.

FRED L. WHIPPLE, *Director*,
Astrophysical Observatory,
Smithsonian Institution.

Cambridge, Mass.

For sale by the Superintendent of Documents, U.S. Government Printing Office
Washington, D.C. 20402 - Price $2.

Contents

Preface

The Special Reports of research in space science were initiated with the Smithsonian Astrophysical Observatory's research program on artificial earth satellites in 1957, and they have provided an avenue of immediate publication which has proved indeed critical to proper elaboration of the field. By early 1963 the 113 Special Reports listed on pages 233 to 244 had been produced and distributed to all institutions participating in the U.S. space-research program and to individual scientists requesting them. The Special Reports have thus become valuable tools for the space scientist.

A number of the purely observational Special Reports are so highly specialized that only the few investigators presently using the data are likely ever to need the information available in them. It is possible that selections from these observational tables may be reproduced elsewhere, but many will not. On the other hand, certain of the Reports record important scientific research that should be available in the general literature.

Hence, the first 10 Special Reports were published as volume 2, number 10, of the *Smithsonian Contributions to Astrophysics*. Here we have selected 29 contributions from Special Reports 11 through 80 as meriting a permanent record. We present them, with such minor revisions as the authors have found necessary to bring them up to date and to clarify them, as volume 6 of the *Contributions to Astrophysics*. Other Special Reports have been published elsewhere in the literature.

To those members of the Observatory staff, and especially to Drs. Jacchia and Whitney, who helped to choose the papers that appear in this volume, I am grateful, as I am to the members of the editorial staff who saw the volume through the press.

FRED L. WHIPPLE, *Director*,
Astrophysical Observatory,
Smithsonian Institution.

Cambridge, Mass., April 2, 1963.

Contributors

R. E. Briggs, mathematician, Smithsonian Astrophysical Observatory.

Giuseppe Colombo, University of Padova, Padova, Italy; celestial mechanician, Smithsonian Astrophysical Observatory.

M. D. Grossi, staff engineer, Raytheon Corporation, Bedford, Massachusetts; electronics engineer, Project Celescope, Smithsonian Astrophysical Observatory.

J. Allen Hynek, director, Dearborn Observatory, Northwestern University, Evanston, Illinois; former associate director, Satellite Tracking Program, Smithsonian Astrophysical Observatory.

Imre Izsak, supervisory astronomer, Smithsonian Astrophysical Observatory.

Luigi G. Jacchia, physicist, Smithsonian Astrophysical Observatory.

Sir Harold Jeffreys, Cambridge University, England; consultant, Smithsonian Astrophysical Observatory.

H. M. Jones, physicist, Massachusetts Institute of Technology, Lincoln Laboratory, Lexington, Massachusetts.

Yoshihide Kozai, astronomer, Tokyo Astronomical Observatory, Tokyo, Japan; former astronomer, Satellite Tracking Program, Smithsonian Astrophysical Observatory.

Karoly Lassovszky, late astronomer, Smithsonian Astrophysical Observatory.

Marcel Nicolet, director, Institut Royal de Météorologie, Brussels, Belgium.

I. I. Shapiro, physicist, Massachusetts Institute of Technology, Lincoln Laboratory, Lexington, Massachusetts.

K. M. Strom, student, Radcliffe College, Cambridge, Massachusetts.

S. E. Strom, physicist, Project Celescope, Smithsonian Astrophysical Observatory.

George Veis, professor of surveying, National Technical University, Athens, Greece; consultant, Smithsonian Astrophysical Observatory.

Charles A. Whitney, physicist, Smithsonian Astrophysical Observatory.

Stanley P. Wyatt, professor of astronomy, University of Illinois Observatory, Urbana, Illinois.

Pedro E. Zadunaisky, director de investigaciones, Instituto de Calculó, Facultad de Ciencias Exactas y Naturales, Universidad de Buenos Aires, Argentina; former astronomer, Smithsonian Astrophysical Observatory.

Research in Space Science

636-014—63——2

Orbital Results for Satellite 1957 $\beta 1$

By Luigi G. Jacchia

This report covers the complete lifetime of Satellite 1957 $\beta 1$. Since all the observations have been reduced anew with improved elements, it supersedes the first set of orbital data (Jacchia, 1958a) that covered the lifetime of the satellite to Feb. 10, 1958.

Method of reduction

Tables 3 and 4 summarize the results of an analysis of approximately 2,800 optical and radio observations, reduced by means of an improved version of the author's subsatellite program (Jacchia, 1958d) which contains the following new features:

Continuously varying perigee distance.—The relation $q=q(a)$ between perigee distance and major axis is determined by fitting the solution of the differential equation $dq/da=f(q,a)$ through well-observed points, and then is fed into the machine program in the form of an approximating equation with 10 numerical coefficients.

A special high-latitude program.—Observations at low and middle latitudes yield independent determinations of the right ascension and of the time of the ascending node. For observations made at high latitudes, near the orbital apex, the effect of observational errors is greatly magnified in the independent solutions. If, however, the position of the node is accurately known for the time of observation, an accurate time for the equatorial crossing can still be obtained. The new feature in the subsatellite program provides for an optional switch to the latter type of reduction when the subsatellite point is within a specified number of degrees of latitude from the apex.

For the computation of the subsatellite points, the following orbital elements were used:

Inclination: $i=65^{\circ}.29$.

Argument of perigee: $\omega=58^{\circ}.0-0^{\circ}.3938(t-T)-2^{\circ}.50\times10^{-4}(t-T)^2-3^{\circ}.1\times10^{-7}(t-T)^3$

(T=1957 Nov. 6.0 U.T.; t in days).

The major axis of the orbit was derived from the nodal period, obtained by differentiation of the interpolating equations that follow:

$$T_{\Omega}=1957\ \text{Nov.}\ 4.41000+0^{d}.0720825n-1^{d}.19\times10^{-6}n^2-0^{d}.03820(e^{0.0017n}-1)+0^{d}.01700\sin(0^{\circ}.237n-128^{\circ}),\quad (0\leq n\leq 1800);\quad (1)$$

$$T_{\Omega}=1958\ \text{March}\ 9.51267+0^{d}.066453(n-1800)-2^{d}.56\times10^{-6}(n-1800)^2-0^{d}.00125927[e^{0.0095(n-1800)}-1]\quad (1800<n\leq 2300);\quad (2)$$

$$T_{\Omega}=1958\ \text{April}\ 10.95583+0^{d}.062547(n-2300)-8^{d}.78\times10^{-6}(n-2300)^2-8^{d}.316\times10^{-5}[e^{0.097(n-2300)}-1]\quad (n>2300).\quad (3)$$

The residuals from these equations never exceed $0^{d}.002$, and the errors in the computed period and heights are negligible in the computation of subsatellite points, nodes, and equatorial crossings.

The relation between the major axis and the perigee distance is given in table 1. Values of dq/da were computed from Sterne's (1958a) equations with the Smithsonian Interim Atmosphere (Sterne, Folkart, and Schilling, 1957) and integrated, starting from the normal point $q=1.03302$ for $a=1.13$. The integration was performed by Jack Slowey, using a special program on the IBM-704 Calculator.

For the reduction of the high-latitude observations, the following equations were used for the position of the ascending node.

$$\alpha_{\Omega}=108^{\circ}.2-2^{\circ}.6079(t-\text{Nov. }6.0)-1^{\circ}.656\times10^{-3}(t-\text{Nov. }6.0)^2-2^{\circ}.08\times10^{-6}(t-\text{Nov. }6.0)^3\quad (4)$$

(for dates before 1958 Mar. 11).

TABLE 1.—*Assumed relation between semimajor axis and perigee distance*

a	q	e
1.15	1.03360	0.1012
1.14	1.03333	.0936
1.13	1.03302	.0858
1.12	1.03268	.0780
1.11	1.03230	.0700
1.10	1.03187	.0619
1.09	1.03137	.0538
1.08	1.03079	.0456
1.07	1.03008	.0373
1.06	1.02920	.0291
1.05	1.02805	.0209
1.04	1.02639	.0131
1.03	1.02370	.0061
1.02	1.01869	.0013

a: Semimajor axis of orbit in units of the earth's equatorial radius.
q: Perigee distance.
e: Orbital eccentricity.

$$\alpha_\Omega = 112^\circ.1 - 3^\circ.175(t - \text{Mar. } 11.0) - 1^\circ.5\times 10^{-4}(t - \text{Mar. } 11.0)^3 \quad (5)$$

(for dates after 1958 Mar. 11).

Results

Normal values of α_Ω at 5-day intervals, together with the observed precession, are given in table 2.

Table 3 gives normal values of T_Ω, the time of the equatorial crossing of the satellite from south to north, at intervals of 25 revolutions. The numbering of the revolutions is the same as in Jacchia (1958a); the first crossing in the list (n=0) was actually the 16th crossing after the launching of the satellite. Also given are the nodal period, P_Ω, and the orbital acceleration dP/dt, in seconds per day; these quantities were obtained by numerical differentiation of T_Ω.

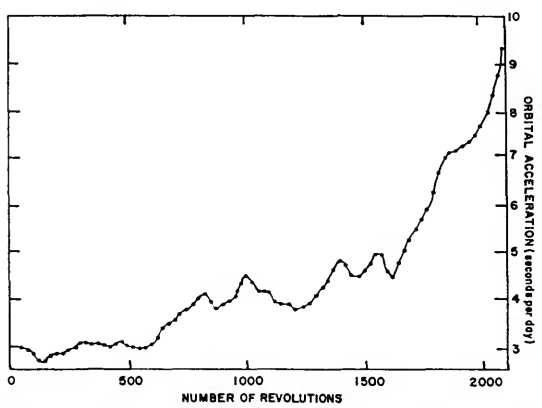

FIGURE 1.—Rate of change of the orbital period as a function of the number of revolutions (n). For a conversion of n to time, see table 2.

TABLE 2.—*Normal values of α_Ω and observed nodal precession*

	t(U.T.)	α_Ω	$d\alpha_\Omega/dt$
1957			
Nov.	6.0	108°.2	−2°.64/day
	11.0	95.0	−2.65
	16.0	81.7	−2.66
	21.0	68.3	−2.67
	26.0	54.8	−2.68
Dec.	1.0	41.5	−2.70
	6.0	28.0	−2.71
	11.0	14.4	−2.73
	16.0	0.7	−2.74
	21.0	346.9	−2.76
	26.0	333.1	−2.78
	31.0	319.1	−2.80
1958			
Jan.	5.0	305.1	−2.82
	10.0	291.0	−2.84
	15.0	276.7	−2.86
	20.0	262.3	−2.88
	25.0	247.9	−2.90
	30.0	233.3	−2.92
Feb.	4.0	218.6	−2.94
	9.0	203.9	−2.96
	14.0	189.0	−2.99
	19.0	174.0	−3.02
	24.0	158.8	−3.05
Mar.	1.0	143.4	−3.09
	6.0	127.8	−3.13
	11.0	112.1	−3.16
	16.0	96.3	−3.20
	21.0	80.2	−3.25
	26.0	63.8	−3.31
	31.0	47.1	−3.37
Apr.	5.0	30.1	−3.45
	10.0	12.7	−3.57
	14.0	358.2	

α_Ω: Right ascension of the ascending node.
$d\alpha_\Omega/dt$: Nodal precession in degrees per day.

The last fifty revolutions are tabulated in greater detail (at intervals of 5 revolutions) in table 4. A plot of dP/dt against n, covering the first 2100 revolutions, is given in figure 1. Due to the slow motion of the perigee for the particular inclination of this satellite, there is no difference, within the tabular accuracy, between the accelerations of the nodal and of the anomalistic period.

TABLE 3.—*Orbital values*

n		t_0(U.T.)	P_0	dP/dt sec./day
	1957			
0	Nov.	4. 39469	(0.072009)	---------
25		6. 19415	. 071947	---------
50		7. 99206	. 071885	−2. 97
75		9. 78842	. 071824	−2. 92
100		11. 58327	. 071764	[−2. 84]
125		[13. 37664]	[. 071706]	[−2. 71]
150		[15. 16860]	[. 071651]	[−2. 66]
175		[16. 95918]	[. 071594]	[−2. 79]
200		[18. 74831]	[. 071536]	[−2. 85]
225		[20. 53596]	[. 071477]	[−2. 86]
250		[22. 32214]	[. 071417]	[−2. 93]
275		[24. 10679]	[. 071356]	[−2. 95]
300		25. 88993	. 071294	[−3. 05]
325		27. 67149	. 071231	−3. 07
350		29. 45146	. 071168	−3. 04
	1957			
375	Dec.	1. 22989	. 071105	−3. 06
400		3. 00673	. 071042	−3. 03
425		4. 78202	. 070981	−2. 99
450		6. 55577	. 070919	−3. 05
475		8. 32796	. 070856	−3. 06
500		10. 09857	. 070794	−3. 03
525		11. 86764	. 070732	−3. 00
550		13. 63516	. 070671	−2. 97
575		15. 40117	. 070610	−2. 96
600		17. 16566	. 070549	−3. 04
625		18. 92860	. 070486	−3. 17
650		20. 68992	. 070419	−3. 37
675		22. 44952	. 070349	−3. 48
700		24. 20735	. 070278	−3. 57
725		25. 96338	. 070204	−3. 68
750		27. 71753	. 070128	−3. 78
775		29. 46977	. 070050	−3. 90
800		31. 22002	. 069970	−4. 05
	1958			
825	Jan.	1. 96825	. 069887	−4. 12
850		3. 71436	. 069804	−3. 96
875		5. 45850	. 069726	−3. 84
900		7. 20068	. 069648	−3. 91
925		8. 94090	. 069569	−3. 97
950		[10. 67911]	[. 069488]	[−4. 08]
975		[12. 41528]	[. 069404]	[−4. 33]
1000		[14. 14928]	[. 069315]	[−4. 51]
1025		[15. 88102]	[. 069225]	[−4. 39]
1050		17. 61056	. 069139	−4. 20
1075		19. 33801	. 069056	−4. 18
1100		21. 06338	. 068973	−4. 15
1125		22. 78666	. 068892	−3. 98
1150		24. 50798	. 068814	−3. 92
1175		26. 22734	. 068735	−3. 91
1200		27. 94476	. 068658	−3. 84
1225		29. 66027	. 068582	−3. 85
1250		31. 37387	. 068505	−3. 90

TABLE 3.—*Orbital values*

n		t_0(U.T.)	P_0	dP/dt sec./day
	1958			
1275	Feb.	2. 08553	. 068428	−3. 94
1300		3. 79525	. 068349	−4. 10
1325		5. 50294	. 068266	−4. 28
1350		7. 20851	. 068180	−4. 42
1375		8. 91190	. 068091	−4. 67
1400		10. 61300	. 067996	−4. 85
1425		12. 31171	. 067901	−4. 75
1450		14. 00809	. 067810	−4. 54
1475		15. 70225	. 067722	−4. 50
1500		17. 39420	. 067633	−4. 61
1525		19. 08389	. 067541	−4. 80
1550		20. 77124	. 067446	−4. 97
1575		22. 45618	. 067349	−4. 94
1600		[24. 13870]	[. 067225]	[−4. 62]
1625		[25. 81897]	[. 067168]	[−4. 52]
1650		[27. 49706]	[. 067077]	[−4. 80]
	1958			
1675	Mar.	[1. 17279]	[. 066981]	[−5. 06]
1700		2. 84608	. 066881	−5. 27
1725		4. 51683	. 066777	−5. 50
1750		6. 18491	. 066669	−5. 69
1775		7. 85025	. 066557	−5. 92
1800		9. 51273	. 066440	−6. 28
1825		11. 17220	. 066315	−6. 72
1850		12. 82844	. 066183	−7. 05
1875		14. 48130	. 066046	−7. 14
1900		16. 13073	. 065909	−7. 21
1925		17. 77672	. 065771	−7. 28
1950		19. 41925	. 065631	−7. 37
1975		21. 05828	. 065490	−7. 51
2000		22. 69375	. 065346	−7. 71
2025		24. 32557	. 065198	−8. 00
2050		25. 95362	. 065044	−8. 38
2075		27. 57771	. 064882	−8. 82
2100		29. 19766	. 064712	−9. 40
2125		30. 81321	. 064529	−10. 28
	1958			
2150	Apr.	1. 42396	. 064327	−11. 34
2175		3. 02941	. 064106	−12. 48
2200		4. 62906	. 063863	−13. 80
2225		6. 22238	. 063596	−15. 3
2250		7. 80859	. 063296	−17. 3
2275		9. 38686	. 062957	−20. 2
2300		10. 95582	. 062547	−25. 3
2325		12. 51318	. 062008	−38. 2
2350		14. 05088	. 06050	−430. :

Values enclosed in brackets are uncertain because of scarcity of observations.

n = Number of revolutions elapsed.
t_0 = Time of ascending-node crossing.
P_0 = Nodal period in days.
dP/dt = Orbital acceleration in seconds per day.

TABLE 4.—*The last 50 revolutions of Satellite 1957 β1*

n	$t_0(U.T.)$	P_0	dP/dt sec./day
	1958 April		
2300	10. 95582	$0^d.062547$	−25. 3
2305	11. 26830	. 062543	−26. 8
2310	11. 58032	. 062355	−28. 0
2315	11. 89184	. 062251	−30. 4
2320	12. 20281	. 062136	−33. 6
2325	12. 51318	. 062008	−38. 2
2330	12. 82285	. 061859	−43. 0
2335	13. 13175	. 061692	−52. 0
2340	13. 43970	. 061477	−69. 0
2345	13. 74637	. 06117	−120. 0
2350	14. 05088	. 06050	−430. 0

The Descent of Satellite 1957 β1

By Luigi G. Jacchia

The present paper [1] covers the final part of the last revolution of Satellite 1957 β1. The observations that are at the basis of this report can be divided into three categories—those from the northeastern United States (table 1), those from ships at sea (table 2), and those from the Caribbean Islands and the northern coast of South America (table 3).

While reliable observations, including altazimuth estimates of sightings, had been received at the Smithsonian Institution Astrophysical Observatory from ships at sea, only isolated and mostly descriptive observations were available from land areas. Therefore, at the suggestion of Dr. F. L. Whipple, Director of the Observatory, the author undertook, at the end of May 1958, a trip to the Caribbean area to collect additional information. In the course of this trip, he visited Antigua, Martinique, Barbados, Trinidad, British Guiana, and Surinam. The information collected is included in table 3.

Reduction of the observations

The observations in table 1, all made at nearly the same time from localities on both sides of the satellite path, provided the means for the computation of an excellent normal point in the trajectory. Its numerical values were:

Longitude:	74°.00 west
Latitude:	41°.40 north
Height:	101 km above sea level
Time:	$1^h45^m25^s$ U.T. (14 April 1958)

A set of orbital trajectories was computed by numerical integration starting from this normal point, with different initial radial-velocity conditions and different (constant) drag parameters, with the ARDC model atmosphere (Minzner and Ripley, 1956), to compute the drag at these low altitudes. For simplicity, these integrations were performed with polar coordinates used in the orbital plane. One of these integrations, whose results are given in table 4, and represented graphically in figure 1, fitted the observations in the Caribbean area within their estimated errors and was chosen as representing the most probable trajectory of the satellite in its final plunge.

The initial conditions and the drag parameter used in this integration were:

Orbital inclination = 65°.29
Total velocity = 7.737×10^5 cm/sec
Radial velocity $(dr/dt) = -1.28\times10^3$ cm/sec
$C_DA/m = K = 0.031$ (c.g.)

In the last quantity, C_D is the drag coefficient; A is the presentation area of the satellite; and m is its mass. The atmosphere was assumed to be rotating solidly with the earth and to have the same density at the same height above sea level, irrespective of latitude. The earth's oblateness and the precessional effects on the orbital plane were taken into account.

In the other experimental trajectories, radial velocities up to -2×10^3 cm/sec and values of K between 0.02 and 1.0 were tried. As should be evident, the effect of such different conditions on the trajectory itself is to vary to a considerable extent the position of the end point, although the subsatellite track is not greatly affected by the changes. The assumption of a constant drag parameter is, of course, a little unrealistic, since the drag coefficient C_D must have been decreasing considerably in the course of the trajectory with the formation of an air cap, while the area-mass ratio A/m must have been increasing due to the continuous shedding of molten metal. Since, however, these two variations must have compensated to a certain extent, the assumption

[1] Essentially an extension of the preceding paper.

TABLE 1.—*Observations over northeastern United States*

Station	Longitude	Latitude	(U.T.) 14 April 1958	Moonwatch observers at α	δ	Z	h	Remarks
	° ′ ″	° ′ ″	h m s	h m	° ′			
Millbrook, New York	73 37 27	+41 51 30	1 45 08	5 05	+45			Magnitude +1. Tail of tiny particles about 1° long, seen more or less all the time; white.
			1 45 35	10 06	0			
			1 46 04	12 10	+23 25			
New Haven, Connecticut	73 00 30	+41 12 35	1 45 47			180°	40°	Blue-white when first seen; magnitude+1; at $1^h45^m42^s$ got brighter (mag. −1) and turned red.
Bryn Athyn, Pennsylvania	75 04	+40 08	1 45 21	17 15	+66			Magnitude +3 to −1; reddish; tail 10′ to 20′ long
			1 45 46	14 39	+13 57			
			Isolated Observers					
Merrow, Connecticut (Mr. R. D. House)	72 19.0	+41 49.4	1 46			NW	25°	Magnitude 1.5 at maximum brightness; red; faint, transparent tail 3° to 5° long, visible only through binoculars.
						W	45	
						S	15	
Pittsford, New York (Mr. R. E. Jenkins)	77 37 41	+43 15 03	1 46 05:	14 24	+20			Magnitude +3.
			1 46 25:	14:	−10:			

is perhaps justified, especially since the agreement between the resulting trajectory and the observations is quite good.

Phases of the trajectory and end point

There is general agreement among practically all observers concerning the developments in the appearance of the object. When seen in the northeastern United States, the satellite already had a faint tail in which sparklike particles could be seen through binoculars. Its visual magnitude, reduced to a standard distance of 100 km (absolute magnitude), was then about +1.0 and the tail could be followed through binoculars for 6 km behind the head, according to the Merrow, Connecticut, observation. After crossing over Long Island, the satellite went unreported for about 5 minutes. When sighted again by ships in the Caribbean, it was at latitude 23° north and had become a spectacular sight. Its tail was 60 km long as seen from Antigua, 80 km long at the latitude of Martinique, and nearly 100 km long as seen from Barbados and Trinidad. (Of all the Caribbean Islands, Barbados was the closest to the satellite's path, about 120 km from the subsatellite track.) When the object was at the latitude of Barbados (13° N), its head, according to the best estimates, had an absolute magnitude of about −7 or −8, and the total light emitted by head and tail must have been close to −9 or −10.

The color of the head was generally described as white with tinges of blue or green, while the tail was described as white, or white-yellowish, near the head, and degrading to a deeper yellow and orange—even red—toward the far end. The "globules" described by all observers close enough to see them were obviously drops of molten metal shed by the object; their observed splitting (A. H. C. Campbell, Barbados) confirms this explanation. Attention is called to the small, semiperiodic light fluctuations observed by Mr. Hart in Barbados, since they might have some bearing on similar phenomena observed in bright fireballs.

Several observers saw a bright flash when the satellite reached 11° or 10° of north latitude and spoke of a "shower of fragments" or "complete disintegration" of the object, but there is

TABLE 2.—*Observations from ships*

Ship	Position of ship Long.(W) °	′	Lat. °	′	14 April 1958 U.T. h	m	Duration of obs.	Appearance*
1. Volvula	65	00	+20	34	1	53	2 min	Moving in direction 328° to 148°.
2. Maron	62	12	+19	54	1	49 (a.)	3–4 min	Moving NNW to SSE.
3. California	60	10	+17	55	1	50		Appeared at $z=330°$, disappeared at $z=150°$.
4. Mitra	64	10	+17	46	1	55	>3 min	Appeared in North, $h=10°$; h max 45° in East; disappeared at $z=140°$, $h=10°$.
5. Duivendijk	61	04	+17	21	1	48 (a.)	2 min	Appeared at $z=350°$, disappeared at $z=160°$; h max=30°.
6. Mormick Sea	53	04	+16	46	1	52 (a.)	2 min	$h=10°$; disappeared at $z=210°$, $h=10°$.
7. Eirmil	55	38	+16	20	1	20		Green flame moving NW to SE.
8. Ells	65	34	+15	53	1	55	3 min	Appeared at $z=30°$, $h=15°$; disappeared at $z=130°$, $h=10°$.
9. Mobil Brilliant	56	30	+15	30	2	10	30 sec	At $z=246°$, $h=17°$; disappeared at $z=205°$, $h=2°$ to 4°.
10. S. Africa Star	62	50	+15	20	1	50	3 min	Moving from NNW to SSE, $h=10°$.
11. Regent Springbok	59	00	+14	30	1	50	2–3 min	Passed overhead; appeared to disintegrate at $h=15°$.
12. Regent Hawk	60	10	+12	37	1	53	20–30 sec	At $z=34°$, $h=16°$; disappeared at $z=94°$
13. K. G. Lohse	52	29	+12	28	1	53 (a.)		Appeared at $z=290°$, disappeared at $z=225°$, $h=3°$ to 5°.
14. Sunkirk	58	03	+12	25	1	51 (a.)	4 min.	Passed overhead.
15. Triton	64	43	+12	06	2	00	1 min	Appeared at $z=55°$, disappeared at $z=95°$, $h=5°$.
16. Omnium Freighter	61	33	+10	37			35 sec	h max=18°.
17. Rio Atuel	59	47	+10	22	1	55	6 min	h max=20°; disappeared in SE at $h=8°$.

*z=azimuth (from North, positive to East); h=altitude above horizon.

no unanimity on this point among the Trinidad witnesses. It seems, however, that when the satellite was disappearing from view in Trinidad, much of the fiery tail had faded out, and only an isolated object (the head, or what remained of it) was still proceeding on its course. This object was seen from British Guiana, at closer range than from Trinidad, as a conspicuous but not spectacular object, which faded out while still well above the horizon in the northeast. This rapid fading out in midair was reported by all observers who managed to follow the course of the object until that point, i.e., the three observers in British Guiana, the witnesses on the vessels *K. G. Lohse* and *Rio Atuel*, and two observers in Trinidad, G. R. Robson and J. Saunders. The disappearance was seen from various directions and corresponded to a point at about 57° of longitude west and 9° north latitude, at a height of some 40 km above sea level.

It appears quite probable that fragments originating in the burst, including the object seen from British Guiana, fell unseen into the Atlantic Ocean along an arc of 100 km or so on the subsatellite track, when their velocity became too low to sustain the light-producing mechanism. The "impact point" recorded in table 4 should not have much more than academic significance, although it is expected that no major fragment succeeded in traveling much more than 1° beyond that point.

Remarks on Table 2

(1) *Volvula:* Long tail.

(2) *Maron:* Many short flames (very bright) behind main body, followed by a long-pointed tail (less lighted).

(4) *Mitra:* Light of flame was equal to that of full moon, brilliant white with long tail of sparks and smoke.

(7) *Eirinil:* Big green flame. Its head was very intensively lighted and its tail faintly. Along the tail there were smaller, bright heads.

(8) *Ells:* Several times brighter than Venus.

(9) *Mobil Brilliant:* When object was ahead ($Z=246°$, $h=17°$), its size was larger than that of Venus, with a tail 11° long. Parts of the head were continually breaking off and following the lower part of the tail, creating a bulge below the tail. Each part was a minia-

TABLE 3.—*Observations from land*

Place	Observer	Longitude (*W*) ° ′	Latitude ° ′	U.T. 14 April 1958	Duration of sighting	Appearance*
St. Thomas, V.I.	1. J. H. Jouett	64 57	+18 21	$1^h30^m-1^h45^m$	2 min	Appeared at $z=40°$, disappeared at $z=110°$.
Antigua, B.W.I.	2. H. Merrifield	61 48	17 10	1^h45^m	4 min	Appeared at $z=20°$, $h=7°$; h max=21°; disappeared at $z=150°$, $h=10°$ (obstacles).
	3. W. P. Novinsky.	61 48	17 10		2 min	h max=30°.
	4. H. Laing	61 48	17 10			When at $z=90°$, $h=27°$; disappeared at $z=133°$, very low.
	5. Y. Carty	61 48	17 10			Disappeared at $z=155°$, very low.
Martinique, F.W.I.	6. R. de Reynal	61 04	14 36		>1 min	Appeared at $z=10°$, $h=15°$; h max=18°; disappeared at 119° behind clouds.
	7. R. de la Coste				>1 min	
	8. Père Théon	61 04	14 36			h max=20°.
	9. Abbé Beaubrun					
St. Lucia, B.W.I.	10. Mrs. N. Moffat	60 55	13 49	1^h53^m	20 sec	
Barbados, B.W.I.	11. R. Parris	59 37	13 15		2.5 min	Appeared at $z=345°$, $h=5°$; at $z=50°$, $h=22°$; at $z=110°$, $h=21°$; disappeared at 145°, $h=6°$, behind trees.
	12. A. Hart	59 35	13 04	1^h50^m	35 sec	Appeared at $z=6°$; at $z=67°$, $h=29°$; disappeared at $z=128°$, $h=13°$, behind clouds.
	13. D. Rufolo	59 34	13 04		≧2 min	Appeared at $z=10°$, $h=12°$; h max=21°; disappeared at $z=100°$, $h=15°$ (behind house).
	14. F. C. Goddard	59 27	13 06			h max=25°–30°.

Additional observers in Barbados: 15. J. Babb; 16. A. H. C. Campbell; 17. L. Hassell; 18. T. Stoute; 19. C. Walcott.

Trinidad, B.W.I.	20. G. R. Robson	61 27	10 19	1^h55^m	30 sec	Appeared at $z=70°$, $h=8°+3°$.
	21. J. Saunders	61 27	10 19	1^h55^m	30 sec	Appeared at $z=70°$, $h=5°30'\pm30'$; disappeared at $z=100°$, $h=1°$–$2°$.
	22. E. H. F. Beadon	61 39	10 39			Appeared in north; disappeared at $z=60°$, $h=3°$, behind mountains.

Observers in Trinidad, who gave rough estimates of h max: 23. A Hinkson (6°); 24. T. R. Ivison (18°); 25. N. McClean (10°–15°); 26. W. Orebaugh (15°); 27. E. Skeen (10°–15°); 28. W. Scott (5°); 29. H. Sookoo (5°–7°); 30. D. St. Aubyn (10°–15°); 31. D. Taylor (5°–10°). Other observers: 32. J. Jackson, 33. R. G. Lovell; 34. M. Tulloch.

British Guiana	35. H. Scott	57 46	6 34			Appeared in north, $h=30°$ (unchecked), disappeared in NE, $h=15°$ (unchecked).
	36. A. Persaud	58 14	6 29	1^h55^m		Appeared in north, $h=15°$; disappeared in ENE at $h=10°$.
	37. E. van Lewin.	58 36	6 36			

*z=azimuth (from north, positive to east); h=altitude above horizon.

ture replica of the larger, but lasted only a very short time. The maximum number at one time must have been about 15. A flash was observed when the object appeared; following the flash, the object emitted a series of four other flashes that were bright but most probably less bright than the first. After closest approach, the tail became foreshortened, and all the object became fainter until it gave one last bright flash; a second afterwards it disappeared, at an altitude of 2 to 4 degrees.

(10) *S. Africa Star:* Tail 20° to 30° long, colored bright orange, silver-blue and green. Crossed (astern of) vessel, appeared to be losing height, and then disintegrated.

(11) *Regent Springbok:* Bright comet-like shape with an associated firepath of smaller glowing bodies. The colorful trail, many miles long, was described as a peacock's tail, each particle glowing through the spectrum from white to deep blue in magnificent display, finally fading away. Sinking in southern sky, spearhead was seen to disintegrate, appearing to do so at 15° above the horizon. Deck and sea around were bathed in pale light as mass crossed overhead.

(12) *Regent Hawk:* When closest, object had tail about 15° long (another report says 20 to 25 times the diameter of the main body) and about 1°.5 broad, in which burning particles were erupting. The main body appeared to have a blue-white head, then a short dark space before the glowing orange-yellow tail. Twenty-seven separate particles were actually counted as they appeared in the main plume. Each followed the main body, and on leaving it developed its own glowing tail. These particles were visible for about one second, starting as a bright white and rapidly darkening to a deep red. The main body was estimated to be about three or four times as bright as Venus at its brightest—while the offshoots were each twice the brightness of Sirius. One observer who saw it in the early stages of its approach states that it was round on top and bright blue-white, but the lower half seemed to be flattened and was more reddish in color, and "sparks" appeared to be coming from the lower half.

(13) *Karl Gunther Lohse:* (account translated and summarized from German): When it appeared, the object had a comet-like shape and was brighter than Jupiter. Toward the end of its trajectory, the body brightened up brilliantly and disintegrated into several glowing parts. A few seconds later all had disappeared.

(14) *Sunkirk:* Was at first believed to be a powerful white searchlight as from an aircraft flying at low altitude. A trail of blue and red fragments could be clearly seen in its wake. Reflection from the object covered a wide area in the sky and a section of the sea was also illuminated by its brilliance.

(16) *Omnium Freighter* (in Port of Spain harbor; account translated and summarized from German): At first the object appeared like a fireball, except that the white glowing tail persisted longer. Tail was "25 to 30 nautical miles long"; from white it degraded into dark red and then into a black smoke trail, where a few isolated sparks still glowed. Through binoculars the body was seen to brighten up several times. The bright light was observed for about 35 seconds, the fainter for some 5 seconds, and the black smoke trail for about 15 seconds, "without seeing the end of it."

(17) *Rio Atuel:* "Satellite appeared like enormous planet, white in color, very bright in head and with reddish trail with spots of lesser intensity as if detached parts from the central nucleus ended in secondary, bluish trail. Disappeared at some 8 degrees altitude after 6 minutes of observation." (This description was sent to the Argentine Association "Amigos de la Astronomia" as a further elaboration on a telegram, in which the vessel had announced it had observed the "total disintegration of Sputnik II.")

Remarks on Table 3

(The numbers in parentheses refer to the observers listed in table 3.)

St. Thomas, V.I.—(1). "Gave appearance of airplane at an altitude of 2500 ft. about 5 miles away. Object seemed dark with cherry-red color at body, changing to almost white at rear end or tail. The cherry-red body was symmetrical, but became uneven aft of the tail."

Antigua, B.W.I.—When first noticed in the north-northeast it looked like a diffuse object, without tail, with diameter not greater than one-tenth of that of the moon (2). As it ap-

proached, a tail was perceived, which at closest approach reached a length of 20° (2) or 30° (3). The object was brightest in front, where the color was yellowish (2). Sparklike particles became detached and were seen especially in the lower part of the tail (2, 3). The central part of the tail appeared of a blue-grayish color; shortly after the main body a dead region (less luminous) could be seen in the tail (2). The end of the tail was mainly composed of particles (2, 3) like flying embers (2). The tail appeared streaked. The greatest intensity was in the upper and lower part, but the lower was brighter (2). The total brightness of the object, including the tail, was comparable with that of the moon at first quarter, but the brilliance of the head was much greater than that of the moon (2). The "sparks" were quite bright at start, but would quickly burn out, in 8–10 seconds; no tail was seen attached to individual sparks (2).

Martinique, F.W.I.—Made its appearance as a white (8, 9) or greenish (7) globe, one-third of the moon in diameter (7); the apparent diameter may not have been real, but due to optical illusion (6). At closest approach the main body was brighter than Venus, some 10 times brighter than Jupiter (6, 7), probably of magnitude −6. The globe was sharply delimited; the tail was attached, but a little separation could be discerned between body and tail (6, 7). At closest approach the length of the tail was 20° (8, 9) or 30° (6, 7) and its color was reddish (6, 7, 8, 9); none of the observers noticed sparks or detached particles, nor any light fluctuations.

St. Lucia, B.W.I.—"Appeared as a blazing orange-yellow ball, about one-fourth the size (in diameter) of the full moon, in the wake of which streamed a long, wide, bright trail of light and sparklike fragments, these appearing as large as an average- or medium-sized star in the sky."

Barbados, B.W.I.—At closest approach the object was cometlike, with a dazzlingly brilliant head, at least as bright as Venus, and a long tail which, as a whole, was several magnitudes brighter than the head, although

TABLE 4.—*Most probable trajectory of descent of Satellite 1957 β1*

Latitude	Longitude (W)	Height (km MSL)	Time (U.T.)
41°. 40	74°. 00	101	$1^h45^m25^s$
24. 0	63. 20	88	1 50 14
22. 0	62. 23	86	1 50 47
20. 0	61. 29	83	1 51 20
18. 0	60. 41	80	1 51 52
16. 0	59. 54	76	1 52 26
14. 0	58. 70	71	1 53 00
12. 0	57. 88	63	1 53 37
10. 0	57. 12	50	1 54 21
9. 0	56. 8	37	1 55 01
8. 6	56. 6	(Impact point)	

less brilliant (12, 19). The head seemed to have a definite diameter, a little less than one-fifth of the diameter of the moon (12); all witnesses asserted that it did not look like a point source of light (16). Its color was described as white with a bluish (12, 16, 19) or blue-greenish (13) tinge. The tail consisted of a bright, flamelike appendage, white (19) or yellowish (13) in color, gradually fading into a more reddish tinge at greater distance from the head (19). Numerous brilliant particles or globules were observed in the tail, especially in the lower part (all observers); their color was white at the beginning, but became reddish as they were left behind, falling, and faded out (12, 13, 19). Each of the globules was followed by a small tail, simulating the shape of the main body (all observers); there were as many as 12 to 18 such "offspring" visible at any time, and some of them subdivided forming two little cometlike objects (16). The length of the flamelike tail was estimated at 10° (13) or 20° (12, 19); some dying-out offspring could be traced as far as 40° from the head. Small fluctuations in brightness were observed in the head, every three seconds or so (12). Most observers saw the object disappear low in the southeast, behind a cloud bank, which became illuminated at the edges. Mr. Hart (12) noticed flashes behind the cloud; there was at least one big flareup after the body disappeared from sight, like a distant flash of lightning. Mr. Walcott (19), who observed the phenomenon from a point several miles away, saw the tail fade out before

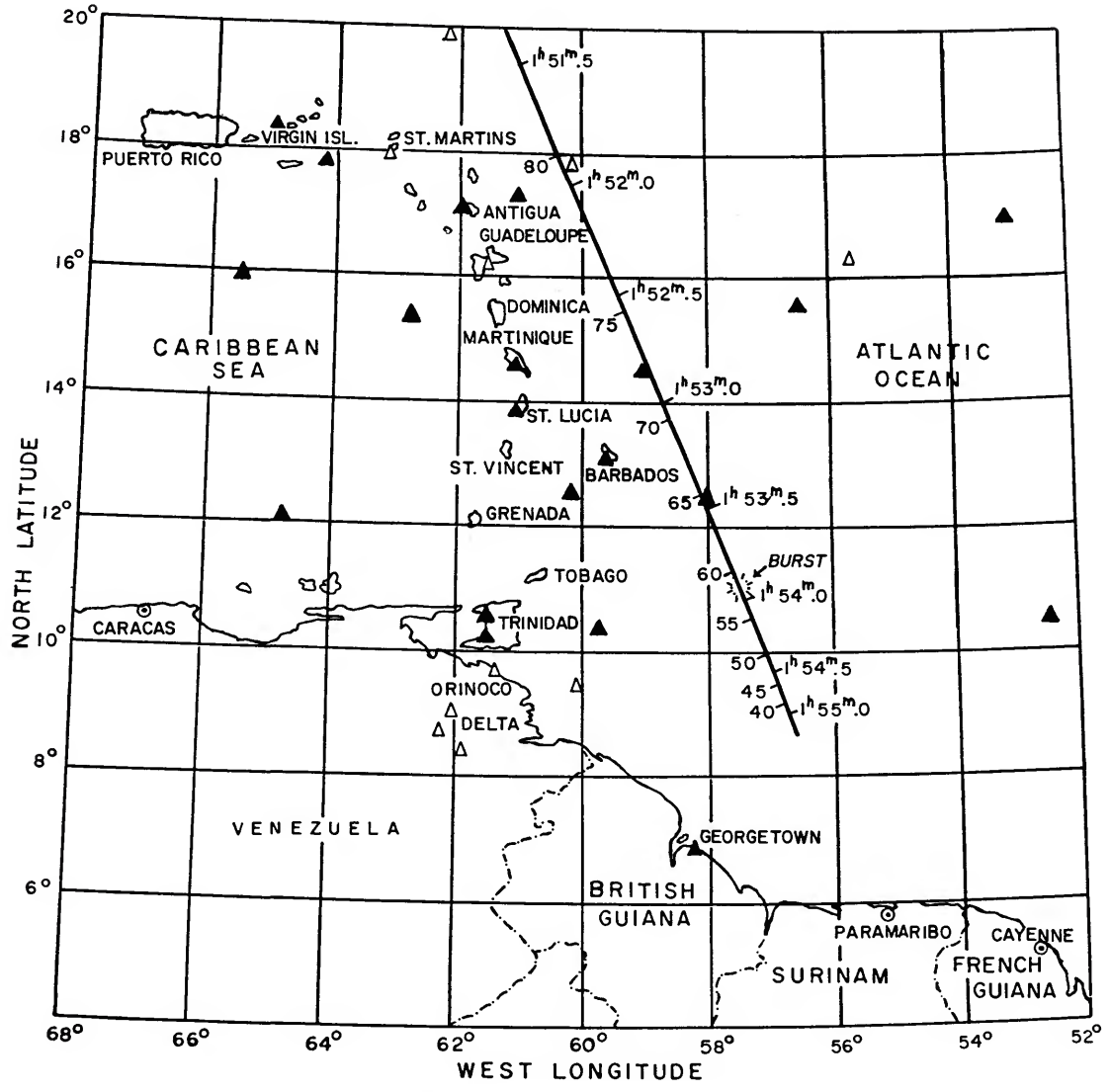

FIGURE 1.—End path of Satellite 1957 β1 in the Caribbean area. Times of arrival and heights above sea level, in kilometers, are marked on the subsatellite track. The black triangles represent localities from which quantitative positional observations were given; qualitative observations came only from the localities marked with open triangles. (Chart reproduced through courtesy of *Sky and Telescope*.)

the object vanished and then saw five or six red pieces fall toward the horizon (hidden by a distant ridge).

Trinidad, B.W.I.—When it appeared in the north-northeast, it was not brighter than an average bright star (30); it rapidly increased in brightness as it approached, and a tail became visible. When it was in the east-northeast it was brighter than any star or planet (all observers agree). The head was variously described as "metallic blue-white" (30), "vivid intense green" (22) or "whitish as a welding flame" (33). The tail was definitely redder than the body (practically all observers), speckled with starlike sparks, at least 10° long (25); some estimated the

maximum length of the tail at 50° (30) or even 60° (29). Some observers (23, 24) mention a definite "burst" at the end of the phenomenon; in other cases it is difficult to decide whether what was described as a burst resulting in a shower of fragments (27, 31) was really an explosion or simply the coming into view of the tail with the spark-like objects in it. Mr. T. R. Ivison (24), who was watching the object together with Mr. W. Orebaugh (26), American Consul General in Trinidad, saw it give out a big white flare, like a magnesium flash, after which it quickly disappeared. Mr. Orebaugh did not mention the flash. Mr. Hinkson (23), a newspaperman who saw the phenomenon from the Piarco Airport, also saw an explosion some 3 seconds before he saw the object disappear. It is remarkable, however, that other observers who had an especially good view of the phenomenon did not mention any burst. Two observers (30, 34) reported that toward the end the fiery tail faded and only the "leader" of the procession of fragments remained visible, only to disappear shortly afterwards.

British Guiana—A. Persaud (36) saw the object at the Atkinson Airport and describes it as brighter than any star or planet, but not spectacular; it had a tail 1° long and seemed to fly parallel to the horizon, from north (where it was first sighted) to northeast. Before it disappeared, in the east-northeast direction, it seemed to drop closer to the horizon. It disappeared quite suddenly while still high (10°, checked by the writer) above the horizon. The color was described as that of an electric bulb. No sparks or fragments were visible during the entire course. H. Scott (35), from a place 20 miles east of Georgetown, describes the object as "white like a white electric light and bright as a bright star." He saw no bursts or fragments. It was like a plane traveling, descending very fast, to about 15° (unchecked) above the horizon, where it disappeared. Steady white light all the time. Mr. E. van Lewin (37) from a boat on the Essequibo River near Bartica describes the color as reddish and saw it "grow smaller until it diminished from view."

Acknowledgments

It is a pleasure to record the enthusiastic help received by the author from the U.S. consular authorities in the various places visited by him to collect information on the demise of Sputnik II. By giving advance publicity to his arrival and arranging for eyewitness interviews at the U.S. Information Libraries or in other suitable locales, they enormously facilitated his task. In particular, the author extends his thanks to Mr. Walter Orebaugh, American consul general in Trinidad; Mr. Jesse M. MacKnight, American consul in Surinam; Mr. A. John Cope, Jr., American consul in British Guiana; Mr. Knox Lamb, American consul, and Mr. Lindsay, consular aid, in Barbados; and Mr. Hopkins, American consul in Martinique. Invaluable aid was given to the writer by the Barbados Astronomical Society and its President, Dr. Harry Bayley (it was shocking to receive the news of Dr. Bayley's death, which occurred on June 14, 1958, only a few days after the writer's visit to the island). A particular acknowledgment is extended to Père Pinchon of the Seminaire-Collège in Fort de France, for his efforts to secure eyewitnesses in Martinique.

The author expresses his indebtedness to Miss Jeannie R. B. Carmichael for her help in computing many of the exacting hand integrations which led to the final trajectory.

Orbital Acceleration of Satellite 1958 $\beta 2$

By Luigi G. Jacchia and R. E. Briggs

The present study is based on an analysis of 1,450 Minitrack observations of Satellite 1958 $\beta 2$ made between March 17 and September 16, 1958. The observations, kindly made available by Project Vanguard at the Naval Research Laboratory, were reduced by use of the subsatellite-point program (Jacchia, 1958d, 1958f), with the assumption of the following values of the elements:

$i = 34^\circ.255$
$q = 1.1028$ earth's equatorial radii
$\alpha_\Omega = 158^\circ.53 - 3^\circ.0126$ (t − 1958 March 16.0)
$\omega = 121^\circ.58 + 4^\circ.4027$ (t − 1958 March 16.0)
(t in days, U.T.).

The resulting times of perigee passage, the anomalistic period P_π, and the orbital acceleration dP/dt, are given in table 1; the last two quantities are shown graphically in figure 1.

It appears that the acceleration varies rhythmically, with cycles of the length of 24 to 37 days; the mean period is close to 30 days. During each of these cycles the acceleration varies over a range of 50 to 100 percent of its mean value; the mean value itself seems to be subject to slower fluctuations. Of particular interest is the sharp rise in the acceleration during the second half of August, when it increased by a factor of 4 in just over two weeks.

A periodicity of approximately 25 days was barely discernible, according to Cornford (1958), in the acceleration of Satellite 1957 $\beta 1$; he mentioned that "this had provoked speculation that the tide-raising force of the moon may play some part," although several other possible sources for the irregularities were envisaged. The acceleration curve (Jacchia, 1958f) does not bear out this periodicity; it seems rather to point to 19-day cycles or to double oscillations with a period of 37 days.

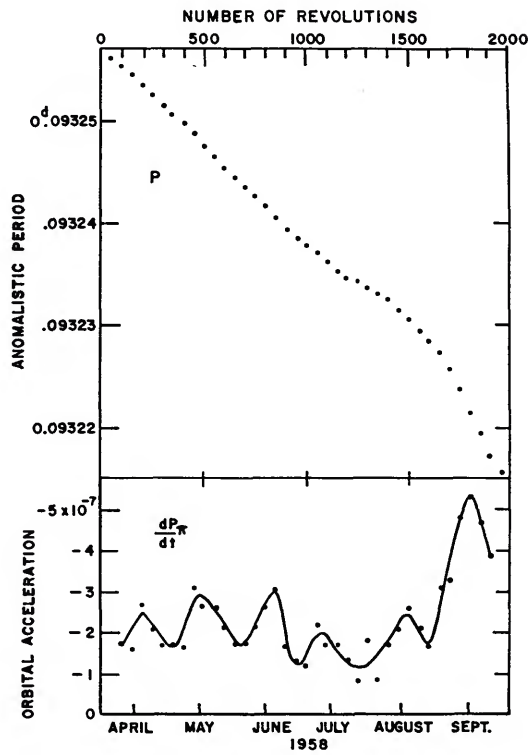

FIGURE 1.—Time variation of anomalistic period and orbital acceleration of Satellite 1958 $\beta 2$.

The fluctuations in Satellite 1958 $\beta 2$, which appear to be too irregular to be explained by tidal phenomena, seem to suggest semiregular changes in the atmospheric density such as could be caused by variable solar radiation—for which one would expect to find occasional periodicities of the order of 27 days and possibly a correlation with geomagnetic activity. A preliminary comparison of the observed accelerations with geomagnetic planetary indices appeared rather inconclusive, although the sharp acceleration maximum near September 1

TABLE 1.—*Orbital elements for Satellite 1958 β2*

No. revolutions n	Times of perigee passage T_n(U.T.)	Anomalistic period P_n (days)	Orbital acceleration dP/dt (days/day)
	1958		
0	Mar. 17.61053		
50	22.27335	0.0932561	
100	26.93614	554	-1.7×10^{-7}
150	31.59889	546	−1.6
200	Apr. 5.26160	536	−2.7
250	9.92425	525	−2.1
300	14.58685	516	−1.7
350	19.24941	508	−1.7
400	23.91193	500	−1.6
450	28.57441	489	−3.1
500	May 3.23682	476	−2.6
550	7.89917	464	−2.6
600	12.56146	453	−2.1
650	17.22370	444	−1.7
700	21.88590	436	−1.7
750	26.54806	427	−2.1
800	31.21017	416	−2.6
850	June 4.87222	403	−3.1
900	9.53420	392	−1.6
950	14.19614	385	−1.3
1000	18.85805	379	−1.2
1050	23.51993	371	−2.2
1100	28.18176	362	−1.7
1150	July 2.84355	354	−1.7
1200	7.50530	347	−1.3
1250	12.16702	342	−0.8
1300	16.82872	336	−1.8
1350	21.49038	330	−0.8
1400	26.15202	324	−1.7
1450	30.81362	315	−2.1
1500	Aug. 4.47517	304	−2.6
1550	9.13666	293	−2.1
1600	13.79810	284	−1.6
1650	18.45950	273	−3.1
1700	23.12083	258	−3.3
1750	27.78208	239	−4.8
1800	Sept. 1.44322	216	−5.3
1850	6.10424	193	−4.7
1900	10.76515	173	−3.9
1950	15.42597	0.0932157	

followed two weeks of strong geomagnetic activity.

It must be emphasized that the accelerations determined from positional observations of artificial satellites cannot be compared, day by day, with geomagnetic or other phenomena, since they are the second-time derivatives of the observed function. At best, the computed accelerations will always be a smoothed-out version of the true accelerations, in which each individual value is the average of a few days.

We may add that the synodic period of precession of the line of apsides for Satellite 1958 β2 amounts to approximately 9,000 revolutions, so that any effect arising from the motion of the perigee from night to day and vice-versa should give origin to fluctuations with a periodicity of this order. This is clearly not true in the present case; in particular, the rapid rise of the acceleration during the second half of August occurred at a time when the perigee was not far from the subsolar point. In a previous report (Jacchia, 1958c), a value $\log \rho = -15.45$ (g/cm^3) was computed for the atmospheric density at perigee height (656 km) under the assumption of an acceleration of -1.95×10^{-7} days per day. The present analysis shows that this value was quite close to the average acceleration in the interval from March to August, 1958. Since, however, the acceleration has shown variations from -1.1×10^{-7} to -5.3×10^{-7} days per day, the computed atmospheric density must be considered to be variable between $\log \rho = -15.0$ and $\log \rho = -15.7$.

A Flashing Satellite for Geodetic Studies

By Charles A. Whitney and George Veis

This paper is intended to provide basic recommendations for an engineering study and design of a flashing geodetic satellite. The study assumes a weight limit of approximately 100 lbs., and a launching time within the near future. On this assumption we have attempted to frame our recommendations as a compromise between what the geodesist would like as an ideal and what the engineer can reasonably be expected to produce within a year. For this reason, we do not discuss the long-range aspects of geodesy or the additional goals that might be attained with a more generous weight limit.

In the first section we outline the aims, the precision required, and the techniques of the geodetic applications of a close satellite; in the second section, we discuss how these factors influence the choice of a satellite orbit; and in the third, we discuss various problems of design and operation. The last section provides a summary of recommendations.

The geodetic aspects

According to the Merriam-Webster unabridged dictionary, geodesy is "that branch of applied mathematics which determines the exact position of points and the figures and areas of large portions of the earth's surface, or the shape and size of the earth, and the variations of terrestrial gravity."

A satellite provided with a mechanism producing flashes of short duration would be highly useful for geodesy.

Accuracy required.—The existing geodetic nets are based on optical (or radio) triangulation for the planimetry and leveling for the altimetry. They are generally accurate to one part in 100,000, which we shall denote as an accuracy of 10^{-5}. The Baltic Geodetic ring is perhaps the most accurate existing net, with an accuracy of about 10^{-6}.

If triangulation techniques are employed to connect these nets, the relative accuracy of the connections will be of the same order as that of the typical base line employed, i.e., 10^{-5}. Therefore, if the absolute accuracy (in meters) of the connections is to equal that existing within the nets, the triangulation scheme must not involve connections over distances significantly greater than the sizes of the nets themselves. If this restriction is observed, triangulation techniques should provide a worldwide geodetic net with an absolute accuracy of about 20 to 30 meters.

In principle, this restriction to tie distances comparable to the length of the base line might be overcome by direct radio-ranging techniques combined with optical triangulation. However, the advantage of such a technique is more apparent than real since, because of the nature of the data, the need to evaluate the propagation velocity and its variations, for example, would probably reduce the relative accuracy to that of the baseline employed, i.e., 10^{-5}.

We adopt the following requirement for the accuracy of measurement of a geodetic satellite: The angles observed must be measured to an accuracy of 10^{-5} radians or 2 seconds of arc. This will generally produce an ellipsoid of uncertainty with a radius of about 15 meters.

For strength in the geometric solutions, observations should be made so that the different lines of sight intersect at nearly right angles. This will usually necessitate restricting observations to elevation angles greater than 30° above the horizon.

On the other hand, since the velocity of the satellite will be about 8 km/sec, to obtain a positional accuracy of 15 meters we must have an accuracy of relative timing better than ± 0.002 second.

Geodetic techniques.—Although the number of possible detailed procedures of observing a satellite for geodetic purposes is very great, there are, in principle, three distinct methods of approaching the problem.

First, a purely geometric procedure can be employed for geodetic connection if the flashes can be observed simultaneously from both of the nets to be connected. Triangulation from each net will give the position of the satellite relative to that net and thus provide the desired three-dimensional connection.

A second method involves fitting an orbit through observations of a set of flashes from one net and of a second set of flashes from another net. We call this the orbital method since we use the orbit as an extrapolation device. Because of uncertainties in the gravitational (and air density) parameters, the method could be used only for flash sets separated by about one orbital revolution or less.

With these two methods of geodetic connection we contrast a third type of analysis, a purely dynamical method in which the coefficients of terms describing the gravitational field are treated as unknowns.

Available data on satellite orbits have already substantially improved the assumed parameters of the earth's gravitational field, through application of what is essentially the dynamical method in which the station positions are treated as knowns. However, data of a rather different nature, such as would be provided by a flashing satellite, are requisites for an efficient program of station-fixing, or geodetic connection.

Choice of the satellite orbit.—There are several differences between the requirements of the geometrical method and those of the orbital method.

Perhaps the most fundamental difference is that the orbital method requires millisecond timing of the flashes, while the geometrical method requires timing just accurate enough to locate the celestial sphere at the time of observation (± 0.05 second). The problem of timing will be discussed later.

Orbital inclination.—The two methods have similar requirements in regard to orbital inclinations. Geodetic connections will be needed primarily in the west-east direction, because the existing nets are generally more extensive in the north-south direction and because transpolar geodetic connections will only rarely be allowed by visibility restrictions. Thus a polar orbit can be ruled out for the general purposes of a geodetic satellite. Polar orbits may be useful in the future, however, for special problems.

A satellite orbit at a height of 500 miles will have a segment more than 30° above the horizon for at least four hours per day from all latitudes less than $i+6°$, where i is the orbital inclination. This would suggest that the inclination could be as much as 6° less than the greatest latitude of the geodetic points to be employed. However, the geometric solutions are greatly strengthened if the satellite does, indeed, pass occasionally to the poleward of these high-latitude stations, or at least through their zeniths.

These considerations, and the geography of northern Europe and Asia, suggest an orbital inclination between 50° and 60° for the first satellites.

We do not feel it advisable (see p. 22) to aim for the critical inclination itself, 64°3, in the neighborhood of which the latitude of perigee changes very slowly. Also, since the high-latitude regions of primary interest to us lie in the northern hemisphere, it would seem advisable to launch the first satellite during the fall season to ensure maximum nighttime visibility in the north during the early, and therefore perhaps more reliable, months of operation.

It is important to note that the success of the geometric method does not require observations to be made in both the northern and southern hemispheres. In other words, the satellite need be observed only from the stations that are to be connected geodetically.

Satellite height.—The height requirements of these two methods differ in the following ways. Ideally, the geometrical procedure would require that the flashes be bright enough to be observed over ground distances of 1,500 to 2,000 miles in order that nets 2,000 miles apart can be connected. Also, the satellite height must be great enough so that, even at this distance, the observed elevation angles will be sufficient (30°) to provide strong trigonometric solutions. These idealized requirements, which demand a satellite height of approximately 2,000 miles, are perhaps rather severe and could be reduced so

that a height of 1,000 to 1,500 miles would suffice.

Height requirements for the orbital method of geodetic connection are more modest, since the satellite need not be observed over such large distances. The height would be chosen so as to keep within tolerable limits the orbital perturbations that result from variations of atmospheric drag and gravitational departures from an ellipsoidal field. So little is known about the exact origin and nature of these smaller-scale gravitational anomalies that it is difficult to predict the rate at which their effect will decrease with height. Through an application of the dynamical method of analysis, determination of this rate will, indeed, be one of the ultimate objectives of observing a geodetic satellite. Thus, considerations of gravitational perturbations do not place a clear-cut minimum on the allowed orbital height.

Atmospheric drag demands a more tangible lower limit on height. For many reasons, the orbital method will probably not be useful in connecting observations separated in time by more than one or two orbital revolutions. We therefore adopt the limiting requirement that the mean atmospheric drag should not displace the satellite from its "undragged" position by more than a few meters during one revolution. This criterion will give an absolute lower limit on perigee height for a satellite of geodetic value.

Analyses of satellite behavior indicate that variations of atmospheric drag, when averaged over 100 revolutions, generally are comparable in magnitude to the mean drag itself. For lack of evidence we may assume that, over intervals of one revolution, the drag variations are of the same magnitude.

The orbit itself will probably have an eccentricity slightly greater than 0.05. Apart from launching difficulties, reasons are given below (p. 22) for an eccentricity of this order. Therefore, we may invert the simplified expression developed by Sterne (1958a) for inferring perigee density from observed changes, and estimate the expected displacements for various orbits. We adopt the Smithsonian Interim Atmosphere No. 2 (Sterne, Folkhart, and Schilling, 1958) for values of average density and employ the drag coefficient ($C_D=2$) used in deriving this model from satellite behavior. For satellites of mean heights between 200 and 800 miles, the following relation is accurate to within a factor 2, which is adequate for present purposes:

$$\delta L=\frac{\rho}{e^{1/2}}\frac{A}{m}10^{16},$$

where δL is the displacement, in meters, produced along the orbit by the average atmospheric drag during one revolution; ρ is the perigee density (gm/cm^3); e is the orbital eccentricity; and A/m is the ratio of effective cross-sectional area to mass of the satellite (cm^2/gm). If we have a satellite with $e=0.05$, $m=50$ kg, $A=0.25$ m^2 and $\delta L\leq 5$, we find a maximum tolerable perigee density of 2×10^{-15} gm/cm^3. This requires the perigee height to be greater than 300 miles, although this figure is not precise since the atmospheric models are rather uncertain at these heights and the density gradient is low because of the high temperature.

For comparison, the hypothetical satellite considered above has a specific gravity (0.58) about 10 percent less than that of the six-inch Vanguard sphere (1958 β2), and an area-mass ratio one-third as great, neglecting antennae. Because of uncertainties and possible fluctuations of atmospheric density at 300 miles, it would seem advisable to aim at a specific gravity somewhat greater than unity, and a minimum perigee height of 400 miles.

We conclude, therefore, that a moderately dense satellite with a perigee height of 400 miles and an apogee height of 1,000 miles would be well suited to the geodetic problems. If the launching vehicle and batteries permit, a more desirable orbit might have a perigee of 500 to 600 miles and an apogee of 1,000 to 1,500 miles.

Operational problems and satellite design

The required accuracy of angular measurement suggests the use of photographic techniques in which the satellite position is measured relative to a star background. Cataloged stellar positions are typically accurate to $\pm0''.5$ of arc, which is entirely adequate.

Parallactic refraction.—Measurement relative to a star background has the advantage that, to the first order, atmospheric refraction is eliminated since the starlight is also refracted. However, there is a small effect, which might be called parallactic refraction, arising from the

fact that the satellite is much closer than the stars. This effect is most severe for low satellites observed near the horizon; for a satellite with $H=500$ km it amounts to 1".5 of arc when the elevation angle is 30°. Since the effect can probably be evaluated to within 10 percent for each observation, the restriction to elevation angles greater than the 30° that is required by geometrical considerations is expected to keep the uncertainties due to parallactic refraction well below timing and measuring errors.

Telescopic focal length.—The position of the center of a circular image on a photographic plate can, with care, be measured to one-fiftieth of its diameter, or about one micron for most photographic plates and telescopes of quality adequate for providing satellite measures. In principle, therefore, a telescopic focal length of 0.5 meter would be sufficiently great to provide positions of the background stars to within 0".5 of arc. In practice, a one-meter focal length will be more nearly compatible with the required aperture.

Duration of flash.—Achieving an angular accuracy of 1 second of arc for the moving satellite image is not easy, for the satellite's apparent angular motion can reach 3,000 seconds of arc per second of time. If the time profile of the light flash were square, the photographic image would become elongated in proportion to the duration of the flash, but it would remain symmetric. Measurements could still attain the required accuracy if the duration of the flash were less than about 0.01 second.

However, a distortion of the satellite image arises from the asymmetry of the light curve of the flash pulses. The light curve shows a rapid increase (a few microseconds) followed by a sharp peak and an exponential decline.

If we represent the light curve by an instantaneous rise to peak intensity I_p, followed by a decline with a half-life τ, in seconds, then the instantaneous intensity $I(t)$, at time t, following the peak is given by the expression,

$$I(t)=I_p e^{-t/\tau}.$$

The nominal exposure time t_n of a flash is taken by convention to be that value of t for which $I(t)/I_p=1/3$, so that $t_n \approx \tau$.

In a typical camera-plate combination the light from a point source is diffused over an area with a diameter of some 20 microns, and the instantaneous spatial profile of light intensity on the plate is well represented by a Gaussian curve. If the photographic plate responded linearly to light, the image could be considered as the sum of a large number of Gaussian curves, arrayed according to the satellite motion, along a line on the plate; the height of the succeeding Gaussians would decrease exponentially. This concept will be very nearly true for images not heavily exposed.

The resulting image will show a well-defined peak of density that will very nearly correspond to the onset of the flash. The observer can be instructed to measure the position of this peak. However, if the image is badly overexposed, the image will saturate, and the peak will become less well defined and will move forward from the instant of onset.

Positional errors thus introduced by varying degrees of image saturation will probably not greatly exceed the distance moved by the light during its nominal exposure time. Thus, these errors can probably be eliminated by keeping t_n less than .001 second and properly diaphragming the observing instruments to avoid heavily overexposing the image.

Atmospheric "tremble" will produce high-frequency angular displacement of the optical image of the satellite. Although the amplitude and frequency spectra of these "seeing excursions" are still under investigation, amplitudes are known to exist as high as 1 second of arc with frequencies greater than 10 to 100 per second. For the stellar background, which will be given exposures of several seconds, these excursions will average to a rather small mean. However, the image of the short flash can be expected to show excursions as great as 1 second of arc even at moderately high elevation angles.

The effects of "tremble," plus the fact that the cost of measuring the photographic plates increases essentially in proportion to the number of plates, suggest that flashes should be arranged in short bursts, or groups, to provide a number of images on each exposed plate.

Brightness of flash.—The brightness of the flash required for detectability by a given telescope depends primarily on the aperture of the telescope objective, the distance to the satellite, the amount of atmospheric absorption,

and the limiting image density considered usable.

A telescopic aperture between 5 and 10 inches would seem optimum in view of the light-gathering power, availability, cost, and ease of installation. Speeds in the region of f/7 would give focal lengths adequate for the desired accuracy of measurement.

The following specification seems to be generally acceptable as a basis for computing the necessary flash brightness: A one-second exposure with a 10-inch aperture gives a workable image of a 10th-magnitude star of solar color at the zenith if fast panchromatic film is used. The xenon discharge tubes do, indeed, have very nearly solar color, and we shall assume the use of panchromatic plate of A.S.A. speed 200.

A 10th-magnitude star as observed at the zenith corresponds to a source of 2.0×10^{-4} candlepower at a distance of one kilometer and with no absorption. With these quantitative conditions, and the inverse-square law of illumination, and the reciprocity law for photographic response, we can easily construct the relation between R, the satellite distance in miles; P, the output in candlepower per second of the flash; A, the aperture of the telescope in inches; and δM, the atmospheric absorption in magnitudes at the zenith distance of observation minus the absorption at the zenith. The relation is given by the equation,

$$\log P=2\log R-2\log A+0.4\,\delta M-1.19.$$

We adopt the values given in table 1 for the atmospheric absorption as a function of zenith distance (Allen, 1957), noting that they apply to a dry, clean atmosphere.

Adopting a reasonable value of 3 candlepower per watt for the efficiency of the discharge tubes, and letting W be the required watt per second rating of the flash unit, we obtain the relation,

$$\log W=2\log R-2\log A+0.4\delta M-1.70.$$

We display the photometric results in table 2, in which satellites at heights of 500 miles and 1,000 miles are treated. For telescopic apertures of 10 inches, the required value of W is given for various values of D, the distance in miles along the earth's surface to the subsatellite point. Angular elevations, h, are also tabulated.

TABLE 1.—*Visual atmospheric absorption*

Zenith distance	Absorption (mag.)	δM (mag.)
0°	0. 21	0. 00
20	0. 22	0. 01
30	0. 24	0. 03
40	0. 27	0. 06
50	0. 32	0. 11
60	0. 42	0. 21
70	0. 61	0. 40

In examining these tables, we must keep several points in mind. 1) Atmospheric absorption increases rapidly with decreasing angular elevation when the elevation becomes less than 40° to 50°. This reduces the efficiency of the flash.

2) If, for reasons of reliability, the purely geometric method of analysis is to be employed for the first satellites, the project will more nearly fulfill its geodetic purpose if stations separated by at least 1,000 to 1,500 miles can simultaneously observe the satellite at an angular elevation greater than 30°. Thus, D should be 750 miles for $h=30°$. This means that the height must be 600 miles at some part of the orbit.

3) Although table 2 is constructed for use with a telescope of 10-inch aperture, the Baker-Nunn satellite-tracking cameras have an aperture of 20 inches, while a much larger number of cameras in the range 5 to 10 inches could be available. These smaller cameras have the advantage of being easily transportable from one site to another.

4) Table 2 is based on general astronomical experience and on a reasonable, though perhaps conservative, value for the luminous efficiency of the flash.

Although further engineering study and testing may show that the power requirements given in this table are larger than necessary, the following comments will probably remain valid: Values of connection distances D up to 680 miles are much more economically obtained for a 500-mile height than for a 1,000-mile height. However, the connection distance can-

TABLE 2a.—*Required flash output*
(H=500 miles)

Subsatellite distance (D)		Angular elevation (h)	Satellite distance (R)	Energy (watt/sec) (W)
0°	0 mi	90°	500 mi	51
2	136	72. 5	525	60
4	271	57	585	72
6	408	45. 5	670	98
8	545	36. 5	775	140
10	680	29	895	200

TABLE 2b.—*Required flash output*
(H=1,000 miles)

Subsatellite distance (D)		Angular elevation (h)	Satellite distance (R)	Energy (watt/sec) (W)
0°	0 mi	90°	1000 mi	200
2	136	80	1015	210
4	271	70	1050	220
6	408	62	1105	260
8	545	53	1175	300
10	680	47	1260	350
12	815	41	1360	420
14	950	35	1475	510

not exceed 700 miles unless the satellite height is greater than 500 miles. Increasing D to 1,000 miles by elevating the satellite to 1,000 miles requires an increase in the flash output by a factor of nearly three.

On the whole, it seems probable that a flash output of 200 to 300 watts per second would be adequate.

The orbital eccentricity.—We have suggested placing the satellite in an orbit with a perigee height of at least 400 miles and an apogee height of 1,000 miles. These are really minimal figures and lead to a mean height of 700 miles and an eccentricity of 0.06. If the orbital inclination differs from 64°3 by at least 5°, the latitude of perigee will vary between positive and negative values numerically equal to the inclination with a total period of some three months. At each observing station, the height of the satellite will thus oscillate between 400 and 1,000 miles. Therefore, depending on the equipment and specific geodetic problem at hand, the observers may choose that observing time at which the height is optimum. With this configuration, the line-of-sight distance to the satellite will vary from 400 miles (perigee at zenith) to some 1,500 miles (apogee at minimum allowable elevation angle). The most "typical" line-of-sight distance will be about 600 miles with an atmospheric attenuation by a factor 0.80.

Flash programming.—The flashes should be grouped in bursts of four to six flashes. The maximum duration of a burst is set by the following considerations. The flashes will be photographed with a telescope that tracks the background stars at the sidereal rate. Background stars are catalogued accurately only to the 9th or 10th magnitude; above this brightness there is an average of 5 stars per square degree. Thus, there is no need for a background exposure going beyond 10th magnitude, which corresponds to 1 second with a 10-inch aperture. In fact, if the background exposure is much greater than this, accuracy may be lost because overexposure and errors of tracking may produce enlargement of the stellar images. Also, the satellite will cross a 5-degree telescopic field in from 15 to 5 seconds; therefore, the burst must last less than 5 seconds.

Flexibility of telescopic angular field and allowable background exposure would seem to demand that the burst duration be less than one second. However, there is no apparent reason for reducing the duration much below one second.

The mean speed of the satellite will be about 250 miles per minute; therefore, a maximum of 1.5 minutes or 375 miles may reasonably be set on the interval between bursts. Provision for a variable interval between flash bursts would be advantageous. From the observers' point of view a 1.5-minute interval would give about three or four usable bursts per passage.

Clearly, the flash need not operate over ground illuminated by the sun. However, a simple sun sensor to cut off the flash when the satellite itself is illuminated would be too restrictive, since for a considerable portion of the orbit, a satellite at 1,000-mile height will be illuminated when ground conditions are favorable for photography. Indeed, this is just the portion of the orbit during which inert satellites are now photographed.

We come finally to the intriguing question of how to provide for timing the flashes and what possibilities exist for ground control over the programming.

We distinguish two types of flash-timing and give them names, for convenience. "Geometric" timing indicates a system by which a simple clock on the satellite activates the bursts at times well enough determined so that observers can photograph the flashes, identify them for the purpose of simultaneous photography from more than one station, and determine the position of the celestial sphere against which the satellite image is measured. An accuracy of 0.05 second would be adequate. "Orbital" timing, on the other hand, means that the satellite carries a clock whose stability and calibration are adequate for the determination of the difference in time between bursts, with an error not to exceed 0.001 second. This clock can be calibrated from the ground.

Operating the satellite.—The simplest and hence the most reliable method for operating the flashing satellite would equip the satellite with a simple clock, whose sole function would be geometric timing. The clock would operate continually, day and night, and would weigh only a few pounds.

In principle, the clock might be made stable enough to allow orbital timing as well, although the requirements for weight and temperature control would be greater. The clock could be calibrated by photoelectric timing through a telescope, although not easily; the data could be analyzed at the individual observing sites or at a central agency, which would publish an ephemeris of flashes. This use of master timing stations would require clock stability sufficient to keep clock errors below 0.001 second per two-hour period, since the time interval between clock checks would be on the order of an orbital period.

The second possible method would include a transmitter on the satellite to emit a radio pulse at the time of the flash. If sufficiently powerful, these pulses could be detected at the observing sites. This technique does not require extreme clock stability. In view of its rewards, this use of an onboard transmitter to provide orbital timing seems highly advisable. If the transmitter failed, the geometric timing would still be available or photoelectric timing could be attempted.

If power requirements dictate a weak pulse, a stable clock could be put on board, and several master timing stations with sensitive receivers could be established to calibrate the clock and prepare an ephemeris of flashes.

This second procedure could be elaborated to enhance greatly the flexibility and efficiency of power utilization. A clock stable to 0.001 or 0.002 second in two hours and operated continually would cause a radio transmitter to emit a pulse, or group of pulses, every 1.5 minutes. When commanded from one, or two, or three master ground stations, a program would be initiated within the satellite to produce a light flash with each radio pulse. The light flashes would be emitted for 100 bursts, or for two and one-half hours, and then stop, although the radio would continue. It might be safer, in view of possible failure, to use the command to suppress the flashes rather than to activate them. By this scheme, the observer could wait for favorable weather and orbital configurations at the observing sites.

One final point concerning the flash programming should be mentioned. If the times of flashes are determined at master stations, rather than at each observing site, it will be necessary to provide a means of identifying the flashes observed at the geodetic stations. The identification of the burst will present no difficulty if the bursts are separated by at least a minute of time. Also, one or two members of a burst might fail to register, due to self-occultation or plate size. If the individual members of the burst are spaced at stable, but unequal, time intervals, they could be identified. For example, a simple pattern of intervals such as 0.2, 0.4 second between the members, would allow a unique determination of the missing member if only three flashes were observed.

Self-occultation could be eliminated at the expense of slightly reduced efficiency, if the satellite had two lamps that flashed simultaneously to illuminate opposite hemispheres. Edgerton's suggestion (personal communication) of employing four lamps, two in each side of the satellite, and letting each lamp

636-014—63——3

produce one member of the burst, would seem an advantage.

Flash lifetime.—It is difficult to place exact limits on the required lifetime of the flash. If the flash operates continually, a minimum lifetime would be about three months, during which the orbital node would have regressed sufficiently to provide visibility at all stations with latitude less than the orbital inclination. This suggests a program lifetime of some 2,000 hours. If, on the other hand, the flash is allowed to operate only during revolutions in a favorable orbit, the efficiency is greatly improved. A fairly complete coverage could probably be obtained with 500 hours of program time. These numbers should be considered lower limits.

Summary

We may summarize our recommendations as follows:

Launch the satellite during the fall months, for maximum visibility in the northern hemisphere. Provide for the operation of the flash, either continuous or intermittent, over a period of at least three months, to allow a complete rotation of the orbit in space.

The best period of operation for the flash program is difficult to estimate, but it should probably be on the order of 500 hours if the command receiver is aboard. If it is not aboard, the time will have to be at least three months or somewhat more than 2,000 hours.

Design the satellite so that (1) a minimum number of flashes is lost by self-occultations; (2) the area-mass ratio is less than 1/20 (cm^2/gm); and (3) the flash output is in the range 200 to 300 watts per second.

Place the satellite in an orbit of inclination $55° \pm 5°$ with a perigee height of 400 miles and an apogee height of 1,000 miles.

In addition to the flash, provide the satellite with the following equipment:

(1) A tracking beacon of Minitrack-type to allow acquisition of the satellite and orbital prediction immediately after launching.
(2) A clock stable enough to give millisecond accuracy over periods of one orbital revolution (nominally, two hours).
(3) A clock-pulse transmitter to emit calibration pulses every ten seconds.
(4) A mechanism to cause a burst of four programmed flashes with every 10th clock pulse (i.e., every 100 seconds).
(5) A command receiver to suppress the flashing for 1,000 clock pulses (3 hours), and thus allow power conservation.

We do not regard the millisecond clock stability as an absolutely essential part of this device, since provision can be made for timing the clock pulses with radio receivers at the observing stations. Such stability would, however, greatly simplify the ground operation and the analysis of data, since it would mean that the timing could be done at two master stations and that analysis of the clock would be allocated to one central group.

The command receiver to allow suppression of the flash is an important part of the device if dry cells are to supply the flash power, since it would quarter the flash power required. Of course, if engineering studies demonstrate the feasibility of using solar energy or a radioactive power supply, the command receiver would be unnecessary.

Acknowledgments

This paper is based, in part, on extensive discussions with J. G. Baker, G. Van Biesbroeck, R. J. Davis, H. E. Edgerton, L. G. Jacchia, R. E. McCrosky. To Fred L. Whipple, Director of the Smithsonian Astrophysical Observatory, we are particularly grateful for thoughtful criticism.

The Earth's Gravitational Potential as Derived From Satellites 1957 β1 and 1958 β2[1]

By Luigi G. Jacchia

An excellent set of 68 orbit determinations of Satellite 1957 β1 (Sputnik II), covering the interval from Nov. 9, 1957 to Apr. 13, 1958, has been published by the Royal Aircraft Establishment, Farnsborough, England (Cornford, 1958). These data permit an accurate interpolation of all orbital elements during the lifetime of the satellite. Since the orbital inclination of this satellite differs by 31° from that of Satellite 1958 β2 (Vanguard)—which, thanks to its high perigee and continuous radio performance, yields highly reliable values for its secular perturbations—it was thought advisable to investigate the possibility of using the two satellites for the independent determination of the second- and fourth-order coefficients of the earth's gravitational potential.

The secular precession $\dot{\Omega}$ of the right ascension of the ascending node, when all distances are expressed in units of the earth's equatorial radius, can be written as follows:

$$\Omega=-n^*a^{-3/2}p^{-2}\cos i\left[J+\frac{J^2}{p^2}\left(\frac{19}{12}\sin^2 i-1\right)-\frac{3}{14}\frac{K}{p^2}(7\sin^2 i-4)\right]. \quad (1)$$

Here a is the major axis of the orbit; n^* is the mean motion of a satellite revolving around a point mass equal to the mass of the earth in an orbit with $a=1$; p is the orbital parameter $[p=a(1-e^2)]$; i is the orbital inclination; J and K are, respectively, the coefficients of the second and fourth harmonics in the earth's gravitational potential. In the above expression, all terms containing J^3, K^2 and higher powers of J and K, as well as their cross-products, have been neglected. We have used $n^*=6135^\circ.58$/day.

For Satellite 1958 β2 we have used the following mean elements, obtained by R. E. Briggs from Naval Research Laboratory orbital data and corrected on the basis of Minitrack observations:

Epoch:	$t_o=1958$ June 18.858
Anomalistic period:	$P_\pi=0^d.0932379$
Eccentricity:	$e=0.19023$
Inclination:	$i=34^\circ.253-0^\circ.00010(t-t_o)$
Right ascension of ascending node:	$\Omega=25^\circ.976-3^\circ.0126(t-t_o)$
Argument of perigee:	$\omega=179^\circ.2+4^\circ.4027(t-t_o)$

(t in days, U.T.).

No departure from linearity can be observed in the motion of the node in the interval from 1958 March 17 to October 10. The estimated error in Ω is $\pm 0^\circ.0002$. From the anomalistic period, using first-order perturbation theory, we can compute $a=1.361527$.

For Satellite 1957 β1 we have interpolated at 10-day intervals, from the data of Royal Aircraft Establishment, the orbital elements in table 1. The nodal precession derived from the data in the last column is tabulated in table 2, together with the individual values of J computed from them, with $K=1.0\times10^{-5}$. These values of J were computed only to test the inner consistency of the data.

To obtain mean values of J and K over the observed interval for Satellite 1957 β1, we have

[1] Manuscript received Nov. 1, 1958.

TABLE 1.—*Orbital elements for Satellite 1957 β1 interpolated from RAE data*

t (0^hU.T.)	a	e	i	ω	Ω
1957					
Nov. 6	1.14601	0.0981	65°.37	59°.3	(108°.3)
16	1.14236	0.0953	.36	55.2	81.69
26	1.13869	0.0926	.34	51.1	54.93
Dec. 6	1.13494	0.0897	.33	47.0	27.95
16	1.13106	0.0867	.32	42.9	0.69
26	1.12694	0.0835	.31	38.7	333.09
1958					
Jan. 5	1.12238	0.0800	.30	34.5	305.11
15	1.11721	0.0759	.29	30.3	276.72
25	1.11193	0.0719	.28	25.8	247.91
Feb. 4	1.10676	0.0678	.27	21.6	218.67
14	1.10138	0.0635	.26	17.3	188.97
24	1.09547	0.0588	.25	12.8	158.76
Mar. 6	1.08877	0.0534	.24	8.3	127.96
16	1.08085	0.0470	.22	3.7	96.45
26	1.07113	0.0392	.21	358.9	64.03
Apr. 5	1.05750	0.0284	65.20	353.7	30.41

integrated equation (1) between the time limits t_1 and t_2, and we thus obtain:

$$\Omega_2-\Omega_1=AJ+BJ^2+CK, \qquad (2)$$

where

$$A=-\int_{t_1}^{t_2} n^* a^{-3/2} p^{-2} \cos i dt=\int_{t_1}^{t_2} f_1 dt,$$

$$B=\int_{t_1}^{t_2} \frac{f_1}{p^2}\left(\frac{19}{12}\sin^2 i-1\right) dt=\int_{t_1}^{t_2} f_2 dt,$$

$$C=-\frac{3}{14}\int_{t_1}^{t_2} \frac{f_1}{p^2}(7\sin^2 i-4)dt=\int_{t_1}^{t_2} f_3 dt.$$

Values of f_1, f_2, and f_3 are given in table 2. Integrating from t_1=1957 Nov. 26.0 to t_2=1958 March 16.0, we obtain (for Satellite 1957 β1):

$$-318°.48=-1°.9624\times10^5 J$$
$$-4°.91\times10^4 J^2+6°.10\times10^4 K. \qquad (3)$$

For Satellite 1958 β2, on the other hand, we have

$$-3°.0126=-1853°.74J+536°J^2-411°K. \qquad (4)$$

Solving equations (3) and (4) simultaneously, we obtain

$$J=0.0016244; \qquad K=6.9\times10^{-6}. \qquad (5)$$

In the interval from t_1 to t_2, the inclination of Satellite 1957 β1 changed by −0°.12. Assuming that the perturbing force which caused this change had an exactly equal effect on the node, i.e., caused an extra precession of the node $\Delta\Omega=-0°.12$, we find for the result:

$$J=.0016241; \qquad K=8.0\times10^{-6}. \qquad (6)$$

The values of K that have been derived from gravity measurements and from different hypotheses concerning the departures of the geoid from a rotational ellipsoid vary between 9.0×10^{-6} and 11.4×10^{-6}. If we wish to adopt the higher of these two values, then we must postulate an extra precession $\Delta\Omega=-0°.47$ in the node of satellite 1957 β1; we then obtain

$$J=0.0016234; \qquad K=11.4\times10^{-6}. \qquad (7)$$

The fact that the rate of change of the orbital inclinations is negative shows that the force responsible for it must be acting in a transverse direction along the general eastward motion of the satellite. Such a force would, if anything, have caused a westward (negative) motion of the nodes; it would seem then that the possibility of a positive excess in the nodal precession due to this cause can be excluded. We can thus consider the value of 6.9×10^{-6}, obtained under the assumption of $\Delta\Omega=0$, as a lower limit for K. It is reasonable to assume that the actual value of K is somewhat smaller than 10×10^{-6}. As to J, it is clear that, no matter what final value is adopted for K, it must be not far from 0.0016240, with an estimated error of $\pm10\times10^{-7}$.

The coefficients J and K are related to the "flattening," α, of the spheroid, by the equations

$$J=\alpha-\frac{1}{2}\rho-\frac{1}{2}\alpha^2+\frac{9}{14}\alpha\rho+\frac{4}{7}\kappa+0(\alpha^3), \qquad (8)$$

$$K=3\alpha^2-\frac{15}{7}\alpha\rho+\frac{24}{7}\kappa+0(\alpha^3). \qquad (9)$$

In these equations $\rho=R\omega^2/k_e^2$, where R is the equatorial radius of the earth, ω is the earth's angular velocity of rotation, and k_e is the "geocentric" gravitational constant; we have adopted $\rho=0.00346149$. The parameter κ is associated with the depression of the spheroid. If we assume that the equipotential surface of the earth is an exact spheroid, we have $\kappa=0$; estimates of κ vary from zero to 6.8×10^{-7}.

TABLE 2.—*Observed values of nodal precession (from RAE data) and individual values of J for Satellite 1957 β1*

t (0^{h}U.T.)	$\dot{\Omega}$ (degrees per day)	f_1 (degrees)	f_2 (degrees)	f_3 (degrees)	$10^3 J$ ($K=1.0\times10^{-5}$)
1957					
Nov. 26	−2.686	−1652.8	−399	+495	1.6275
Dec. 6	−2.711	−1670.9	−405	503	1.6248
16	−2.742	−1690.0	−412	512	1.6249
26	−2.778	−1710.5	−420	521	1.6265
1958					
Jan. 5	−2.818	−1733.7	−428	531	1.6278
15	−2.860	−1760.5	−438	544	1.6270
25	−2.902	−1788.5	−448	556	1.6250
Feb. 4	−2.946	−1816.6	−458	569	1.6242
14	−2.994	−1846.6	−469	583	1.6238
24	−3.049	−1880.3	−482	599	1.6240
Mar. 6	−3.113	−1919.6	−497	618	1.6242
16	−3.191	−1967.6	−516	641	1.6243

For $J=0.0016240$ we obtain $\alpha=1/298.26$ under the assumption of $\kappa=0$, and $\alpha=1/298.30$ assuming $\kappa=6.8\times10^{-7}$. The corresponding values of K are 8.8×10^{-6} when $\kappa=0$, and $K=11.2\times10^{-6}$ when $\kappa=6.8\times10^{-7}$. Since, to first-order, $d\left(\frac{1}{\alpha}\right)=-\frac{1}{\alpha^2}\,dJ$ and $dK=6\alpha dJ$, we find that a change of $+10\times10^{-7}$ in J will result in a change of $-.09$ in $\frac{1}{\alpha}$, but of only -2×10^{-8} in K; (that is, K as derived from equation (9) is unaffected by any reasonable error in J). We are thus led to the following most probable values with their estimated errors:

$$J=0.001624\pm.000001$$
$$K=9(\pm2)\times10^{-6}$$
$$1/\alpha=298.28\pm.11$$
$$\kappa=3(\pm3)\times10^{-7}.$$

The value of $1/\alpha$ given above is in essential agreement with the values of $1/298.0\pm0.3$ and $1/298.38\pm.07$ derived by the U.S. Army Map Service (O'Keefe, Hertz, and Marchant, 1958) from Satellites 1958 Alpha and 1958 β2. It should be noted, however, that this flattening derived from dynamic data does not necessarily have the same meaning as the flattening determined from geodetic measurements on the earth's surface. As pointed out by G. Veis (private communication), the "dynamic" flattening is the flattening of a fictitious, equipotential spheroid containing all the earth's mass, which will give rise to the observed gravitational potential. This fictitious spheroid does not necessarily coincide with the spheroids obtained from geodetic observations, which need special assumptions to correct for the effect of masses left outside the geoid.

The Diurnal Effect in the Orbital Acceleration of Satellite 1957 $\beta 1$[1]

By Luigi G. Jacchia

A tabulation of the orbital acceleration of Satellite 1957 $\beta 1$ has been given in Jacchia (1958c). At the time the report was written there was still some uncertainty—at least in the writer's mind—about the origin of the fluctuations in the observed accelerations. Since then observations (Jacchia and Briggs, 1958) of Satellite 1958 $\beta 2$ (Vanguard) have made it clear that the fluctuations are not caused by a change in the effective presentation area of the satellite, but are of atmospheric origin. It seems appropriate, therefore, to reappraise the results for Satellite 1957 $\beta 1$ in this light. In particular, it may be of some interest to check the acceleration curve for the presence of a diurnal effect, which should manifest itself as the perigee changes its position with respect to the sun.

Table 1 gives, at 10-day intervals, the geocentric angular distance ψ between the perigee and the sun, together with other basic quantities: the argument of perigee ω; the right ascension of the ascending node α_Ω; the right ascension α_π; and the declination δ_π of the perigee. The number of revolutions n corresponding to each date has the same origin as in Jacchia (1958c). The observed accelerations are plotted in figure 1, at the bottom of which the angle ψ is graphed for comparison.

There seems to be little doubt about the presence of the diurnal effect. Apart from shorter, superimposed fluctuations, the departures of the observed acceleration from a smooth curve are very closely in phase with the ψ curve. The effect is gradual, and there is no evidence of a discontinuity at the time when the perigee crosses from light into shadow, or from shadow into light. The observed semiamplitude of the diurnal effect is roughly 10 percent of the acceleration. Since the corresponding semiamplitude in ψ was 60°, we can say that the magnitude d of the diurnal effect can be expressed as

$$d=.0017A(\psi-\psi_0),$$

where A is the undisturbed acceleration and $\psi-\psi_0$ is expressed in degrees; ψ_0 is a reference angle comprised between 90° and the zenith distance of the horizon at perigee height—depending on the assumption concerning the effective height at which the diurnal effect operates. During the time interval covered by table 1, the height of the geometric horizon at perigee height decreased from 104°.6 to 103°.3.

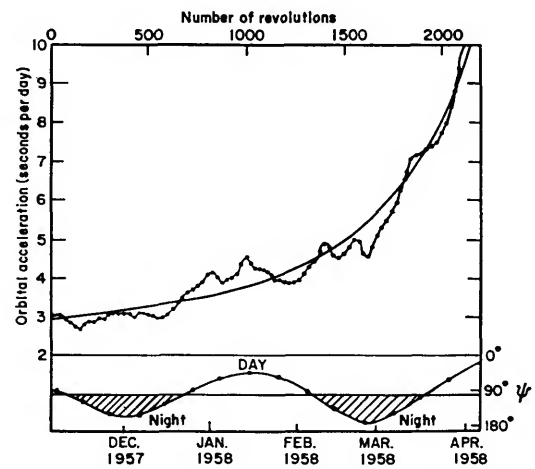

FIGURE 1.—Orbital acceleration of Satellite 1957 $\beta 1$, compared with the geocentric angular distance ψ between the sun and perigee. A smooth curve has been drawn for reference through the jagged acceleration curve (top). When ψ is approximately 104° (bottom), perigee is at the divide between light and shadow.

[1] Manuscript received Dec. 15, 1958.

TABLE 1.—*Position of perigee with respect to sun for Satellite 1957 β1*

t(U.T.)	n	ω	α_Ω	α_τ	δ_τ	ψ
1957						
Nov. 6.0	22	59°.3	108°.3	143°.6	+51°.4	94°.6
16.0	162	55.2	81.7	112.8	48.2	122.4
26.0	302	51.1	54.9	82.4	45.0	150.2
Dec. 6.0	442	47.0	28.0	52.2	41.6	154.5
16.0	583	42.9	0.7	22.0	38.2	126.5
26.0	725	38.7	333.1	351.7	34.6	93.6
1958						
Jan. 5.0	867	34.5	305.1	321.2	31.0	63.7
15.0	1012	30.3	276.7	290.5	27.3	48.8
25.0	1157	25.8	247.9	259.4	23.3	62.8
Feb. 4.0	1303	21.6	218.7	228.1	19.5	94.5
14.0	1450	17.3	189.0	196.5	15.7	132.2
24.0	1598	12.8	158.8	164.3	11.6	172.3
Mar. 6.0	1747	8.3	128.0	131.5	7.5	145.6
16.0	1898	3.7	96.5	98.1	+3.4	102.9
26.0	2051	358.9	64.0	63.5	−1.0	59.2
Apr. 5.0	2206	353.7	30.4	27.7	−5.7	18.3

An Empirical Formula for Ephemerides of Satellites Near the End of Their Lifetime[1]

By Luigi G. Jacchia

In a post-mortem analysis of Satellite 1957 $\beta 1$, searching for a simple function that would represent the period variation of the satellite during its last few hundred revolutions, the author found a relation between the period and the number of remaining revolutions. This turned out to be extremely useful in making predictions during the last week of the lifetime of Satellite 1958 $\delta 1$. Since some interest has been expressed concerning prediction techniques at the end of a satellite's lifetime, we think we are justified in presenting a brief discussion of this formula, in spite of its purely empirical character.

Let n be the number of revolutions of a satellite, counted from an arbitrary origin, and n^* be the number of the last revolution in such count. Moreover, let P be the orbital period of the satellite at the n^{th} revolution, and P^* be a critical period, constant for each satellite.

For Satellite 1957 $\beta 1$, the author found that during the last 100 revolutions the relation

$$\frac{d \log (P-P^*)}{d \log (n^*-n)}=\text{constant}=k \qquad (1)$$

was almost rigorously satisfied when P^* was put equal to 0^d06030.

For Satellite 1958 $\delta 1$ the same relation held equally true, with P^* again 0^d06030. Since the area/mass ratio was very similar for the two satellites, k itself was nearly identical in the two cases (0.406 for 1957 $\beta 1$, and 0.403 for 1958 $\delta 1$). A plot of log $(P-P^*)$ against log (n^*-n) for both satellites is shown in figure 1.

It will be noticed that the critical period $P^*=0^d0603=86.8$ minutes is just about the value of the period that a satellite reaches in the course of the last revolution, when it starts in its final descent arc; the corresponding height in a circular orbit is 120 km above the equator. This critical height should not be too different from one satellite to the other, so it stands to reason that P^* can always be taken equal to 0^d0603, thus eliminating one unknown parameter in equation (1).

From equation (1) we have, by integration

$$\log (P-P^*)=\log b+k \log(n^*-n), \qquad (2)$$

or

$$P=P^*+b(n-n^*)^k, \qquad (3)$$

where b is a constant. Integrating again, we obtain

$$T=a+P^*(n^*-n)-\frac{b}{k+1}(n^*-n)^{k+1}, \qquad (4)$$

where T is the time of ascending-node crossing (or any other crossing from which the period P is determined), and a is another constant.

A comparison of the observed instants of ascending-node crossings with instants computed by equation (4) with suitable parameters is given in tables 1 and 2, for both Satellites 1957 $\beta 1$ and 1958 $\delta 1$. It will be seen that the residuals in both cases amount to only a moderate number of seconds. The equations used are:

For Satellite 1957 $\beta 1$:

$$T=1958 \text{ Apr. } 8.02102+0.0603(n_B-2250) -0.0003275(2350-n_B)^{1.406}. \qquad (5)$$

For Satellite 1958 $\delta 1$:

$$T=1958 \text{ Nov. } 27.16316+0.0603(n_D-2790) -0.00032894(2897-n_D)^{1.403}. \qquad (6)$$

[1] Manuscript received Dec. 15, 1958.

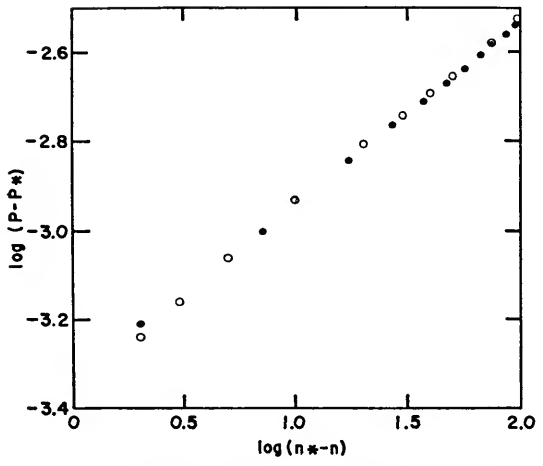

FIGURE 1.—Plot of log $(P-P^*)$ against log $(n-n^*)$ for Satellites 1957 $\beta 1$ (open circles) and 1958 $\delta 1$ (dots).

Counted from an arbitrary origin, n_B and n_D represent the number of revolutions for each of the two satellites. The quantity Δn tabulated for 1958 $\delta 1$ is the difference between n_D and the value of n_B for which the first satellite had the same period. As can be seen, the two satellites were out of phase by 544 revolutions at the start of the tabulation, but the difference increased slowly, at a nearly constant rate. This circumstance made it possible to have an independent estimate of n^*—i.e., of the time of demise—for 1958 $\delta 1$. A similar procedure could have been used, presumably, even if the area/mass ratio of the second satellite had been widely different; in that case, however, a scaling factor in n would have been advisable before computing Δn.

It should be clear that for a determination of the parameters k and n^* it is simpler to use the observed periods P, rather than the crossing times T. If we write log $(n^*-n)=x$, and log $(P-P^*)=y$, and select three corresponding sets of x and y (subscripts 1, 2, 3), the procedure is to find by trial and error a value of n^* that will satisfy the relation,

$$\frac{x_2-x_1}{x_3-x_2}=\frac{y_2-y_1}{y_3-y_2}, \tag{7}$$

which derives from equation (1). Once n^* is found, we have

$$k=\frac{x_3-x_1}{y_3-y_1}, \tag{8}$$

after which a and b can be determined from two observed values of T.

It should be obvious that equation (1) cannot be expected to hold throughout the lifetime of a satellite, especially in the case of those with highly eccentric orbits, so that the formula does not appear suitable for the computation of long-range life expectancies of satellites. It does appear, however, that toward the end of a satellite's lifetime, when formulas based on the orbital eccentricity are bound to fail, this empirical formula may offer a distinct advantage.

TABLE 1.—*Comparison of the last revolutions of Satellite $\beta 1$ with ephemerides*

n_B	t_Ω obs.	O-C	P	log (n^*-n_B) $(n^*=2350)$	log $(P-P^*)$ $(P^*=.0603)$
2250	Apr. 7. 80859	. 00000	¢063296	2. 0000	7. 4765–10
2275	9. 38686	+. 00010	. 062957	1. 8751	7. 4244
2300	10. 95582	−. 00004	. 062547	1. 6989	7. 3516
2310	11. 58032	−. 00013	. 062355	1. 6021	7. 3128
2320	12. 20281	−. 00012	. 062136	1. 4771	7. 2639
2330	12. 82285	−. 00007	. 061859	1. 3010	7. 1928
2340	13. 43970	+. 00002	. 061477	1. 0000	7. 0708
2345	13. 74637	. 00000	. 06117	0. 6990	6. 940
2347	13. 86853	−. 00006	. 06099	0. 4771	6. 839
2348	13. 92947	−. 00008	. 06088	0. 3010	6. 763
2349	13. 99028	−. 00011	. 06072	0. 0000	6. 623
2350	14. 05088	−. 00014	(. 06050)	[last revolution]	

TABLE 2.—*Comparison of the last revolutions of Satellite 51 with ephemerides*

n_D	t_0 obs.	O-C	P	log (n^*-n_D) (n^*=2897)	log (P-P^*) (P^*=.0603)	Δn
2790	Nov. 26. 93177	. 00000	d 063347	2. 0294	7. 4839–10	544
2800	27. 56463	+. 00010	. 063224	1. 9868	7. 4660	545
2810	28. 19623	+. 00016	. 063096	1. 9395	7. 4465	545
2820	28. 82651	+. 00019	. 062957	1. 8865	7. 4244	545
2830	29. 45533	+. 00015	. 062804	1. 8261	7. 3986	546
2840	30. 08256	+. 00003	. 062641	1. 7559	7. 3694	546
2850	30. 70811	−. 00009	. 062472	1. 6721	7. 3369	546
2860	Dec. 1. 33186	−. 00013	. 062272	1. 5682	7. 2949	546. 0
2870	1. 95348	−. 00016	. 062046	1. 4314	7. 2420	546. 4
2880	2. 57255	−. 00009	. 061756	1. 2304	7. 1632	546. 8
2890	3. 18814	+. 00003	. 061304	0. 8451	7. 0017	547. 0
2895	3. 49371	−. 00007	. 06090	0. 3010	6. 778	547. 2
2896	3. 55456	−. 00007	. 06080	0. 0000	6. 690	547. 4
2897	3. 61530	+. 00005	(. 06067)	[last revolution]		

The Structure of the High Atmosphere: I. Linear Models

By Charles A. Whitney

This paper is the first of two on the structure of the terrestrial atmosphere above 100 km as inferred from data on artificial satellites. Orbital accelerations derived by analyses performed at the Smithsonian Astrophysical Observatory will be employed to infer atmospheric densities near the perigee heights of the satellites.

Despite remaining uncertainties in charge-accumulation effects on the drag parameters (Schilling and Whitney, 1958), computations neglecting these effects give the most reliable data available on densities above 100 km.

The principal aim of this first paper is the presentation of a homogeneous set of mean satellite data and the fitting of three simple models to the inferred densities. These models, being based on sectionally linear distributions of molecular temperature, must not be considered as more than smoothing operators for the satellite data. On the other hand, these models provide an excellent basis for a study of the range of models that will fit the satellite data. They allow a demonstration of the uncertainties inherent in the derivation of a temperature distribution from data on the density distribution.

The nature of the high atmosphere

Although I shall defer detailed discussions of the physical nature of the high atmosphere to later papers, several outstanding features must be mentioned at the outset. The reader is referred to the literature (Kuiper, 1952; 1954) for more detailed discussions and further references.

First, the chemical composition of the atmosphere above 80 km is not well known. Molecular oxygen undergoes dissociation somewhere between 90 and 200 km; the details of the transition evidently undergo significant temporal and geographic variations. Auroral spectra indicate the presence of molecular nitrogen to 500 km at least; and although it must be partially dissociated at such heights, the working approximation that nitrogen is molecular is sufficient for discussions of mean molecular weight.

Also, diffusional separation of molecules of differing weights is significant above 120 to 150 km.

The variation of molecular weight resulting from these effects makes it convenient to employ a molecular temperature rather than true temperature in establishing preliminary models. A molecular temperature, T_m, may be defined as

$$T_m = \frac{M_0}{M} T, \tag{1}$$

where M and T are the true molecular weight and temperature, and M_0 is a reference molecular weight, conveniently taken as the molecular weight at the ground or at the greatest height for which it is well known.

Although radiative effects are important at lower levels, it seems fairly certain that conduction plays the major role in heat balance above 300 km (Spitzer, 1952). This statement may not be valid during times of large ultraviolet excess in solar radiation. Chapman's (1957) suggestion that the high atmosphere is heated by conduction from the solar corona is clearly of basic importance in this regard.

The concept of an exosphere has been rediscussed by Spitzer (1952). The base of the

exosphere, or the critical level, is defined as that level at which "a fraction $1/e$ of a group of very fast particles moving upward . . . will experience no collision as they go to infinitely greater heights." The atmosphere above the critical level is essentially isothermal, and diffusional separation must take place.

For neutral particles the number density at the critical level is given by

$$n_c=\frac{1}{4\sigma\mathscr{H}} \tag{2}$$

where σ is the typical atomic cross section (6.8×10^{-16} cm^2) and $\mathscr{H}$ is the scale height.

Nature of the data

Orbital accelerations employed in this paper for deriving densities have been obtained from second differences of the times of perigee passage. In practice it has been found necessary to employ intervals of at least 30 to 50 orbital revolutions in deriving accelerations, so the data are averaged over several days.

The accelerations thus derived have shown, for all satellites, semiperiodic fluctuation with mean periods around 28 to 30 days. Although I suggested (Whitney, 1958) that for 1958 Alpha this could be explained by systematic variations in geometric effective cross section, this interpretation is no longer valid. Jacchia (1959e) has shown a remarkable correlation between the variations experienced by Satellites 1958 $\beta2$ (Vanguard) and 1958 $\delta1$ (the rocket of Sputnik III). Further examination removes all doubt that this correlation is ubiquitous, all satellites showing virtually simultaneous maxima and minima of acceleration. Although these variations are only semiregular, they show mean semiamplitudes of 15 percent to 50 percent; Satellite 1958 $\beta2$, the highest satellite, shows the greatest amplitude.

Priester (1958) has recently discovered a surprisingly close positive correlation between the daily averages of 20-cm radiation and the variable acceleration of 1957 $\beta2$ as derived by Jacchia for the interval Nov. 1, 1957, to Feb. 10, 1958. Priester notes that Elwert's work (1956) indicates that these atmospheric fluctuations may be produced by 6 A to 30 A radiation from coronal condensations.

The satellite data show an increase with perigee height of the amplitude of the acceleration variations. In discussion, Jacchia and I noted that this indicates a change of density gradient over a rather large depth interval in the atmosphere, since the mean density gradient probably decreases with increasing height.

The discoveries of Jacchia and Priester will be of tremendous importance in studying the high atmosphere, since they imply the existence of worldwide, synchronous variations of density. Jacchia has also shown that there is a term in the acceleration of Satellite 1958 $\delta1$ that can be correlated with the zenith distance of the sun at the subperigee point.

At this time it seems best to proceed by averaging out these periodic fluctuations and deriving densities from mean accelerations over several months. I have taken the data, insofar as possible, from the spring and early summer months of 1958 in order to eliminate possible difficulties from longer-period terms.

Also, rocket data provide evidence for rather considerable latitudinal, short-period or irregular fluctuations of atmospheric density at high elevations. However, an earlier analysis has shown that there is no evidence in the data for Satellite 1958 Epsilon of any severe latitudinal changes of mean density at $Z=260$ km. Therefore, I have combined data from different latitudes in the present study.

It is hoped that the mean models thus obtained will provide a basis for a "differential corrections" study of the fluctuations observed.

The satellite data

Using Sterne's formula (1958c) and applying also the major portion of his correction for the assumed solid-body rotation of the atmosphere, I have derived atmosphere densities from accelerations. (I am indebted to Dr. Sterne for providing me with this correction prior to publication.) The data pertinent to the use of these formulas are assembled in table 1.

For two reasons, I have taken all geometric perigee heights, Z_p, in km as measured from a sphere of radius 6378 km. First, the motions of the lines of apsides were, in most cases, rather large in the intervals covered; and second, the mean accelerations could not be defined so well that a few kilometers would be significant.

TABLE 1.—*Satellite data*

Satellite	Height of perigee		Semimajor axis a	Eccentricity e	Acceleration $\dot{P}$ (sec/day)	Mass-area ratio m/A (gm/cm ^{2})	Length (cm)
	Geocentric Z_p (km)	Geopotential H_p (km)					
1957 $\alpha 2$	220	213	1.086	.0482	−2.4	24.1	58
1958 Alpha	360	341	1.2276	.139	−0.455	5.5	200
1958 $\beta 2$	656	594	1.3619	.190	−0.017	3.97	15
1958 Gamma	185	180	1.211	.153	−12.6*	5.6	200
1958 Epsilon	257	247	1.1883	.125	−1.72	6.4	200

*Derived from curve communicated by J. Siry.

The quantity H_p is the geopotential height of perigee derived from the relation

$$H=Z\left(1+\frac{Z}{6357}\right)^{-1}. \qquad (3)$$

Geopotential height, like molecular temperature, is an artifice used to facilitate the integration of the equation of hydrostatic equilibrium.

Since Sterne's formula for the density at perigee actually gives $\rho_p \mathscr{H}^{-1/2}$ where $\mathscr{H}$ is the scale height just above perigee, it is necessary to have an approximate model before densities can be derived. I have, therefore, proceeded by successive approximations. In table 2 are given the densities as derived from scale heights given by models 4 and 5 described below. The densities derived from the scale heights of model 4 are the values used in constructing models 4 and 5, and represent the results of iteration. Actually, the process had converged after only one adjustment, since the densities are insensitive to the model employed. Thus, although model 5 is not rigorously self-consistent, further adjustment would produce only a trivial change. Table 2 also includes the drag coefficient, C_D, used in deriving the densities. These values are consistent with the densities of model 4 and their derivation is discussed later (see p. 41).

The convergence of such an iteration process can be speeded through a technique which was apparently first employed at the Vanguard Computing Center and reported by J. W. Siry (1960; see also King-Hele, 1959).

TABLE 2.—*Atmospheric densities from satellite accelerations*

Satellite	H_p	C_D	$\log_{10}\rho$ (gm/cm^3)	
			Model 4	Model 5
1958 Gamma	180	1.2	−11.86	−11.91
1957 $\alpha 2$	213	1.9	−12.37	−12.40
1958 Epsilon	247	1.9	−13.00	−13.02
1958 Alpha	341	2.0	−13.74	−13.75
1958 $\beta 2$	594	2.0	−15.47	−15.45

Sterne's formula for the satellite acceleration may be written

$$\rho_p^* \sqrt{\mathscr{H}^*} = \dot{P} f(e).$$

In this form, $f(e)$ is a known function of the orbital elements whose relative error is much less than the relative error of $\dot{P}$, the observed acceleration. The quantity ρ_p^* is the true value of density at perigee, and $\mathscr{H}^*$ is the true value of scale height at perigee.

If Sterne's formula is employed with an assumed scale height, $\mathscr{H}$, which is not the true value, then the derived density ρ_p will differ from the true density. In fact, the relative error of the derived perigee density is one-half the relative error of the assumed scale height.

Suppose, however, we modify Sterne's formula and use it to derive the density at some height above the perigee. Denote this height by $h\mathscr{H}$, where h is dimensionless. The essence of the present technique is to choose h so that the derived density falls nearly on the true

density curve regardless of moderate errors in $\mathscr{H}$. Siry has called h the isopycnotic height.

Explicitly, we first write Sterne's formula in terms of the assumed scale height and the derived density at perigee,

$$\dot{P}f(e)=\rho_p\sqrt{\mathscr{H}}.$$

Denote as $\rho(H_p+h\mathscr{H})$ the derived density at a height $h\mathscr{H}$ above the perigee, whose height is H_p. Then

$$\rho(H_p+h\mathscr{H})=\rho_p e^{-h}.$$

Therefore, the density derived for the height $H_p+h\mathscr{H}$ may be written

$$\rho(H_p+h\mathscr{H})=\dot{P}f(e)\frac{e^{-h}}{\sqrt{\mathscr{H}}}.$$

On the other hand, the true density at the assumed height $H_p+h\mathscr{H}$ is

$$\rho^*(H_p+h\mathscr{H})=\rho_p^* e^{-h\mathscr{H}/\mathscr{H}^*}=\dot{P}f(e)\frac{e^{-h\mathscr{H}/\mathscr{H}^*}}{\sqrt{\mathscr{H}^*}}.$$

The isopycnotic height, h_p, is that value of h for which

$$\rho^*(H_p+h\mathscr{H})=\rho(H_p+h\mathscr{H}).$$

It may be found by equating the expressions above, i.e., from

$$\frac{e^{-h}p}{\sqrt{\mathscr{H}}}=\frac{e^{-h}p^{\mathscr{H}/\mathscr{H}^*}}{\sqrt{\mathscr{H}^*}}.$$

Clearly h depends on $\mathscr{H}/\mathscr{H}^*$, the error in the assumed value of , but fortunately the dependence is not strong.

For small errors, i.e.,

$$\left|\frac{\mathscr{H}}{\mathscr{H}^*}-1\right|\ll 1,$$

we find

$$h_p=\frac{1}{2}.$$

When the error of $\mathscr{H}$ cannot be assumed small we must proceed numerically and choose that isopycnotic height that is appropriate to the estimated uncertainty of $\mathscr{H}$.

TABLE 3.—*Percent errors of derived densities*

$\mathscr{H}/\mathscr{H}^*$	h			
	0	0.43	0.5	1.0
1.0	0.0	0.0	0.0	0.0
1.1	−4.6	−0.5	+0.2	+5.4
1.2	−8.7	−0.5	0.9	11.5
1.3	−12.3	−0.2	1.9	18.4
1.4	−15.5	+0.4	3.2	26.1
1.5	−18.3	+1.2	+4.8	+34.6

In a qualitative way the basis of the technique is the following. If the assumed scale height is too large, the derived density will be too small. However, this density will be applied at too great a height. When $h=h_p$, these errors cancel.

In table 3 we illustrate the power of this technique by listing the percent error in derived density as a function of $\mathscr{H}/\mathscr{H}^*$ and the adopted value of h.

On the basis of this table, it appears that the appropriate choice, if the atmosphere were truly exponential, would lie in the range

$$0.5>h>0.43,$$

the upper limit being favored when the uncertainty of $\mathscr{H}$ is small.

Therefore, we conclude that when Sterne's formula is written in the form

$$\rho(H_p+0.43\mathscr{H})=\dot{P}f(e)\frac{e^{-0.43}}{\sqrt{\mathscr{H}}},$$

the derived densities will be virtually unaffected by errors of up to 50 percent in the assumed value of $\mathscr{H}$.

An earlier linear model

Sterne, Folkart, and Schilling (1957) derived three tentative model atmospheres from a density at $Z=200$ km evaluated from the acceleration of Satellite 1957 $\alpha 2$. They adopted the formula,

$$\rho(220)=4.5\times 10^{-13}\text{ gm cm}^{-3},$$

and forced the temperatures and densities of these models to fit the ARDC model (Minzner and Ripley, 1956) at $Z'=80$, 90, and 100 km, by adjustment of the constant temperature

gradient above Z'. These models were designated Interim Atmospheres Nos. 1, 2, and 3, respectively. The defining relations are:

Model 2.

$$T_m = -603.3 + 9.0167H,$$

$$\log \rho = 2.588 - 4.79 \log T_m.$$

In these relations, and in those to follow, logarithms are to the base 10, densities are in gm/cm^3, and heights are in kilometers. The molecular temperature for this model is defined by equation (1), and $M_0 = 28.966$.

The densities given by this model are plotted against geometric height in figure 1. Considering that this model, which the authors preferred over models 1 and 3, was based on data from a single satellite, it is remarkably good even at 500 km. However, since the later data seem to deviate systematically, I have considered it worth while to construct further models.

Models 4 and 5

I have extended the calculations of Sterne *et al.* (1957) by adjusting the height Z', at which the ARDC model is fitted, and L the temperature gradient above Z', to produce a fit to the satellite data of table 2 at heights of 260 and 656 km. Explicitly the model fits, by construction, the data at

$$Z' = 88.4, \log \rho = -8.29, T_m = 196.9.$$

The defining relations are:

Model 4.

$$T_m = -465.6 + 7.641H$$

$$\log \rho = 4.311 - 5.4712 \log T_m.$$

The densities given by this model are plotted in figure 1; they seem to be a significant improvement over those of model 2. Furthermore, the excellence of the over-all fit of model 4 to the data indicates that the assumption of a constant temperature gradient above 100 km is adequate.

In order to estimate the range in models permitted by satellite data, I have constructed a fifth linear model based on rather different assumptions. Models 4 and 5 are in no way limiting cases on acceptable models. However, being based on independent boundary conditions at the bottom and on rather different temperature assumptions, they might be considered as independent samples of acceptable models. In this sense, the differences between them give a reasonable, rather than an extreme, estimate of the remaining uncertainties.

I have constructed this fifth model by forcing the density through three points and the temperature through one. For the lowest point I took $T = 150°$K, $M = 28.57$, log $\rho = -8.66$ at $H = 90$ km. These values are nearly those given by Nicolet's tabulation (1958a). The height of 90 km was chosen as the maximum height at which uncertainties in the dissociation and diffusion are insignificant.

The atmosphere was assumed to have constant, but different, temperature gradients above and below 150 km. The dividing height of 150 km was chosen arbitrarily as representing, roughly, an elevation at which the nature of the atmosphere changes significantly (in relation to diffusion and O_2 dissociation). Also, it is a convenient round number near the lowest satellite perigee.

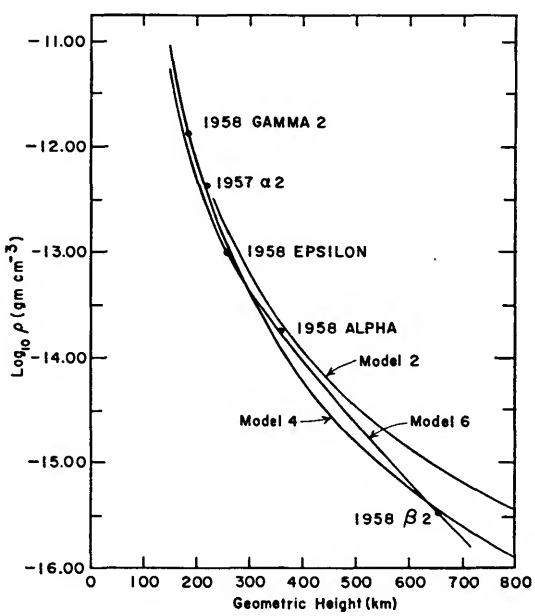

FIGURE 1.—Atmospheric densities given by models 2, 4, and 6, plotted against geometric height.

The model is described by the following formulas, whose derivation is standard (see Sterne *et al.*, 1957):

$$\left.\begin{aligned} T_m &= 150 + L'(H-90), \\ \log \rho &= \log \rho(90) - \left(1+\frac{33.76}{L'}\right)\log\left(\frac{T_m(H)}{T_m(90)}\right). \end{aligned}\right\} \quad 90<H<150.$$

$$\left.\begin{aligned} T_m &= 150 + 60L' + L''(H-150), \\ \log \rho &= \log \rho(150) - \left(1+\frac{33.76}{L''}\right)\log\left(\frac{T_m(H)}{T_m(150)}\right). \end{aligned}\right\} \quad H>150.$$

In these relations L' and L'' are the temperature gradients (°K/km) below and above 150 km, and T_m is related to the true temperature through equation (1), with $M_0=28.57$.

After several trials, a pair of L' and L'' was found that fit the required densities. These lead to the defining relations:

Model 5.

$$\left.\begin{aligned} T_m &= -966 + 12.4H \\ \log \rho &= -0.56 - 3.723 \log T_m \end{aligned}\right\} 90<H<150.$$

$$\left.\begin{aligned} T_m &= -111 + 6.70H \\ \log \rho &= 6.275 - 6.039 \log T_m \end{aligned}\right\} H>150.$$

As a measure of the uncertainties within the framework of this particular model, I have evaluated the following partial derivatives for heights of 260 and 656 km:

$$\left(\frac{\partial \log \rho}{\partial L'}\right)_{260} = 0.12, \qquad \left(\frac{\partial \log \rho}{\partial L'}\right)_{656} = 0.19,$$

$$\left(\frac{\partial \log \rho}{\partial L''}\right)_{260} = 0.01, \qquad \left(\frac{\partial \log \rho}{\partial L''}\right)_{656} = 0.21.$$

Taking $\Delta \log \rho = \pm 0.1$ as a reasonable upper limit on the uncertainty in the basic data, we see that the temperature gradients for this particular model are reliable only to approximately $\pm 0.5°$ K/km.

The actual uncertainties, however (see below), are considerably greater.

Model 6

Considerable interest is attached to the temperature gradient above 300 to 400 km.

Bates (1951) has shown that absorption of ultraviolet solar radiation appears insufficient to maintain a significant positive temperature gradient above the F layer. If such a gradient indeed exists, it will probably be explained by conduction from above, as outlined by Chapman (1957).

Unfortunately, the satellite data give only two mean-density values above 300 km, so this question probably remains an open one. As an experiment I have constructed model 6 in the following manner. From model 4, I derived densities at $Z=300$ km leads to $T_m=2527°$ K ($M_0=28.966$) above this height. To fit the model to lower levels I assumed a constant temperature gradient and forced the temperature to $T=150°$K at $H=90$ km (Nicolet, 1958a). It was not necessary to assume a density at heights other than $Z=300$ and 600 km.

The resulting model is described by the following equations:

Model 6.

$$\left.\begin{aligned} T_m &= -751°.44 + 10.016H \\ \log \rho &= 1.274 - 4.411 \log T_m \end{aligned}\right\} 90<H<287.$$

$$\left.\begin{aligned} T_m &= 2123° \text{ K} \\ \log \rho &= 11.404 - .0069591H \end{aligned}\right\} H>287.$$

The densities given by this model are graphed in figure 1 and they seem to fit the data quite well. Also, at $H=90$ km, this model gives $\log \rho = -8.32$, in excellent accord with $\log \rho = -8.31$, given by the ARDC model.

Table 4 compares the densities and molecular-scale temperatures given by models 4 and 6.

The results of this comparison are neither surprising nor encouraging. Although the tem-

TABLE 4.—*Densities (log ρ) and temperatures (T_m) given by linear models*

Height Z(km)	Model 4		Model 6	
	T_m	log ρ	T_m	log ρ
200	1017	−12.14	1192	−12.30
300	1727	−13.40	2123	−13.40
400	2407	−14.19	2123	−14.02
500	3080	−14.78	2123	−14.63
600	3722	−15.22	2123	−15.22

peratures agree well at low heights and near 350 km, as they must, they differ considerably at heights greater than 400 km. I would not say that it is possible at present to choose between these two nonphysical models.

The base of the exosphere

Equation (2) has been used to evaluate Z_c, the geometric height of the critical level, or base of the exosphere. For model 2, $Z_c=630$ km; for model 4, $Z_c=500$ km. If the numerical coefficients of equation (2) are correct, the value of Z_c as given by model 4 is probably accurate to 20 km for the mean atmosphere during the early summer of 1958.

At $Z=500$ km, model 4 gives $T_m=3080°$ K, and model 6 gives $T_m=2123°$ K. If, as seems likely from Nicolet's (1958a) discussion and further results to be presented in Paper II (p. 43), we may assume the gas at this level to be pure oxygen, then these molecular temperatures lead to true temperatures of 1700° K and 1200° K, respectively.

These values are lower than 2250° K, the lower limit derived by Nicolet for the required escape of helium, but the discrepancy may not be serious. Further, the present data do not exclude the possibility of a rise to 2000° K somewhat below 500 km, since these data determine only the mean temperature and not its detailed distribution.

The drag coefficient

Dr. R. M. L. Baker, Jr., of Aeronutronic Systems, Inc., Glendale, Calif., kindly made available, prior to publication, his formula for the drag coefficient C_D in the transition region. The expression is of the form,

$$C_D=C_{D_0}\left[1+\left(\frac{2}{C_{D_0}}-1\right)\exp\left(-\sigma C\right)\right],$$

where σ is a dimensionless atmospheric density; $C_{D_0}=C_D(\sigma=1)$; and C is related to the ratio of mean free path to body size.

Employing Baker's formula and the atmospheric densities of model 4, I have computed C_D for the transition region. I have adopted the velocity $v=8$ km/sec for the satellites, and $M_cT_s=8000°$ K, where M_c is the dimensionless molecular weight of the particles "emitted" from the satellite and T_s is the surface temperature of the satellite. Table 5 gives representative values of C_D; Z is the geometric height of the satellite, and d is its "typical" linear dimension.

TABLE 5.—*Transitional drag coefficient* (C_D)

Height Z(km)	Drag coefficient for satellite of linear dimension d (meters)			
	1m	3m	10m	30m
160	0. 99	0. 92	0. 92	0. 92
180	1. 30	. 96	. 92	. 92
200	1. 60	1. 21	. 92	. 92
220	1. 79	1. 48	1. 04	. 92
240	1. 89	1. 68	1. 26	. 95
260	1. 93	1. 81	1. 48	1. 06
280	1. 96	1. 88	1. 65	1. 24
300	1. 98	1. 92	1. 77	1. 43
320	1. 99	1. 95	1. 75	1. 59
340	2. 0	1. 97	1. 90	1. 69

Since the algebraic representation of C_D is rather arbitrary, the details of the transitional C_D are not too reliable. However, the heights of the transition regions of various satellite sizes are probably fairly accurate.

Baker's formula leaves little doubt that variations of C_D from the conventional value of two, employed heretofore in deriving satellite densities, are significant. There may, of course, be an increase of C_D due to plasma effects.

The possible implications of Baker's results for analyses of satellite data are manifest. I shall defer a discussion of some of these possibilities to later papers, and merely state that I have used these values in computing the densities for table 4. The changes introduced by values of $C_D<2$ are important only for the two lowest satellites considered in the present analysis.

The Structure of the High Atmosphere: II. A Conduction Model

By Charles A. Whitney

In the first paper of this series (Whitney, 1959), I summarized the values of atmospheric densities as derived from satellite accelerations. In an attempt to smooth the data, I constructed three models with sectionally constant temperature gradients. Such models, although fitting the data quite well and providing a useful basis for discussion, are admittedly nonphysical.

Nicolet (1958b) has outlined several aspects of physical models for the high atmosphere. In this paper I shall construct a conduction model based on his discussion.

Algebraic description of the conduction model

The total heat flux F carried downward by conduction across a geocentric sphere of radius r is given by the equation

$$F=4\pi r^2 BT^{1/2}\frac{dT}{dr}, \tag{1}$$

where $BT^{1/2}$ is the coefficient of conduction.

On the assumption that radiative losses may be neglected, F is a constant, and equation (1) may be integrated directly. It is convenient to measure heights from a reference level whose geocentric distance is r_0. Let z be the geometric height measured from this level and T_0 be the temperature at $z=0$. If T_h is the temperature at $z=h$, then the temperature T at the general level is given by the equation

$$\frac{T^{3/2}-T_0^{3/2}}{T_h^{3/2}-T_0^{3/2}}=\frac{z}{h}\,\frac{r_0+h}{r_0+z}. \tag{2}$$

Also, if $r=r_0+z$, the flux per unit area, E, follows from the relation

$$E(r)=\frac{r_0 r_h}{r^2}\,\frac{2}{3}\,B\,\frac{T^{3/2}-T_0^{3/2}}{h}. \tag{3}$$

If diffusive equilibrium holds above $z=0$, and $N_0(M)$ and $N(M)$ are the number densities of particles of molecular weight M(gm) at height $z=0$ and at the general level, respectively, we find the following approximate relation, valid to within several percent in $N(M)$:

$$\log\frac{N(M)}{N_0(M)}=-\log\frac{T}{T_0}$$
$$-1.3029 r_0 K_0\left(\frac{R}{r}\right)^2\frac{[(\alpha+3)z/r_0]^{1/3}-1}{\alpha+3}, \tag{4}$$

where

$$K_0=\frac{g_0 M}{kT_0},$$
$$\alpha=\frac{r_h}{h}\left[\left(\frac{T_h}{T_0}\right)^{3/2}-1\right].$$

Also $g_0=980.7$ cm sec^{-2}, R is the radius of the earth, and all distances are measured in centimeters. Logarithms are to the base 10.

The density ρ at any level is then derived from the sum of the partial densities,

$$\rho=\Sigma MN(M), \tag{5}$$

and the mean molecular weight $\overline{M}$ follows from the relation

$$\overline{M}=\frac{\rho}{\Sigma N(M)}. \tag{6}$$

Construction of the model

I have assumed, following Nicolet's suggestion, that the important atmospheric constituents are N_2 and O. Also, I have adopted the value $T_0=560°$ at $z=0$, where z is measured from a geometric height of 140 km, and

$$n=\frac{N(\mathrm{O})}{N(\mathrm{N_2})}=\frac{5.60\times10^{10}}{4.15\times10^{10}}=1.35, \qquad \text{at } z=0.$$

TABLE 1.—*Atmospheric properties (model no. 7)*

Geometric height z (km)	T (°K)	$N(O)$ (cm^{-3})	$N(N_2)$ (cm^{-3})	log ρ (gm cm^{-3})	$\bar{\mu}$	$\mathscr{R}$ (erg cm^{-3} sec^{-1})
140	560	1.39×10^{11}	1.03×10^{11}	−11.07	21.10	2.29×10^{-7}
175	677	4.01×10^{10}	1.40×10^{10}	−11.76	19.11	6.62×10^{-8}
200	754	1.94×10^{10}	4.26×10^{9}	−12.15	18.16	3.20×10^{-8}
250	898	5.58×10^{9}	5.47×10^{8}	−12.76	17.07	9.21×10^{-9}
300	1026	1.94×10^{9}	9.54×10^{7}	−13.25	16.56	3.21×10^{-9}
350	1146	7.80×10^{8}	2.10×10^{7}	−13.66	16.31	1.29×10^{-9}
400	1258	3.44×10^{8}	5.36×10^{6}	−14.03	16.18	5.67×10^{-10}
450	1364	1.85×10^{8}	1.92×10^{6}	−14.30	16.12	2.71×10^{-10}
500	1465	8.30×10^{7}	5.00×10^{5}	−14.65	16.07	1.37×10^{-10}
600	1653	2.47×10^{7}	6.55×10^{4}	−15.18	16.03	4.08×10^{-11}

The value of $T_h(h=360$ km) and $N_0(O)$ were adjusted to fit the satellite data, and the results were the following: At $z=0$,

$$N_0(0)=1.39\times10^{11},\ N_0(N_2)=1.03\times10^{11}.$$

These concentrations are 2.48 times those suggested by Nicolet. At $h=360$ km (a real height of 500 km above the earth),

$$T_h=1465°\text{ K},$$

$$E=0.27\text{ erg cm}^{-2},$$

$$F=1.609\times10^{18}\text{ erg/sec}.$$

Table 1 lists some physical properties of this atmosphere as functions of height Z from the earth's surface.

The mean molecular weight μ is defined by $\mu=\bar{M}/1.673\times10^{-24}$. The column headed $\mathscr{R}$ gives the rate of radiation (erg cm^{-3} sec^{-1}) from atomic oxygen according to Nicolet (1958):

$$\mathscr{R}=1.65\times10^{-18}N(O). \quad (7)$$

The densities of model 7 are plotted against geometric height in figure 1 for comparison with the satellite data. The over-all fit to the data is quite adequate, and I conclude that the form of the density profile predicted by the conductive atmosphere is not inconsistent with present data.

The temperature of model 7 is plotted as the solid smooth curve in figure 2. The temperature curves given by models 4 and 6 (Whitney, 1959), included for comparison, were derived from the molecular-scale temperature by use of the mean molecular weights of model 7 (table 1). The spread of temperature above 250 km is rather large, considering how well these models fit the satellite data; this spread results from the coarseness of the data and the nature of the equation of hydrostatic equilibrium.

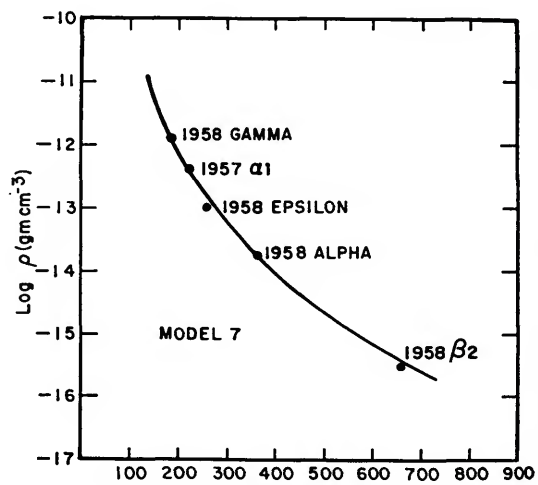

FIGURE 1.—Densities of model 7 plotted against geometric height.

Domain of failure of the conductive atmosphere

The temperature equation (2) is based on the assumption that the global conductive flux F is independent of height. If there are radiative sources and sinks of energy, the transfer equation may be written:

$$\frac{\partial}{\partial r} F(r)=4\pi r^2(\mathscr{R}-A), \tag{8}$$

where $\mathscr{R}$ and A are the rates of emission and absorption per unit volume per second. In general, the forms of A and $\mathscr{R}$ will require numerical integration of equation (8).

Introducing the explicit form for F and performing the indicated differentiation, we see that equation (8) becomes

$$\frac{2}{r}+\frac{1}{2T}\frac{dT}{dr}+\left(\frac{dT}{dr}\right)^{-1}\frac{d^2T}{dr^2}=\frac{4\pi r^2(\mathscr{R}-A)}{F(r)}. \tag{9}$$

It is convenient to put this equation into dimensionless form by expressing the temperature in terms of the temperature, T_0, at a reference level of geocentric distance r_0. Writing

$$r=xr_0, \tag{10a}$$

$$T=\tau T_0, \tag{10b}$$

and introducing

$$y=\frac{r_0}{T_0}\frac{dT}{dr}=\frac{d\tau}{dx}, \tag{11a}$$

$$z=\tau^{1/2}, \tag{11b}$$

I find the following pair of first-order equations in y, z and x:

$$\frac{2zy}{x}+\frac{y^2}{2z}+z\frac{dy}{dx}=\frac{4\pi r_0^3(\mathscr{R}-A)}{4\pi r_0 BT_0^{3/2}}, \tag{12}$$

$$y=2z\frac{dz}{dx}. \tag{13}$$

This pair can be integrated downward from the following boundary conditions:

$$\text{At } x=1(r=r_0)\text{: } z^2=\tau=1,\ y=y_0.$$

The value of y_0 follows from the physical conditions at r_0 through the following relation,

$$F_0=4\pi r_0 BT_0^{3/2}y_0, \tag{14}$$

where F_0 is the assumed global flux at the reference level. Alternatively, y_0 may be evaluated from the value T_0 and an assumed temperature gradient, with the use of equation (11a).

If the value of $\mathscr{R}-A$ is known from an initial model as a function of height, equations (10) through (14) suffice to determine $T(r)$ in the presence of conductive and radiative heat transfer.

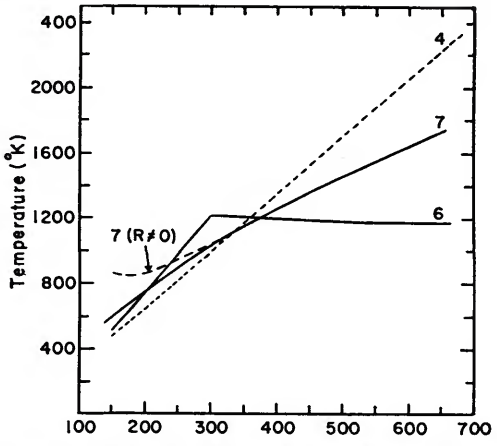

FIGURE 2.—Temperatures of models 7, 6, and 4, plotted against geometric height.

As a simple test of the region of failure of the conductive model, I have performed a numerical integration of these equations, setting $A=0$ and adopting equation (7) for the radiative loss due to oxygen. Of course, in reality the radiative absorption A is finite, and will to a large extent compensate the radiative loss. For this reason, the present test should give a sure indication of the level below which the conductive model fails.

The results of this test are shown in table 2, which compares the temperatures and global fluxes obtained with and without the radiative-loss term. The tabulation indicated quite clearly that, within the framework of model 7, radiative-*emission* terms are not significant above 200 km. It should be borne in mind, however, that radiative-absorption terms may significantly perturb the temperature distribu-

TABLE 2.—*Effect of radiative loss*

Height (km)	$\mathscr{R}-A=0$	$A=0$, $\mathscr{R}=\mathscr{R}(O_2)$	
	T(°K)	T(°K)	F/F_0
500	1465	1465	1.000
400	1258	1259	0.982
300	1026	1046	0.880
200	754	851	.446
150	595	859	.400

tion below 300 km. The temperatures computed with radiative losses are plotted in figure 2 as the dashed branch of model 7.

Conclusions

In summary, it appears that through adjustment of parameters, the conductive model can be made consistent with present satellite data. The total flux required, $F=1.61\times10^{18}$ erg sec^{-1}, or $E=0.27$ erg cm^{-2} sec^{-1}, is comfortably below 2.4×10^{19} erg sec^{-1}, the amount of solar coronal heat estimated by Chapman (1957) to be available for such conduction in the earth's upper atmosphere.

As indicated by figure 2, the temperature distribution above 250 km is still open to considerable uncertainty insofar as *direct* evidence from satellite data is concerned. However, the data are of such a quality that within the framework of a particular theoretical or semi-theoretical model the temperature distribution can be determined with a fairly small uncertainty.

I shall repeat two comments made in the first paper. First, the satellite data show a definite correlation with solar activity. For this reason considerable care must be exercised in combining data from different epochs. The present data represent an average over several months during 1958, with the exception of the data from Satellite 1957 $\alpha2$. Second, although satellite data give no evidence for a considerable latitude-dependence of density, the nature of the data tends to obscure such a dependence.

Evidently the present type of data derived from the acceleration of dense satellites is of principal value in deriving a global picture of the density structure, and not for fine structure of either a temporal or a spatial nature. It is to be anticipated that balloon satellites of small mass-area ratio will offer an improved picture of the more rapid variations.

On the Effects of the Sun and the Moon upon the Motion of a Close-Earth Satellite

By Yoshihide Kozai

In the present paper I shall treat the lunar and solar perturbations of a close-earth satellite whose radius is very small compared with that of the moon.

Since the disturbing functions of both the sun and the moon have similar forms, only the method of deriving the perturbation for the moon will be described here.

If we denote the geocentric radius vector of the satellite and of the moon by $\mathbf{r}$ and $\mathbf{r}'$, respectively, and expand the disturbing function R into a power series of r/r', a small quantity, we obtain the expression,

$$R=\frac{Gm'}{r'}\left(\frac{1}{r'}+\frac{r^2}{r'^2}S_2+\frac{r^3}{r'^3}S_3+\ldots\right), \quad (1)$$

where G is the constant of gravity; m' is the mass ratio of the moon with respect to the earth; and S_i is the Legendre polynomial of the i^{th} order; that is,

$$\left.\begin{aligned} &S_2=\frac{3}{2}s^2-\frac{1}{2},\ S_3=\frac{5}{2}s^3-\frac{3}{2}s,\\ &s=\mathbf{r}\,\mathbf{r}'/r\,r' \end{aligned}\right\}. \quad (2)$$

We can omit the first term, which does not depend on the orbital elements of the satellite. Since we cannot expect any secular contributions from the odd-order terms, I will derive the perturbation produced from the second-order term.

Adopting geocentric coordinates, with x-axis directed towards the equinox and z-axis towards the north pole, we have the following three conponents of $\mathbf{r}$ (by using the conventional orbital elements):

$$\left.\begin{aligned} \frac{x}{r}&=\cos(L+\Omega)+2\sin^2\frac{i}{2}\sin L\sin\Omega,\\ \frac{y}{r}&=\sin(L+\Omega)-2\sin^2\frac{i}{2}\sin L\cos\Omega,\\ \frac{z}{r}&=\sin i\sin L \end{aligned}\right\}, \quad (3)$$

where L is the argument of latitude. We derive similar expressions for the moon, using primed letters to represent elements referred to the equator. Then s is expressed as follows:

$$\begin{aligned} s=&\frac{xx'+yy'+zz'}{rr'}\\ =&\cos(L+\Omega-L'-\Omega')\\ &-2\sin^2\frac{i}{2}\sin L\sin(L'+\Omega'-\Omega)\\ &-2\sin^2\frac{i'}{2}\sin L'\sin(L+\Omega-\Omega')\\ &+4\sin^2\frac{i}{2}\sin^2\frac{i'}{2}\sin L\sin L'\cos(\Omega-\Omega')\\ &+\sin i\sin i'\sin L\sin L'. \end{aligned} \quad (4)$$

It is convenient to express the disturbing function by mean longitudes λ and λ' and by other orbital elements. Dropping all terms depending on the mean longitude of the satellite, which have little effect on the satellite's motion, we have as the principal terms of the disturbing function:

$$\begin{aligned} R=n'^2m'a^2\Big[&\{1+3e'\cos(\lambda'-\omega'-\Omega')\}\\ &\times\left\{\left(1+\frac{3}{2}e^2\right)A+\frac{15}{8}e^2B\right\}\\ &-4e'\sin(\lambda'-\omega'-\Omega')\\ &\times\left\{\left(1+\frac{3}{2}e^2\right)A'+\frac{15}{8}e^2B'\right\}\Big], \end{aligned} \quad (5)$$

where

$$A=\frac{1}{4}\left(1-\frac{3}{2}\sin^2 i\right)\left(1-\frac{3}{2}\sin^2 i'\right)$$
$$+\frac{3}{16}\sin 2i \sin 2i' \cos(\Omega-\Omega')$$
$$+\frac{3}{16}\sin^2 i \sin^2 i' \cos 2(\Omega-\Omega')$$
$$+\frac{3}{8}\sin^2 i'\left(1-\frac{3}{2}\sin^2 i\right)\cos 2(\lambda'-\Omega')$$
$$+\frac{3}{8}\sin^2 i \cos^4\frac{i'}{2}\cos 2(\lambda'-\Omega)$$
$$-\frac{3}{8}\sin 2i \sin i' \cos^2\frac{i'}{2}\cos(2\lambda'-\Omega-\Omega')$$
$$+\frac{3}{8}\sin^2 i \sin^4\frac{i'}{2}\cos 2(\lambda'-2\Omega'+\Omega)$$
$$+\frac{3}{8}\sin 2i \sin i' \sin^2\frac{i'}{2}\cos(2\lambda'+\Omega-3\Omega'),$$

$$B=\cos^4\frac{i}{2}\cos^4\frac{i'}{2}\cos 2(\lambda'-\omega-\Omega)$$
$$+\frac{1}{2}\sin^2 i\left(1-\frac{3}{2}\sin^2 i'\right)\cos 2\omega$$
$$+\frac{1}{2}\cos^4\frac{i}{2}\sin^2 i' \cos 2(\omega+\Omega-\Omega')$$
$$+\sin^4\frac{i}{2}\cos^4\frac{i'}{2}\cos 2(\omega-\Omega+\lambda')$$
$$+\cos^4\frac{i}{2}\sin^4\frac{i'}{2}\cos 2(\omega+\Omega+\lambda'-2\Omega')$$
$$+\sin^4\frac{i}{2}\sin^4\frac{i'}{2}\cos 2(\lambda'-2\Omega'-\omega+\Omega)$$
$$+\frac{3}{8}\sin^2 i \sin^2 i' \cos 2(\lambda'-\Omega'-\omega)$$
$$+\frac{3}{8}\sin^2 i \sin^2 i' \cos 2(\lambda'+\omega-\Omega')$$
$$+\sin i \cos^2\frac{i}{2}\sin i' \cos^2\frac{i'}{2}\cos(2\lambda'-\Omega'-2\omega-\Omega)$$
$$-\frac{1}{2}\sin i \cos^2\frac{i}{2}\sin 2i' \cos(2\omega+\Omega-\Omega')$$
$$+\frac{1}{2}\sin^4\frac{i}{2}\sin^2 i' \cos 2(\omega-\Omega+\Omega')$$
$$+\frac{1}{2}\sin i \sin^2\frac{i}{2}\sin 2i' \cos(2\omega-\Omega+\Omega')$$
$$+\sin i \sin^2\frac{i}{2}\sin i' \cos^2\frac{i'}{2}\cos(2\lambda'+2\omega-\Omega-\Omega')$$
$$-\sin i \cos^2\frac{i}{2}\sin i' \sin^2\frac{i'}{2}\cos(2\lambda'+2\omega+\Omega-3\Omega')$$
$$+\sin i \sin^2\frac{i}{2}\sin i' \sin^2\frac{i'}{2}\cos(2\lambda'-3\Omega'-2\omega+\Omega).$$

By selecting all terms depending on λ' and by replacing cos by sin, we can also derive expressions for A' and B', from A and B.

The variations of e and i are obtained from the equations:

$$\left.\begin{aligned}\frac{de}{dt}&=-\frac{\sqrt{1-e^2}}{na^2e}\frac{\partial R}{\partial\omega},\\ \frac{di}{dt}&=\frac{\cos i}{na^2\sqrt{1-e^2}\sin i}\frac{\partial R}{\partial\omega}\\ &\quad-\frac{1}{na^2\sqrt{1-e^2}\sin i}\frac{\partial R}{\partial\Omega}\end{aligned}\right\}. \quad (6)$$

By using the variations δe and δi, we can derive $\delta\omega$ and $\delta\Omega$ from the formulas

$$\left.\begin{aligned}\frac{d\omega}{dt}&=-\frac{\cos i}{na^2\sqrt{1-e^2}\sin i}\frac{\partial R}{\partial i}+\frac{\sqrt{1-e^2}}{na^2e}\frac{\partial R}{\partial e}\\ &\quad+\frac{d\dot\omega}{de}\delta e+\frac{d\dot\omega}{di}\delta i,\\ \frac{d\Omega}{dt}&=\frac{1}{na^2\sqrt{1-e^2}\sin i}\frac{\partial R}{\partial i}+\frac{d\dot\Omega}{de}\delta e+\frac{d\dot\Omega}{di}\delta i,\end{aligned}\right\} \quad (7)$$

where

$$\dot\omega=\frac{A_2}{p^2}n\frac{4-5\sin^2 i}{2},$$

$$\dot\Omega=-\frac{A_2}{p^2}n\cos i.$$

It is remarkable that these disturbing functions do not affect the semimajor axis. In the righthand sides of the equations, i',

the inclination of the lunar path to the equator, is changing gradually, but we may regard it as constant during one year or so.

As for the secular terms of Ω and ω, we have

$$\left.\begin{aligned}\frac{d\Omega}{dt}&=-\frac{3}{4}\frac{n'^2}{n}m'\frac{\cos i}{\sqrt{1-e^2}}\\&\quad\times\left(1+\frac{3}{2}e^2\right)\left(1-\frac{3}{2}\sin^2 i'\right),\\\frac{d\omega}{dt}&=\frac{3}{4}\frac{n'^2}{n}m'\frac{1}{\sqrt{1-e^2}}\\&\quad\times\left(2-\frac{5}{2}\sin^2 i+\frac{1}{2}e^2\right)\left(1-\frac{3}{2}\sin^2 i'\right),\end{aligned}\right\}\quad(8)$$

where

$$\sin^2 i'=\frac{1}{2}\sin^2 J(1+\cos^2\epsilon)+\sin^2\epsilon\cos^2 J+\frac{1}{2}\sin 2\epsilon\sin 2J\cos N-\frac{1}{2}\sin^2 J\sin^2\epsilon\cos 2N.$$

Here J and N are the lunar inclination and the longitude of the ascending node referred to the ecliptic; and ϵ is the obliquity. We can find the values of J, N and λ' in the American Ephemeris.

If we set $m'=1$, and $J=0$, we can derive the solar perturbations from the same equations.

The Earth's Gravitational Potential Derived from the Motion of Satellite 1958 $\beta 2$

By Yoshihide Kozai

O'Keefe and Eckles (1958) recently reported that the long-period (80-day) variations in the eccentricity of the orbit of Satellite 1958 $\beta 2$ (Vanguard) can be explained by a north-south asymmetry in the gravitational potential of the earth. That is, the axial symmetry of the field is retained, but the third harmonic in latitude is added. Explicitly, it is assumed that the potential of the earth is

$$U=\frac{GM}{r}\left\{1+\frac{A_2}{r^2}\left(\frac{1}{3}-\sin^2\delta\right)+\frac{A_3}{r^3}\left(\frac{5}{2}\sin^3\delta-\frac{3}{2}\sin\delta\right)+\frac{A_4}{r^4}\left(\frac{3}{35}+\frac{1}{7}\sin^2\delta-\frac{1}{4}\sin^2 2\delta\right)\right\}, \quad (1)$$

at a point whose declination is δ and whose geocentric distance is r. In this expression, A_2, A_3, and A_4 are constant, G is the constant of gravitation, and M is the mass of the earth.

Expressing U_3, the part of the third harmonic, in terms of the conventional orbital elements, rather than declination and radius vector, and eliminating terms depending on mean longitude, I find the long-period part of U_3 to be as follows:

$$(U_3)_{L.P.}=GM\frac{3}{2}\frac{A_3}{a^4}\sin i\left(\frac{5}{4}\sin^2 i-1\right)\times e(1-e^2)^{-\frac{5}{2}}\sin\omega, \quad (2)$$

where i is the inclination of the orbital plane to the equator, a is the semimajor axis, and ω is the argument of perigee.

We note that no secular variations of the orbital elements are produced by this odd harmonic in the potential and that the coefficient of $\cos 3\omega$ is zero.

The equations for the variation of the elements produced by the third harmonic are the following:

$$\begin{aligned}
\frac{d\delta a}{dt}&=0,\\
\frac{d\delta e}{dt}&=-\frac{\sqrt{1-e^2}}{na^2e}\frac{\partial U_3}{\partial\omega},\\
\frac{d\delta i}{dt}&=\frac{\cos i}{na^2\sqrt{1-e^2}\sin i}\frac{\partial U_3}{\partial\omega},\\
\frac{d\delta\Omega}{dt}&=\frac{1}{na^2\sqrt{1-e^2}\sin i}\frac{\partial U_3}{\partial i}+\frac{d\dot{\Omega}}{di}\delta i+\frac{d\dot{\Omega}}{de}\delta e,\\
\frac{d\delta\omega}{dt}&=-\frac{\cos i}{na^2\sqrt{1-e^2}\sin i}\frac{\partial U_3}{\partial i}+\frac{\sqrt{1-e^2}}{na^2e}\frac{\partial U_3}{\partial e}+\frac{d\dot{\omega}}{di}\delta i+\frac{d\dot{\omega}}{de}\delta e, \quad (3)
\end{aligned}$$

where n is the mean motion, Ω is the longitude of the ascending node, and

$$\begin{aligned}
\dot{\Omega}&=-\frac{A_2}{p^2}n\cos i,\\
\dot{\omega}&=\frac{A_2}{p^2}n\frac{4-5\sin^2 i}{2},\\
p&=a(1-e^2). \quad (4)
\end{aligned}$$

Integrating these equations we have the following results:

$$\begin{aligned}
\delta e&=\frac{3}{4}\frac{A_3}{A_2a}\sin i\sin\omega,\\
\delta i&=-\frac{3}{4}\frac{A_3}{A_2p}e\cos i\sin\omega,\\
\delta\omega&=\frac{3}{4}\frac{A_3}{A_2p}\frac{\sin^2 i-e^2\cos^2 i}{\sin i}\frac{1}{e}\cos\omega,\\
\delta\Omega&=\frac{3}{4}\frac{A_3}{A_2p}\frac{\cos i}{\sin i}e\cos\omega. \quad (5)
\end{aligned}$$

To confirm the suggestion of O'Keefe and Eckles, I analyzed the orbital elements of Satellite 1958 $\beta 2$ from June 19, 1958, to Jan. 29, 1959; they were furnished by the Vanguard Computing Center.

At first I subtracted the effect of air-drag as given by the following formulas,[1] under the assumption that the perigee height is not changed through this period:

$$\Delta e=\frac{1-e}{a}\Delta a,$$

$$\Delta\Omega=-\frac{A_2}{3p^2}\cos i\left[\frac{7-e}{1+e}\right]\Delta M,$$

$$\Delta\omega=\frac{A_2}{3p^2}\,\frac{4-5\sin^2 i}{2}\left[\frac{7-e}{1+e}\right]\Delta M,$$

$$\Delta M=\int \Delta n\, dt \qquad (6)$$

where Δa, Δn and Δe are deviations from the values for Oct. 16 $12^h\ 27^m$ (U.T.) 1958.

Then I also subtracted solar and lunar perturbations (Kozai, 1959c) as follows:

$$\begin{aligned}
\delta e\times 10^4 &= -1.7\cos 2(\omega+\Omega-\lambda_\odot)\\
&\quad +0.5\cos(2\omega+2\Omega-3\lambda_\odot+\pi_\odot)\\
&\quad +0.1\cos 2(\omega+\Omega-\lambda_{\mathbb{C}}),\\
\delta i &= 0^\circ.003\cos\Omega,\\
\delta\omega &= 0^\circ.011\sin 2(\omega+\Omega-\lambda_\odot)\\
&\quad -0^\circ.062\sin(2\omega+2\Omega-3\lambda_\odot+\pi_\odot)\\
&\quad +0^\circ.003\sin(2\omega+\Omega-2\lambda_\odot)\\
&\quad +0^\circ.005\sin\Omega+0^\circ.055\sin N_{\mathbb{C}},\\
\delta\Omega &= -0^\circ.001\sin 2\lambda_\odot+0^\circ.028\sin 2(\omega+\Omega-\lambda_\odot)\\
&\quad +0^\circ.001\sin 2(\lambda_\odot-\Omega)\\
&\quad +0^\circ.032\sin(2\omega+2\Omega-3\lambda_\odot+\pi_\odot)\\
&\quad -0^\circ.005\sin\Omega-0^\circ.039\sin N_{\mathbb{C}}, \qquad (7)
\end{aligned}$$

where $\lambda_\odot$ is the mean longitude; $\pi_\odot$ is the longitude of perigee of the sun; $\lambda_{\mathbb{C}}$ is the mean longitude of the moon; and $N_{\mathbb{C}}$ is the longitude of the ascending node of the lunar path referred to the ecliptic.

Then assuming that the periodic inequalities are due to the third harmonics we obtain the variations given in table 1.

[1] K. Squires, private communication to Dr. C. A. Whitney.

TABLE 1.—*Variations in orbital elements*

Inequality	Observed	Computed
δe	$(0.43\pm0.02)\times10^{-3}\sin\omega$	0.42×10^{-3}
δi	$-(0^\circ.007\pm0^\circ.001)\sin\omega$	$-0^\circ.007$
$\delta\omega$	$(0^\circ.106\pm0^\circ.010)\cos\omega$	$0^\circ.122$
$\delta\Omega$	$(0^\circ.018\pm0^\circ.003)\cos\omega$	$0^\circ.012$

Figure 1 shows the observed values plotted against theoretical values for this same period, June 19, 1958, to Jan. 29, 1959.

Assigning to each observed amplitude the weight that is reciprocally proportional to the square of the probable error, we have as the coefficient of the third harmonic,

$$\frac{A_3}{a_e^3}=(2.20\pm0.08)\times10^{-6}.$$

The predicted amplitudes from this value are also shown in figure 1.

The values of the secular motions of the node and the perigee, given in table 2, correspond to the following quantities:

$n=3862^\circ.640$, anomalistic mean motion per day,
$e=0.190\ 00$,
$i=34^\circ.250$.

To compare with my results,

$$\begin{aligned}
\dot\Omega &= -\frac{A_2}{p^2}n\left\{1-\frac{A_2}{a^2}\left(\frac{1}{2}-\frac{4}{3}\sin^2 i\right)\right\}\cos i\\
&\quad -\frac{A_4}{a^4}n\left(\frac{6}{7}-\frac{3}{2}\sin^2 i\right)\left(1+\frac{11}{2}e^2\right)\cos i,\\
\dot\omega &= \frac{A_2}{p^2}n\,(4-5\sin^2 i)\left\{\frac{1}{2}+\frac{A_2}{a^2}\left(1-\frac{31}{48}\sin^2 i\right)\right\}\\
&\quad +\frac{A_4}{a^4}n\,\frac{3}{112}\Big\{4(16-62\sin^2 i+49\sin^4 i)\\
&\quad +e^2(328-1244\sin^2 i+973\sin^4 i)\Big\}, \qquad (8)
\end{aligned}$$

TABLE 2.—*Secular motions of node* ($\dot\Omega$) *and perigee* ($\dot\omega$)

Motions	Node $\dot\Omega$	Perigee $\dot\omega$
Observed (per day)	$-3^\circ.015\ 07\pm4$	$4^\circ.404\ 62\pm10$
Solar part	$-0.000\ 13$	$0.000\ 18$
Lunar part	$-0.000\ 28$	$0.000\ 39$
Corrected	$-3.014\ 66$	$4.404\ 05$

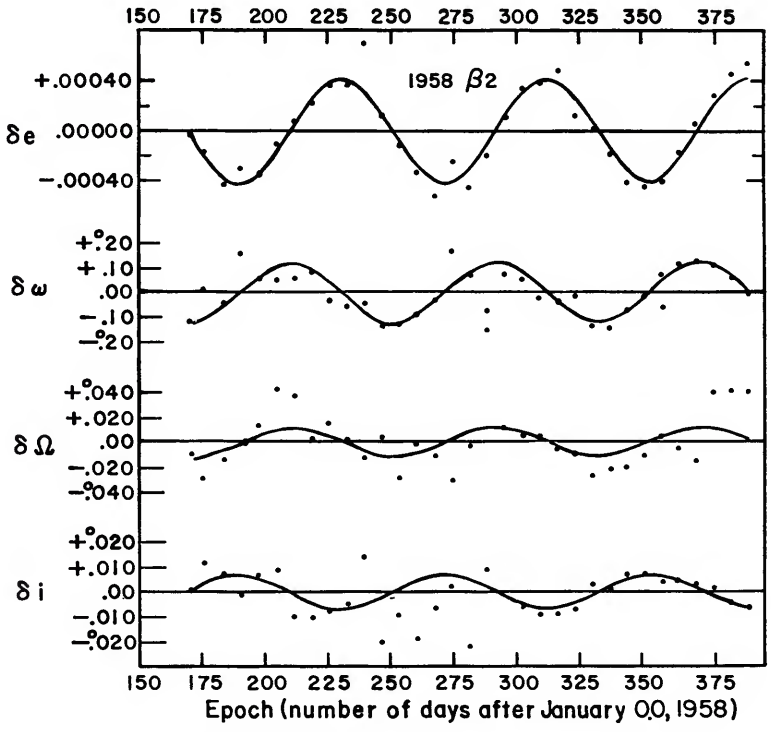

FIGURE 1.—Observed values (dots) and theoretical values (solid lines) of variations in orbital elements due to the third harmonic. Each point represents 7 days.

we must subtract solar and lunar perturbations from the observed values. The solar and lunar parts have been derived from the following equations:

$$\delta\dot{\Omega}=-\frac{3}{4}\frac{n_{\mathbb{C}}}{n}\,n_{\mathbb{C}}m_{\mathbb{C}}\left(1-\frac{3}{2}b^2\right)\times\frac{1}{\sqrt{1-e^2}}\left(1+\frac{3}{2}e^2\right)\cos i,$$

$$\delta\dot{\omega}=\frac{3}{4}\frac{n_{\mathbb{C}}}{n}\,n_{\mathbb{C}}m_{\mathbb{C}}\left(1-\frac{3}{2}b^2\right)\times\frac{1}{\sqrt{1-e^2}}\left(2-\frac{5}{2}\sin^2 i+\frac{1}{2}e^2\right), \quad (9)$$

where

$$b^2=\frac{1}{2}\sin^2 J(1+\cos^2\epsilon)+\sin^2\epsilon\cos^2 J.$$

Here $m_{\mathbb{C}}$ is the mass ratio of the moon to the earth; J is the inclination of lunar path to the ecliptic; and ϵ is the obliquity. If we set $n_{\mathbb{C}}=n_{\odot}$, $m_{\mathbb{C}}=1$ and $J=0$, we can also derive the solar secular perturbation from these equations.

Then from $\dot{\Omega}$ and $\dot{\omega}$ I derived the following:

$$\frac{A_2}{a_e^2}=1.6208\times10^{-3},$$

$$\frac{A_4}{a_e^4}=2.1\times10^{-5}.$$

I am grateful to Drs. C. A. Whitney, L. G. Jacchia and G. Veis for their valuable discussions.

Solar Effects on the Acceleration of Artificial Satellites

By Luigi G. Jacchia

Slow fluctuations connected with variable solar radiation

The atmospheric drag that artificial satellites experience around perigee causes them to lose energy and to fall into orbits with smaller major axes and shorter periods of revolution. The change in period that the satellite undergoes from one revolution to the next is called the "secular acceleration"; in this discussion the term "acceleration" will refer to the nondimensional quantity dP/dt, when P is the period of revolution, and t is the time.

Erratic changes in the acceleration of a satellite were first detected by this writer in an analysis of the observations of Satellite 1957 Beta (Jacchia, 1958e; 1958a). At first it was not clear whether these changes were owing to variations in the presentation area of the satellite or to density variations in the atmosphere, but when their presence was detected also in Satellite 1958 $\beta 2$ (the spherical Vanguard) no doubt was left about their atmospheric origin. The presence of a 27-day periodicity pointed to variable solar radiation as the cause of the atmospheric fluctuations (Jacchia and Briggs, 1958). The discovery that the accelerations of Satellites 1958 $\beta 2$ and 1958 $\delta 1$ varied more or less in unison (Jacchia, 1959a; 1959e) and that those of the other satellites followed the same rhythm proved that the atmospheric fluctuations at their origin are truly global.

In a communication dated December 18, 1958, Dr. W. Priester of Bonn, Germany, pointed out a remarkable similarity between my acceleration curve of Satellite 1957 $\beta 1$ (Jacchia, 1958b) and the 20-cm solar-flux curve in the interval from November 11, 1957, to February 10, 1958. I had no 20-cm solar data at hand, but had 10.7-cm data from the National Research Council in Ottawa; a comparison of the satellite curves with these data, extended over a whole year, showed a correlation that could be classified as little short of perfect. The amplitude of the fluctuations increased with the perigee height of the satellite. They amounted to about 20 percent in typical, well-defined 27-day cycles in the acceleration of Satellite 1958 $\delta 1$ (perigee height 200 km), but to about 70 percent in corresponding cycles of Satellite 1958 $\beta 2$ (perigee height 650 km).

Transient fluctuations connected with magnetic storms

The 10.7-cm radiation is closely correlated with the sunspot numbers, so an excellent correlation also exists between satellite accelerations and sunspot numbers. Searching for further clues about the nature of the radiation that interacts with the upper atmosphere, I reduced anew all the available observations of Satellites 1958 $\beta 2$ (about 2500) and 1958 $\delta 1$ (about 9000) with the best elements at hand and obtained more accurate accelerations at twice the original resolution. The results are plotted in figure 1, together with the 10.7-cm solar-radiation curve (Jacchia, 1959b). As can be seen, the correlation with the solar radiation is remarkably good, even in details, for the high-flying, spherical Satellite 1958 $\beta 2$ (Vanguard), for which accurate, well-distributed Minitrack observations were available throughout. For Satellite 1958 $\delta 1$ the observations are mostly optical, less accurate, and more irregularly distributed, with occasional periods of near-invisibility; these facts, together with the elongated shape,

636-014—63——5

may have contributed somewhat to the poor correlation for 1958 δ1.

The procedure for computing the accelerations was the following. Residuals of individual nodal (for 1958 δ1) or perigee (for 1958 β2) passages from empirical equations were plotted and ordinates on the residual curves were read off at intervals of 25 revolutions; the resulting table was then differenced and accelerations were computed from the differences. The residual curve for 1958 δ1 is a succession of long, smooth waves of great amplitude that are mainly due to the 27-day fluctuations. At only two spots in the whole curve is the smooth succession of long waves interrupted by a transient, short-lived but unmistakable secondary

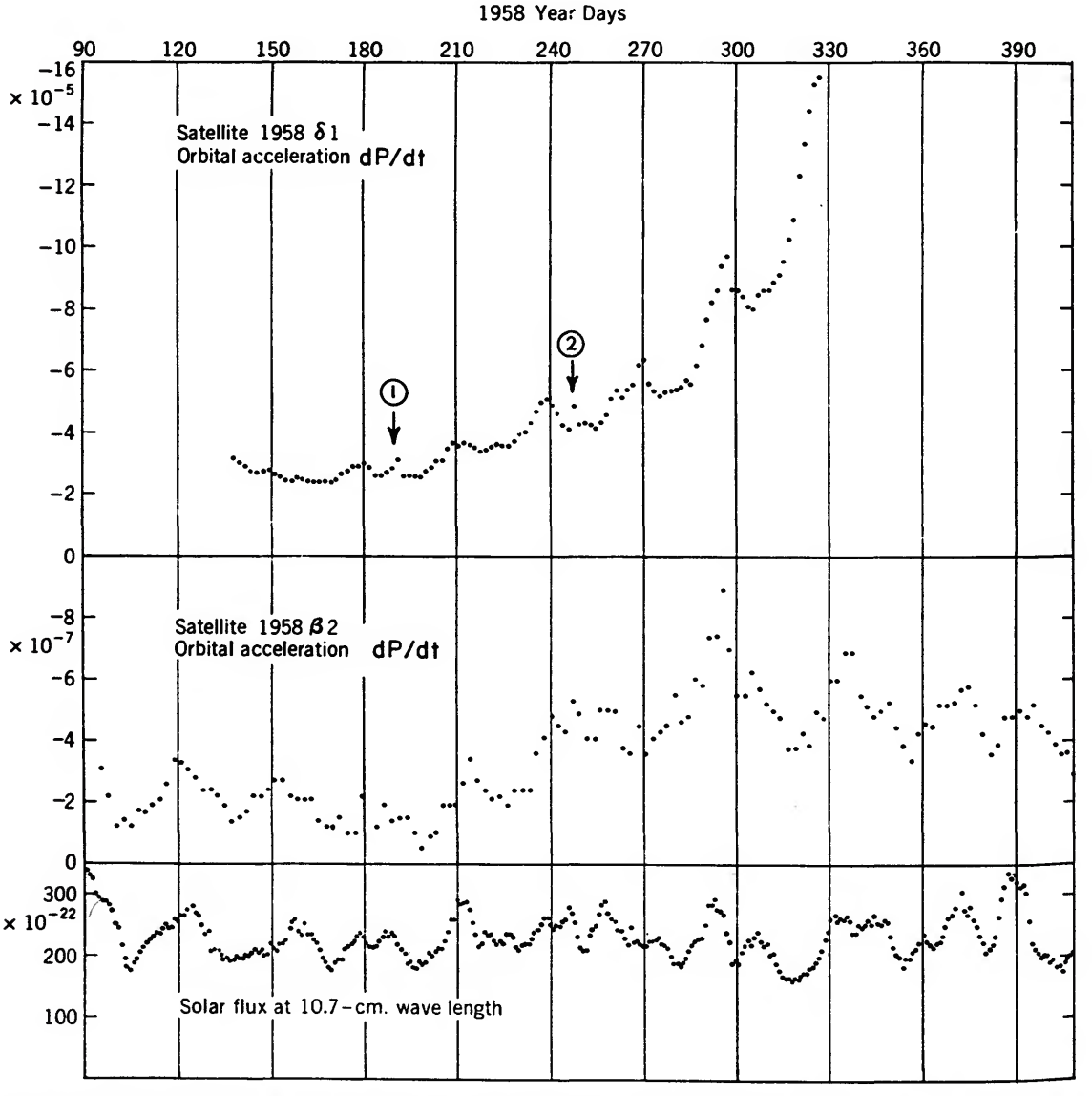

FIGURE 1.—Secular accelerations of Satellites 1958 δ1 and 1958 β2 compared with the 10.7-cm solar flux. The dates of the two great geomagnetic disturbances, July 8–9 and September 4, 1958, are marked (1) and (2), respectively. Accelerations were computed at intervals of 25 revolutions.

oscillation. The dates of these disturbances are July 8 to 9 and September 4, 1958; they are exactly coincident with the only two great geomagnetic disturbances that occurred during the satellite's lifetime. Both magnetic storms followed, at the usual one-day interval, the appearance of a flare of importance 3+ on the sun.

Although the original accelerations had a resolution of 25 revolutions, it appeared possible to obtain accelerations with a resolution of 10 revolutions around the critical dates, and these—computed at intervals of 5 revolutions—are plotted in figure 2 together with the three-hourly geomagnetic planetary indices Kp (Jacchia, 1959b). It is quite evident that in both the July and the September events, there was no immediate response at the time when the flare appeared, and that the atmospheric disturbance—an increase in density—proceeded nearly

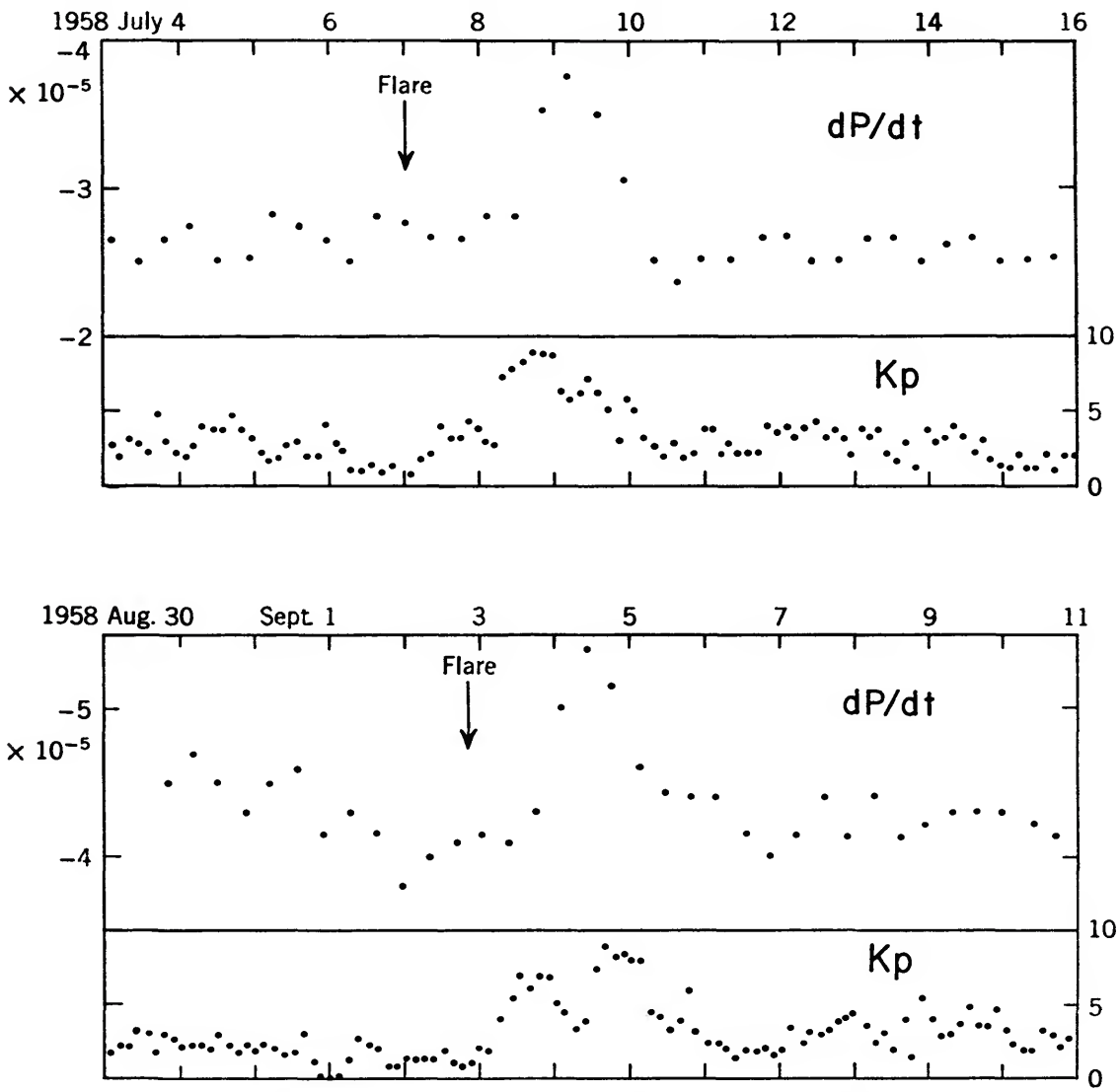

FIGURE 2.—Secular accelerations of Satellite 1958 δ1 computed with a resolution of 10 revolutions around the dates of two great geomagnetic disturbances and compared with the three-hour geomagnetic planetary indices K_p. The instants of the flares that preceded the magnetic storms are marked on the diagram.

synchronously with the magnetic disturbance. The increase in the acceleration amounted to 40 percent in the July 8 event and to a little more than 30 percent in the event of September 4. These are actually lower limits, inasmuch as the limited resolution may have smoothed out the peaks (with a resolution of 25 revolutions the peaks are highly reduced, as can be seen in figure 1, where the two disturbances are marked (1) and (2) respectively.) Since the amplitude of the 27-day oscillations did not exceed 20 percent for this satellite (1958 $\delta 1$), it appears that the corpuscular radiation capable of causing a first-rate geomagnetic disturbance has a greater, although more transient, effect on the atmospheric density at the 200-km level, than the ordinary fluctuation in solar radiation associated with the 27-day period. That this latter radiation might also be corpuscular in nature appeared possible, in view of the failure of the atmospheric density to react promptly to the stream of electromagnetic radiation that accompanies the appearance of a flare. Wave radiation could not be ruled out, however, since the duration of a flare is much shorter than that of a magnetic storm, and the effect of a transient drag perturbation on the satellite position is proportional to the square of the duration.

No disturbance could be detected in the residual curves for Satellite 1958 $\beta 2$ around the two critical dates in July and September. This could be due to the much smaller value of the acceleration for this satellite, which would make a short-lived perturbation difficult to detect. Otherwise, we should conclude that during a violent magnetic storm the atmospheric layers in the 200-km zone are more strongly affected than those at a height of 600 to 700 km. Judging by the increase of the 27-day fluctuations with height, it appears that in ordinary conditions the opposite situation prevails, with the higher levels affected more than the lower. It might be of interest to remark that at the time of the July disturbance the latitude of perigee of Satellite 1958 $\delta 1$ was $+35°$; at the time of the September disturbance it was $+15°$; the corresponding geocentric angular distances between sun and perigee were 110° and 77°, respectively.

Diurnal effects

The existence of a "diurnal" effect, i.e., a variation of the acceleration with the geocentric angular distance between the sun and the satellite's perigee, was announced by this writer for Satellite 1957 $\beta 1$ (Jacchia, 1959c). The published amplitude of the effect—about 20 percent—is almost certainly too large, much of the fluctuation being probably due to a slow variation of solar radiation superimposed on the shorter, erratic fluctuations. This slow variation is quite evident in the 10.7-cm flux curve (fig. 3), but was unknown to the author when the paper was written. Only a bare suggestion of a diurnal effect is discernible in the acceleration curve of Satellite 1958 $\delta 1$.

A much larger diurnal effect is suggested by the acceleration curves of the higher-perigee Satellites 1958 Alpha and 1958 $\beta 2$ (fig. 4), but the picture here seems to be complicated by a major perturbation of the atmosphere that started in the second half of August 1958, and continued for two or three months, and possibly longer. This perturbation occurred when the perigee of Satellite 1958 Alpha was in daylight and raised the acceleration level to extremely high values, which were never reached again when the perigee returned to the same position with respect to the sun the following year (April to August, 1959). The global nature of the perturbation is evidenced by the extremely rapid and perfectly synchronous rise in the accelerations of both satellites between August 17 and August 27, 1958. The curve of the 10.7-cm solar flux does not offer any clear-cut clue to the cause of this perturbation. For some time the writer was tempted to speculate about the effect of stored corpuscular radiation following major magnetic storms, but it must be admitted that the evidence for such a mechanism is not very convincing.

Due to the presence of the large atmospheric perturbation, it is difficult to draw definite conclusions regarding the amplitude and the phase of the diurnal effect in Satellite 1958 Alpha and 1958 $\beta 2$. Although the 1958 parts of both curves suggest a phase lag of some 30° to 50° in $\alpha\pi - \alpha_\odot$ ($\alpha\pi$=R.A. of perigee, $\alpha_\odot$= R.A. of sun), the 1959 portion of the 1958 Alpha

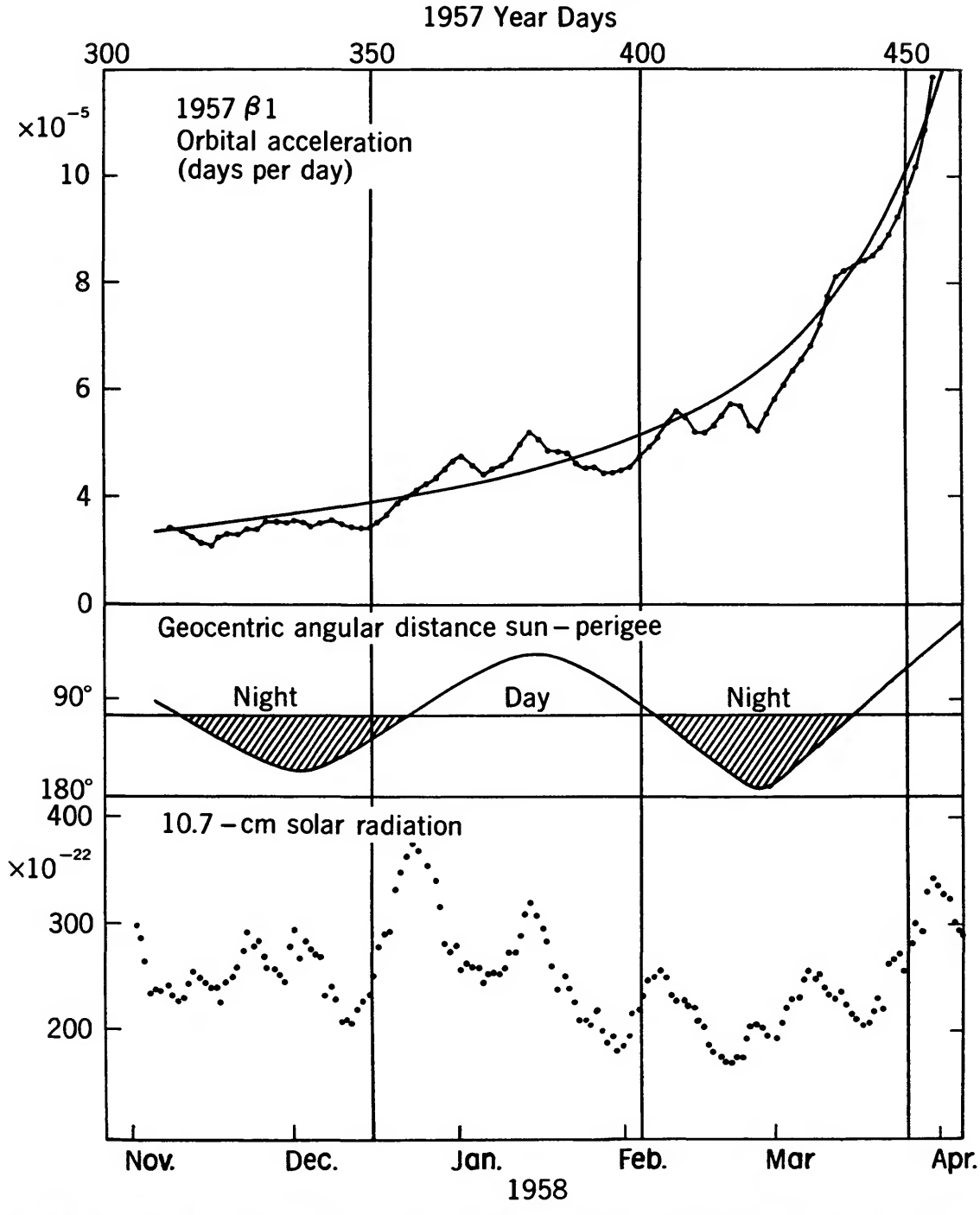

FIGURE 3.—The diurnal effect in Satellite 1957 β1. Accelerations (top) are compared with angular distances sun-perigee and with the solar flux at 10.7 cm. The smooth line in the acceleration diagram was drawn as a visual aid.

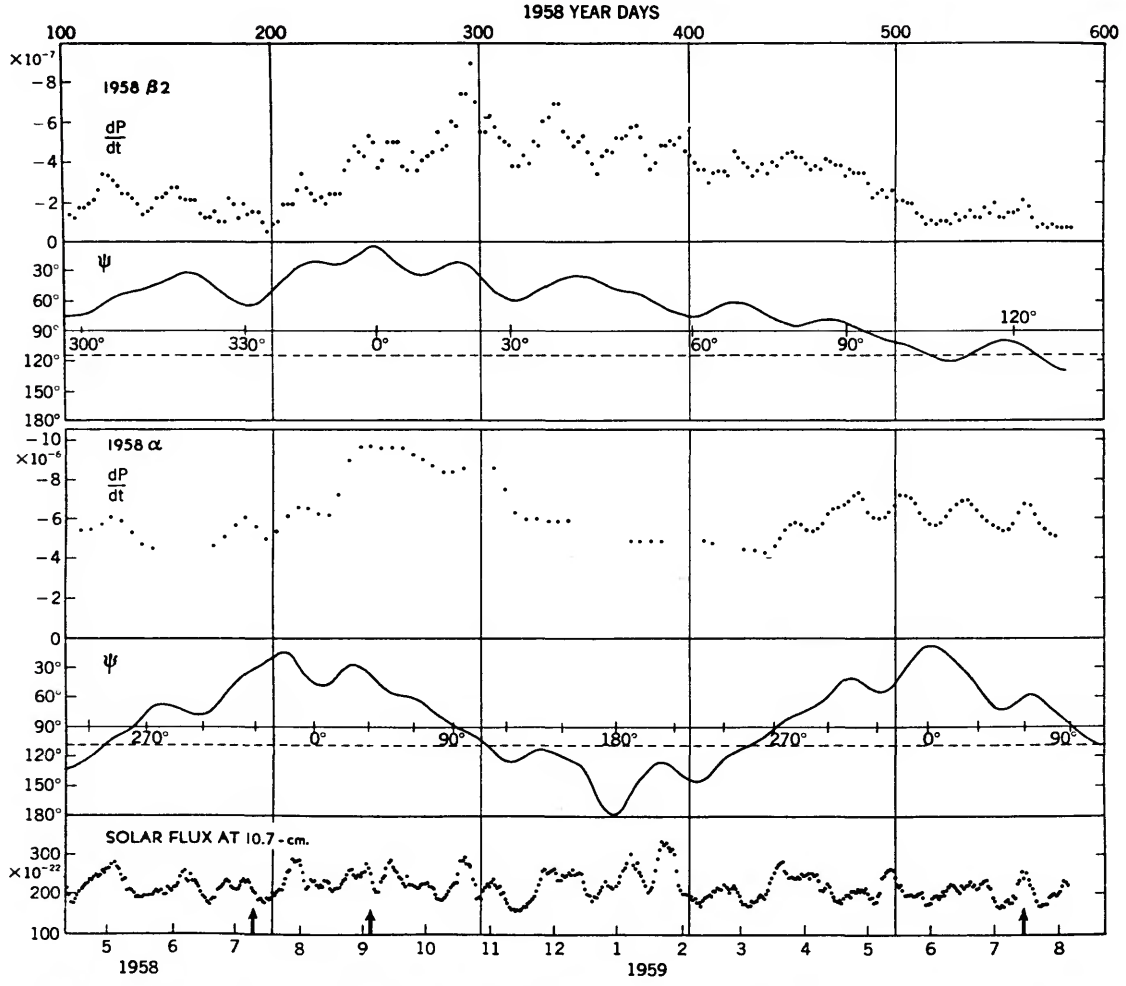

FIGURE 4.—Acceleration of Satellites 1958 $\beta 2$ and 1958 Alpha, compared with angular distances sun-perigee ψ and with the solar flux at 10.7 cm. Values of the difference in right ascension between the satellite's perigee and the sun $(\alpha_s - \alpha_\odot)$ are marked on the horizontal line corresponding to $\psi = 90°$.

curve seems to be reasonably well in phase. The ratio of mean maximum to mean minimum acceleration due to purely diurnal effect should be about 1.4 or 1.5 for 1958 Alpha (perigee height 350 km) and 7 or more for 1958 $\beta 2$ (perigee height 650 km). The mean maximum and minimum values are those obtained by passing a mean curve through the monthly oscillations connected with the solar flux. Such a large variation of the effect with height indicates that the density profile and the scale height of the atmosphere above 300 km differ markedly in the bright and in the dark hemispheres. Preliminary computations show that to account for the effect, the scale height must vary by a factor of about two at the 650-km level.

A remarkable feature that emerges from figure 4 is the disappearance of the monthly oscillations when the perigee comes from daylight into night. The phenomenon is present in both satellites (1958 Alpha and 1958 $\beta 2$). Since atmospheric variations with constant amplitude are reflected in the acceleration curves with amplitudes proportional to the mean acceleration itself, part of the variation in the amplitude of the fluctuation observed in 1958 $\beta 2$ is only apparent. If, however, we

compare the curves of 1958 $\beta 2$ in the period April to July, 1958, and in May, 1959, when the mean acceleration was about the same ($dP/dt \approx -2 \times 10^{-7}$), we can notice the difference in behavior between the first interval, when the perigee was in daylight, and the second interval, during which the perigee was crossing into the dark hemisphere. The 10.7-cm solar flux was actively oscillating during both intervals, and the oscillations are clearly visible in 1958 Alpha also during the second interval, at which time this satellite had its perigee in daylight.

The disappearance of the oscillations in the dark hemisphere would be expected if the variable radiation responsible for them was wave radiation. In view of the association of the 10.7-cm flux with sunspots and with ion density in the F layer, the association of this type of atmospheric oscillation with wave radiation would seem to make good sense. We should not forget that for the low-perigee Satellites 1957 Beta and 1958 $\delta 1$, the monthly oscillations persisted also when the perigee was in the dark hemisphere. A look at the acceleration curves for these two satellites shows, however, that during such periods the amplitude of the oscillations was definitely smaller.

Summary and conclusions

Summarizing, we find that four distinct types of fluctuations can be distinguished in the acceleration of satellites.

(1) Fluctuations that follow the rhythm of the solar flux at 2800 mc (10.7-cm wavelength). These fluctuations increase in amplitude with height and become smaller or disappear when the perigee is in darkness. Very probably these fluctuations reflect variations in atmospheric density caused by variable short-wave solar radiation (extreme ultraviolet).

(2) A slow fluctuation connected with the position of the perigee with respect to the subsolar point ("diurnal effect"). This effect is small at the 200-km level, but becomes very large at heights above 350 km. This effect is intimately connected with (1) and should have the same primary agent (ultraviolet absorption) as its origin. It reflects a difference in the density profiles of the bright and the dark hemispheres of the earth.

(3) Transient fluctuations accompanying magnetic storms. These perturbations are seemingly of corpuscular origin and should reflect a heating of the atmosphere through some interaction with corpuscular radiation.

(4) Erratic fluctuations of unexplained origin, such as the perturbation of August and September, 1958. A comparison with conditions in the radiation belts may provide a clue to this effect.

Explanation of tables

For Satellite 1958 Alpha the accelerations are given at equal time intervals, at 0^h U.T. For 1958 $\beta 2$ and 1958 $\delta 1$ the accelerations are tabulated at equal intervals of revolutions (N). Uncertain values are in parentheses.

In Tables 2a, 2b and 2c, the tabulated angle ψ is the geocentric angular distance between sun and perigee; α_π is the right ascension of perigee; and $\alpha_\odot$ is the right ascension of the sun.

Acknowledgments

The accelerations of 1958 $\beta 2$ were obtained by Mr. R. E. Briggs, using the author's "subsatellite point program," in which each observation yields a time of perigee or nodal passage.

The writer is indebted to Mr. Pedro Zadunaisky for communicating to him, in advance of publication, the results of 109 orbital determinations for Satellite 1958 Alpha. These orbits were computed by the differential-correction method of Dr. George Veis, from Minitrack and Baker-Nunn camera observations. The orbits were computed, whenever possible, at 3-day intervals, although in some sections intervals of 6 days and more became necessary. Each orbit yielded a value of the mean motion of the satellite for a central epoch, and accelerations were derived from these mean motions.

Mr. Stephen Maran assisted in the preparation of most of the tables.

TABLE 1a.—*Secular accelerations of Satellite 1958 Alpha*

Date 1958		10^6 dP/dt	Date 1958		10^6 dP/dt	Date 1958		10^6 dP/dt	Date 1958		10^5 dP/dt
Feb.	16	−4.9	Aug.	5	−6.6	Jan.	17	−4.9	May	12	−6.36
	21	−4.2		10	−6.3		22	−4.9		14.5	−6.74
	26	−4.1		15	−6.2		27	(−5.0)		17	−7.26
Mar.	3	−4.7		20	−7.3	Feb.	1	(−5.0)		19.5	−7.22
	8	−5.3		25	−9.0		6	(−5.0)		22	−7.10
	13	−5.7		30	−9.7		11	−4.9		24.5	−6.78
	18	−5.9	Sept.	4	−9.7		16	−4.8		27	−6.32
	23	(−6.0)		9	−9.6		21	(−4.7)		29.5	−5.96
	28	(−6.1)		14	−9.6		26	(−4.6)	June	1	−5.76
Apr.	2	(−6.2)		19	−9.6	Mar.	3	−4.5		3.5	−5.70
	7	(−6.2)		24	−9.3		8	−4.4		6	−5.86
	12	(−5.8)		29	−9.0		13	−4.3		8.5	−6.14
	17	−5.4	Oct.	4	−8.7		18	−4.7		11	−6.48
	22	−5.4		9	−8.4		20.5	−5.06		13.5	−6.78
	27	−5.7		14	−8.4		23	−5.48		16	−6.94
May	2	−6.1		19	−8.6		25.5	−5.76		18.5	−6.98
	7	−5.9		24	(−8.7)		28	−5.82		21	−6.76
	12	−5.3		29	(−8.7)		30.5	(−5.70)		23.5	−6.46
	17	−4.7	Nov.	3	−8.6	Apr.	2	(−5.48)		26	−6.16
	22	−4.5		8	−7.5		4.5	−5.36		28.5	−5.94
	27	(−4.9)		13	−6.3		7	−5.46	July	1	−5.76
June	1	(−5.0)		18	−6.0		9.5	−5.78		3.5	−5.56
	6	(−4.7)		23	−6.0		12	−6.26		6	−5.42
	11	(−4.4)		28	−5.9		14.5	−6.52		8.5	−5.46
	16	(−4.3)	Dec.	3	−5.9		17	−6.60		11	−5.80
	21	−4.6		8	−5.9		19.5	−6.72		13.5	−6.34
	26	−5.1		13	(−5.6)		22	−6.94		16	−6.80
July	1	−5.7		18	(−5.5)		24.5	−7.20		18.5	−6.70
	6	−6.1		23	(−5.4)		27	−7.32		21	−6.18
	11	−5.6		28	(−5.2)		29.5	−7.00		23.5	−5.74
	16	−5.0	1959			May	2	−6.36		26	−5.50
	21	−5.4	Jan.	2	(−5.0)		4.5	−6.08		28.5	−5.26
	26	−6.2		7	−4.9		7	−6.06		31	−5.14
	31	−6.6		12	−4.9		9.5	−6.10			

TABLE 1b.—*Secular accelerations of Satellite 1958 β2*

N		Date 1958	10^7 dP/dt	N		Date 1958	10^7 dP/dt	N		Date 1958	10^7 dP/dt
0	Mar.	17.61	-----	500	May	3.24	−3.1	1000	June	18.86	−1.2
25		19.94	−2.4	525		5.57	−2.8	1025		21.19	−1.5
50		22.27	−2.1	550		7.90	−2.4	1050		23.52	−1.0
75		24.60	−0.9	575		10.23	−2.4	1075		25.85	−1.0
100		26.94	−1.0	600		12.56	−2.2	1100		28.18	−2.2
125		29.97	−1.5	625		14.89	−1.9	1125		30.51	−1.9
150		31.60	−2.4	650		17.22	−1.4	1150	July	2.84	−1.2
175	Apr.	2.93	−2.7	675		19.55	−1.5	1175		5.17	−1.9
200		5.26	−3.1	700		21.89	−1.7	1200		7.51	−1.4
225		7.59	−2.2	725		24.22	−2.2	1225		9.84	−1.5
250		9.92	−1.2	750		26.55	−2.2	1250		12.17	−1.5
275		12.26	−1.4	775		28.88	−2.4	1275		14.50	−1.0
300		14.59	−1.2	800		31.21	−2.7	1300		16.83	−0.5
325		16.92	−1.7	825	June	8.54	−2.7	1325		19.16	−0.9
350		19.25	−1.7	850		4.87	−2.2	1350		21.49	−1.0
375		21.58	−1.9	875		7.20	−2.1	1375		23.82	−1.9
400		23.91	−2.1	900		9.53	−2.1	1400		26.15	−1.9
425		26.24	−2.6	925		11.87	−2.1	1425		28.48	−1.9
450		28.57	−3.4	950		14.20	−1.4	1450		30.81	−2.6
475		30.91	−3.3	975		16.53	−1.2	1475	Aug.	2.14	−3.4

TABLE 1b.—*Secular accelerations of Satellite 1958 β2*—Continued

N	Date 1959	$10^7\ dP/dt$	N	Date 1958	$10^7\ dP/dt$	N	Date 1959	$10^7\ dP/dt$
1500	Aug. 4.48	−2.7	2850	Dec. 8.30	−5.2	4175	Apr. 10.71	−4.1
1525	6.81	−2.4	2875	10.63	−4.8	4200	13.04	−4.0
1550	9.14	−2.1	2900	12.96	−5.0	4225	15.37	−3.8
1575	11.47	−2.2	2925	15.29	−5.3	4250	17.70	−3.8
1600	13.80	−1.9	2950	17.62	−4.5	4275	20.02	−3.3
1625	16.13	−2.4	2975	19.95	−3.9	4300	22.35	−3.6
1650	18.46	−2.4	3000	22.27	−3.4	4325	24.68	−3.4
1675	20.79	−2.4	3025	24.60	−4.3	4350	27.01	−3.4
1700	23.12	−3.6	3050	26.93	−4.6	4375	29.34	−3.4
1725	25.45	−4.1	3075	29.26	−4.5	4400	May 1.66	−2.9
1750	27.78	−4.8	3100	31.59	−5.2	4425	3.99	−2.2
1775	30.11	−4.5		1959		4450	6.32	−2.4
1800	Sept. 1.44	−4.3	3125	Jan. 2.92	−5.2	4475	8.65	−2.6
1825	3.77	−5.3	3150	5.25	−5.3	4500	10.97	−2.2
1850	6.10	−4.8	3175	7.58	−5.7	4525	13.30	−2.8
1875	8.43	−4.1	3200	9.91	−5.8	4550	15.63	−2.4
1900	10.77	−4.1	3225	12.24	−5.2	4575	17.96	−2.1
1925	13.10	−5.0	3250	14.56	−4.3	4600	20.29	−1.9
1950	15.43	−5.0	3275	16.89	−3.6	4625	22.61	−1.9
1975	17.76	−5.0	3300	19.22	−3.9	4650	24.94	−1.4
2000	20.09	−3.8	3325	21.55	−4.8	4675	27.27	−1.2
2025	22.42	−3.6	3350	23.88	−4.8	4700	29.60	−0.9
2050	24.75	−4.5	3375	26.21	−5.0	4725	31.92	−1.0
2075	27.08	−3.6	3400	28.54	−4.8	4750	June 3.25	−0.9
2100	29.41	−4.1	3425	30.87	−5.2	4775	5.58	−1.0
2125	Oct. 1.74	−4.3	3450	Feb. 2.19	−4.5	4800	7.91	−1.0
2150	4.07	−4.5	3475	4.52	−4.3	4825	10.23	−0.9
2175	6.40	−5.5	3500	6.85	−3.9	4850	12.56	−1.4
2200	8.73	−4.6	3525	9.18	−3.6	4875	14.89	−1.0
2225	11.06	−4.8	3550	11.51	−3.6	4900	17.22	−1.2
2250	13.39	−6.0	3575	13.84	−2.9	4925	19.54	−1.5
2275	15.72	−5.8	3600	16.16	−3.4	4950	21.87	−1.2
2300	18.05	−7.4	3625	18.49	−3.5	4975	24.20	−1.2
2325	20.38	−7.4	3650	20.82	−3.5	5000	26.53	−1.7
2350	22.71	−8.9	3675	23.15	−3.3	5025	28.85	−1.4
2375	25.04	−7.0	3700	25.48	−4.5	5050	July 1.18	−1.9
2400	27.37	−5.5	3725	27.81	−4.1	5075	3.51	−1.2
2425	29.70	−5.5	3750	Mar. 2.14	−4.0	5100	5.84	−1.2
2450	Nov. 1.03	−6.3	3775	4.46	−3.4	5125	8.16	−1.4
2475	3.36	−5.7	3800	6.79	−3.6	5150	10.49	−1.4
2500	5.69	−5.2	3825	9.12	−3.6	5175	12.82	−1.5
2525	8.02	−5.0	3850	11.45	−3.8	5200	15.15	−2.1
2550	10.35	−4.8	3875	13.78	−3.4	5225	17.47	−1.7
2575	12.68	−3.8	3900	16.10	−4.0	5250	19.80	−1.4
2600	15.01	−3.8	3925	18.43	−3.8	5275	22.13	−1.2
2625	17.34	−4.3	3950	20.76	−4.3	5300	24.46	−0.5
2650	19.66	−3.9	3975	23.09	−4.3	5325	26.78	−0.7
2675	21.99	−5.0	4000	25.42	−4.5	5350	29.11	−0.9
2700	24.32	−4.8	4025	27.75	−4.3	5375	31.44	−0.7
2725	26.65	−6.0	4050	30.07	−4.1	5400	Aug. 2.77	−0.7
2750	28.98	−6.3	4075	Apr. 1.40	−3.8	5425	5.09	−0.7
2775	Dec. 1.31	−6.9	4100	3.73	−3.6	5450	7.42	−0.7
2800	3.64	−6.9	4125	6.06	−3.8			
2825	5.97	−5.5	4150	8.39	−3.6			

TABLE 1c.—*Secular accelerations of Satellite 1958 δ2*

N	Date 1958		$10^5\ dP/dt$	N	Date 1958		$10^5\ dP/dt$	N	Date 1958		$10^5\ dP/dt$
0	May	16.02		1050	July	31.09	−3.63	2100	Oct.	12.39	−5.57
25		17.86	−3.13	1075	Aug.	1.87	−3.59	2125		14.09	−6.17
50		19.69	−2.98	1100		3.66	−3.51	2150		15.79	−6.82
75		21.52	−2.87	1125		5.44	−3.37	2175		17.48	−7.66
100		23.36	−2.73	1150		7.21	−3.44	2200		19.17	−8.20
125		25.19	−2.70	1175		8.99	−3.53	2225		20.86	−8.59
150		27.02	−2.73	1200		10.77	−3.63	2250		22.54	−9.38
175		28.85	−2.76	1225		12.54	−3.56	2275		24.22	−9.71
200		30.67	−2.63	1250		14.31	−3.57	2300		25.89	−8.61
225	June	1.50	−2.56	1275		16.08	−3.71	2325		27.56	−8.58
250		3.32	−2.44	1300		17.85	−3.96	2350		29.23	−8.40
275		5.15	−2.41	1325		19.62	−4.03	2375		30.89	−8.06
300		6.97	−2.50	1350		21.39	−4.31	2400	Nov.	1.55	−7.99
325		8.79	−2.46	1375		23.15	−4.68	2425		3.21	−8.46
350		10.61	−2.42	1400		24.91	−4.96	2450		4.86	−8.60
375		12.43	−2.38	1425		26.67	−5.01	2475		6.52	−8.61
400		14.25	−2.38	1450		28.43	−4.87	2500		8.16	−8.85
425		16.06	−2.39	1475		30.18	−4.60	2525		9.80	−9.12
450		17.88	−2.35	1500		31.94	−4.25	2550		11.44	−9.55
475		19.69	−2.45	1525	Sept.	2.69	−4.11	2575		13.08	−10.26
500		21.51	−2.65	1550		4.44	−4.85	2600		14.71	−10.88
525		23.32	−2.73	1575		6.19	−4.27	2625		16.34	−12.31
550		25.13	−2.87	1600		7.93	−4.31	2650		17.96	−13.36
575		26.94	−2.90	1625		9.68	−4.25	2675		19.58	−14.42
600		28.75	−2.99	1650		11.42	−4.14	2700		21.19	−15.28
625		30.56	−2.85	1675		13.16	−4.33	2725		22.79	−15.49
650	July	2.36	−2.59	1700		14.90	−4.58	2750		24.39	−16.58
675		4.17	−2.59	1725		16.63	−5.12	2775		25.98	−18.01
700		5.97	−2.70	1750		18.37	−5.34	2800		27.56	−20.15
725		7.77	−2.84	1775		20.10	−5.13	2810		28.20	−21.4
750		9.58	−3.11	1800		21.83	−5.37	2820		28.83	−23.0
775		11.37	−2.56	1825		23.55	−5.54	2830		29.46	−25.0
800		13.17	−2.59	1850		25.58	−6.19	2840		30.08	−27.0
825		14.97	−2.56	1875		27.00	−6.35	2850		30.71	−29.1
850		16.77	−2.54	1900		28.72	−5.56	2860	Dec.	1.33	−32.
875		18.56	−2.74	1925		30.44	−5.34	2865		1.64	−37.
900		20.36	−2.86	1950	Oct.	2.15	−5.22	2870		1.95	−41.
925		22.15	−3.08	1975		3.86	−5.30	2875		2.26	−46.
950		23.94	−3.09	2000		5.57	−5.34	2880		2.57	−52.
975		25.73	−3.47	2025		7.28	−5.39	2885		2.88	−70.
1000		27.52	−3.66	2050		8.99	−5.47	2890		3.19	−101.
1025		29.30	−3.58	2075		10.69	−5.68	2895		3.49	−160.

TABLE 2a.—*Relative positions of sun and perigee for Satellite 1958 Alpha*

Date	$\alpha_\pi - \alpha_\odot$	ψ	Date	$\alpha_\pi - \alpha_\odot$	ψ	Date	$\alpha_\pi - \alpha_\odot$	ψ
1958			Aug. 15	14.3	47.8	Feb. 21	239.7	121.4
Feb. 6	159.0	159.8	25	24.9	28.8	Mar. 3	250.7	109.6
16	161.4	144.2	Sept. 4	31.5	36.0	13	257.9	99.0
26	178.7	138.1	14	53.5	56.1	23	280.6	80.7
Mar. 8	191.6	160.8	24	59.8	59.9	Apr. 2	286.4	73.1
18	195.6	153.7	Oct. 4	70.8	71.6	12	300.6	59.9
28	215.7	132.0	14	91.1	88.3	22	319.2	39.7
Apr. 7	225.7	133.1	24	94.7	97.2	May 2	323.1	50.3
17	231.3	129.0	Nov. 3	110.9	115.6	12	343.5	52.1
27	252.6	111.6	13	125.5	127.2	22	354.1	24.2
May 7	259.0	99.9	23	128.5	114.1	June 1	1.1	7.1
17	267.1	82.8	Dec. 3	142.4	116.0	11	22.8	20.9
27	287.2	66.5	13	155.6	124.7	21	27.0	42.7
June 6	290.4	75.0	23	162.4	163.2	July 1	41.6	68.9
16	302.1	78.7	1959			11	58.0	66.8
26	319.1	57.6	Jan. 2	182.8	176.9	21	62.0	57.2
July 6	321.4	37.0	12	186.2	148.3	31	84.1	75.9
16	337.4	23.1	22	199.3	123.9	Aug. 10	92.8	93.1
26	351.2	11.7	Feb. 1	216.3	138.4	20	103.6	108.1
Aug. 5	354.5	39.6	11	219.4	142.0			

TABLE 2b.—*Relative positions of sun and perigee for Satellite 1958 β2*

Date	$\alpha_\pi - \alpha_\odot$	ψ	Date	$\alpha_\pi - \alpha_\odot$	ψ	Date	$\alpha_\pi - \alpha_\odot$	ψ
1958			Sept. 27	5.9	32.9	Apr. 5	79.1	78.3
Mar. 21	292.7	68.9	Oct. 7	18.1	28.5	15	82.0	78.4
31	290.6	69.2	17	19.4	19.4	25	94.5	86.8
Apr. 10	291.4	74.6	27	17.4	34.6	May 5	100.3	95.0
20	302.7	70.8	Nov. 6	23.3	53.7	15	97.6	99.7
30	311.5	59.5	16	34.6	58.2	25	98.9	107.3
May 10	309.7	51.6	26	35.8	46.0	June 4	110.1	118.6
20	309.1	47.1	Dec. 6	36.0	34.7	14	116.0	120.3
30	318.6	38.3	16	36.0	33.0	24	113.0	108.4
June 9	327.0	30.3	26	47.0	42.2	July 4	113.0	98.0
19	325.1	41.1	1959			14	123.8	102.9
29	323.3	58.4	Jan. 5	48.2	47.5	24	130.9	117.6
July 9	332.0	62.6	15	44.3	55.8	Aug. 3	128.6	127.9
19	341.5	49.2	25	47.7	68.4	13	130.0	132.2
29	340.7	28.5	Feb. 4	59.4	74.3	23	140.0	137.4
Aug. 8	339.0	20.3	14	62.9	67.5	Sept. 2	149.0	147.4
18	347.3	23.7	24	60.1	59.0	12	148.0	147.3
28	358.7	16.5	Mar. 6	63.3	64.1	22	148.2	140.0
Sept. 7	359.4	1.9	16	76.1	77.1	Oct. 2	153.2	140.2
17	358.0	21.9	26	81.3	82.0	12	168.6	160.8

TABLE 2c.—*Relative positions of sun and perigee for Satellite 1958 δ1*

Date	$\alpha_\pi - \alpha_\odot$	ψ	Date	$\alpha_\pi - \alpha_\odot$	ψ	Date	$\alpha_\pi - \alpha_\odot$	ψ
1958			July 24	84.5	75.6	Oct. 2	171.7	171.2
May 15	0.6	34.1	Aug. 3	45.6	42.9	12	131.1	131.1
25	320.8	42.4	13	6.8	10.2	22	89.7	89.6
June 4	281.2	66.0	23	328.5	31.3	Nov. 1	47.3	47.5
14	242.0	92.3	Sept. 2	289.8	68.8	11	3.7	9.6
24	202.3	112.9	12	250.9	107.4	21	318.2	40.8
July 4	162.9	117.9	22	211.6	146.9	Dec. 1	270.6	83.5
14	123.6	102.8						

Note on the Secular Motions of the Node and Perigee of an Artificial Satellite

By Yoshihide Kozai

The values of the coefficients of the second and the fourth harmonics of the earth's gravitational potential, which I derived (Kozai, 1959a) from the motion of the node and perigee of Satellite 1958 $\beta 2$, the first Vanguard, are quite different from those obtained by other authors. Recently I discovered an error in my formula for the secular motion of the perigee as it appeared in the previous paper. Instead of

$$\dot{\omega}=\frac{A_2}{p^2}n(4-5\sin^2 i)\left\{\frac{1}{2}+\frac{A_2}{a^2}\left(1-\frac{31}{48}\sin^2 i\right)\right\},$$

we must read

$$\dot{\omega}=\frac{A_2}{p^2}n(4-5\sin^2 i)\left\{\frac{1}{2}+\frac{29}{48}\frac{A_2}{a^2}\sin^2 i\right\}.$$

This change should give more reasonable values for the coefficients. In the meantime, however, I have derived more complete formulas for the secular motions of the node and perigee, which are applicable to any satellite even if its eccentricity is not small. They are of closed form as far as the terms of order of A_2^2/a^4.

The new formulas are:

$$\dot{\Omega}=-\frac{A_2}{p^2}n\cos i\left[1+\frac{A_2}{p^2}\left\{\frac{3}{2}+\frac{e^2}{6}-2\sqrt{1-e^2}-\sin^2 i\left(\frac{5}{3}-\frac{5}{24}e^2-3\sqrt{1-e^2}\right)\right\}\right]-\frac{A_4}{p^4}n\cos i\left(\frac{6}{7}-\frac{3}{2}\sin^2 i\right)\left(1+\frac{3}{2}e^2\right);$$

$$\dot{\omega}=\frac{A_2}{p^2}n\left(2-\frac{5}{2}\sin^2 i\right)\left[1+\frac{A_2}{p^2}\left\{2+\frac{e^2}{2}-2\sqrt{1-e^2}-\sin^2 i\left(\frac{43}{24}-\frac{e^2}{48}-3\sqrt{1-e^2}\right)\right\}\right]-\frac{5}{12}\frac{A_2^2}{p^4}ne^2\cos^4 i+\frac{A_4}{p^4}n\left[\frac{12}{7}-\frac{93}{14}\sin^2 i+\frac{21}{4}\sin^4 i+e^2\left(\frac{27}{14}-\frac{189}{28}\sin^2 i+\frac{81}{16}\sin^4 i\right)\right]$$

Here n is the anomalistic mean motion; and $p=a(1-e^2)$; i and e are their mean values over an entire orbital period; and a is determined from the equation

$$n^2a^3=GM\left\{1-\frac{A_2}{p^2}\sqrt{1-e^2}\left(1-\frac{3}{2}\sin^2 i\right)\right\}.$$

I used the following data of Satellite 1958 $\beta 2$ for Oct. 16, $12^h\ 27^m$ (U.T.), 1958, as given in Special Report No. 22 (Kozai, 1959):

$\dot{\Omega}=-3.^\circ014\ 66$ per day,
$\dot{\omega}=4.^\circ404\ 05$ per day,
$n=3862.^\circ640$ per day,
$e=0.190\ 00$,
$i=34.^\circ250$,

and derived the following values:

$$\frac{A_2}{a_e^2}=1.6232\times10^{-3},$$

$$\frac{A_4}{a_e^4}=0.94\times10^{-5}.$$

These values are reasonable and are not very much different from those obtained by other authors.

Anticipated Orbital Perturbations of Satellite 1959 δ2

By Yoshihide Kozai and Charles A. Whitney

The orbit of Satellite 1959 δ2, the "Paddle-Wheel," is significantly affected by lunar and solar perturbations. Thus, Satellite 1959 δ2 is unique among satellites launched to date, and we believe it worthwhile to publish the present analysis to provide a basis for anticipating its orbital behavior.

Starting from the orbital elements provided by the National Aeronautics and Space Administration for September 3, 1959, we have carried out numerical integration to predict the future behavior of this satellite. These integrations, based on a variation of parameters, are preliminary in nature. Techniques for a more precise analysis of the orbit are in preparation.

The equations employed are outlined below. The technique of integration was a simple one, taking the semimajor axis as independent variable.

The perturbation equations

Solar and lunar perturbations.—Variations of the orbital eccentricity due to the moon and the sun are expressed by the equation (Kozai, 1959c),

$$\frac{de}{dt}=-\frac{\sqrt{1-e^2}}{na^2e}\frac{\partial R}{\partial \omega}, \tag{1}$$

where the principal terms of R are:

$$\begin{aligned}R=\frac{15}{8}e^2a^2\Big[&n_\odot^2\cos^4\frac{i}{2}\cos^4\frac{\epsilon}{2}\cos 2(\lambda_\odot-\omega-\Omega)\\&+\frac{1}{2}(n_\mathbb{C}^2m_\mathbb{C}+n_\odot^2)\sin^2 i\left(1-\frac{3}{2}\sin^2\epsilon\right)\cos 2\omega\\&+\frac{1}{2}n_\mathbb{C}^2m_\mathbb{C}\Big\{\sin^2\epsilon\cos^4\frac{i}{2}\cos 2(\omega+\Omega-\Omega_\mathbb{C})\\&-\sin i\cos^2\frac{i}{2}\sin 2\epsilon\cos(2\omega+\Omega-\Omega_\mathbb{C})\Big\}\\&+\frac{1}{2}n_\odot^2\Big\{\sin^2\epsilon\cos^4\frac{i}{2}\cos 2(\omega+\Omega)\\&-\sin i\cos^2\frac{i}{2}\sin 2\epsilon\cos(2\omega+\Omega)\Big\}\\&+n_\odot^2\sin i\cos^2\frac{i}{2}\sin\epsilon\cos^2\frac{\epsilon}{2}\\&\cos(2\lambda_\odot-2\omega-\Omega)\Big].\end{aligned} \tag{2}$$

Here, $n_\odot$ is the mean motion of the sun; $n_\mathbb{C}$, that of the moon; ϵ, the obliquity; $\lambda_\odot$, the mean longitude of the sun; $m_\mathbb{C}$, the mass of the moon (the unit is the mass of the earth); and $\Omega_\mathbb{C}$, the longitude of the ascending node of the moon with respect to the earth's equator. On the right side of equation (2), i, Ω, and ω may be considered unaffected by the moon and the sun.

As the semimajor axis does not change rapidly due to the moon and the sun, the variation of the perigee distance q is given by the equation

$$\frac{dq}{dt}=-a\frac{de}{dt}. \tag{3}$$

Oblateness.—The rates of change of the argument of perigee and the right ascension of the ascending node were computed from the usual first-order equations,

$$\begin{aligned}\frac{d\omega}{dN}&=\frac{J}{p^2}(2-2.5\sin^2 i),\\\frac{d\Omega}{dN}&=-\frac{J}{p^2}\cos i,\end{aligned} \tag{4}$$

where N is the revolution number, and $p=$

$a(1-e^2)$. The value $J=.0016230$ was employed, as well as the equation,

$$P=.0586745a^{3/2}, \tag{5}$$

relating the orbital period in days to the semimajor axis in units of 6378.388 km.

Atmospheric Drag.—The effects of atmospheric drag on the orbital energy and the perigee height were introduced in the following manner.

The effect on perigee height was computed from the approximation

$$\frac{dq}{dQ}=\frac{H}{ae}, \tag{6}$$

where H is the atmospheric scale height. This relation can be transformed to the equation

$$\frac{dq}{da}=\frac{2}{Kae+1}, \tag{7}$$

where $K=H^{-1}$. This approximation is valid for orbits of high eccentricity, but clearly it is very poor for low eccentricities. We do not feel that the present calculations would be significantly affected by a more precise computation of dq/da.

The drag effect on orbital period was evaluated with a formula derived to be valid for a wide range of eccentricities.

The loss of energy due to drag may be written as

$$du=\frac{C_D}{2}A\rho w^2 ds, \tag{8}$$

where C_D is the drag coefficient; A is the satellite's effective cross-sectional area; ρ is the atmospheric density; w is the orbital velocity; and ds is the differential of distance along the orbit.

For the orbital velocity we substituted the value at perigee,

$$w^2=k^2\frac{1+e}{a(1-e)}.$$

For ds we used the equations,

$$\frac{ds}{dv}=r\left(1+\left(\frac{1}{r}\frac{dr}{dv}\right)^2\right)^{1/2},$$

$$\frac{dr}{dv}=r\frac{\sin v}{1+e\cos v}. \tag{9}$$

On the assumption that v, the true anomaly, is much less than one radian in the region of significant drag, we derived the equation,

$$ds=a(1-e)\left(1+\frac{e}{1+e}v^2\right)dv. \tag{10}$$

We further assumed that the atmospheric density above perigee can be represented by an exponential function of height, writing $\rho(v)=\rho(q)\exp\left(-K(q)\{r(v)-q\}\right)$.

We then found that

$$du=\frac{C_D}{2}A\rho(q)k^2(1+e)\left(1+\frac{e}{1+e}v^2\right)\exp\left(-\frac{Kqev^2}{2(1+e)}\right)dv. \tag{11}$$

Integrating over true anomaly and employing the relation

$$da=\frac{a^2}{mk^2}du,$$

where m is the satellite mass, led to the following expression for Δa, the change of semimajor axis per revolution:

$$\Delta a=\sqrt{\frac{\pi}{2}}C_D\frac{A}{m}\rho(q)\frac{(1+e)^{3/2}}{\sqrt{Kqe}}a^2\left(1+\frac{1}{Kq}\right). \tag{12}$$

We note that the integration around an orbit is performed with an exponential atmosphere. However, because of the wide range of perigee heights produced by the lunar and solar perturbations, it was not sufficiently accurate to assume that the entire atmosphere was isothermal.

We employed the following formulas for $\rho(q)$ and $K(q)$:

$$\rho(q)=7.94\times10^{-11}\exp\left[-161.55(q-1)+2.3029\exp\left(-138.46(q-1)+2.8\right)\right],$$

$$K(q)=161.55+318.86\exp\left(-138.46(q-1)+2.8\right), \tag{13}$$

where ρ is in gm/cm^3; q is in units of 6378.388 km; and K is in km^{-1}.

Table 1 lists the values of $\log_{10}\rho$ derived from this model and from the Smithsonian

TABLE 1.—*Atmospheric densities*

Height (km)	$\log_{10} \rho$(gm/cm³)	
	Approximation	Model 4
150	−11.12	−11.08
180	−11.75	−11.77
210	−12.24	−12.29
240	−12.65	−12.73
270	−13.02	−13.09

Astrophysical Observatory Interim Model Atmosphere No. 4 (Whitney, 1959).

Numerical results

The perturbed orbit has been calculated from the following initial orbit:

Epoch 1959 September 3.150 GMT
a=4.3446
e=.7604
i=47°.10
ω=41°.66
Ω=55°.62

The results are summarized in figures 1, 2, and 3. The arrows indicate the date of satellite launching. These figures show integrations for two values of A/m, in order to indicate the sensitivity of the orbit to variations of atmospheric density and effective area of the satellite.

The semiannual variation of perigee distance is produced by the solar perturbation and does not drastically affect the satellite lifetime. The lunar perturbation produces the rapid drop of perigee around 600 days after September 3, 1959 and ends the life of the satellite.

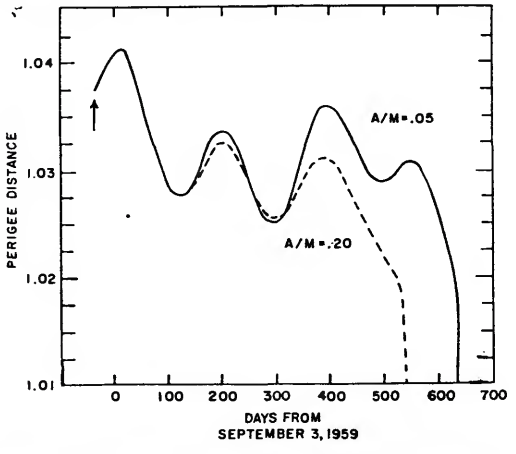

FIGURE 1.—Expected perigee distance of 1959 δ2 measured in units of earth radii.

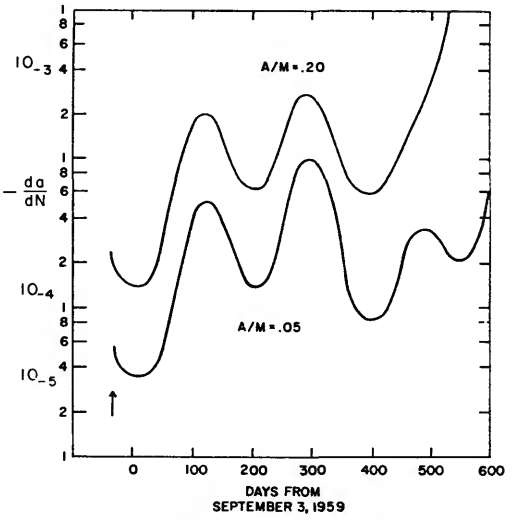

FIGURE 2.—Expected acceleration of Satellite 1959 δ2 given in terms of the decrease of semimajor axis (in earth radii) per revolution.

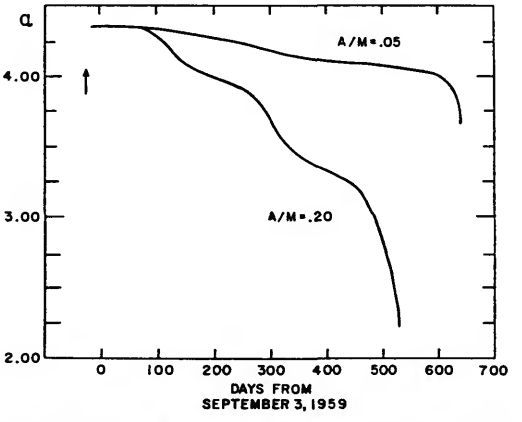

FIGURE 3.—Expected semimajor axis of 1959 δ2 measured in earth radii.

The two "acceleration" curves of da/dN, plotted logarithmically, are essentially mirror images of the curve of perigee height.

From observations of this satellite during the first month of flight, Dr. Don Lautman has derived an acceleration of

$$\frac{da}{dN} = -1.5 \times 10^{-4} \text{ earth radii.}$$

This value falls between the plotted curves.

On the Effects of Image Motion on the Accuracy of Measurement of a Flashing Satellite

By J. Allen Hynek

Artificial satellites carrying flashing lights that can be triggered by internal programming or by command from earth have frequently been proposed as a means of increasing the geodetic usefulness of the satellites. Individual flash durations of less than a millisecond, or a pattern of such bursts, have been suggested. According to this proposal, such flashes would allow us to fix the linear position of a typical close satellite to within 25 feet, and simultaneous observations of a given flash from two or, preferably, more stations would not only permit us to fix the position with a high degree of accuracy, but would also obviate the necessity for precision timing of the observations.

These suggestions, insofar as they concern positional accuracy, overlook salient astrometric facts relating to atmospheric unsteadiness and image motion, which can cause the instantaneous photographic position of the satellite image to differ from its "true" position by easily as much as 2 or 3 seconds of arc.

Observers have long known, for example, that if exposures are too short—under a minute of time—the accuracy of measures of stellar parallax is apt to suffer. The mean position of the wandering image will not be the same as the centroid of an image formed by a longer exposure. Instantaneous visual measures will likewise suffer. It has also been recognized that asteroid positions obtained from relatively long exposures are more accurate than those made visually by filar micrometer, since the photographic method integrates the random [1] motion of the image, while the visual observation does not.

The motion of a stellar image, apart from its scintillation (defined solely as changes of brightness with time, independent of image size or motion), can be measured in a number of ways. For measurements in the focal plane, motion pictures of an image and the associated focal-plane reticle can be made, or the images can be allowed to trail on the film by diurnal motion or by motion of the film itself. The stellar image can also be photographed extra-focally, preferably by rapid-sequence photographs. The successive frames then show the motion of the motley array of bright-image elements, each arising from a separate portion of the incoming wavefront, warped by atmospheric irregularity in the neighborhood of the telescope. From the motion of the elements of the extra-focal image, the motion of the centroid of the focal image can be derived.

Observations of the "dance" of stellar images have been made by many astronomers. As part of a research program on fluctuations of starlight, carried out several years ago by a group associated with the writer at the McMillin Observatory,[2] R. Hosfeld (1954) made quantitative measures that apply directly to the problem of flashing satellites. It should be pointed out that the numbers obtained are characteristic of seeing conditions in the Ohio Valley region but may not be representative for the entire country.

It is particularly instructive to study the motion of the two small, extra-focal image elements formed by admitting starlight to the telescope through two relatively small, equal apertures; Hosfeld used two circular apertures of 3-inch diameter whose centers were separated by 9

[1] Private communication from J. Ashbrook.

[2] Work sponsored by Geophysics Research Directorate, Air Force Cambridge Research Center (Contract No. 19(604)-41).

inches. The separation of these two elements is related to the motion of the focal image, in that the latter motion is one-half the motion of the two extra-focal images as measured by the difference between their maximum and minimum separations.

It is also instructive to observe focal-plane images directly. Motion pictures of the movement of focal images of stars reveal a surprising amount of change of image structure, and of the motion of the "centroid" of the image. Deviations of an image from a mean position can also be recorded by allowing an image to trail on a photographic plate, or by having a film or plate move linearly while being exposed. These and successive-frame photography of extra-focal images showed that the average image motion is 2.2 seconds of arc during night hours, and 3.1 during the daytime. The random motion of Capella during the daytime is shown in figure 1. The consecutive points are separated in time by $\frac{1}{32}$ second; points can be as far apart in distance as 5 seconds of arc.

The image of a satellite flash, therefore, may appear at a position several seconds of arc away from the "true" position of the satellite. Simultaneous observations from two or more stations will not necessarily tend to cancel the effect; if the errors are of opposite sign, they can yield a position error as great as 10 seconds of arc.

A pattern of bursts of individual short flashes would, in the mean, tend to produce a reliable

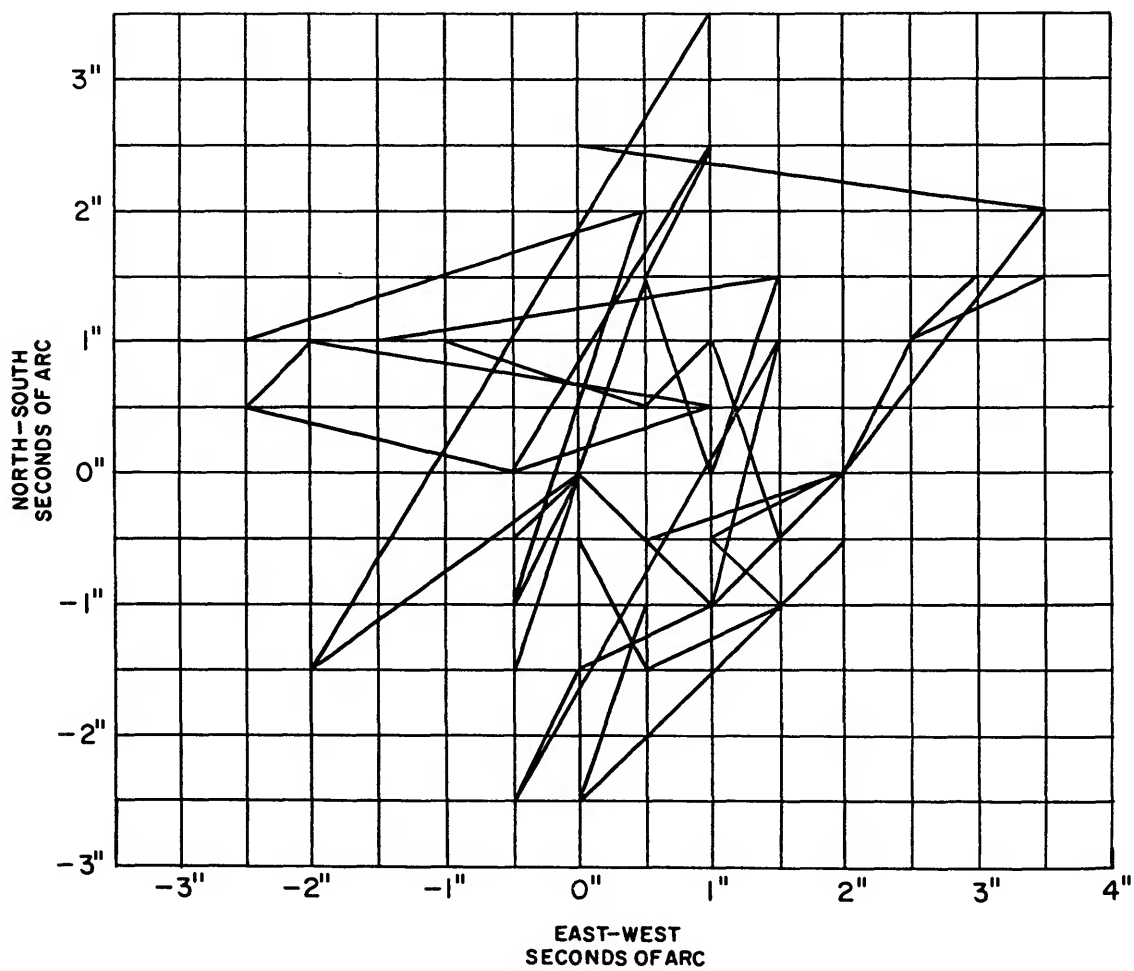

FIGURE 1.—Random walk of Capella during two seconds of time.

position, although the position of each individual flash would be subject to large error. It would appear unfortunately, therefore, that as long as satellites must be observed through an appreciable atmosphere, the use of very short flashes for geodetic purposes will tend to increase rather than to decrease the positional error, if accuracies of a second of arc are required.

The study of image structure and motion carried out by the Ohio State group and others shows that such motions are to be ascribed to atmospheric disturbances in the general neighborhood of the telescope, and not to the disturbances at the heights of the order of the height of the tropopause that cause scintillation. That is, the positional errors under discussion are not introduced by stellar twinkling, as might at first be thought, but by local wavefront changes. Since these atmospheric disturbances are local, a proper location of the observing sites would help to minimize the effects of the disturbances.

Several independent lines of evidence indicate that stellar scintillation does not cause shifts in image position. The immediate cause of scintillation is the play upon the telescope objective of the interference pattern induced by the atmosphere. One can easily observe this by placing his unaided eye at the focal plane of a telescope of moderate size that is trained on a bright star. The entire telescope objective is then seen to be illuminated. If the observer uses his eye as a field lens, he discerns the rapidly moving and changing pattern of starlight.

A more slowly moving pattern of light, suggestive of a viscous flow, is apparent if the image is examined at a point slightly beyond the focal plane of the telescope. These relatively slow-moving light patterns represent deformations of the wavefront responsible for image motions and explain the fact that elements in an extra-focal image tend to persist in form and position for large fractions of a second, quite unlike the kaleidoscopic changes seen on the objective itself which even successive photographic exposures of 0.01 second are generally unable to "stop."

The distinction between image motion and stellar scintillation can be illustrated in many ways (Hosfeld, 1954). For example, the images of double stars show random scintillation but coordinated motion; with increasing zenith distance, scintillation increases more rapidly than does image motion; we can induce image motion artificially, but not scintillation except by interfering with the beam at relatively large distances.

One might suppose that since the images of components of a double star move coordinately, as do indeed the images of stars in a field nearly a degree across, the flashing satellite and the stars would exhibit the same image motion. This supposition, of course, does not hold, since the stellar exposure would obviously be many times as long as that for the satellite flash, and the image of each star would therefore represent the integral of many excursions from the mean position.

In long exposures of faint stars, a larger number of developable emulsion grains accumulate near the mean stellar position than elsewhere. The rapid motion of images to points away from the mean position contribute, at most, to the slight halo around the stellar image. For the average stellar image, 30 to 40 microns in diameter and corresponding to many seconds of arc, the position can be measured within an accuracy of about 2 microns. Because the centroid of a stellar image corresponds to the true position of the star, such accuracy is meaningful; in the case of the image of a short flash from a satellite, it is apt to be misleading.

The Effect of a Variable Scale Height on Determinations of Atmospheric Density from Satellite Accelerations

By Luigi G. Jacchia

The anomalistic period P of an artificial satellite changes under the action of atmospheric drag. The rate of change can be expressed very approximately (Sterne, 1958a; King-Hele, Cook, and Walker, 1959) by the equation

$$\frac{dP}{dt}=-3C_D\frac{A}{m}a\int_0^\pi\frac{(1+e\cos E)^{3/2}}{(1-e\cos E)^{1/2}}\rho\,dE. \quad (1)$$

The symbols are defined as follows:

C_D=drag coefficient,
A=effective cross section of satellite,
m=mass of satellite,
a=semimajor axis of satellite's orbit,
e=orbital eccentricity of satellite,
E=eccentric anomaly,
ρ=atmospheric density.

Equation (1) assumes a stationary atmosphere; the effect of atmospheric rotation has been evaluated by Sterne (1959). The only approximation made in equation (1) is that the orbit can be defined by a set of Keplerian elements in the course of one revolution; in the general case, therefore, the error arising from this approximation is entirely negligible.

Useful formulas for computing atmospheric densities from satellite accelerations can be derived from equation (1) on the assumption of a spherically symmetrical atmosphere in which the density varies exponentially with height (Sterne, 1958b; Groves, 1958; King-Hele, Cook and Walker, 1959). The procedure consists in replacing ρ by the expression

$$\rho=\rho_p\exp\left(-\frac{r-q}{H}\right), \quad (2)$$

(where ρ_p is the atmospheric density at perigee; r the geocentric distance; q the perigee distance; and H a constant, the density scale height), and in expanding the integrand as a power series of e. The integral can then be evaluated in terms of Bessel functions of the first kind of imaginary argument $I_n(x)$, with $x=ae/H$. For small eccentricities, the Bessel functions can be replaced by their expansion at the origin; for larger eccentricities, use is made of their asymptotic expansions (King-Hele, Cook and Walker, 1959).

Formulas of the type just described have been used by all investigators in deriving atmospheric densities from satellite accelerations. If the density scale height H varies with height, instead of being a constant, the use of such formulas causes a systematic error. It is the purpose of this note to evaluate the size of this error.

Let us assume, for simplicity, that H varies linearly with height, and that H_p is the value of H at perigee; we shall then have

$$H=H_p+\beta(r-q); \quad (3)$$

and, since by definition

$$\frac{1}{H}=-\frac{1}{\rho}\frac{d\rho}{dr},$$

we obtain, by integration,

$$\rho=\rho_p\left[1+\frac{\beta}{H_p}(r-q)\right]^{-\frac{1}{\beta}} \quad (4)$$

The gradient β of the density scale height is a nondimensional quantity. Recent atmos-

pheric results (Jacchia, 1960a) have shown that at the height of 400 km $\beta \approx +0.1$ in the dark hemisphere and $\beta \approx +0.2$ in the center of the diurnal bulge. The density scale height itself is of the order of 55 km at night and 72 km in the diurnal bulge, for the same height of 400 km above the geoid.

Replacing ρ in equation (1) by the expressions of equations (2) and (4) respectively, and using the same values for ρ_p and H_p in both cases, we obtain two values of $\frac{d\rho}{dt}$, whose ratio R is 1 for $\beta=0$ and >1 for positive values of β. The explicit value of R is

$$R=\frac{\int_0^\pi f(e,E)\exp\left(-\frac{r-q}{H_p}\right)dE}{\int_0^\pi f(e,E)\left[1+\frac{\beta}{H_p}(r-q)\right]^{-\frac{1}{\beta}}dE}, \quad (5)$$

where

$$f(e,E)=\frac{(1+e\cos E)^{3/2}}{(1-e\cos E)^{1/2}}.$$

It should be apparent that $R-1$ is the relative error that is committed when ρ_p is determined from equation (1) under the assumption that $\beta=0$.

The values of R to be found in table 1 were computed by numerical evaluation of the integrals of equation (5), with the value, $H_p=0.01$ earth's radii=63.78 km. Extensive use was made of the "logarithmic" finite-difference method of integration introduced by the author (Jacchia, 1955), which is highly advantageous when the integrand is a near-exponential function.

It has been assumed at the outset that for values of H_p different from 63.78 km, R must differ from the values given in table 1. Sample integrations with $H_p=31.89$ km seem, however, to reproduce table 1 to the last digit. The reason for this fact is not obvious to this writer. No serious attempt has been made to prove that $\partial R/\partial H_p=0$; the problem is hereby left to an investigator endowed with greater persistence or deeper mathematical insight.

It will be noticed that, while $R-1$ is nearly proportional to β for any given value of e, its behavior is quite different when its variation in function of e is considered for a given β (figures 1 and 2). For $e=0$, we must obviously have $R=1$, irrespective of β; even an extremely small eccentricity, however, will make R considerably different from unity when $\beta \neq 0$, and for any given value of β, R reaches a maximum for $e \approx 0.02$. For greater values of e, R becomes a little smaller and rapidly approaches a nearly asymptotic value, which is practically reached for $e=0.2$.

It is a pleasure to acknowledge the expert help of Miss J. R. B. Carmichael, who performed most of the numerical integrations.

TABLE 1.—*Values of R for $H_p=63.78$ km*

e	Values of R		
	$\beta=0$	$\beta=0.1$	$\beta=0.2$
0.00	1.000	1.000	1.000
0.01	1.000	1.032	1.061
0.02	1.000	1.050	1.100
0.05	1.000	1.044	1.095
0.10	1.000	1.040	1.086
0.20	1.000	1.039	1.083
0.40	1.000	1.039	1.082
0.60	1.000	1.039	1.082
1.00	1.000	1.039	1.083

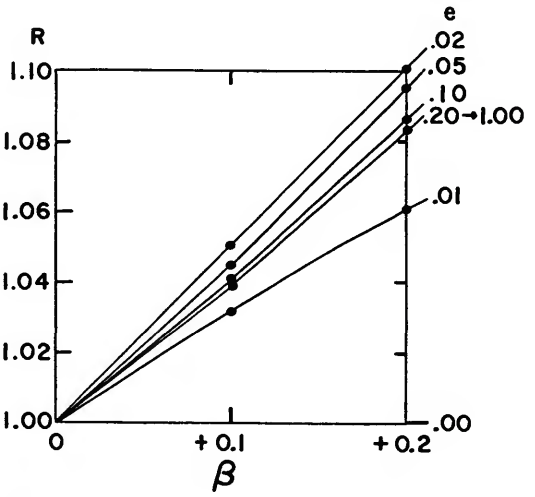

FIGURE 1.—Variation of R (see equation (5)) in function of the scale-height gradient β for different orbital eccentricities. The relative error of densities determined using formulas that assume $\beta=0$ is given by $R-1$. Scale height at perigee, $H_p=63.78$ km.

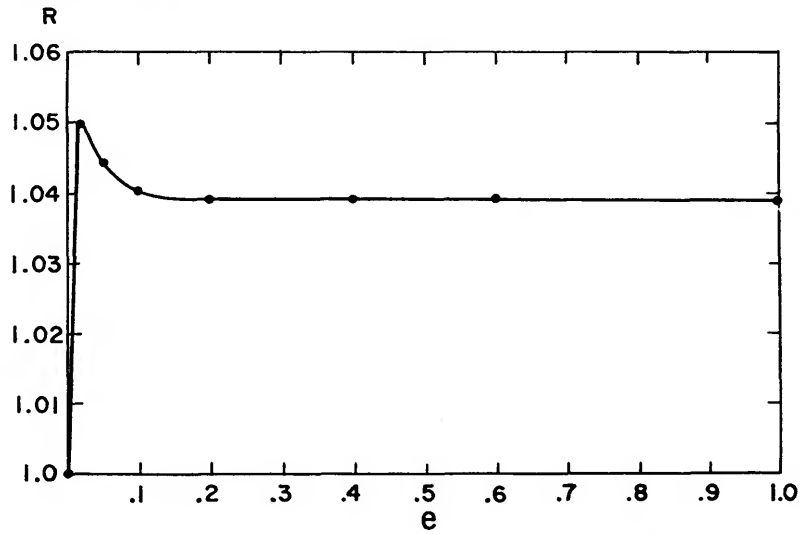

FIGURE 2.—Variation of R in function of e for $\beta=+0.1$. (For R see legend to fig. 1.)
Scale height at perigee, $H_p=63.78$ km.

A Second-Order Solution of Vinti's Dynamical Problem

By Imre G. Izsak

The accurate description of the motion of artificial satellites has presented a new problem in celestial mechanics. It is true that satellites of some other planets—for instance, the five inner satellites of Jupiter and the five inner satellites of Saturn—have quite significant perturbations caused by the oblateness of the parent planet, but the obtainable planetocentric accuracy of the observations did not demand a highly sophisticated theory. In the case of artificial satellites of the earth, however, the accuracy of the topocentric observations made by the Baker-Nunn cameras amounts to a few seconds of arc. That means we have a geocentric accuracy of about one second of arc, while the time record is accurate to a few thousandths of a second. It would be very difficult to construct an analytical theory that would represent the motion with such an accuracy, either for the computation of exact ephemerides or, what is even more important, for the best possible use of the observations. The oblateness perturbations are only a part of the factors that influence the satellite motion, of course. For instance, we know that low-orbiting satellites suffer large perturbations of an "irregular" character caused by atmospheric drag, and that high-orbiting satellites are affected by luni-solar perturbations. Solar-radiation pressure is another factor complicating the situation, especially in the case of satellites with small mass/area ratio. The present paper deals with the motion in the gravitational field of the earth.

Although a great many papers devoted to this problem exist in the recent literature, the most comprehensive investigations were presented in papers by Brouwer (1959), Garfinkel (1959), and Kozai (1959b), all of which appeared in the celebrated November 1959 issue of *Astronomical Journal*. These authors treated, by different methods, the first- and second-order secular perturbations, as well as the first-order long-periodic and short-periodic perturbations of the orbital elements, where order refers to the oblateness parameter. Less related to the present subject is the very powerful semianalytical method for the computation of gravitational perturbations developed by Musen (1959).

The distinction among the different kinds of perturbations has significance not only from the theoretical but also from the practical point of view. In theoretical work, the secular, long-periodic, and short-periodic terms are usually obtained by different techniques. In practical work, for instance in an orbit improvement program, the short-periodic terms are used for the reduction of the real motion of the satellite, as reflected in the observations, to a certain mean elliptical motion. The secular and long-periodic variations are still present in this mean elliptical orbit and can be obtained with a high degree of accuracy by the use of many revolutions of the satellite.

If the coefficients of these terms are expressed as functions of the orbital elements and the geophysical constants, the latter can be determined. The next step beyond the work of Brouwer, Garfinkel, and Kozai would be to obtain the second-order short-periodic perturbations. As far as I can see, this would be a rather tedious undertaking with their methods, because it involves several multiplications of Fourier series. In this paper I shall adopt a quite different approach, based on a remarkable approximation to the actual gravitational field of the earth, originated by Vinti (1959).

Vinti's dynamical system

On the assumption that the earth is an axially symmetric oblate body, its potential can be developed into the series

$$V=-\frac{\mu}{r}\left\{1-\sum_{n=1}^{\infty} J_n\left(\frac{a_E}{r}\right)^n P_n(\sin\delta)\right\}, \tag{1}$$

where $\mu=fm_E=398.618\pm.003$ Mm^3 ksec^{-2} (O'Keefe, Eckels, and Squires, 1959),

f is the gravitational constant,
m_E and a_E are the mass and the equatorial radius of the earth,
the J_n denote geophysical constants,
r and δ are the geocentric distance and declination of the satellite,
and the $P_n(\sin\delta)$ are Legendre polynomials.

According to the latest determination[1] by Kozai (1961b), we have the following values of the J_n:

$$J_2=(1.08219\pm.00002)\times10^{-3}, \qquad J_3=-(2.29\pm.02)\times10^{-6},$$
$$J_4=-(2.12\pm.04)\times10^{-6}, \qquad J_5=-(2.3\pm.2)\times10^{-7}.$$

Thus J_3, J_4, and J_5 can be considered as of the second order with respect to J_2.

Vinti has shown that if the relations

$$J_{2n}=(-1)^{n+1}J_2^n, \qquad J_{2n+1}=(-1)^n J_1 J_2^n$$

are valid, the dynamical system $\ddot{r}=-\nabla V$ can be solved exactly; or to be more precise, the integration of the differential equations can be reduced to quadratures. It is expedient to note here that the representation of the coordinates as functions of time or of another independent variable may still be a difficult problem, involving the solution of a system of simultaneous equations. This is sometimes called the inversion problem and will play an important role in this paper. From the values of the J_n given above it follows that for the gravitational field of the earth Vinti's relation $J_4=-J_2^2$ is not satisfied; instead we have

$$D_4=J_4+J_2^2=-.95\times10^{-6}.$$

On the other hand, J_1 is practically zero; hence it can not be used to generate the coefficients of the odd harmonics. Nevertheless, the potential function

$$\hat{V}=-\frac{\mu}{r}\left\{1+\sum_{n=1}^{\infty}(-J_2)^n\left(\frac{a_E}{r}\right)^{2n}P_{2n}(\sin\delta)\right\}, \tag{2}$$

containing only the even harmonics, is a very good approximation to the potential function (1), the difference

$$V-\hat{V}=\frac{\mu}{r}\left\{J_3\left(\frac{a_E}{r}\right)^3P_3(\sin\delta)+D_4\left(\frac{a_E}{r}\right)^4P_4(\sin\delta)+J_5\left(\frac{a_E}{r}\right)^5P_5(\sin\delta)+\ldots\right\}$$

being of the second order in the oblateness parameter J_2. We call the differential system, $\ddot{r}=-\nabla\hat{V}$, Vinti's dynamical system. If this has been solved, the perturbations due to $V-\hat{V}$ can be treated by a first-order method, that is, without multiplications of Fourier series.

[1] Note added on this appearance of paper: Recent values of the geophysical constants as determined by Kozai (1962) are:

$J_2=(1.08248\pm.00004)\times10^{-3}$ $\quad$ $J_3=-(2.562\pm.007)\times10^{-6}$
$J_4=-(1.84\pm.09)\times10^{-6}$ $\quad$ $J_5=-(6.4\pm.7)\times10^{-8}$
$J_6=(3.9\pm.9)\times10^{-7}$ $\quad$ $J_7=-(4.7\pm.1)\times10^{-7}$.

It follows that $D_4=-.67\times10^{-6}$; therefore, Vinti's approximation is better than expected two years ago.

Oblate-spheroidal coordinates

At this point it is necessary to introduce oblate-spheroidal coordinates, which are defined by the equations

$$x=\sqrt{\rho^2+c^2}\sqrt{1-\sigma^2}\cos\alpha$$

$$y=\sqrt{\rho^2+c^2}\sqrt{1-\sigma^2}\sin\alpha \qquad r=\sqrt{\rho^2+c^2(1-\sigma^2)}$$

$$z=\rho\sigma. \tag{3}$$

It follows that

$$\dot{x}^2+\dot{y}^2+\dot{z}^2=\frac{\rho^2+c^2\sigma^2}{\rho^2+c^2}\dot{\rho}^2+\frac{\rho^2+c^2\sigma^2}{1-\sigma^2}\dot{\sigma}^2+(\rho^2+c^2)(1-\sigma^2)\dot{\alpha}^2.$$

The coordinate α is the right ascension of the satellite, and the surfaces α=constant are meridian planes.

The equation of the surfaces ρ=constant in rectangular coordinates is

$$\frac{x^2+y^2}{\rho^2+c^2}+\frac{z^2}{\rho^2}=1.$$

Consequently, these equations describe oblate spheroids, the intersections with the meridian planes being confocal ellipses of linear eccentricity c, and semiminor axis ρ.

Similarly, for the surfaces σ=constant we have the equation

$$\frac{x^2+y^2}{c^2(1-\sigma^2)}-\frac{z^2}{c^2\sigma^2}=1,$$

which describes one-sheet hyperboloids of revolution, the intersections with the meridian planes being confocal hyperbolas of linear eccentricity c. The geometrical meaning of the coordinate σ is the sine of half the angle between the asymptotes.

In the present application the constant c is meant to take care of the earth's oblateness, and is necessarily small relative to the equatorial radius of the earth. This means that, far enough from the origin, the coordinate surfaces ρ=constant and σ=constant are nearly spheres and cones, respectively. Solving the equations (3) for ρ^2 and σ^2 we get

$$\rho^2=\frac{r^2-c^2}{2}\left\{1+\sqrt{1+\left(\frac{2cz}{r^2-c^2}\right)^2}\right\}, \qquad \sigma^2=\frac{2z^2}{r^2-c^2}\left\{1+\sqrt{1+\left(\frac{2cz}{r^2-c^2}\right)^2}\right\}^{-1};$$

the developments in spherical coordinates,

$$\rho=r\left\{1-\frac{1}{2}\left(\frac{c}{r}\right)^2(1-\sin^2\delta)-\frac{1}{8}\left(\frac{c}{r}\right)^4(1-\sin^2\delta)(1-5\sin^2\delta)-\dots\right\},$$

$$\sigma=\sin\delta\left\{1+\frac{1}{2}\left(\frac{c}{r}\right)^2(1-\sin^2\delta)+\frac{1}{8}\left(\frac{c}{r}\right)^4(1-\sin^2\delta)(3-7\sin^2\delta)+\dots\right\},$$

are easily derived from the preceding relations.

Vinti obtained the potential (2) by asking himself: What is the most general solution $\hat{V}(\rho,\sigma)$ of the Laplace equation

$$\frac{\partial}{\partial\rho}\left\{(\rho^2+c^2)\frac{\partial\hat{V}}{\rho\partial}\right\}+\frac{\partial}{\partial\sigma}\left\{(1-\sigma^2)\frac{\partial\hat{V}}{\partial\sigma}\right\}=0$$

for a gravitational potential which makes the Hamilton-Jacobi equation

$$\frac{1}{2(\rho^2+c^2\sigma^2)}\left\{(\rho^2+c^2)\left(\frac{\partial\hat{W}}{\partial\rho}\right)^2+(1-\sigma^2)\left(\frac{\partial\hat{W}}{\partial\sigma}\right)^2+\left(\frac{1}{1-\sigma^2}-\frac{c^2}{\rho^2+c^2}\right)\left(\frac{\partial\hat{W}}{\partial\alpha}\right)^2\right\}+\hat{V}(\rho,\sigma)=\hat{h}$$

separable in these oblate-spheroidal coordinates? Requiring further that the solution should have no singularities except a pole at the origin, and that as well as axial symmetry it should also possess equatorial symmetry, he found that $\hat{V}(\rho,\sigma)=\frac{b\rho}{\rho^2+c^2\sigma^2}$, where b is a constant. In order to see that this is the same as equation (2), let us expand it into a series of spherical harmonics.

Obviously, $b\rho(\rho^2+c^2\sigma^2)^{-1}=bRe\{(\rho+ic\sigma)^{-1}\}$. But

$$(\rho+ic\sigma)^2=(\rho^2-c^2\sigma^2)+2ic\rho\sigma=(r^2-c^2)+2icz=r^2\{1-2(-icr^{-1})\sin\delta+(-icr^{-1})^2\},$$

so that by the definition of the Legendre polynomials

$$(\rho+ic\sigma)^{-1}=r^{-1}\{1-2(-icr^{-1})\sin\delta+(-icr^{-1})^2\}^{-\frac{1}{2}}=r^{-1}\sum_{n=0}^{\infty}(-icr^{-1})^nP_n(\sin\delta).$$

Taking the real part of this equation we get

$$b\rho(\rho^2+c^2\sigma^2)^{-1}=br^{-1}\left\{1+\sum_{n=1}^{\infty}(-c^2r^{-2})^nP_{2n}(\sin\delta)\right\},$$

and comparing it with the equation (2) we see that we must choose

$$b=-\mu, \qquad c^2=J_2a_E^2.$$

The above value of J_2 and the value $a_E=6378.388$ km give $c=209.828$ km.

Separable dynamical systems of Stäckel's type

Vinti's dynamical system belongs to an important type of solvable problem in analytical dynamics, known as dynamical systems of Stäckel's type. The essentials of these systems can be summarized as follows. Let

$$\Phi=\begin{bmatrix}\phi_{11}(q_1) & \cdots & \phi_{1n}(q_1)\\ \cdot & & \cdot\\ \cdot & & \cdot\\ \cdot & & \cdot\\ \phi_{n1}(q_n) & \cdots & \phi_{nn}(q_n)\end{bmatrix}$$

be a nonsingular matrix, in which the elements of the jth row depend upon the jth coordinate only. We call the inverse $\Psi=\Phi^{-1}$ of such a matrix a Stäckel matrix, the elements of which depend on all the coordinates $q_1, \ldots, q_n$, in general.

As was shown by Stäckel (1891) (see Charlier, 1927), a Hamilton-Jacobi equation of the form

$$H\left(\frac{\partial W}{\partial q}\middle| q\right)=\frac{1}{2}\sum_{j=1}^{n}a_j(q)\left(\frac{\partial W}{\partial q_j}\right)^2+V(q)=h$$

can be solved by the method of separation of the variables if, and only if, the coefficients $a_j(q)$ constitute the first (or any) row of a Stäckel matrix such that $a_j(q)=\psi_{1j}(q)$, and the potential energy can be represented in the form

$$V(q)=\sum_{j=1}^{n}\psi_{1j}(q)\chi_j(q_j),$$

where the functions $\chi_j(q_j)$ depend on the jth coordinate only. Such a dynamical system is said to

be of Stäckel's type. For our present purposes it is sufficient to see that the separation follows from these conditions.

Indeed, the function $W(q|\alpha)$ defined by the equations

$$W(q|\alpha)=\sum_{j=1}^{n} W(q_j|\alpha),$$

$$W(q_j|\alpha)=\sqrt{2}\int_{q_j^0(\alpha)}^{q_j}\sqrt{\sum_{k=1}^{n}\alpha_k\phi_{jk}(q_j)-\chi_j(q_j)}\;dq_j \tag{4}$$

contains n arbitrary constants, $\alpha_1=h$, α_2, . . . , α_n, and is a complete solution of the Hamilton-Jacobi equation:

$$\frac{1}{2}\sum_{j=1}^{n}\psi_{1j}\left(\frac{\partial W}{\partial q_j}\right)^2=\sum_{j=1}^{n}\left\{\psi_{1j}(q)\left[\sum_{k=1}^{n}\alpha_k\phi_{jk}(q_j)-\chi_j(q_j)\right]\right\}$$

$$=\sum_{k=1}^{n}\alpha_k\delta_{1k}-\sum_{j=1}^{n}\psi_{1j}(q)\chi_j(q_j)=h-V.$$

According to Jacobi's theorem, the solution of the canonical system $\dot{p}_j=-\dfrac{\partial H}{\partial q_j}$, $\dot{q}=\dfrac{\partial H}{\partial p_j}$ is then given implicitly by the equations

$$p_j=\frac{\partial(Wq|\alpha)}{\partial q_j}\qquad(j=1,\ldots,n),$$

$$\frac{\partial W(q|\alpha)}{\partial\alpha_1}=t+\beta_1,\qquad\frac{\partial W(q|\alpha)}{\partial\alpha_2}=\beta_2,\ldots,\qquad\frac{\partial W(q|\alpha)}{\partial\alpha_n}=\beta_n, \tag{5}$$

where the β_j are the other n constants of integration.

We can also say that a dynamical system with the Hamiltonian function

$$H(p|q)=\frac{1}{2}\sum_{j=1}^{n}\psi_{1j}(q)p_j^2+\sum_{j=1}^{n}\psi_{1j}(q)\chi_j(q_j)$$

has a system of n quadratic integrals

$$\frac{1}{2}\sum_{j=1}^{n}\psi_{ij}(q)p_j^2+\sum_{j=1}^{n}\psi_{ij}(q)\chi_j(q_j)=\alpha_i,\qquad(i=1,\ldots,n)$$

in involution.

The separability of the variables is a formal property, and it occurs only in appropriate coordinate systems.

In the most important practical applications the functions of q_j under the square root sign in equations (4) must all be positive inside closed intervals I_j and must vanish in the first order at their endpoints. Then the solutions $q_j=q_j(t|\alpha|\beta)$, $p_j=p_j(t|\alpha|\beta)$ of equations (5) can be represented for $-\infty<t<+\infty$ by multiple Fourier series (at least in general). This is the ideal of celestial mechanics. However, in the much more difficult problems with which it deals, such a representation can be only an approximation, valid only in a finite interval of time.

I shall now describe briefly an important special case of Stäckel-type dynamical systems. The natural context for the treatment of these dynamical systems of Liouville's type seems to be the apparatus of the Lagrange equations:

$$\frac{d}{dt}\left(\frac{\partial L}{\partial\dot{q}_j}\right)-\frac{\partial L}{\partial q_j}=0.$$

It can be shown (Whittaker, 1959) that if the Lagrangian function has the structure

$$L=\frac{1}{2}\{u(q)\}\left\{\sum_{j=1}^{n}v_j(q_j)\dot{q}_j^2\right\}+\{u(q)\}^{-1}\left\{\sum_{j=1}^{n}w_j(q_j)\right\}, \tag{6}$$

where $u(q)=\sum_{i=1}^{n} u_i(q_i)$, and the functions $u_i(q_i)$, $v_j(q_j)$, $w_j(q_j)$ depend on the indicated coordinate only, the Lagrange equations possess the "integrals"

$$\frac{1}{2}\{u(q)\}^2 v_j(q_j)\dot{q}_j^2=hu_j(q_j)+w_j(q_j)+c_j. \tag{7}$$

Here h means the energy constant, the $c_1, \ldots, c_{n-1}$ are independent constants of integration, but

$$c_n=-\sum_{i=1}^{n-1} c_i.$$

Actually, in Whittaker's book we find the not-quite-fortunate specialization $v_j(q_j)=1$; however, it is easy to generalize his procedure.

The importance of this type lies in the fact that the inversion problem associated with it can be much simplified. Indeed, if we introduce a new "independent" variable τ by the differential relation

$$\frac{d\tau}{dt}=\frac{\Gamma}{u(q)}, \tag{8}$$

where Γ denotes a conveniently chosen constant, the "integrals" (7) take the form,

$$\frac{\Gamma^2}{2} v_j(q_j)\left(\frac{dq_j}{d\tau}\right)^2=hu_j(q_j)+w_j(q_j)+c_j.$$

These equations can be integrated again immediately, giving the relation

$$\Gamma\int_{q_j^\circ(h|c)}^{q_j}\frac{\sqrt{v_j}dq_j}{\sqrt{\{2hu_j(q_j)+w_j(q_j)+c_j\}}}=\tau+d_j, \tag{9}$$

where the d_j represent n new constants of integration. Each of the equations (9) contains only a single q_j, instead of containing them all as in equations (5) in the case of a general Stäckel-type dynamical system. In other words, a dynamical system of Liouville's type of n degrees of freedom splits up into n dynamical systems of one degree of freedom. After the coordinates q_j have been obtained as functions of the parameter τ, the time dependence of the motion is given by the integral of equation (8); that is,

$$\sum_{i=1}^{n}\int_0^\tau u_i(q_i(\tau))d\tau=\Gamma(t-t_0).$$

The Hamiltonian function belonging to the Lagrangian function (6) is

$$H=\frac{1}{2}\{u(q)\}^{-1}\left\{\sum_{j=1}^{n}[v_j(q_j)]^{-1}p_j^2\right\}\{-u(q)\}^{-1}\left\{\sum_{j=1}^{n} w_j(q_j)\right\}.$$

It is easy to see that to write it in Stäckel's form we have to choose:

$$\Phi=\begin{bmatrix} u_1v_1 & v_1 & 0 & 0 & \ldots & 0 & 0 \\ u_2v_2 & 0 & v_2 & 0 & \ldots & 0 & 0 \\ u_3v_3 & 0 & 0 & v_3 & \ldots & 0 & 0 \\ \cdot & \cdot & \cdot & \cdot & \cdots & \cdot & \cdot \\ \cdot & \cdot & \cdot & \cdot & \cdots & \cdot & \cdot \\ \cdot & \cdot & \cdot & \cdot & \cdots & \cdot & \cdot \\ u_{n-1}v_{n-1} & 0 & 0 & 0 & \ldots & 0 & v_{n-1} \\ u_nv_n & -v_n & -v_n & -v_n & \ldots & -v_n & -v_n \end{bmatrix},$$

and $$\chi_j = -v_j w_j.$$

For $n=2$, Stäckel's type is not more general than that of Liouville.

The integration of Vinti's dynamical system

Let us now proceed with the integration of Vinti's dynamical system. To convince ourselves that the Hamilton-Jacobi equation

$$\frac{1}{2(\rho^2+c^2\sigma^2)}\left\{(\rho^2+c^2)\left(\frac{\partial \hat{W}}{\partial \rho}\right)^2+(1-\sigma^2)\left(\frac{\partial \hat{W}}{\partial \sigma}\right)^2+\left(\frac{1}{1-\sigma^2}-\frac{c^2}{\rho^2+c^2}\right)\left(\frac{\partial \hat{W}}{\partial \alpha}\right)^2\right\}-\frac{\mu\rho}{\rho^2+c^2\sigma^2}=\hat{h}, \tag{10}$$

is of Stäckel's type, let us put

$$\Phi=\begin{bmatrix} \frac{\rho^2}{\rho^2+c^2} & -\frac{1}{2(\rho^2+c^2)} & \frac{c^2}{2(\rho^2+c^2)^2} \\ \frac{c^2\sigma^2}{1-\sigma^2} & \frac{1}{2(1-\sigma^2)} & -\frac{1}{2(1-\sigma^2)^2} \\ 0 & 0 & \frac{1}{2} \end{bmatrix}, \quad \begin{matrix} \chi_1=\frac{\mu\rho}{\rho^2+c^2} \\ \text{and } \chi_2=0 \\ \chi_3=0. \end{matrix} \tag{11}$$

Then, $\det \Phi=\frac{\rho^2+c^2\sigma^2}{4(\rho^2+c^2)(1-\sigma^2)}\neq 0$ except for polar orbits, and

$$\Psi=\Phi^{-1}=\begin{bmatrix} \frac{\rho^2+c^2}{\rho^2+c^2\sigma^2} & \frac{1-\sigma^2}{\rho^2+c^2\sigma^2} & \frac{1}{\rho^2+c^2\sigma^2}\left(\frac{1}{1-\sigma^2}-\frac{c^2}{\rho^2+c^2}\right) \\ \frac{-2c^2(\rho^2+c^2)\sigma^2}{\rho^2+c^2\sigma^2} & \frac{2\rho^2(1-\sigma^2)}{\rho^2+c^2\sigma^2} & \frac{2}{\rho^2+c^2\sigma^2}\left(\frac{\rho^2}{1-\sigma^2}+\frac{c^4\sigma^2}{\rho^2+c^2}\right) \\ 0 & 0 & 2 \end{bmatrix}.$$

The first line in this Stäckel matrix agrees with the coefficients in the Hamilton-Jacobi equation (10).

The second line permits us to write down immediately the quadratic integral,

$$-\frac{c^2(\rho^2+c^2)\sigma^2}{\rho^2+c^2\sigma^2}p_\rho^2+\frac{\rho^2(1-\sigma^2)}{\rho^2+c^2\sigma^2}p_\sigma^2+\frac{1}{\rho^2+c^2\sigma^2}\left(\frac{\rho^2}{1-\sigma^2}+\frac{c^4\sigma^2}{\rho^2+c^2}\right)p_\alpha^2-\frac{2c^2\mu\rho\sigma^2}{\rho^2+c^2\sigma^2}=\hat{C}^2.$$

For $\sigma=0$, that is, for an equatorial crossing, the expression on the left side is positive. This is why we are permitted to write the constant of integration as $\hat{C}^2$. The value of $\hat{C}$ is close to that of the magnitude of the nonconstant angular momentum, the difference being $O(c^2)$.

The third line corresponds to the square of the linear integral $p_\alpha=\hat{G}$, which results from the fact that α is an ignorable coordinate; $\hat{G}$ is the z-component of the angular momentum, and is positive or negative according as the motion is direct or retrograde.

In order to obtain a complete solution of the Hamilton-Jacobi equation (10), substitute the expressions of ϕ_{ij} and χ_j given by equations (11) into the general formulas (4). By a suitable choice of the lower limits of integration we get

$$\hat{W}(\rho,\sigma,\alpha|\hat{h},\hat{C},\hat{G})=\int_{\rho_1}^{\rho}\frac{\sqrt{P(\rho)}}{\rho^2+c^2}\,d\rho+\int_0^{\sigma}\frac{\sqrt{Q(\sigma)}}{1-\sigma^2}\,d\sigma+\hat{G}\alpha, \tag{12}$$

where $P(\rho)=2\hat{h}\rho^4+2\mu\rho^3-(\hat{C}^2-2c^2\hat{h})\rho^2+2c^2\mu\rho-c^2(\hat{C}^2-\hat{G}^2)$

and $Q(\sigma)=-2c^2\hat{h}\sigma^4-(\hat{C}^2-2c^2\hat{h})\sigma^2+(\hat{C}^2-\hat{G}^2)$ are two quartics fundamental in this theory.

The qualitative nature of the motion depends on the character of the roots of the quartic equations $P(\rho)=0$ and $Q(\sigma)=0$. There are several cases to distinguish according to different values of the constants of integration $\hat{h}$, $\hat{C}$, $\hat{G}$. In this paper, however, we are interested only in the kind of motion for which $\rho(t)$ oscillates between two real roots ρ_1 and ρ_2 that are bigger than the equatorial radius of the earth, and $\sigma(t)$ oscillates between two real roots $-\sigma_1$ and $+\sigma_1$ that are smaller than 1. The condition $\rho_1=\rho_2$, that is, $\rho(t)\equiv\rho_1$, characterizes "circular" orbits, and the condition $\sigma_1=0$, that is $\sigma(t)\equiv 0$ corresponds to orbits in the equatorial plane of the earth.

Because for $c=0$ (two-body problem) the motion would be elliptic, parabolic, or hyperbolic according as the constant of energy is negative, zero, or positive, it is reasonable to assume that in our problem $\hat{h}<0$. Further, we must have $Q(\sigma)\geqq 0$ during the motion, especially for $\sigma=0$, and this condition gives $\hat{C}^2\geqq\hat{G}^2$. Then it is clear that the equation $Q(\sigma)=0$ will have four real roots σ_1, $-\sigma_1$, σ_2, $-\sigma_2$ with the following properties: $0\leqq\sigma_1<1$, $\sigma_2\gg 1$. For $c=0$ the equation $P(\rho)=0$ would have two positive roots and zero as a double root. The roots for small values of c can differ from these roots only by small amounts; that is, we shall expect two finite roots ρ_1 and ρ_2, corresponding to "perigee" and "apogee" respectively; furthermore, we shall expect two infinitesimal roots ρ_3 and ρ_4, which are in general complex but become real in the case of very small inclinations. We shall have opportunity to return to this point later. It would hardly be worth the labor to obtain the exact, and necessarily rather complicated, algebraic conditions needed for the characterization of all these circumstances.

Let us return to the complete solution (12). Differentiating with respect to $\hat{h}$, $\hat{C}$, $\hat{G}$, we should consider the lower limit ρ_1 as a function of the quantities $\rho_1(\hat{h}, \hat{C}, \hat{G})$. But because the integrand is zero for $\rho=\rho_1$, the result is the same as if ρ_1 were independent of $\hat{h}$, $\hat{C}$, $\hat{G}$. We obtain the following implicit equations for the determination of $\rho(t)$, $\sigma(t)$, $\alpha(t)$:

$$\frac{\partial\hat{W}}{\partial\hat{h}}=\int_{\rho_1}^{\rho}\frac{\rho^2 d\rho}{\sqrt{P(\rho)}}+c^2\int_0^{\sigma}\frac{\sigma^2 d\sigma}{\sqrt{Q(\sigma)}}=t-\hat{t}, \tag{13}$$

$$\frac{\partial\hat{W}}{\partial\hat{C}}=-\hat{C}\int_{\rho_1}^{\rho}\frac{d\rho}{\sqrt{P(\rho)}}+\hat{C}\int_0^{\sigma}\frac{d\sigma}{\sqrt{Q(\sigma)}}=\hat{\omega}, \tag{14}$$

$$\frac{\partial\hat{W}}{\partial\hat{G}}=c^2\hat{G}\int_{\rho_1}^{\rho}\frac{d\rho}{(\rho^2+c^2)\sqrt{P(\rho)}}-\hat{G}\int_0^{\sigma}\frac{d\sigma}{(1-\sigma^2)\sqrt{Q(\sigma)}}+\alpha=\hat{\Omega}. \tag{15}$$

The sign of the square root of $P(\rho)$ has to be considered as positive if ρ is increasing from ρ_1 to ρ_2, but negative if ρ is decreasing from ρ_2 to ρ_1. A similar requirement holds for the square root of $Q(\sigma)$, the limits being $-\sigma_1$ and $+\sigma_1$. The symbols $\hat{t}$, $\hat{\omega}$, and $\hat{\Omega}$ denote three constants of integration whose meanings are related to the time at perigee, the argument of perigee, and the right ascension of the node in a Keplerian motion, respectively. The caret above the letters serves to distinguish the canonical set of elements $\hat{h}$, $\hat{C}$, $\hat{G}$; $-\hat{t}$, $\hat{\omega}$, $\hat{\Omega}$ from other elements to be introduced later, which will be more convenient in the development of the theory. The chief merit of the canonical elements (automatically introduced in the method of separation of the variables) lies in the fact that the variations of these elements in the case of a perturbed motion are described by a canonical system of differential equations.

To represent the coordinates as functions of time we would have to solve equations (13) and (14) for ρ and σ, then substitute $\rho(t)$ and $\sigma(t)$ into equation (15). This is a very hard task to carry out and, by the way, an impractical procedure. Instead, we relate ρ and σ to another "independent"

variable v, analogous to the true anomaly in a Keplerian motion, as follows. If we put

$$\Gamma \int_{\rho_1}^{\rho} \frac{d\rho}{\sqrt{P(\rho)}} = v, \tag{16}$$

where Γ is a constant (depending on $\hat{h}$, $\hat{C}$, $\hat{G}$) to be defined later, equation (14) becomes

$$\hat{C} \int_0^{\sigma} \frac{d\sigma}{\sqrt{Q(\sigma)}} = \frac{\hat{C}}{\Gamma} v + \hat{\omega}. \tag{17}$$

For a certain $\rho=\rho_1$ we will have $v=0$, while $\sigma=0$ will correspond to $v_0=-\Gamma\hat{\omega}/\hat{C}$. If we introduce and use Jacobian elliptic functions, we can easily invert relations (16) and (17) to obtain ρ and σ as functions of v. Then equations (15) and (13) take the form

$$\alpha - \hat{\Omega} = \frac{\hat{G}}{\Gamma} \int_{v_0}^{v} \frac{dv}{1-\sigma^2} - \frac{c^2\hat{G}}{\Gamma} \int_0^{v} \frac{dv}{\rho^2+c^2}, \tag{18}$$

$$t - \hat{t} = \frac{1}{\Gamma} \int_0^{v} \rho^2 dv + \frac{c^2}{\Gamma} \int_{v_0}^{v} \sigma^2 dv. \tag{19}$$

The first of these equations gives α as a function of v; the second is equivalent to Kepler's equation in a Keplerian motion.

Without going into details, we remark that the above simplification of the inversion problem is made possible by the circumstance that α is an ignorable coordinate. If we first carried out the reduction to two degrees of freedom by using the integral $p_\alpha=(\rho^2+c^2)(1-\sigma^2)\dot{\alpha}=\hat{G}$, we would then obtain a dynamical system of Liouville's type.

Introduction of elliptic functions [2]

We propose next to reduce the elliptic integrals of the first kind in equations (16) and (17) to Legendre's normal form.

For this purpose let us seek a linear transformation with real coefficients of the complex ρ-plane,

$$\rho = \frac{p+d_*\xi}{1+e_*\xi}, \tag{20}$$

such that the roots ρ_1, ρ_2, ρ_3, and ρ_4 of the equation $P(\rho)=0$ are mapped onto the points $\xi_1=1$, $\xi_2=-1$, $\xi_3=i/m$, and $\xi_4=-i/m$, respectively. The quantity m is considered to be real or pure imaginary, according as the roots ρ_3 and ρ_4 are (conjugate) complex or real. Because three points and their images already determine a linear transformation, this number m cannot be chosen arbitrarily. Indeed, the cross ratio is an invariant of the linear transformation; that is,

$$\frac{\rho_1-\rho_3}{\rho_1-\rho_4} : \frac{\rho_2-\rho_3}{\rho_2-\rho_4} = \frac{\xi_1-\xi_3}{\xi_1-\xi_4} : \frac{\xi_2-\xi_3}{\xi_2-\xi_4} = \left(\frac{1+im}{1-im}\right)^2.$$

We have to determine p, d_*, e_* and m as functions of the roots ρ_1, ρ_2, ρ_3 and ρ_4; or if the latter are written in the form

$$\rho_1=a(1-e), \qquad \rho_2=a(1+e), \qquad \rho_3=a(\kappa-i\lambda), \qquad \rho_4=a(\kappa+i\lambda), \tag{21}$$

as functions of a, e, κ, and λ. The first two of these equations give the definition of the orbital

[2] Detailed references with regard to elliptic functions seem unnecessary. The book of Whittaker and Watson (1958) can serve as a general reference.

elements a and e; although the orbit is not an exact ellipse, we can still call them the semimajor axis and the eccentricity. It will be shown later how κ and λ are determined as functions of a, e, and s.

The relations $\rho_j=\frac{p+d_*\xi_j}{1+e_*\xi_j}$ $(j=1, 2, 3, 4)$ with the values of ξ_j given above can be written in the form:

$$\begin{aligned} &p+d_*-\rho_1 e_*=\rho_1,\\ &p-d_*+\rho_2 e_*=\rho_2,\\ &-imp+d_*-\rho_3 e_*=-im\rho_3,\\ &imp+d_*-\rho_4 e_*=im\rho_4. \end{aligned} \tag{22}$$

Solving the first two of these equations for p and d_* we obtain

$$\begin{aligned} p&=\frac{\rho_1+\rho_2}{2}-\frac{\rho_2-\rho_1}{2}e_*=a(1-ee_*),\\ d_*&=\frac{\rho_1+\rho_2}{2}e_*-\frac{\rho_2-\rho_1}{2}=a(e_*-e). \end{aligned} \tag{23}$$

Also, transformation (20) becomes

$$\rho=a\frac{(1-ee_*)+(e_*-e)\xi}{1+e_*\xi}=a\left(1-e\frac{e_*+\xi}{1+e_*\xi}\right).$$

In order to obtain convenient relations for the determination of e_* and m, take the sum of the products of equations (22) by $-1, 1, 1, 1$, and use the factors $im, im, 1, -1$ in the same way. These combinations yield:

$$\{(\rho_1+\rho_2)-(\rho_3+\rho_4)\}e_*=\{(\rho_2-\rho_1)+(\rho_4-\rho_3)im\}$$

and

$$\{(\rho_4-\rho_3)+(\rho_2-\rho_1)im\}e_*=\{(\rho_1+\rho_2)-(\rho_3+\rho_4)\}im,$$

or, taking relations (21) into consideration, we obtain:

$$(1-\kappa)e_*=e-\lambda m, \text{ and } (\lambda+em)e_*=(1-\kappa)m. \tag{24}$$

Eliminating e_* or m between these equations, we obtain second-degree equations for the determination of m or e_*, which can be written as

$$\frac{m}{1-m^2}=\frac{e\lambda}{(1-\kappa)^2-(e^2-\lambda^2)} \tag{25}$$

and

$$\frac{e_*}{1+e_*^2}=\frac{(1-\kappa)e}{(1-\kappa)^2+(e^2+\lambda^2)}. \tag{26}$$

Having the choice between two possible values of m and e_*, we require that m and e_* be close to 0 and e, respectively. For $e=0$ both m and e_* vanish.

Now let us apply the linear transformation (20) to the elliptic integral (16). The radicand can be written in the form $P(\rho)=2\hat{h}\prod_{j=1}^{4}(\rho-\rho_j)$, where

$$\rho-\rho_j=\frac{\Delta}{1+e_*\xi}\frac{\xi_j-\xi}{1+e_*\xi_j}, \tag{27}$$

and

$$\Delta=pe_*-d_*=ae(1-e_*^2). \tag{28}$$

As a consequence of our choice of the ξ_j, we have

$$\prod_{j=1}^{4} \frac{\xi_j-\xi}{1+e_*\xi_j}=-\frac{(1-\xi^2)(1+m^2\xi^2)}{(1-e_*^2)(e_*^2+m^2)},$$

so that

$$\sqrt{P(\rho)}=\sqrt{\frac{-2\hat{h}}{(1-e_*^2)(e_*^2+m^2)}}\left(\frac{\Delta}{1+e_*\xi}\right)^2\sqrt{(1-\xi^2)(1+m^2\xi^2)}.$$

On the other hand, $d\rho=-\frac{\Delta}{(1+e_*\xi)^2}\,d\xi$. Consequently, the integral (16) takes the form

$$\frac{-\Gamma}{A_*}\int_0^{\xi}\frac{d\xi}{\sqrt{(1-\xi^2)(1+m^2\xi^2)}}=v, \text{ with } A_*=\sqrt{\frac{-2\hat{h}\Delta^2}{(1-e_*^2)(e_*^2+m^2)}},$$

which is still not Legendre's normal form. That form, however, can be obtained at once by putting

$$\xi=\sqrt{1-\eta^2}, \qquad d\xi=-\eta d\eta/\sqrt{1-\eta^2}; \qquad \frac{\Gamma}{A}\int_0^{\eta}\frac{d\eta}{\sqrt{(1-\eta^2)(1-k^2\eta^2)}}=v,$$

where

$$A=\sqrt{\frac{-2\hat{h}\Delta^2(1+m^2)}{(1-e_*^2)(e_*^2+m^2)}} \tag{29}$$

and

$$k=m/\sqrt{1+m^2}. \tag{30}$$

The inverse functions $\eta(v)$ and $\xi(v)$ are now given by the definition of the Jacobian elliptic functions with modulus k as

$$\eta=\mathrm{sn}\left(\frac{A}{\Gamma}v|k^2\right) \text{ and } \xi=\mathrm{cn}\left(\frac{A}{\Gamma}v|k^2\right).$$

This is the point where we can determine the constant Γ by demanding that the period of the functions $\xi(v)$ should be 2π. Because the real quarter-period of $cn(z|k^2)$ is

$$K=\frac{\pi}{2}\left\{1+\left(\frac{1}{2}\right)^2k^2+\left(\frac{1\cdot 3}{2\cdot 4}\right)^2k^4+\ldots\right\}, \tag{31}$$

we must have $\xi=cn\left(\frac{2K}{\pi}v|k^2\right)$, that is,

$$\Gamma=\frac{\pi}{2K}A. \tag{32}$$

The reduction of the elliptic integral (17) is quite immediate, as the quartic $Q(\sigma)$ contains merely even powers of σ. Let us write

$$Q(\sigma)=(\hat{C}^2-\hat{G}^2)(1-\sigma^2/\sigma_1^2)(1-\sigma^2/\sigma_2^2)$$

and apply the transformation $\sigma/\sigma_1=\zeta$. When we introduce the notation $\sigma_1/\sigma_2=l$, equation (17) becomes

$$\frac{\hat{C}\sigma_1}{\sqrt{\hat{C}^2-\hat{G}^2}}\int_0^{\zeta}\frac{d\zeta}{\sqrt{(1-\zeta^2)(1-l^2\zeta^2)}}=\frac{\hat{C}}{\Gamma}v+\hat{\omega},$$

and this form can be inverted to give the expression $\sigma=\sigma_1 sn\left(\frac{\sqrt{\hat{C}^2-\hat{G}^2}}{\Gamma\sigma_1}(v-v_0)|l^2\right)$, where v_0 means $-\Gamma\hat{\omega}/\hat{C}$ as in equations (18) and (19).

It is advisable to introduce some new notations. First, because σ oscillates between the values $-\sigma_1$ and σ_1, we can think of σ_1 as the sine of the "inclination" I of the orbit; let us denote it by $s=\sin I$. Second, we shall need the real quarter-period L belonging to the modulus l, that is,

$$L=\frac{\pi}{2}\left\{1+\left(\frac{1}{2}\right)^2 l^2+\left(\frac{1\cdot 3}{2\cdot 4}\right)^2 l^4+\ldots\right\}. \tag{33}$$

Third, we define an "argument of perigee" $\bar{\omega}$ as a linear function of v by the equation

$$\frac{2L}{\pi}(v+\bar{\omega})=\frac{\sqrt{\hat{C}^2-\hat{G}^2}}{\Gamma s}(v-v_0).$$

Then if we put $\bar{\omega}=\epsilon v+\omega$, the small quantity

$$\epsilon=\frac{\pi}{2L}\frac{\sqrt{\hat{C}^2-\hat{G}^2}}{\Gamma s}-1 \tag{34}$$

will be the motion of perigee, and

$$\omega=-\frac{\pi}{2L}\frac{\sqrt{\hat{C}^2-\hat{G}^2}}{\Gamma s}v_0=\frac{\pi}{2L}\frac{\sqrt{\hat{C}^2-\hat{G}^2}}{\hat{C}s}\hat{\omega}, \tag{35}$$

a constant close to the canonical element $\hat{\omega}$.

Summarizing the results of this section, we have obtained the explicit representation of the coordinates ρ and σ as functions of the true anomaly v in the following form:

$$\rho=\frac{p+d_*\mathrm{cn}\left(\frac{2K}{\pi}v|k^2\right)}{1+e_*\mathrm{cn}\left(\frac{2K}{\pi}v|k^2\right)} \tag{36}$$

and

$$\sigma=s\,\mathrm{sn}\left(\frac{2L}{\pi}(v+\bar{\omega})|l^2\right). \tag{37}$$

These formulas correspond to $r=\frac{p}{1+e\cos v}$ and $\sin\delta=s\sin(v+\omega)$ in a Keplerian motion.[3]

Determination of the constants e_*, k^2, l^2, and ϵ

In the preceding section we gave the definitions of the orbital elements a, e, and s, which can be thought of as three independent constants of integration replacing the canonical elements $\hat{h}$, $\hat{C}$, and $\hat{G}$. The other fundamental constants e_*, k^2, l^2, and ϵ must be expressed as functions of these orbital elements.

According to the equations (25), (26), and (30), we first of all have to determine the quantities κ and λ in terms of a, e, and s. The coefficients and the roots of the quartic equation $P(\rho)=0$ are related to those of $Q(\sigma)=0$ in the following manner:

$$2a(1+\kappa)=-\mu/\hat{h}$$

$$a^2[(1-e^2)+4\kappa+(\kappa^2+\lambda^2)]=-(\hat{C}^2-2c^2\hat{h})/2\hat{h}=c^2(s^2+s^2/l^2)$$

[3] Just before finishing the manuscript I received a copy of a very interesting paper on the present subject by Davis and Stein (1960), in which the relevant elliptic integrals were reduced by the same transformations that I was using. In other aspects, however, the goal of these authors is quite different from that of my paper. They were primarily concerned with the development of a satellite orbit compntation program, and not with the construction of an analytical theory in the spirit of celestial mechanics. In particular, Davis and Stein do not seem to be interested in the explicit representation of the several fundamental constants as functions of the orbital elements.

$$2a^3[(1-e^2)\kappa+(\kappa^2+\lambda^2)]=-c^2\mu/\hat{h}$$

$$a^4(1-e^2)(\kappa^2+\lambda^2)=-c^2(\hat{C}^2-\hat{G}^2)/2\hat{h}=c^4s^2(s^2/l^2). \tag{38}$$

After introduction of the dimensionless, small parameter $\nu=c/a$, the elimination of $\hat{h}$ between the first and third equations gives $(1-e^2-\nu^2)\kappa+(\kappa^2+\lambda^2)=\nu^2$.

Similarly, eliminating s^2/l^2 between the second and fourth equations we get

$$-4\nu^2s^2\kappa+(1-e^2-\nu^2s^2)(\kappa^2+\lambda^2)=\nu^2s^2(1-e^2-\nu^2s^2).$$

These two equations determine the roots $\rho_3=a(\kappa-i\lambda)$ and $\rho_4=a(\kappa+i\lambda)$ in terms of the orbital elements a, e, and s. We obtain first

$$\kappa=\frac{\nu^2(1-s^2)(1-e^2-\nu^2s^2)}{(1-e^2-\nu^2)(1-e^2-\nu^2s^2)+4\nu^2s^2} \tag{39}$$

and

$$\kappa^2+\lambda^2=\frac{\nu^2s^2(1\{-e^2-\nu^2)(1-e^2-\nu^2s^2)+4\nu^2\}}{(1-e^2-\nu^2)(1-e^2-\nu^2s^2)+4\nu^2s^2}; \tag{40}$$

or, developing in powers of ν^2,

$$\kappa=\frac{\nu^2(1-s^2)}{1-e^2}+\frac{\nu^4(1-s^2)}{(1-e^2)^3}(1-4s^2-e^2)+\ldots \tag{41}$$

and

$$\kappa^2+\lambda^2=\nu^2s^2+\frac{4\nu^4s^2}{(1-e^2)^2}(1-s^2)+\frac{4\nu^6s^2}{(1-e^2)^4}(1-s^2)[(1-3s^2)-(1+s^2)e^2]+\ldots. \tag{42}$$

(Although the present theory is confined to the order of ν^4, the last ν^6 term will be needed in the computation of ϵ, the motion of perigee to the order of ν^4.) Then

$$\lambda^2=\nu^2s^2-\frac{\nu^4}{(1-e^2)^2}(1-s^2)(1-5s^2)+\ldots. \tag{43}$$

This expression shows that for very low inclinations λ becomes imaginary, i.e., ρ_3 and ρ_4 become real, as stated before. The value of the inclination for which λ becomes zero is approximately given by the formula $s^2=\nu^2/(1-e^2)^2$. For artificial satellites of the earth, ν^2 is of the order 10^{-3} and the eccentricity is small, in general; hence this inclination is about 2°.

Returning now to our original purpose, we remark that the last of equations (38) written in the form $l^2=\frac{\nu^2s^2}{1-e^2}\frac{\nu^2s^2}{\kappa^2+\lambda^2}$ and equation (40) give immediately

$$l^2=\frac{\nu^2s^2}{1-e^2}\frac{(1-e^2-\nu^2)(1-e^2-\nu^2s^2)+4\nu^2s^2}{(1-e^2-\nu^2)(1-e^2-\nu^2s^2)+4\nu^2},$$

for the parameter of the elliptic function in equation (37). Or, developing in powers of ν^2, we obtain

$$l^2=\frac{\nu^2s^2}{1-e^2}-\frac{4\nu^4s^2}{(1-e^2)^3}(1-s^2)+\ldots. \tag{44}$$

The quantities e_*, m, and k are given as algebraic functions of the orbital elements by equations (25), (26), (30), (39), and (40). However, since their closed expressions are too complicated to be useful in numerical computations, we instead seek to represent them by power series in ν^2. Putting $e_*=e\{1+\nu^2x+\nu^4y+\ldots\}$, we have $\frac{1+e_*^2}{e_*/e}=(1+e^2)-\nu^2(1-e^2)x+\nu^4[x^2-(1-e^2)y]+\ldots.$ On the other hand, $\frac{(1-\kappa)^2+(e^2+\lambda^2)}{(1-\kappa)}=(1+e^2)-\frac{(1-e^2)\kappa-(\kappa^2+\lambda^2)}{(1-\kappa)}$

$$=(1+e^2)-[(1-e^2)\kappa-(\kappa^2+\lambda^2)]-[(1-e^2)\kappa-(\kappa^2+\lambda^2)]\kappa-\ldots.$$

From equations (41) and (42) it follows that $(1-e^2)\kappa-(\kappa^2+\lambda^2)=\nu^2(1-2s^2)+\frac{\nu^4}{(1-e^2)^2}(1-s^2)(1-8s^2-e^2)+\ldots$, and $[(1-e^2)\kappa-(\kappa^2+\lambda^2)]\kappa=\frac{\nu^4}{1-e^2}(1-s^2)(1-2s^2)$. Then the reciprocal of equation (26) becomes $-\nu^2(1-e^2)x+\nu^4[x^2-(1-e^2)y]+\ldots=-\nu^2(1-2s^2)-\frac{2\nu^4}{(1-e^2)^2}(1-s^2)[(1-5s^2)-(1-s^2)e^2]+\ldots$, and, determining x and y by comparison of the coefficients, we obtain:

$$e_*=e\left\{1+\frac{\nu^2}{1-e^2}(1-2s^2)+\frac{\nu^4}{(1-e^2)^3}[(3-16s^2+14s^4)-2(1-s^2)^2e^2]+\ldots\right\}. \tag{45}$$

The equation (25) for the determination of m as a function of e, κ, and λ, contains also the first power of λ which, because of the branch-point at $s^2=\nu^2/(1-e^2)^2+\ldots$, cannot be represented as a power series in ν^2. In other words, this branch-point is also a singularity of m. Therefore, we shall take the square of equation (25). Working with power series, we can determine immediately the parameter $k^2=m^2/(1+m^2)$ of the elliptic functions in equation (36). Putting $k^2=e^2\{\nu^2x+\nu^4y+\ldots\}$, we have $\frac{m^2}{(1-m^2)^2}=\frac{k^2(1-k^2)}{(1-2k^2)^2}=k^2(1+3k^2+\ldots)=e^2\{\nu^2x+\nu^4(3e^2x^2+y)+\ldots\}$. On the other hand,

$$\left\{\frac{e\lambda}{(1-\kappa)^2-(e^2-\lambda^2)}\right\}^2=\frac{e^2\lambda^2}{(1-e^2)^2}\left\{1+2\left[\frac{2\kappa-(\kappa^2+\lambda^2)}{1-e^2}\right]+\ldots\right\}.$$

From equations (41) and (42) it follows that

$$\frac{2\kappa-(\kappa^2+\lambda^2)}{1-e^2}=\frac{\nu^2}{(1-e^2)^2}[(2-3s^2)+s^2e^2]+\frac{2\nu^4}{(1-e^2)^4}[(1-7s^2+6s^4)-(1-3s^2+2s^4)e^2]+\ldots, \tag{46}$$

and using equation (43) we get

$$\left\{\frac{e\lambda}{(1-\kappa)^2-(e^2-\lambda^2)}\right\}^2=e^2\left\{\frac{\nu^2}{(1-e^2)^2}s^2-\frac{\nu^4}{(1-e^2)^4}[(1-10s^2+11s^4)-2s^4e^2]+\ldots\right\}.$$

A comparison of the coefficients gives x and y, and we obtain

$$k^2=\frac{\nu^2e^2}{(1-e^2)^2}s^2-\frac{\nu^4e^2}{(1-e^2)^4}[(1-10s^2+11s^4)+s^4e^2]+\ldots. \tag{47}$$

The computation of ϵ is somewhat more tedious. It is given by equations (34) and (32), or, what is the same, by

$$1+\epsilon=\frac{\sqrt{\hat{C}^2-\hat{G}^2}}{As}\frac{K}{L}. \tag{48}$$

The quarter-periods K and L can be considered as already known quantities, expressed in terms of the orbital elements by use of equations (31), (33) and (47), (44). Let us transform the expression of A as given by equation (29) into a more convenient one. Recalling equations (21), (27), and (28), we can write

$$2ai\lambda=\rho_4-\rho_3=\frac{\Delta}{1+e_*\xi_4}\frac{\xi_3-\xi_4}{1+e_*\xi_3}=\frac{2\Delta im}{e_*^2+m^2},$$

or

$$\frac{\Delta^2}{(1-e_*^2)(e_*^2+m^2)}=a^2\frac{e\lambda}{m}. \tag{49}$$

Then equations (48) and (29) yield $1+\epsilon=\sqrt{\frac{\hat{C}^2-\hat{G}^2}{-2\hat{h}a^2s^2}}\sqrt{\frac{m}{e\lambda}}\frac{1}{\sqrt{1+m^2}}\frac{K}{L}$. But from the last of equa-

tions (38) we have $\frac{\hat{C}^2-\hat{G}^2}{-2\hat{h}a^2}=(1-e^2)\frac{\kappa^2+\lambda^2}{\nu^2}$, and equation (25) gives $\frac{m}{e\lambda}=\frac{1-m^2}{(1-\kappa)^2-(e^2-\lambda^2)}$; hence,

$$1+\epsilon=\sqrt{\frac{\kappa^2+\lambda^2}{\nu^2 s^2}}\sqrt{\frac{1-e^2}{(1-\kappa)^2-(e^2-\lambda^2)}}\sqrt{\frac{1-m^2}{1+m^2}}\frac{K}{L}.$$

Let us develop this expression into a power series of the small parameter ν^2. The first radicand is given by equation (42), and the third can be written as $\sqrt{1-2k^2}$, by use of equation (30). Developing the second radicand, we use equation (46), as follows:

$$\begin{aligned}\frac{1-e^2}{(1-\kappa)^2-(e^2-\lambda^2)}&=\frac{1}{1-\dfrac{2\kappa-(\kappa^2-\lambda^2)}{1-e^2}}\\&=1+\frac{2\kappa-(\kappa^2+\lambda^2)}{1-e^2}+\left[\frac{2\kappa-(\kappa^2+\lambda^2)}{1-e^2}\right]^2+\cdots\\&=1+\frac{\nu^2}{(1-e^2)^2}[(2-3s^2)+s^2e^2]+\frac{\nu^4}{(1-e^2)^4}[(6-26s^2+21s^4)-(2-10s^2+10s^4)e^2+s^4e^4]+\ldots.\end{aligned}$$

The square roots of this series and of equation (42) are:

$$\sqrt{\frac{1-e^2}{(1-\kappa)^2-(e^2-\lambda^2)}}=1+\frac{\nu^2}{2(1-e^2)^2}[(2-3s^2)+s^2e^2]+\frac{\nu^4}{8(1-e^2)^4}[(20-92s^2+75s^4)-(8-36s^2+34s^4)e^2+3s^4e^4]+\ldots \quad (50)$$

and

$$\sqrt{\frac{\kappa^2+\lambda^2}{\nu^2s^2}}=1+\frac{2\nu^2}{(1-e^2)^2}(1-s^2)-\frac{2\nu^4}{(1-e^2)^4}[(2s^2-2s^4)+(1-s^4)e^2]+\ldots. \quad (51)$$

Furthermore, in virtue of relations (31), (33), (44), and (47), we have

$$\begin{aligned}\sqrt{1-2k^2}\frac{K}{L}&=(1-k^2-k^4/2-\ldots)\frac{1+k^2/4+9k^4/64+\ldots}{1+l^2/4+9l^4/64+\ldots}\\&=1-\frac{1}{4}(3k^2+l^2)-\frac{1}{64}(39k^4-12k^2l^2+5l^4)-\ldots\\&=1-\frac{\nu^2}{4(1-e^2)^2}(s^2+2s^2e^2)+\frac{\nu^4}{64(1-e^2)^4}[(64s^2-69s^4)+(48-544s^2+614s^4)e^2-8s^4e^4]+\ldots. \quad (52)\end{aligned}$$

Multiplying the series (50), (51), and (52), we obtain the motion of perigee as:

$$\epsilon=\frac{\nu^2}{4(1-e^2)^2}(12-15s^2)+\frac{\nu^4}{64(1-e^2)^4}[(288-1296s^2+1035s^4)-(144+288s^2-510s^4)e^2]+\ldots. \quad (53)$$

Development of Fourier series for the right ascension and the generalized Kepler's equation

By now, the coordinates ρ and σ are known functions of the true anomaly v and the orbital elements a, e, and s. These coordinates were represented by the closed expressions (36) and (37), and the relevant constants were given by the series (45), (47), (44), and (53). Our next task is to elaborate the equations (18) and (19) to expedient formulas for the right ascension of the satellite and a generalized Kepler's equation, respectively. Since these equations contain elliptic integrals of the second and third kind, we cannot hope to obtain concise expressions for them. In the spirit of celestial mechanics, we propose to deduce Fourier series well adapted for numerical computations. We would like to point out, however, that the role of these Fourier series is not the same as in the customary constructions of satellite theories, where Fourier series are used from the very beginning

to obtain successive approximations of different orders to the solution. The exact solution of Vinti's dynamical system has already been defined by equations (36), (37), (18), and (19); our problem is "only" to bring the latter two equations to an explicit form. This can be done by developing "known" functions into multiple Fourier series.

To begin with, let us consider the first term in equation (18), which, taking into consideration equation (37), and using the abbreviated notation

$$w=v+\bar{\omega}=(1+\epsilon)v+\omega, \tag{54}$$

we can write

$$\frac{\hat{G}}{\Gamma(1+\epsilon)}\int_0^w \frac{dw}{1-s^2\mathrm{sn}^2\left(\frac{2L}{\pi}w \mid l^2\right)}, \tag{55}$$

where the integral is essentially of the standard form of the elliptic integral of the third kind, and can be expressed by the Jacobian Θ-function with (in our case) imaginary argument. It is instructive, however, to deduce directly the Fourier series of the integrand by the theory of residues, and then to integrate it as follows.

The function $1/[1-s^2\mathrm{sn}^2(z|l^2)]$ of the complex variable z is doubly periodic with periods $2L$ and $2iL'$, regular at all points of the fundamental period-parallelogram $0, 2L, 2L+2iL', 2iL'$, except at two simple poles z_1 and z_2, where the denominator becomes zero. A little consideration shows that, for $l<s<1$, these poles must be of the form $z_1=L+iy$, $z_2=L+2iL'-iy$, with $0<y<L'$. Now let us determine the residues of the above function at these poles by seeking the first terms in its Laurent series. Since the Taylor series of $\mathrm{sn}^2 z$ near $z_j (j=1, 2)$ begins with $\mathrm{sn}^2(z_j+\delta)=\mathrm{sn}^2 z_j + (2\,\mathrm{sn}\,z_j\,\mathrm{cn}\,z_j\,\mathrm{dn}\,z_j)\delta+O(\delta^2)$ and $1-s^2\mathrm{sn}^2\,z_j=0$, we obtain $\{1-s^2\,\mathrm{sn}^2\,(z_j+\delta)\}^{-1}=-\{2s^2\,\mathrm{sn}\,z_j\,\mathrm{cn}\,z_j\,\mathrm{dn}\,z_j\}^{-1}\delta^{-1}+O(1)$. But at the pole z_1 the values of the Jacobian elliptic functions are $\mathrm{sn}\,z_1=1/s$, $\mathrm{cn}\,z_1=-i\sqrt{1-s^2}/s$, $\mathrm{dn}\,z_1=\sqrt{1-l^2/s^2}$; at z_2, on the other hand, $\mathrm{sn}\,z_2=1/s$, $\mathrm{cn}\,z_2=-i\sqrt{1-s^2}/s$, $\mathrm{dn}\,z_2=-\sqrt{1-l^2/s^2}$. Consequently, the residues of the function $1/[1-s^2\,\mathrm{sn}^2(z|l^2)]$ at the poles z_1 and z_2 will be

$$\frac{-i/2}{\sqrt{1-s^2}\sqrt{1-l^2/s^2}} \text{ and } \frac{i/2}{\sqrt{1-s^2}\sqrt{1-l^2/s^2}},$$ and, changing the argument from z to $\frac{2L}{\pi}w$, those of the

integrand in expression (55) will be:

$$\frac{-i\pi/4L}{\sqrt{1-s^2}\sqrt{1-l^2/s^2}} \text{ and } \frac{i\pi/4L}{\sqrt{1-s^2}\sqrt{1-l^2/s^2}}. \tag{56}$$

The coefficients of the Fourier series

$$\frac{1}{1-s^2\mathrm{sn}^2\left(\frac{2L}{\pi}w \mid l^2\right)}=a_0+2\sum_{n=1}^{\infty} a_{2n}\cos 2nw \tag{57}$$

are given by the expression

$$a_{2n}=\frac{1}{\pi}\int_0^{\pi}\frac{\exp(2inw)}{1-s^2\mathrm{sn}^2\left(\frac{2L}{\pi}w|l^2\right)}dw.$$

If we extend the path of integration over the entire period-parallelogram, then from the periodic properties of the elliptic function $\mathrm{sn}\left(\frac{2L}{\pi}w|l^2\right)$ and $\exp(2inw)$ it follows that

$$\oint=\int_0^{\pi}+\int_{\pi}^{\pi+\pi iL'/L}+\int_{\pi+\pi iL'/L}^{\pi iL'/L}+\int_{\pi iL'/L}^{0}=(1-q^{2n})\int_0^{\pi}=\pi(1-q^{2n})a_{2n}, \tag{58}$$

where

$$q=\exp(-\pi L'/L). \tag{59}$$

The only singularity of the function exp $(2inw)$ being at infinity, the residues of the integrand are the values (56) multiplied by exp $(2inw_1)$ and exp $(2inw_2)$ respectively. Here w_1 and w_2 are the points corresponding to z_1 and z_2, namely $\frac{\pi}{2L}(L+iy)=\frac{\pi}{2}+iY$, and $\frac{\pi}{2L}(L+2iL'-iy)=\frac{\pi}{2}+i\pi\frac{L'}{L}-iY$, where $Y=\frac{\pi}{2L}y$, so that using the definition (59), we see that exp $(2inw_1)=(-1)^n$ exp $(-2nY)$ and exp $(2inw_2)=(-1)^n q^{2n}$ exp $(2nY)$. Then, according to the theorem of residues we have

$$\frac{1}{2\pi i}\oint = \text{Res}\,(w_1)+\text{Res}\,(w_2)=\frac{-i\pi/4L}{\sqrt{1-s^2}\sqrt{1-l^2/s^2}}(-1)^n\{\exp(-2nY)-q^{2n}\exp(2nY)\}.$$

Comparison of this result with relation (58) gives, for $n\neq 0$,

$$a_{2n}=\frac{\pi}{2L}\frac{(-1)^n}{\sqrt{1-s^2}\sqrt{1-l^2/s^2}}\frac{\tau^{2n}-(q/\tau)^{2n}}{1-q^{2n}} \tag{60}$$

with

$$\tau=\exp(-Y)=\exp\left(-\frac{\pi}{2L}y\right). \tag{61}$$

This procedure cannot be applied to the determination of the coefficient a_0, because for $n=0$ the divisor $1-q^{2n}$ becomes zero. But substituting $w=0$ in equation (57) we see that the constant term in our Fourier series will be represented by the infinite series

$$a_0=1-2\sum_{n=1}^{\infty}a_{2n}. \tag{62}$$

A consideration of the merits of the method of residues leads to the following remarks. Besides unquestionable elegance, the chief advantage of the method consists in giving an expression for all the coefficients of the Fourier series. In a satellite theory, though, we represent these coefficients in terms of the orbital elements as power series in the small parameter ν^2, and this is not easy if we base this development on equations (60) and (61).[4] For example, we had first to develop the quantity y, then Y and $\tau=\exp(-Y)$, the latter being approximately the tangent of half the inclination. Also, some simple transformations of the expressions (60) and (62) should be made to show that their finite parts (not containing ν^2) are identical with formulas for a Keplerian motion. In the case of the ρ-integrals in equations (18) and (19) we had to handle even more complicated expressions. These difficulties make it advisable to seek for a more elementary process that will yield the first coefficients of the Fourier series in a rather immediate way. From the theoretical point of view, the arguments v and w are the most natural ones: to the equations (36) and (37) there correspond Fourier series whose arguments are multiples of the single arguments v and w, respectively; and equations (18) and (19) give rise to the sum of two such series. In other words, none of these Fourier series contains trigonometric terms with arguments of the form $\alpha v+\beta w$; in particular, there are no long-periodic terms whatsoever. The more elementary process we are going to follow now will make use of other arguments, which are not linearly connected with each other but will permit us to deduce relatively simple formulas well adapted for numerical computations.

Let us consider again expression (55), and introduce a new variable ψ, the so-called amplitude of $\frac{2L}{\pi}w$ by the definition

$$\text{sn}\left(\frac{2L}{\pi}w\,|\,l^2\right)=\sin\psi. \tag{63}$$

[4] Note added on this appearance of paper: A consistent application of the method of residues seems now to me the preferable procedure.

Simultaneously we will have

$$\mathrm{cn}\left(\frac{2L}{\pi}w|l^2\right)=\cos\psi \text{ and } \mathrm{dn}\left(\frac{2L}{\pi}w|l^2\right)=\sqrt{1-l^2\sin^2\psi};$$

moreover,

$$dw=\frac{\pi}{2L}\frac{d\psi}{\sqrt{1-l^2\sin^2\psi}},$$

so that the expression (55) becomes

$$\frac{\hat{G}}{\Gamma(1+\epsilon)}\frac{\pi}{2L}\int_0^{\psi}\frac{d\psi}{(1-s^2\sin^2\psi)\sqrt{1-l^2\sin^2\psi}}. \tag{64}$$

As shown in the theory of elliptic functions,

$$\psi=\mathrm{am}\left(\frac{2L}{\pi}w|l^2\right)=w+2\sum_{n=1}^{\infty}\frac{q^n\sin 2nw}{n(1+q^{2n})},$$

where

$$q=\exp(-\pi L'/L)=\frac{l^2}{16}\left(1+\frac{l^2}{2}+\frac{21\,l^4}{64}+\ldots\right);$$

or, with sufficient accuracy for our purposes,

$$\psi=w+\frac{l^2}{8}\left(1+\frac{l^2}{2}\right)\sin 2w+\frac{l^4}{256}\sin 4w+\ldots, \tag{65}$$

the inverse relation of which is

$$w=\psi-\frac{l^2}{8}\left(1+\frac{l^2}{2}\right)\sin 2\psi+\frac{3}{256}\frac{l^4}{}\sin 4\psi-\ldots. \tag{66}$$

The development of the integrand in expression (64) into a Fourier series turns out to be simpler, if we include in it the constant factor $\frac{\hat{G}}{\Gamma(1+\epsilon)}\frac{\pi}{2L}$. First of all, according to equation (34) we have $\frac{1}{\Gamma(1+\epsilon)}\frac{\pi}{2L}=\frac{s}{\sqrt{\hat{C}^2-\hat{G}^2}}$, and from the second and fourth of equations (38) it follows that $1-\hat{G}^2/\hat{C}^2=\frac{s^2}{1-(1-s^2)\,l^2/s^2}$, or what is essentially the same, $\frac{\hat{G}^2}{\hat{C}^2-\hat{G}^2}=\frac{1-s^2}{s^2}(1-l^2/s^2)$. Hence expression (64) can be brought to the form

$$\int_0^{\psi}\frac{\sqrt{1-s^2}\sqrt{1-l^2/s^2}\,d\psi}{(1-s^2\sin^2\psi)\sqrt{1-l^2\sin^2\psi}}.$$

Proceeding now to its development, we put $\frac{1-l^2/s^2}{1-l^2\sin^2\psi}=1-\frac{l^2}{s^2}\frac{1-s^2\sin^2\psi}{1-l^2\sin^2\psi}$, from which we obtain

$$\sqrt{\frac{1-l^2/s^2}{1-l^2\sin^2\psi}}=1-\frac{1}{2}\frac{l^2}{s^2}\frac{1-s^2\sin^2\psi}{1-l^2\sin^2\psi}-\frac{1}{8}\left(\frac{l^2}{s^2}\frac{1-s^2\sin^2\psi}{1-l^2\sin^2\psi}\right)^2-\ldots$$

$$=1-\frac{l^2}{2s^2}(1-s^2\sin^2\psi)-\frac{l^4}{8s^4}(1-s^2\sin^2\psi)(1+3s^2\sin^2\psi)-\ldots,$$

so that the integral becomes

$$\int_0^{\psi} \frac{\sqrt{1-s^2}\sqrt{1-l^2/s^2}d\psi}{(1-s^2\sin^2\psi)\sqrt{1-l^2\sin^2\psi}} = \int_0^{\psi} \frac{\sqrt{1-s^2}d\psi}{1-s^2\sin^2\psi} - \left[\frac{l^2}{2s^2}+\frac{l^4}{16s^4}(2+3s^2)\right]\sqrt{1-s^2}\psi + \frac{3l^4}{32s^2}\sqrt{1-s^2}\sin 2\psi + \ldots. \quad (67)$$

The elementary integral on the right side is familiar to us from the theory of Keplerian motion:

$$\int_0^{\psi} \frac{\sqrt{1-s^2}d\psi}{1-s^2\sin^2\psi} = \tan^{-1}(\sqrt{1-s^2}\tan\psi).$$

There is not much to say about the second integral in equation (19). Its value is needed only up to $O(\nu^2)$, which turns out to be:

$$\begin{aligned}\int_{v_0}^{v} \sigma^2 dv &= \frac{s^2}{1+\epsilon}\int_0^{w} \mathrm{sn}^2\left(\frac{2L}{\pi}w|l^2\right)dw = \frac{s^2}{1+\epsilon}\frac{\pi}{2L}\int_0^{\psi}\frac{\sin^2\psi}{\sqrt{1-l^2\sin^2\psi}}d\psi \\ &= \frac{s^2}{1+\epsilon}\frac{\pi}{2L}\int_0^{\psi}\left\{\left(\frac{1}{2}+\frac{3l^2}{16}\right)-\left(\frac{1}{2}+\frac{l^2}{4}\right)\cos 2\psi+\frac{l^2}{16}\cos 4\psi-\ldots\right\} \\ &= \frac{s^2}{1+\epsilon}\frac{\pi}{2L}\left\{\left(\frac{1}{2}+\frac{3l^2}{16}\right)\psi-\left(\frac{1}{4}+\frac{l^2}{8}\right)\sin 2\psi+\frac{l^2}{64}\sin 4\psi-\ldots\right\}. \end{aligned} \quad (68)$$

To develop the second integral in equation (18), we define a new variable ϕ, the amplitude of $\frac{2K}{\pi}v$ by the equation

$$\mathrm{sn}\left(\frac{2K}{\pi}v|k^2\right) = \sin\phi, \quad (69)$$

which is analogous to equation (63); the integral to be evaluated is then

$$\int_0^{v}\frac{c^2dv}{\rho^2+c^2} = \frac{\pi}{2K}\int_0^{\phi}\frac{c^2}{\rho^2+c^2}\frac{d\phi}{\sqrt{1-k^2\sin^2\phi}},$$

where

$$\rho = a\frac{(1-ee_*)+(e_*-e)\cos\phi}{1+e_*\cos\phi}. \quad (70)$$

Again, we try to obtain a Fourier series in the argument ϕ by developing first the integrand according to powers of ν^2, which is the only reasonable method we can think of.

Anticipating the not surprising result, that the coefficient of a trigonometric term with argument $n\phi$ will contain e^n as a factor, we shall use here the notations

$$\begin{aligned}\nu_1 &= \frac{\nu^2}{(1-e^2)^2}, \\ k_1 = k^2/e^2 &= \frac{\nu^2}{(1-e^2)^2}s^2+\ldots = \nu_1 s^2+\ldots, \\ \delta_1 = \frac{e_*-e}{(1-e^2)e} &= \frac{\nu^2}{(1-e^2)^2}(1-2s^2)+\ldots = \nu_1(1-2s^2)+\ldots, \end{aligned} \quad (71)$$

so that

$$\frac{c}{\rho} = \sqrt{\nu_1}\frac{1+[1+(1-e^2)\delta_1]e\cos\phi}{(1-\delta_1e^2)+\delta_1e\cos\phi} = \sqrt{\nu_1}\{(1+\delta_1e^2)+e\cos\phi-\delta_1e^2\cos^2\phi+\ldots\},$$

and

$$\frac{1}{\sqrt{1-k^2\sin^2\phi}}=1+\frac{k^2}{2}\sin^2\phi+\ldots=\left(1+\frac{k_1}{2}e^2\right)-\frac{k_1}{2}e^2\cos^2\phi+\ldots.$$

If, as always, we neglect terms of $O(\nu^6)$, we have

$$\frac{c^2/(\rho^2+c^2)}{\sqrt{1-k^2\sin^2\phi}}=\left(\frac{c}{\rho}\right)^2\left\{\left(1+\frac{k_1}{2}e^2\right)-\frac{k_1}{2}e^2\cos^2\phi+\ldots\right\}-\left(\frac{c}{\rho}\right)^4+\cdots,$$

which upon substitution of

$$\left(\frac{c}{\rho}\right)^2=\nu_1\{(1+2\delta_1e^2)+2(1+\delta_1e^2)e\cos\phi+(1-2\delta_1)e^2\cos^2\phi-2\delta_1e^3\cos^3\phi+\ldots\}$$

and

$$\left(\frac{c}{\rho}\right)^4=\nu_1^2\{1+4e\cos\phi+6e^2\cos^2\phi+4e^3\cos^3\phi+e^4\cos^4\phi+\ldots\}$$

becomes

$$\frac{c^2/(\rho^2+c^2)}{\sqrt{1-k^2\sin^2\phi}}=\nu_1\left\{\left[(1-\nu_1)+\left(2\delta_1+\frac{k_1}{2}\right)e^2\right]+[(2-4\nu_1)+(2\delta_1+k_1)e^2]e\cos\phi\right.$$
$$\left.+\left[(1-6\nu_1-2\delta_1)-\frac{k_1}{2}(1-e^2)\right]e^2\cos^2\phi-(4\nu_1+2\delta_1+k_1)e^3\cos^3\phi-\left(\nu_1+\frac{k_1}{2}\right)e^4\cos^2\phi+\ldots\right\}.$$

Expressing the powers of the cosine by cosines of multiple angles, and integrating, we obtain

$$\int_0^\phi\frac{c^2d\phi}{(\rho^2+c^2)\sqrt{1-k^2\sin^2\phi}}=\nu_1\left[(1-\nu_1)+\left(\frac{1}{2}-3\nu_1+\delta_1+\frac{k_1}{4}\right)e^2-\left(\frac{3\nu_1}{8}-\frac{k_1}{16}\right)e^4\right]\phi$$
$$+\nu_1\left[(2-4\nu_1)-\left(3\nu_1-\frac{\delta_1}{2}-\frac{k_1}{4}\right)e^2\right]e\sin\phi+\frac{\nu_1}{2}\left[\left(\frac{1}{2}-3\nu_1-\delta_1-\frac{k_1}{4}\right)-\frac{\nu_1}{2}e^2\right]e^2\sin 2\phi$$
$$-\frac{\nu_1}{3}\left(\nu_1+\frac{\delta_1}{2}+\frac{k_1}{4}\right)e^3\sin 3\phi-\frac{\nu_1}{4}\left(\frac{\nu_1}{8}+\frac{k_1}{16}\right)e^4\sin 4\phi+\ldots. \quad (72)$$

In order to deal with the first integral in equation (19), that is,

$$\int_0^v\rho^2dv=\frac{\pi}{2K}a^2\int_0^\phi\frac{(\rho/a)^2d\phi}{\sqrt{1-k^2\sin^2\phi}},$$

we have to introduce some analogue of the eccentric anomaly in a Keplerian motion. It seemed to us that the following procedure is a quite natural one for this purpose.

The above integrand can be represented up to $O(\nu^4)$ as a linear combination of the functions D^{-2}, D^{-1}, 1, D, D^2 with constant coefficients, where the abbreviation $D=1+e_*\cos\phi$ stands for the denominator of ρ. The integrals of the 1, D, and D^2 terms (all representing "perturbations") can immediately be expressed by ϕ, sin ϕ and sin 2ϕ:

$$\int_0^\phi d\phi=\phi,$$
$$\int_0^\phi Dd\phi=\phi+e_*\sin\phi,$$
$$\int_0^\phi D^2d\phi=\left(1+\frac{e_*^2}{2}\right)\phi+2e_*\sin\phi+\frac{e_*^2}{4}\sin 2\phi. \quad (73)$$

Furthermore, if we define the eccentric anomaly E by

$$\cos E=\frac{e_*+\cos\phi}{1+e_*\cos\phi},\qquad \sin E=\frac{\sqrt{1-e_*^2}\sin\phi}{1+e_*\cos\phi}, \tag{74}$$

so that $\frac{dE}{d\phi}=\frac{\sqrt{1-e_*^2}}{1+e_*\cos\phi}$, then we have

$$\int_0^\phi D^{-2}d\phi=\frac{E-e_*\sin E}{(\sqrt{1-e_*^2})^3},$$

$$\int_0^\phi D^{-1}d\phi=\frac{E}{\sqrt{1-e_*^2}}. \tag{75}$$

As a consequence of this definition of the eccentric anomaly and equation (70) we can write

$$\rho=a(1-e\cos E), \tag{76}$$

which is the same expression as that for the radius vector r in a Keplerian motion.

Turning now to the execution of this development we put

$$\delta_2=(e_*-e)/e_*=\frac{\nu^2}{1-e^2}(1-2s^2)+\frac{\nu^4}{(1-e^2)^3}[(2-12s^2+10s^4)-(1-2s^4)e^2]+\ldots, \tag{77}$$

and

$$k_2=k^2(1-e_*^2)/e_*^2=\frac{\nu^2}{1-e^2}s^2-\frac{\nu^4}{(1-e^2)^3}[(1-8s^2+7s^4)+s^4e^2]+\ldots, \tag{78}$$

to give $(1-ee_*)+(e_*-e)\cos\phi=(1-e_*^2)(1-\delta_2)+\delta_2D$ and $(1-e_*^2)k^2\sin^2\phi=-k_2[(1-e_*^2)-2D+D^2]$. Furthermore we have

$$(1-e_*^2)^{-2}(\rho/a)^2=(1-\delta_2)^2D^{-2}+2(1-\delta_2)\delta_2(1-e_*^2)^{-1}D^{-1}+\delta_2^2(1-e_*^2)^{-2} \tag{79}$$

and

$$\frac{(1-e_*^2)^2}{\sqrt{1-k^2\sin^2\phi}}=(1-e_*^2)^2\left\{1+\frac{k^2}{2}\sin^2\phi+\frac{3k^4}{8}\sin^4\phi+\ldots\right\}=(1-e_*^2)^2\left(1-\frac{k_2}{2}+\frac{3k_2^2}{8}\right)$$
$$+(1-e_*^2)k_2\left(1-\frac{3k_2}{2}\right)D-\frac{k_2}{2}\left[(1-e_*^2)-\frac{3k_2}{2}(3-e_*^2)\right]D^2-\frac{3k_2^2}{8}(4D^3-D^4)+\ldots. \tag{80}$$

Multiplication of equations (79) and (80) yields the integrand in question in the required form:

$$\frac{(\rho/a)^2}{\sqrt{1-k^2\sin^2\phi}}=(1-e_*^2)^2\left[(1-\delta_2)^2-\frac{k_2}{2}\left(1-2\delta_2-\frac{3k_2}{4}\right)\right]D^{-2}$$
$$+(1-e_*^2)\left[2(1-\delta_2)\delta_2+k_2\left(1-3\delta_2-\frac{3k_2}{2}\right)\right]D^{-1}$$
$$-\left[\frac{k_2}{2}(1-e_*^2)-\delta_2^2-k_2\left(\delta_2+\frac{3k_2}{4}\right)(3-e_*^2)\right]-k_2\left(\delta_2+\frac{3k_2}{2}\right)D+\frac{3k_2^2}{8}D^2+\ldots.$$

Now all we have to do is to apply the rules of integration (73) and (75); we obtain

$$\int_0^\phi\frac{(\rho/a)^2d\phi}{\sqrt{1-k^2\sin^2\phi}}=\sqrt{1-e_*^2}\left[(1-\delta_2^2)+\frac{k_2}{2}\left(1-4\delta_2-\frac{9k_2}{4}\right)\right]E$$
$$-\sqrt{1-e_*^2}\left[(1-\delta_2)-\frac{k_2}{2}\left(1-\delta_2-\frac{3k_2}{4}\right)\right]e\sin E$$
$$-\left[\frac{k_2}{2}(1-e_*^2)-\delta_2^2-k_2\left(\delta_2+\frac{9k_2}{16}\right)(2-e_*^2)\right]\phi-k_2\left(\delta_2+\frac{3k_2}{4}\right)e\sin\phi+\frac{3k_2^2}{32}e^2\sin 2\phi+\ldots. \tag{81}$$

Let us remark, in addition, that the above expansion features first the powers of the eccentricity e_* as a factor of the trigonometric terms. These were converted to powers of the eccentricity e by using the relation $e=e_*(1-\delta_2)$. If we neglect quantities of $O(\nu^6)$, this transformation makes a difference only in the coefficient of sin E.

The explicit form of the solution

For purely practical purposes, we have already solved the proposed problem, because equations (18), (19), (36), (37), and the Fourier series (67), (68), (72), (81) of the integrals, together with the definitions of the relevant constants, permit us to compute the position of the satellite for a given time. This form of the results, however, is not completely satisfactory from the theoretical point of view, until we express all the appearing constants explicitly as functions of the orbital elements. No difficulties of principle are involved in carrying out this program, just a few multiplications of power series, of which only terms up to $O(\nu^4)$ are required. As a by-product, we shall have opportunity to define and express the motion of the node and the mean motion of the satellite in an appropriate way.

Let us rewrite equations (18) and (19) corresponding to the results reached in the previous chapter, taking into consideration also the definition (32) of the constant Γ:

$$\alpha-\hat{\Omega}=\int_0^{\psi}\frac{\sqrt{1-s^2}\sqrt{1-l^2/s^2}d\psi}{(1-s^2\sin^2\psi)\sqrt{1-l^2\sin^2\psi}}-\frac{\hat{G}}{A}\int_0^{\phi}\frac{c^2d\phi}{(\rho^2+c^2)\sqrt{1-k^2\sin^2\phi}}, \tag{82}$$

$$t-\hat{t}=\frac{a^2}{A}\left\{\int_0^{\phi}\frac{(\rho/a)^2d\phi}{\sqrt{1-k^2\sin^2\phi}}+\frac{K/L}{1+\epsilon}\nu^2s^2\int_0^{\psi}\frac{\sin^2\psi d\psi}{\sqrt{1-l^2\sin^2\psi}}\right\}. \tag{83}$$

These formulas indicate that we still have to determine the expansions of the constants a^2/A up to $O(\nu^4)$, and $\hat{G}/A$ and $\frac{K/L}{1+\epsilon}$ up to $O(\nu^2)$.

According to equations (28), (29), and (30) we have

$$\frac{\sqrt{-2\hat{h}a^2}}{A}=\sqrt{\frac{e_*^2+k^2(1-e_*^2)}{e^2(1-e_*^2)}}, \tag{84}$$

and the first of equations (38) gives $-2\hat{h}=\frac{\mu}{a(1+\kappa)}$.

It was found convenient to define at this point another semimajor axis and an auxiliary mean motion by the Keplerian relations

$$\hat{a}=\frac{\mu}{-2\hat{h}}=a(1+\kappa) \text{ and } \hat{n}=\sqrt{\frac{\mu}{\hat{a}^3}}; \tag{85}$$

also, we define a "mean anomaly" by $\hat{M}=\hat{n}(t-\hat{t})$. Instead of equation (84) we can then write $\hat{n}\frac{a^2}{A}=\frac{1}{1+\kappa}\sqrt{\frac{e_*^2+k^2(1-e_*^2)}{e^2(1-e_*^2)}}$, or remembering the definitions (77) and (78) of the quantities k_2 and δ_2, we have

$$\hat{n}\frac{a^2}{A}=\frac{1}{\sqrt{1-e_*^2}}\frac{\sqrt{1+k_2}}{(1+\kappa)(1-\delta_2)}. \tag{86}$$

Preparing for the derivation of our final results we obtain the following developments immediately from the definitions of the relevant quantities:

$$\hat{n}=\sqrt{\frac{\mu}{a^3}}\left\{1-\frac{3\nu^2(1-s^2)}{2(1-e^2)}+\frac{3\nu^4(1-s^2)}{8(1-e^2)^3}[(1+11s^2)-(1-5s^2)e^2]-\ldots\right\} \tag{87}$$

and

$$\frac{\sqrt{1+k_2}}{(1+\kappa)(1-\delta_2)}=1-\frac{\nu^2 s^2}{2(1-e^2)}+\frac{\nu^4}{8(1-e^2)^3}[(12-48s^2+39s^4)-(8-16s^2+7s^4)e^2]-\ldots. \tag{88}$$

Let us come to the determination of the constant $\hat{G}/A$. From the second and fourth of equations (38) we have $\frac{\hat{G}^2}{-2\hat{h}a^2}=(1-s^2)(s^2\nu^2/l^2-\nu^2)$, which, combined with equation (84), gives $\frac{\hat{G}}{A}=\sqrt{1-s^2}\sqrt{s^2\nu^2/l^2-\nu^2}\sqrt{\frac{e_*^2/e^2}{1-e_*^2}+k^2/e^2}$. The development of this quantity can be obtained by use of equations (44), (45), and (47) as

$$\frac{\hat{G}}{A}=\sqrt{1-s^2}\left\{1+\frac{\nu^2}{2(1-e^2)^2}[(5-7s^2)+(1-s^2)e^2]+\ldots\right\}. \tag{89}$$

Finally, the third constant to consider becomes simply

$$\frac{K/L}{1+\epsilon}=1+\left(\frac{k^2-l^2}{4}-\epsilon\right)+\ldots=1-\frac{\nu^2}{2(1-e^2)^2}[(6-7s^2)-s^2e^2]+\ldots. \tag{90}$$

How to express equations (82) and (83) in an explicit form is now obvious. In formulas (67), (68), (72), and (81) we have to substitute the developments (44), (71), (47), (77), and (78) of the figuring constants, and carry out the multiplication by the constants (89), (86), and (90). The details of these elementary but somewhat lengthy operations will not be given here; rather we confine ourselves to giving the results, which are:

$$\begin{aligned}\alpha-\hat{\Omega}=&\tan^{-1}(\sqrt{1-s^2}\tan\psi)-\left\{\frac{\nu^2\sqrt{1-s^2}}{2(1-e^2)}-\frac{\nu^4\sqrt{1-s^2}}{16(1-e^2)^3}[(30-35s^2)+(2+3s^2)e^2]\right\}\psi\\
&+\frac{3\nu^4\sqrt{1-s^2}}{32(1-e^2)^2}s^2\sin 2\psi-\left\{\frac{\nu^2\sqrt{1-s^2}}{2(1-e^2)^2}(2+e^2)+\frac{\nu^4\sqrt{1-s^2}}{16(1-e^2)^4}[(24-56s^2)-(4+64s^2)e^2-(2+3s^2)e^4]\right\}\phi\\
&-\left\{\frac{2\nu^2\sqrt{1-s^2}}{(1-e^2)^2}+\frac{\nu^4\sqrt{1-s^2}}{4(1-e^2)^4}[(4-28s^2)-(6+7s^2)e^2]\right\}e\sin\phi\\
&-\left\{\frac{\nu^2\sqrt{1-s^2}}{4(1-e^2)^2}-\frac{\nu^4\sqrt{1-s^2}}{8(1-e^2)^4}[11+(1+s^2)e^2]\right\}e^2\sin 2\phi\\
&+\frac{\nu^4\sqrt{1-s^2}}{4(1-e^2)^4}(2-s^2)e^3\sin 3\phi+\frac{\nu^4\sqrt{1-s^2}}{64(1-e^2)^4}(2+s^2)e^4\sin 4\phi+O(\nu^6)\end{aligned} \tag{91}$$

and

$$\begin{aligned}\hat{M}=\hat{n}(t-\hat{t})=&E-\left\{1-\frac{\nu^2(1-s^2)}{1-e^2}+\frac{\nu^4(1-s^2)}{(1-e^2)^3}s^2(3+e^2)\right\}e\sin E\\
&-\left\{\frac{\nu^2\sqrt{1-e^2}}{2(1-e^2)}s^2-\frac{\nu^4\sqrt{1-e^2}}{16(1-e^2)^3}[(24-96s^2+78s^4)-(8-11s^2)s^2e^2]\right\}\phi-\frac{\nu^4\sqrt{1-e^2}}{4(1-e^2)^3}(4-5s^2)s^2e\sin\phi\\
&+\frac{3\nu^4\sqrt{1-e^2}}{32(1-e^2)^3}s^4e^2\sin 2\phi+\left\{\frac{\nu^2\sqrt{1-e^2}}{2(1-e^2)}-\frac{\nu^4\sqrt{1-e^2}}{16(1-e^2)^3}[(24-27s^2)-(8-11s^2)e^2]\right\}s^2\psi\\
&-\left\{\frac{\nu^2\sqrt{1-e^2}}{4(1-e^2)}-\frac{\nu^4\sqrt{1-e^2}}{8(1-e^2)^3}[(6-7s^2)-(2-3s^2)e^2]\right\}s^2\sin 2\psi+\frac{\nu^4\sqrt{1-e^2}}{64(1-e^2)^2}s^4\sin 4\psi+O(\nu^6).\end{aligned} \tag{92}$$

The connection between the arguments ϕ and ψ is expressed according to equations (54) and (66), and the analogous equations for the argument v, by the relation

$$\psi-\frac{l^2}{8}\left(1+\frac{l^2}{2}\right)\sin 2\psi+\frac{3l^4}{256}\sin 4\psi-\ldots=(1+\epsilon)\left\{\phi-\frac{k^2}{8}\left(1+\frac{k^2}{2}\right)\sin 2\phi+\frac{3k^4}{256}\sin 4\phi-\ldots\right\}+\omega. \quad (93)$$

It seems appropriate to comment on the developments in this paper with the same reminder Dr. Brouwer used in the conclusion to his paper (1959): "Anyone who has ever carried out developments of the type presented here knows that extreme caution is necessary if errors are to be avoided, even if the method used is straightforward."

All the necessary computations I performed at least twice, and in two different ways whenever possible. Unfortunately, such a procedure in itself cannot guarantee that there is not a single mistake in the formulas.

I make some further remarks concerning the derivation and form of the results. Certain simplifications in the formulas suggest that by handling the constants in a more efficient way it should be possible to arrive at a shorter derivation of expressions (91) and (92). (For instance, due to the definition (85) of the quantity $\hat{n}$, the coefficient of the eccentric anomaly E becomes 1. This is in agreement with earlier, unpublished results of the present writer. Furthermore, the coefficient of $e \sin E$ is simply $-1/(1+\kappa)$, at least up to $O(\nu^4)$.) Admittedly, it would be more elegant to use the linearly connected arguments v and w in the developments instead of ϕ and ψ.

A rather pleasant job has still to be done, namely, the determination of the motion of the node and that of the anomalistic and draconitic mean motion of the satellite.

Since we have not yet mentioned the "plane" of the orbit, we have had no chance to define its ascending node on the equator, whose mean rate of change should be obtained now. The idea of the motion of the node comes originally from perturbation theories based on the concept of osculating orbital elements. In a theory like this one, which uses a pure coordinate method, the motion of the node can nevertheless be defined in a formal way.

Let us consider again the expressions (91) and (92), in which the fundamental arguments are ϕ and ψ, the first being a "true anomaly" and the second an "argument of latitude." As known from the theory of Keplerian motion, the following expansions hold true:

$$\tan^{-1}\left(\sqrt{1-s^2}\tan\psi\right)=\psi+\sum_{j=1}^{\infty}\frac{(-\tau^2)^j}{j}\sin 2j\psi,$$

where $s=\sin I$, $\tau=\tan\frac{I}{2}$, and $E=\phi+2\sum_{j=1}^{\infty}\frac{(-\vartheta)^j}{j}\sin j\phi$, where $\vartheta=(1-\sqrt{1-e_*^2})/e_*=\frac{e_*}{2}\left(1+\frac{e_*^2}{4}+\ldots\right)$.

This means that equations (91) and (92) could be written in the forms

$$\alpha-\hat{\Omega}=(1+\delta)\psi+\theta\phi+D(\psi)+F(\phi) \quad (94)$$

and

$$(1+\beta)\phi+\gamma\psi+B(\phi)+C(\psi)=\hat{M}, \quad (95)$$

where δ, θ, β, and γ are constants of $O(\nu^2)$, and the Latin capitals denote Fourier series in the indicated arguments. We are not going to substitute series expansions for closed expressions in any practical application, of course. All we are interested in is the possibility of these expansions, and the fact that we can read off the coefficients of the secular terms immediately from equations (91) and (92); we shall need them soon. Moreover, according to equation (93), the relation between the arguments ϕ and ψ is of the form

$$-(1+\epsilon)\phi+\psi+G(\phi)+H(\psi)=\omega, \quad (96)$$

where, as before, ϵ is the motion of perigee given by equation (53), and the Fourier series $G(\phi)$ and $H(\psi)$ are of $O(\nu^2)$.

When the argument ψ increases from 0 to 2π, i.e., the satellite makes a complete revolution with respect to the equator, the right ascension α changes by 2π minus a quantity of $O(\nu^2)$. This small amount can be thought of as the regression of the node, yet it is in general not the same for consecutive revolutions. But equations (94) and (96) imply that $\lim_{\Delta\psi\to\infty} \frac{\alpha(\psi+\Delta\psi)-\alpha(\psi)}{\Delta\psi}$ exists, its value being $(1+\delta)+\theta/(1+\epsilon)$. We can call the small quantity $\eta=\delta+\frac{\theta}{1+\epsilon}$ the motion of the node. Comparison of equation (91) and (94) yields the values of the constants δ and θ, and ϵ is already known. In this way we obtain for the motion of the node the formula

$$\eta=-\frac{3\nu^2\sqrt{1-s^2}}{2(1-e^2)^2}+\frac{3\nu^4\sqrt{1-s^2}}{16(1-e^2)^4}[(18-13s^2)+24s^2e^2]-\ldots. \tag{97}$$

To determine the anomalistic and draconitic mean motion of the satellite we proceed as follows. Ignoring their physical meaning in connection with the motion of a satellite, let us consider equations (95) and (96) as relations between two pairs of variables, partly ϕ and ψ, partly $\hat{M}$ and ω. We are interested in periodicity properties of the functions defined by these equations. First of all, it is clear that for any integers i and j the identities $\hat{M}(\phi+2\pi i,\ \psi+2\pi j)-\hat{M}(\phi,\ \psi)=2\pi i(1+\beta)+2\pi j\gamma$, and $\omega(\phi+2\pi i,\ \psi+2\pi j)-\omega(\phi,\ \psi)=-2\pi i(1+\epsilon)+2\pi j$ are valid. To simplify them, we shall perform the linear transformation $\hat{M}=(1+\beta)M+\gamma N,\ \omega=-(1+\epsilon)M+N$, the inverse of which is $M=\frac{\hat{M}-\gamma\omega}{(1+\beta)+(1+\epsilon)\gamma},\ N=\frac{(1+\epsilon)\hat{M}+(1+\beta)\omega}{(1+\beta)+(1+\epsilon)\gamma}$. The periodicity properties of the functions $M(\phi,\ \psi)$ and $N(\phi,\ \psi)$ will be expressed by the identities $M(\phi+2\pi i,\ \psi+2\pi j)-M(\phi,\ \psi)=2\pi i$ and $N(\phi+2\pi i,\ \psi+2\pi j)-N(\phi,\ \psi)=2\pi j$. Then a little consideration reveals that, if we assume the existence of uniquely determined inverse functions $\phi(M,\ N)$ and $\psi(M,\ N)$, their periodicity properties must be the same, that is,

$$\begin{aligned}\phi(M+2\pi i,\ N+2\pi j)-\phi(M,\ N)&=2\pi i\\ \psi(M+2\pi i,\ N+2\pi j)-\psi(M,\ N)&=2\pi j.\end{aligned} \tag{98}$$

As we see, the inversion problem of the basic equations (13), (14), and (15) has been changed to that of the equations (92) and (93); in this altered form, however, the problem is almost trivial.

Now, equations (98) mean that the functions $\phi(M,\ N)-M$, and $\psi(M,\ N)-N$ can be expressed as Fourier series in the two arguments M and N. Consequently, if we again consider $\hat{M}$, M and N as linear functions of the time, and define the anomalistic and draconitic mean motion of the satellite by the limits $n_\phi=\lim_{T\to\infty}\frac{\phi(t+T)-\phi(t)}{T}$, $n_\psi=\lim_{T\to\infty}\frac{\psi(t+T)-\psi(t)}{T}$, then we have

$$n_\phi=\frac{\hat{n}}{(1+\beta)+(1+\epsilon)\gamma}=\hat{n}\left\{1-\frac{3\nu^4\sqrt{1-e^2}}{16(1-e^2)^3}(8-32s^2+25s^4)+\ldots\right\}, \tag{99}$$

and

$$n_\psi=(1+\epsilon)n_\phi. \tag{100}$$

It is interesting to observe that up to $O(\nu^2)$ the mean motion n_ϕ depends only on the total energy h of the system.

Summary

The second-order solution of Vinti's dynamical problem is represented in the following form, well adapted for numerical computations.

The radius vector and the sine of the declination are given by the formulas

$$r=a\sqrt{(1-e\cos E)^2+\nu^2(1-s^2\sin^2\psi)}, \qquad \sin\delta=\frac{s\sin\psi}{\sqrt{1+\nu^2\dfrac{1-s^2\sin^2\psi}{(1-e\cos E)^2}}}.$$

Actually, these expressions are exact, i.e., valid to any order of approximation. They can be thought of as representing a transformation from the coordinates r and δ to the angular variables E and ψ. Then the right ascension of the satellite and the generalized Kepler's equation are found to be the Fourier series with secular terms, (91) and (92). The relation between the true anomaly ϕ and the argument of latitude ψ is expressed by equation (93), and equation (74) is the definition of the eccentric anomaly E.

The orbital elements a, e, $s=\sin I$, $\hat{i}$, $\hat{\Omega}$, and ω serve as the fundamental constants of integration. Other important constants are:

a second eccentricity, e_*;
the parameters k^2 and l^2 of the elliptic functions encountered in this theory;
the motion of the perigee, ϵ;
the motion of the node, η;
the auxiliary mean motion of the satellite, $\hat{n}$
the anomalistic and draconitic mean motions of the satellite, n_ϕ and $n_\psi=(1+\epsilon)n_\phi$.

These constants are given as functions of the orbital elements by the expansions (45), (47), (44), (53), (97), (87), and (99).

No small divisors appear in this theory; neither ϵ, which becomes 0 in the case of the critical inclination 63°26′, nor e, which is troublesome in some methods using orbital elements instead of coordinates. The absence of ϵ as a divisor reflects the fact that the solution of Vinti's dynamical problem can be exactly represented by (rapidly) convergent trigonometric series. The absence of e as a divisor lends itself to a discussion of the case of very small eccentricities.[6] This problem and the perturbations due to the potential $V-\hat{V}$ will be treated later in another paper.

Appendix

For the sake of completeness, I give here the expressions for the right ascension of the satellite and the generalized Kepler equation, in case one prefers to use the arguments v and $w=(1+\epsilon)v+\omega$ instead of ϕ and ψ:

$$\alpha-\Omega_*=\tan^{-1}\left\{\sqrt{1-s^2}\,\mathrm{tn}\left(\frac{2L}{\pi}w\middle|l^2\right)\right\}-\left\{\frac{3\nu^2\sqrt{1-s^2}}{2(1-e^2)^2}-\frac{3\nu^4\sqrt{1-s^2}}{16(1-e^2)^4}[(18-13s^2)+24s^2e^2]\right\}w$$
$$+\frac{\nu^4\sqrt{1-s^2}}{32(1-e^2)^2}s^2\sin 2w-\left\{\frac{2\nu^2\sqrt{1-s^2}}{(1-e^2)^2}+\frac{\nu^4\sqrt{1-s^2}}{8(1-e^2)^4}[(8-56s^2)-(12+13s^2)e^2]\right\}e\sin v$$
$$-\left\{\frac{\nu^2\sqrt{1-s^2}}{4(1-e^2)^2}-\frac{\nu^4\sqrt{1-s^2}}{16(1-e^2)^4}[(22-2s^2)+(2+s^2)e^2]\right\}e^2\sin 2v$$
$$+\frac{\nu^4\sqrt{1-s^2}}{8(1-e^2)^4}(4-3s^2)e^3\sin 3v+\frac{\nu^4\sqrt{1-s^2}}{64(1-e^2)^4}(2-s^2)e^4\sin 4v+O(\nu^6),$$

[6] After the completion of this paper, I found that a very interesting investigation into the geometry of satellite orbits has appeared in several recent papers by Strubel, the latest of which (Strubel, 1960) seems to be the most complete. He paid special attention to the problem of very small eccentricities, and to that of the critical inclination.

and

$$M_*=\hat{n}(t-t_*)=E-\left\{1-\frac{\nu^2(1-s^2)}{1-e^2}+\frac{\nu^4(1-s^2)}{(1-e^2)^3}\,s^2(3+e^2)\right\}\,e\sin E$$
$$+\frac{3\nu^4\sqrt{1-e^2}}{16(1-e^2)^3}\,(8-32s^2+25s^4)v-\frac{\nu^4\sqrt{1-e^2}}{4(1-e^2)^3}\,(4-5s^2)s^2e\sin v+\frac{\nu^4\sqrt{1-e^2}}{32(1-e^2)^3}\,s^4e^2\sin 2v$$
$$-\left\{\frac{\nu^2\sqrt{1-e^2}}{4(1-e^2)}-\frac{\nu^4\sqrt{1-e^2}}{16(1-e^2)^3}\,[(12-13s^2)-(4-5s^2)e^2]\right\}s^2\sin 2w-\frac{\nu^4\sqrt{1-e^2}}{64(1-e^2)^2}\,s^4\sin 4w+O(\nu^6).$$

The differences between Ω_* and $\hat{\Omega}$ and between M_* and $\hat{M}$ are constants of $O(\nu^2)$. This form of the results is easily derived from equations (91) and (92) by substituting into these equations the expansions

$$\phi=v+\frac{\nu^2s^2e^2}{8(1-e^2)^2}\sin 2v+\ldots,$$

$$\psi=w+\frac{\nu^2s^2}{8(1-e^2)}\sin 2w+\ldots,$$

$$\sin\phi=\left[1+\frac{\nu^2s^2e^2}{16(1-e^2)^2}\right]\sin v+\frac{\nu^2s^2e^2}{16(1-e^2)^2}\sin 3v+\ldots,$$

$$\sin 2\phi=\sin 2v+\frac{\nu^2s^2e^2}{8(1-e^2)^2}\sin 4v+\ldots,$$

$$\sin 2\psi=\sin 2w+\frac{\nu^2s^2}{8(1-e^2)}\sin 4w+\ldots.$$

If the inclination is near 90°, the right ascension does not seem to be a proper coordinate of the satellite, because its finite part becomes a discontinuous function of w for $s=1$. To avoid this unessential singularity, we could obtain another interesting and useful form of the results by introducing a slowly rotating reference plane, with constant inclination I, and right ascension of the ascending node $\bar{\Omega}=\Omega_*+\eta w$.

Effects of Solar-Radiation Pressure on the Motion of an Artificial Satellite

By Yoshihide Kozai

The effects of solar-radiation pressure on the motion of an artificial satellite have been studied by several authors (Musen, 1960; Parkinson, Jones, and Shapiro, 1960). As they predicted, the orbit of Satellite 1960 ι 1 (Echo I) has been greatly affected by the solar-radiation pressure (Shapiro and Jones, 1960). And even for Satellite 1958 $\beta 2$ (Vanguard I), which is of moderate size, Musen, Bryant, and Bailie (1960) found that the discrepancy between the observed and computed values of perigee height could be explained by the solar-radiation effect.

When the author (Kozai, 1959a, 1961b) derived several constants of the earth's gravitational potential from the motion of artificial satellites, he did not take this effect into consideration. Although the effect is very small for the average satellite, it must be considered in the future in the reduction of observations.

In the present paper the author wants to study this problem in order to reduce the observations of satellites of moderate size. The analytical expressions for the perturbations of the first order are easily obtained; however, the two limits of integration are derived by numerical methods.

Disturbing functions

The equations of variations to be solved are the following:

$$\frac{da}{dt}=\frac{2na^3}{\sqrt{1-e^2}}F\left\{S(v)\sin v+T(v)\frac{p}{r}\right\},$$

$$\frac{de}{dt}=na^2\sqrt{1-e^2}F\left[S(v)\sin v+T(v)\left\{\cos v+\frac{1}{e}\left(1-\frac{r}{a}\right)\right\}\right],$$

$$\frac{di}{dt}=\frac{na^2}{\sqrt{1-e^2}}WF\frac{r}{a}\cos L,$$

$$\sin i\frac{d\Omega}{dt}=\frac{na^2}{\sqrt{1-e^2}}WF\frac{r}{a}\sin L,$$

$$\frac{d\omega}{dt}=-\cos i\frac{d\Omega}{dt}+na^2\frac{\sqrt{1-e^2}}{e}F\left[-S(v)\cos v+T(v)\left(1+\frac{r}{p}\right)\sin v\right],$$

$$\frac{dM}{dt}=n-2a^2FS(v)\frac{r}{a}-\sqrt{1-e^2}\left(\frac{d\omega}{dt}+\cos i\frac{d\Omega}{dt}\right), \quad (1)$$

where the conventional notations are used for the orbital elements, $L=v+\omega$, $p=a(1-e^2)$; $n^2a^3FS(v)$, $n^2a^3FT(v)$, and n^2a^3FW are three components of the disturbing force due to the solar-radiation pressure in the direction of the radius vector of the satellite, in the direction perpendicular to it in the orbital plane, and in the normal to the orbital plane; and F is a product of the area-mass ratio, solar-radiation pressure, and a reciprocal of GM.

To derive the expressions of $S(v)$, $T(v)$, and W, we make the following assumptions:

(1) The distance of the sun and the satellite is infinite; that is, the parallax of the sun is negligible.

(2) The solar flux is constant along the orbit of the satellite if there is no shadow.

(3) There is no re-radiation from the surface of the earth.

Then the expressions are the following:

$$S(v)=-\cos^2\frac{i}{2}\cos^2\frac{\epsilon}{2}\cos(\lambda_\odot-L-\Omega)-\sin^2\frac{i}{2}\sin^2\frac{\epsilon}{2}\cos(\lambda_\odot+\Omega-L)$$

$$-\frac{1}{2}\sin i \sin\epsilon \{\cos(\lambda_\odot - L) - \cos(-\lambda_\odot - L)\}$$
$$-\sin^2\frac{i}{2}\cos^2\frac{\epsilon}{2}\cos(\Omega-\lambda_\odot-L)$$
$$-\cos^2\frac{i}{2}\sin^2\frac{\epsilon}{2}\cos(-\lambda_\odot-L-\Omega),$$

$$W=\sin i\cos^2\frac{\epsilon}{2}\sin(\lambda_\odot-\Omega) - \sin i\sin^2\frac{\epsilon}{2}\sin(\lambda_\odot+\Omega) - \cos i\sin\epsilon\sin\lambda_\odot, \quad (2)$$

where $\lambda_\odot$ is the longitude of the sun, and ϵ is the obliquity. The expression of $T(v)$ is obtained if cos in $S(v)$ is replaced by sin except for the trigonometrical terms with an argument i, ϵ, $i/2$, or $\epsilon/2$.

Solutions

There is a very important difference between the solar-radiation force and the gravitational force. The solar-radiation force is sometimes a discontinuous function of time because when the satellite enters the shadow, its motion is free from this effect.

Suppose that the satellite exits from the shadow at a point where the corresponding eccentric anomaly of the satellite is E_1, and enters the shadow at E_2. If the force is continuous, the integral of the short-periodic effect can be neglected. However, for this case there is a possibility that this effect will be cumulative to a certain amount during a long interval of time. Therefore, the short-periodic terms must be kept in the solutions.

By use of the eccentric anomaly E as the independent variable, the perturbations of the first order after one revolution can be derived in closed forms as follows:

$$\delta a = 2a^3F\Big|(S\cos E + T\sqrt{1-e^2}\sin E)\Big|_{E_1}^{E_2},$$

$$\delta e = a^2F\sqrt{1-e^2}\Big[\Big|\frac{1}{4}S\sqrt{1-e^2}\cos 2E + T\Big(-2e\sin E+\frac{1}{4}\sin 2E\Big)\Big|_{E_1}^{E_2} + \frac{3}{2}\int T dE\Big],$$

$$\delta i = a^2F\frac{W}{\sqrt{1-e^2}}\Big[\Big|\Big\{(1+e^2)\sin E - \frac{e}{4}\sin 2E\Big\}\cos\omega + \sqrt{1-e^2}\Big(\cos E-\frac{e}{4}\cos 2E\Big)\sin\omega\Big|_{E_1}^{E_2} - \frac{3}{2}e\int W\cos\omega dE\Big],$$

$$\sin i\,\delta\Omega = a^2F\frac{W}{\sqrt{1-e^2}}\Big[\Big|\Big\{(1+e^2)\sin E - \frac{e}{4}\sin 2E\Big\}\sin\omega - \sqrt{1-e^2}\Big(\cos E-\frac{e}{4}\cos 2E\Big)\cos\omega\Big|_{E_1}^{E_2} - \frac{3}{2}e\int W\sin\omega dE\Big],$$

$$\delta\omega = -\cos i\,\delta\Omega + a^2F\frac{\sqrt{1-e^2}}{e}\Big[\Big|S\Big(e\sin E+\frac{1}{4}\sin 2E\Big) + T\sqrt{1-e^2}\Big(e\cos E - \frac{1}{4}\cos 2E\Big)\Big|_{E_1}^{E_2} - \frac{3}{2}\int S dE\Big],$$

$$\delta M = -\frac{3}{2}\int_0^{2\pi}\frac{\delta a}{a}dM - \sqrt{1-e^2}\,\delta\omega - \sqrt{1-e^2}\cos i\,\delta\Omega - 2a^2F\Big[\Big|S\{(1+e^2)\sin E - \frac{e}{4}\sin 2E\} - T\sqrt{1-e^2}(\cos E - \frac{e}{4}\cos 2E)\Big|_{E_1}^{E_2} - \frac{3}{2}e\int S dE\Big], \quad (3)$$

where the limits of integration are E_1 and E_2 unless other values are written; S and T are the expressions of $S(v)$ and $T(v)$, in which L is replaced by ω; that is,

$$S = S(0),$$
$$T = T(0). \quad (4)$$

If the satellite does not enter the shadow during one revolution, the terms depending explicitly on E vanish, and in particular, δa vanishes.

In the expressions of $\delta\omega$ and $\delta\Omega$, indirect effects of the solar-radiation pressure through $\dot{\omega}$ and $\dot{\Omega}$ must be considered as follows:

$$\frac{d\delta\omega}{dt}=\frac{d\dot{\omega}}{de}\delta e+\frac{d\dot{\omega}}{di}\delta i+\frac{d\dot{\omega}}{da}\delta a,$$

$$\frac{d\delta\Omega}{dt}=\frac{d\dot{\Omega}}{de}\delta e+\frac{d\dot{\Omega}}{di}\delta i+\frac{d\dot{\Omega}}{da}\delta a. \qquad (5)$$

Shadow equation

If the geocentric angular distance between the sun and the satellite is denoted by α, the shadow boundary is expressed by the equation,

$$r\sin\alpha=a_{\oplus}, \qquad (6)$$

where $a_{\oplus}$ is the radius of the earth and is assumed to be constant. The following relations hold among r/a, E, S, T and α:

$$\frac{r}{a}\cos\alpha=-S(\cos E-e)-T\sqrt{1-e^2}\sin E,$$

$$\frac{r}{a}=1-e\cos E. \qquad (7)$$

If ω, Ω, and $\lambda_{\odot}$ are assumed to be constant during one revolution of the satellite, S, T and e can also be regarded as constant; then E can be derived from equation (6).

However, as the equation is of the fourth degree with respect to sin E or cos E, it is very difficult to get general analytical solutions except for a circular orbit. If the orbit is circular, the terms of odd powers of sin E or cos E disappear, and the equation becomes quadratic for $\cos^2 E$ or $\sin^2 E$. And it is almost impossible to expand the solutions into power series of the eccentricity because of slow convergency. Even if the series is convergent, it is possible that the equation has no real root even though the equation has two real roots for the circular orbit, and *vice versa*.

Therefore, the author thinks that equation (7) must be solved numerically for every revolution. There are four roots; however, under a condition that cos α must be negative, the number reduces to two, at most. If there is no real root, the satellite does not enter the shadow. And if there is only one real root, the satellite touches the shadow at one point.

Numerical examples

The author has devised a program to calculate these effects on the IBM–704 computer. This program computes the inequalities of the orbital elements due to the solar-radiation pressure, if the approximate expressions of the orbital elements are known.

As an example, inequalities of the orbital elements for Satellite 1958 β 2 during the period 36526–36615 (Modified Julian Days) are plotted in figure 1. This computation is based on an estimated acceleration of 9.7×10^{-6} cm/sec^2 (Musen, Bryant, and Bailie, 1960). The semimajor axis is expressed in earth equatorial radii, and the mean anomaly is in revolutions. The author (Kozai, 1961b) earlier used the same observations to derive geodetic constants; the effect of the solar-radiation pressure was partly taken into account in that reduction.

The perturbations for Satellite 1960 ι1 have been roughly computed by this program, and have been checked with observed values. As the eccentricity is small (order of 10^{-2}), the change of the argument of perigee is very rapid due to the solar radiation. For this case it is

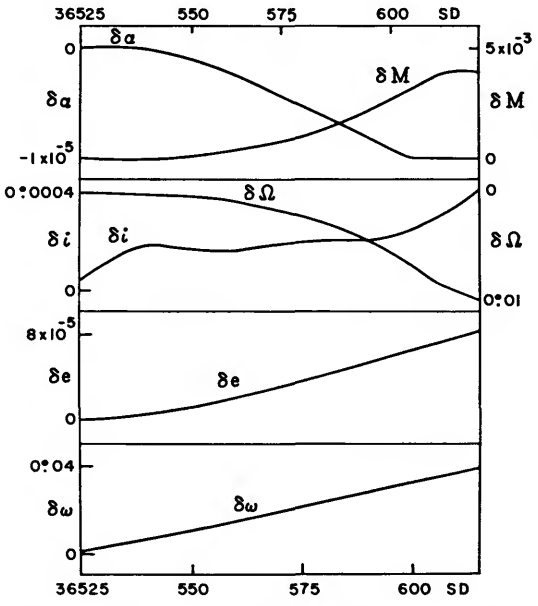

FIGURE 1.—Inequalities of the orbital elements due to the solar-radiation pressure for Satellite 1958 β2.

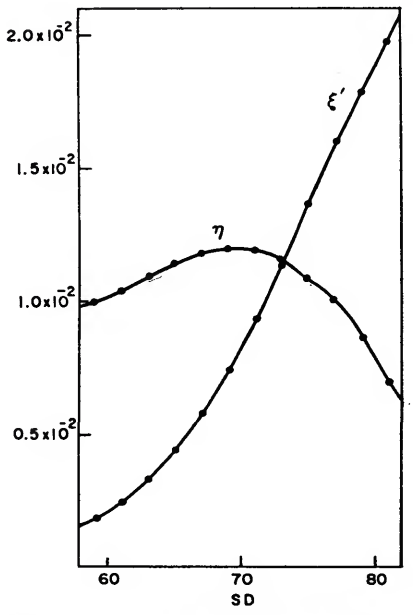

FIGURE 2.—Variations of ξ' and η for Satellite 1960 ι1 with observed values represented by dots. Epochs are given in 37100 (MJD).

better to use, instead of e and ω, $\xi=e \sin \omega$, $\eta=e \cos \omega$.

The following expressions are derived under an assumption that the satellite never enters the shadow, and they are compared with observations in figure 2:

$$\xi=\xi'+0.00066,$$

$$\xi'=0.04409 \sin (91^\circ.99+2^\circ.965t) + 0.03579 \sin (\lambda_\odot-\Omega)+0.00188 \sin (\lambda_\odot+\Omega) - 0.00519 \sin \lambda_\odot,$$

$$\eta=0.04409 \cos (91^\circ.99+2^\circ.965t) + 0.03373 \cos (\lambda_\odot-\Omega)-0.00200 \cos (\lambda_\odot+\Omega) - 0.00169 \cos \lambda_\odot, \quad (8)$$

where 0.00066 in ξ appears because of the odd harmonic of the earth's potential; 0.04409 is the so-called proper eccentricity; and other terms are due to the solar-radiation pressure. The time t is measured from 37171.0 (MJD) in days. The proper eccentricity and the phase angle 91°.99 are determined from observations by the method of least squares. The acceleration is also determined to be $(4.470 \pm 0.024) \times 10^{-3}$.

Although the satellite entered the shadow after 37171 (MJD), the above expressions can follow the actual variations quite well.

The Effect of Radiation Pressure on the Secular Acceleration of Satellites

By Stanley P. Wyatt

The secular perturbations of a satellite orbit arising from solar-radiation pressure have been discussed recently (Musen, 1960; Musen, Bryant, and Bailie, 1960; Parkinson, Jones, and Shapiro, 1960). In particular, the variations of 1 or 2 km in the perigee height of Satellite 1958 $\beta 2$ (Vanguard I) predicted by Musen and his collaborators, when combined with the gravitational effects of the sun and moon, agree very well with the observed changes during the first two years in orbit. Very recently, much larger variations of eccentricity and perigee height of Satellite 1960 $\iota 1$ (Echo I) during its early life have been observed and found to be in excellent accord with theory (Jastrow and Bryant, 1960; Shapiro and Jones, 1960).

The problem to be considered here concerns the short-term secular variations in period to be expected from solar-radiation pressure. The secular acceleration of a satellite as a function of the time can often be derived from observation with considerable accuracy. As is well known, these accelerations, $\Delta P/P$, may then be employed to deduce values of $\rho_q\sqrt{H_q}$, where ρ_q and H_q are the density and scale height of the atmosphere at the locations of perigee. The question naturally arises how high in the atmosphere it is legitimate to deduce these parameters from the observed period changes. Are there other perturbing forces, in addition to atmospheric drag, that will produce finite values of $\Delta P/P$? If so, how can their effects be eliminated in order to avoid erroneous conclusions about the structure of the thermosphere? In what follows it will be shown that the effect of solar radiation on the week-to-week variation in period is negligible when a satellite is continually in sunshine. Later, however, because of the motion of sun, node, and perigee, the satellite must spend some of its time passing through the earth's shadow; the secular acceleration due to the force of sunlight may then exceed that due to atmospheric drag at heights above 800 km or so.

The perturbing acceleration due to radiation pressure

A satellite of average physical cross-section A and mass m at distance $r_\odot=1$ a.u. from the sun intercepts energy at the rate $L_\odot A/4\pi r_\odot^2$, where $L_\odot$ is the total power output of the sun. Hence the momentum gained per unit time, or repulsive force, is of amount $L_\odot A/4\pi c r_\odot^2$, where c is the velocity of light. If the incident energy is reflected specularly or is absorbed and re-emitted isotropically, virtually no net momentum is carried away. We therefore assume that the radial acceleration has a magnitude

$$f=(A/m)L_\odot/4\pi c r_\odot^2. \tag{1}$$

We also assume for simplicity that during the few hours a satellite spends revolving once around the earth the vector **f** is a constant relative to the satellite's orbit. We thus ignore a variety of small effects: (1) possible variations of the solar constant; (2) the minuscule change in the solar distance; (3) the slight motion of the sun in right ascension and declination; (4) the motion of the satellite's node; (5) the motion of the satellite's perigee; and (6) the Poynting-Robertson drag. The magnitude of **f** is probably constant to good accuracy. The change in direction of **f**, through items (3), (4), and (5), amounts at most to a few tenths of a degree during one typical orbital period. Item (6)

modifies the direction of **f** by less than one minute of arc. The influence of all these factors on the secular acceleration of a satellite is ordinarily much smaller than that due to the earth's shadow, and we shall not consider them here.

A more important effect appears to be re-radiation of sunlight from the earth. When the sun is overhead, a satellite at a typical height experiences an upward push due to the reflected component of sunlight amounting to at least 20 percent of the downward push of direct sunlight. When the sun is at larger zenith distances, the effect is less important, but is complicated by the fact that the repulsive force is no longer quite radial from the center of the earth. Over the entire earth the magnitude of the mean outward acceleration due both to the reflected sunlight and to the infrared radiation by the surface and atmosphere is less than 20 percent of that due to direct sunlight for satellites with perigee heights greater than 800 km. Although it is desirable that the influence of terrestrial re-radiation be calculated, we shall not attempt to do so in this study.

The secular acceleration of a satellite

The instantaneous time rate of change of semimajor axis of an earth satellite is given (e.g., Moulton, 1914; Smart, 1953) by

$$\frac{da}{dt}=\frac{Pe\sin\theta}{\pi\sqrt{1-e^2}}R+\frac{P(1+e\cos\theta)}{\pi\sqrt{1-e^2}}S, \tag{2}$$

where P is the orbital period, e the eccentricity, θ the true anomaly, R the component of **f** directed radially away from the center of the earth, and S the component in the satellite's orbit plane at right angles to the radius vector and making an angle less than 90° with the velocity vector of the satellite. To change this expression to the rate of change of period with true anomaly, we make use of the law of areas, the polar equation of the orbit, and the derivative of Kepler's third law. Substitution gives

$$\frac{dP}{d\theta}=\frac{dP}{da}\frac{da}{dt}\frac{dt}{d\theta}=\frac{3Pa^2(1-e^2)}{GM_\oplus}\left[\frac{Re\sin\theta+S(1+e\cos\theta)}{(1+e\cos\theta)^2}\right]. \tag{3}$$

The components of the disturbing acceleration may be deduced from figures 1 and 2. The xy-plane coincides with the orbit plane of the satellite, Q is the direction of perigee, and P the instantaneous position of the satellite. The direction of the sun is S, inclined by an angle $i'\equiv ZS$ from the orbit normal. The direction J defines the direction of the x-axis and is the intersection of the orbit plane

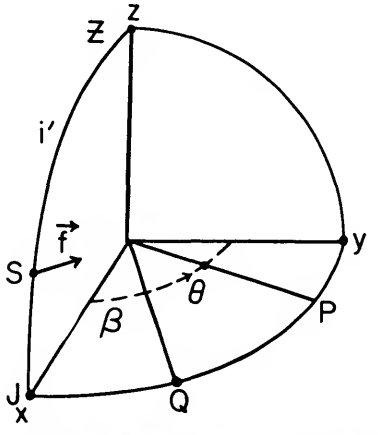

FIGURE 1.—The celestial sphere, showing the direction of the orbit normal Z, of the sun S, of perigee Q, and of the instantaneous satellite position P. The direction of the radiation vector is from S toward the origin.

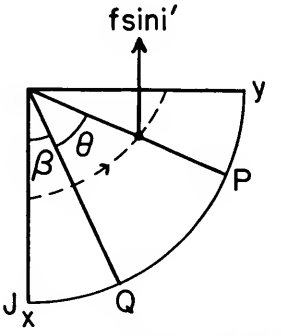

FIGURE 2.—The satellite's orbit plane, with symbols as in figure 1. The component of the perturbing acceleration due to solar-radiation pressure is $f \sin i'$ and is directed toward the negative x-axis.

and a perpendicular plane which contains the sun. The instantaneous true anomaly of the satellite is $\theta \equiv QP$; we define the angle $\beta \equiv JQ$. Figure 2 shows that the total magnitude of the perturbing acceleration in the orbit plane is $f \sin i'$; the radial and transverse components are therefore

$$R = -f \sin i' \cos(\theta+\beta),$$
$$S = +f \sin i' \sin(\theta+\beta). \tag{4}$$

Substituting equations (4) in equation (3) and integrating around the orbit, we find that the secular acceleration of an earth satellite due to the pressure of sunlight is

$$\frac{\Delta P}{P} = \frac{1}{P}\int_0^{2\pi} \frac{dP}{d\theta}\, d\theta = \frac{3a^2(1-e^2) f \sin i'}{GM_\oplus} \int_{0,\theta_2}^{\theta_1,2\pi} \frac{[\cos\beta \sin\theta + \sin\beta(e+\cos\theta)]}{(1+e\cos\theta)^2}\, d\theta. \tag{5}$$

Again, it should be stressed that the assumptions implicit in this formulation are that **f** has a constant magnitude as the orbit is described and also that the angles i' and β are constant during this interval. The limits of integration on the right side of equation (5) account for the fact that in the general case a satellite will enter the earth's shadow when the true anomaly is θ_1 and emerge when it is θ_2. During this time, of course, the perturbing acceleration vanishes. The first term in the integrand is readily evaluated, while the second term is found on substituting the well-known relation $\tan(\theta/2) = (1+e)^{1/2}(1-e)^{-1/2} \tan(E/2)$, where E is the eccentric anomaly. The value of the integral is

$$\frac{e^{-1}\cos\beta + \sin\beta\sin\theta}{1+e\cos\theta}\Bigg|_{0,\theta_2}^{\theta_1,2\pi} = -\frac{e^{-1}\cos\beta + \sin\beta\sin\theta}{1+e\cos\theta}\Bigg|_{\theta_1}^{\theta_2}$$
$$= \left[-\frac{\cos\beta}{e} + \frac{\cos(\beta+\theta)}{1+e\cos\theta}\right]\Bigg|_{\theta_1}^{\theta_2} = \frac{\cos(\beta+\theta)}{1+e\cos\theta}\Bigg|_{\theta_1}^{\theta_2}. \tag{6}$$

When equations (1) and (6) are substituted in equation (5), the expression for the secular acceleration of a satellite due to solar-radiation pressure becomes

$$\frac{\Delta P}{P} = \frac{3(A/m) L_\odot a^2(1-e^2)\sin i'}{4\pi c r_\odot^2 GM_\oplus} \left[\frac{\cos(\beta+\theta)}{1+e\cos\theta}\right]\Bigg|_{\theta_1}^{\theta_2}. \tag{7}$$

It is convenient for numerical purposes to describe the physical characteristics of the satellite itself by a dimensionless quantity D_s such that $(A/m) = D_s$ cm²/gm, and also to express the ratio of perigee distance to the earth's equatorial radius by another dimensionless quantity K such that $q/R_\oplus \equiv a(1-e)/R_\oplus = K \geqq 1$. Then equation (7) simplifies to

$$\frac{\Delta P}{P} = \frac{3D_s L_\odot R_\oplus^2 K^2(1+e)\sin i'}{4\pi c r_\odot^2 GM_\oplus(1-e)} \left[\frac{\cos(\beta+\theta)}{1+e\cos\theta}\right]\Bigg|_{\theta_1}^{\theta_2}$$
$$= 1.40\times10^{-7} D_s K^2 \frac{(1+e)}{(1-e)} \sin i' \left[\frac{\cos(\beta+\theta)}{1+e\cos\theta}\right]\Bigg|_{\theta_1}^{\theta_2}. \tag{8}$$

The earth's shadow

To evaluate the bracket in equation (8) we must know the values of the true anomaly, θ_1 and θ_2, at which the satellite enters and leaves the earth's shadow. To keep the problem tractable we assume, without appreciable error, that the shadow is a circular cylinder of radius $R_\oplus$, with axis of course in the anti-sun direction. The intersection of this cylinder with the orbit plane is a semi-ellipse, as shown in figure 3. Its equation in the coordinate system already defined is

$$x^2 \cos^2 i' + y^2 = R_\oplus^2, \qquad x \leqq 0. \tag{9}$$

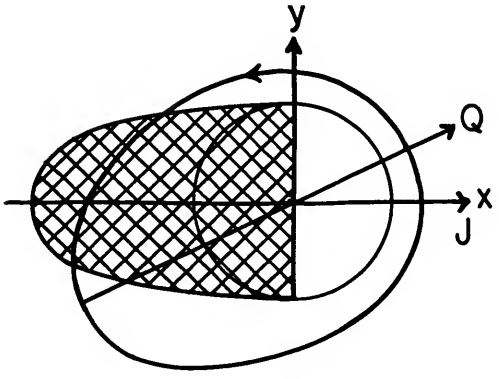

FIGURE 3.—The general geometrical relation of a satellite's orbit and the semi-ellipse of the earth's cylindrical shadow projected onto the orbit plane.

Transforming to polar coordinates and equating to the expression for the satellite's orbit, we find the values of θ_1 and θ_2 are the two solutions of

$$\frac{R_\oplus^2}{1-\sin^2 i' \cos^2(\beta+\theta)}=\frac{a^2(1-e^2)^2}{(1+e\cos\theta)^2}, \qquad \frac{\pi}{2}\leqq\beta+\theta\leqq\frac{3\pi}{2}. \tag{10}$$

If there are no solutions in the second and third quadrants, the satellite is in sunshine all around the orbit; if there is one solution, $\theta_1=\theta_2$, the satellite touches the shadow at only one place and spends none of its time in darkness. As before, we may substitute $q/R_\oplus=K\geqq 1$; then θ_1 and θ_2 are the two solutions of

$$(1+e\cos\theta)^2=K^2(1+e)^2[1-\sin^2 i' \cos^2(\beta+\theta)], \qquad \frac{\pi}{2}\leqq\beta+\theta\leqq\frac{3\pi}{2}. \tag{11}$$

The specific values of θ_1 and θ_2 for a given high satellite can be found by computing i' and β for every few days and solving equation (11) by graphical or other approximate methods. The angle i', between the orbit normal and the sun, is given by

$$\cos i'=\cos i \sin\delta_\odot+\sin i \cos\delta_\odot \sin(\alpha_N-\alpha_\odot), \tag{12}$$

where i is the inclination of the orbit plane to the equator, $\alpha_\odot$ and $\delta_\odot$ are the right ascension and declination of the sun, and α_N is the right ascension of the ascending node. The angle β can be found from

$$\cos\beta \sin i'=\sin\delta_\odot \sin\delta_Q+\cos\delta_\odot \cos\delta_Q \cos(\alpha_Q-\alpha_\odot), \tag{13}$$

where α_Q and δ_Q are the right ascension and declination of perigee. When the angles of entry and exit, θ_1 and θ_2, have been found for various epochs they may then be used in equation (8) to compute predicted secular accelerations as a function of the time.

When we abandon consideration of a specific satellite and ask for a general solution of equation (11) to be substituted in equation (8) for $\Delta P/P$, the problem is formidably complex because the angles of entry and exit depend on four arbitary parameters. Let us therefore first consider some specific applications that will perhaps elucidate the effect of radiation pressure on the period changes of a high satellite and then proceed to develop a quasi-general solution as a power series in the eccentricity. (For objections to this procedure, see Kozai, 1961a, especially page 30.)

Special cases of orbital orientation and shape

(a) *Orbit normal pointing toward the sun.*—Here $i'=0°$ and therefore the right side of equation (8) is zero. Physically, no satellite can spend a finite fraction of its time in the earth's shadow, even if $K=1$.

(b) *Satellite in sunshine all around the orbit.*—If i' is sufficiently small, the satellite will see the sun above the earth's horizon continually, as was the case with Echo I (1960 ι1) during its first two

weeks aloft in August, 1960. Under such conditions, even if i' is not zero, $\Delta P/P=0$. Mathematically, the left side of equation (6) is to be evaluated from 0 to 2π, and the result is zero. Regarded physically, the perturbing effects cancel on opposite sides of the orbit. The null result here is like that of the solar gravitational perturbation of a satellite, where there is never a "shadow" in which to hide: the secular acceleration is zero when **f** is regarded as a constant vector relative to the satellite orbit.

(c) *The circular orbit, i' arbitrary.*—To find the period change of a satellite in a circular orbit and spending time in the earth's shadow, set $e=0$ in equation (8) and note that, by symmetry, $(\beta+\theta_2)=2\pi-(\beta+\theta_1)$. Evaluating the bracket, we see that $\Delta P/P=0$. Because of the symmetry the momentum loss while the satellite is moving toward the solar hemisphere is just balanced by the momentum gain when it is moving toward the opposite hemisphere.

(d) *The angle $\beta=0°$ or $180°$, i' arbitrary.*—By symmetry, $\theta_2=2\pi-\theta_1$. The bracket in equation (8) is therefore zero and hence $\Delta P/P=0$ for this case also, the interpretation being similar to that of case (c).

(e) *The asymmetric case with $i'=90°$, $\beta=90°$ or $270°$.*—It may be thought from all the foregoing that radiation pressure has no effect at all on satellite accelerations. The present example is intended to show otherwise. It is also one that can be evaluated without great difficulty. When $\beta=90°$ the solution of equation (11) gives $\cos\theta_1=[K(1+e)-e]^{-1}$ and $\cos\theta_2=-[K(1+e)+e]^{-1}$. Substitution in equation (8) shows that for $i'=90°$, $\beta=90°$, the secular acceleration is

$$\frac{\Delta P}{P}=-1.40\times10^{-7}D_*U(K,e),$$

$$U(K,e)=\frac{K\sqrt{1+e}}{1-e}\{\sqrt{(K^2-1)+e(K^2+1)+2Ke}-\sqrt{(K^2-1)+e(K^2+1)-2Ke}\}, \tag{14}$$

the period decreasing with the time. If $\beta=270°$ the effect is equal and opposite, the period increasing secularly. Although I have not tried to prove it, this special example probably reveals about the maximum secular acceleration to be expected from radiation pressure. For one thing, with $i'=90°$ the full force of sunlight is in the orbit plane; for another, with $\beta=90°$ or 270° the effects of asymmetry are large. Table 1 presents numerical values of $U(K, e)$ for several relevant values of the eccentricity e, and the perigee distance $K=q/R_\oplus$.

TABLE 1.—*Values of* U(K, e) *for use with equations (14)*

K	$e=0.00$	0.01	0.02	0.05	0.10	0.15	0.20	0.30	0.40	0.50
1.00	0.00	0.20	0.29	0.48	0.74	0.98	1.22	1.78	2.49	3.46
1.05	0.00	0.06	0.12	0.27	0.49	0.71	0.93	1.45	2.10	2.99
1.10	0.00	0.05	0.10	0.23	0.45	0.66	0.88	1.39	2.04	2.94
1.15	0.00	0.05	0.09	0.22	0.42	0.63	0.86	1.37	2.04	2.94
1.20	0.00	0.04	0.09	0.21	0.41	0.62	0.85	1.37	2.05	2.98
1.30	0.00	0.04	0.08	0.20	0.41	0.62	0.86	1.40	2.11	3.09
1.40	0.00	0.04	0.08	0.20	0.41	0.63	0.88	1.45	2.19	3.22
1.50	0.00	0.04	0.08	0.20	0.42	0.65	0.91	1.51	2.29	3.38

Inspection of the table reveals several points. First, the secular acceleration is zero for circular orbits of all sizes, as expected. Second, for any fixed value of the perigee distance, $U(K,e)$ increases monotonically with e, because of the increasing asymmetry of the passage through the earth's shadow. Third, for any fixed value of the eccentricity, $U(K,e)$ has a relative maximum for the smallest possible orbit ($K=1$), falls to an absolute minimum at some intermediate value of K, and then rises once again. Interpreted physically, for a fixed e there is maximum asymmetry for $K=1$, while there is none at all as $K\to\infty$ and the earth's shadowing effect becomes infinitesimal. With increasing K, however, the decrease in asymmetry is compensated and then overtaken by the

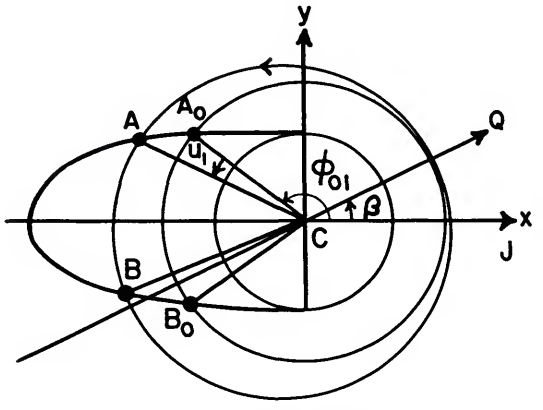

FIGURE 4.—The construction for a nearly circular orbit. The semi-ellipse of the projected shadow is shown, as are also the orbit and its inscribed circle of radius equal to the perigee distance. Notation as in case (f).

decreasing gravitational control of the earth on the satellite. When $U(K, e)$ is differentiated partially with respect to K, it is found that the absolute minimum occurs at a perigee of

$$K^2=\frac{(5+4e^2)+3\sqrt{1+8e^2}}{4(1+e)^2}. \tag{15}$$

For any eccentricity in the range $0.0 \leqq e \leqq 0.5$ the minimum value of $U(K, e)$ may be found by adopting the smallest value in any given column of table 1, because the absolute minima for all these eccentricities occur within the range of K that is tabulated. Thus, for this particular orientation and independently of K, the magnitude of $\Delta P/P$ ranges from zero for a circular orbit to at least 0.5×10^{-7} D_s at $e=0.10$, at least $1.1\times10^{-7}D_s$ at $e=0.20$, and at least 4.1×10^{-7} D_s at $e=0.50$.

(f) *The orbit of low eccentricity.*—A quasi-general solution for the secular acceleration may be developed as a power series in e. In equations (8) and (11) make the substitution $\phi=\beta+\theta$, where r and ϕ are polar coordinates in the orbit plane as defined by the coordinate system of figure 2, such that $x=r\cos\phi$, $y=r\sin\phi$. Next circumscribe a circle of radius q around the center of the earth, as shown in figure 4. In the figure, $\angle JCA=\phi_1$ and $\angle JCB=\phi_2$. Define $\phi_1=\phi_{01}+u_1$, $\phi_2=\phi_{02}+u_2$, where u_1 and u_2 are small quantities if the eccentricity is small and zero for a circular orbit. As can be seen from figure 4, $\phi_{01}=\angle JCA_0$ and must lie in the second quadrant, while $\phi_{02}=\angle JCB_0$ and must lie in the third quadrant. The solution of equation (11) with $e=0$ gives

$$\cos\phi_{01}=\cos\phi_{02}=-\frac{\sqrt{K^2-1}}{K\sin i'}\equiv-\nu, \qquad \nu\geqq0,$$

$$\sin\phi_{01}=-\sin\phi_{02}=\frac{\sqrt{1-K^2\cos^2 i'}}{K\sin i'}\equiv\mu, \qquad \mu\geqq0. \tag{16}$$

Now set $u_1=a_1e+a_2e^2+\ldots$, $u_2=b_1e+b_2e^2+\ldots$, substitute each in equation (11), and then equate coefficients of like powers of e in order to obtain expressions for $a_1, a_2, \ldots, b_1, b_2, \ldots$. Then return to equation (8) for the secular acceleration and expand it similarly as a power series in e, a series which will of course contain $a_1, a_2, \ldots, b_1, b_2, \ldots$. Substitution of the explicit expressions for these coefficients, already found above, then gives the secular acceleration as a power series in e to any degree of accuracy. Unfortunately, of course, the greater the desirable degree of accuracy, the greater is the undesirable degree of complexity in working out the coefficients. I find the quasi-general solution, as far as order e^2, to be

$$\frac{\Delta P}{P}=-1.40\times10^{-7}D_sY(K, e, \beta, i'),$$

$$Y(K, e, \beta, i')=\frac{2K^3e\mu\sin\beta}{\sqrt{K^2-1}}\left[1+2e(1+\nu\cos\beta)-\frac{e(1+\nu^3\cos\beta)}{\mu^2(K^2-1)}\right]+0(e^3), \tag{17}$$

where μ and ν are given by equations (16).

This expression has both merits and demerits. It vanishes, as it should, for a circular orbit. For a finite eccentricity it is zero for $\beta=0°$ or 180°, as expected from case (c). Also, if we set $i'=90°$ and $\beta=90°$ in equation (17), it is found to agree with the exact equation (14) when the latter is expanded to the second order in e. The acceleration predicted by each formula for this special situation is

$$\frac{\Delta P}{P}=-1.40\times10^{-7}D_s\left[\frac{2K^2e}{\sqrt{K^2-1}}\left\{1+\frac{e(K^2-2)}{(K^2-1)}\right\}\right]. \tag{18}$$

Although equation (17) is consistent with some of the foregoing special cases, it arouses suspicion on at least two grounds. First, consider a time when $\mu=0$ and therefore by equation (16) $\phi_{01}=\phi_{02}=180°$. The final term in equation (17) suggests an infinite secular acceleration under these conditions. Actually, this particular situation occurs when the circumscribed circle of figure 4 touches the projected shadow at one and only one point—on the anti-sun axis. It is readily seen, therefore, that no satellite traveling on any orbit whose inscribed circle is such that $\mu=0$ can spend a finite fraction of its period in darkness. The difficulty here is a mathematical one rather than a physical one, and as has already been pointed out $\Delta P/P=0$ on all occasions when equation (11) has less than two solutions. A second, and legitimate, suspicion is aroused when $K=1$ in equation (17). It is not enough to dismiss this problem with the comment that any satellite with $K=1$ is itself in grave trouble; we deal with this problem as case (h).

(g) *The orbit of low eccentricity, $i'=90°$.*—Specializing equations (16) and (17) for those times when the radiation force lies fully in the orbit plane, we find that

$$Y(K,e,\beta,90°)=eV(K,\beta)\left[1+e\left\{\frac{K^2-2}{K^2-1}+\frac{\cos\beta\sqrt{K^2-1}}{K}\right\}+\ldots\right],$$

$$V(K,\beta)=\frac{2K^2\sin\beta}{\sqrt{K^2-1}}. \tag{19}$$

Table 2 gives values of $V(K, \beta)$ for several combinations of K and β and may be used to estimate quickly the leading term of equation (19). The absolute value of the second term is less than 20 percent of the leading term for all values of β at $K=1.05$ if $e<0.022$; at $K=1.10$ if $e<0.048$; at $K=1.15$ if $e<0.077$; at $K=1.20$ if $e<0.109$; at $K=1.30$ if $e<0.184$; at $K=1.40$ if $e<0.270$; and at $K=1.50$ if $e<0.211$. The minimum absolute contribution of the second term occurs in the neighborhood of $K=\sqrt{2}$ and then rises again with increasing perigee distance until for very large orbits 20 percent contribution occurs at $e=0.100$. The sign of the second term is usually negative for $K<\sqrt{2}$ and is negative for all values of β provided $K<1.27$.

From this specific example it appears likely that equations (16) and (17) constitute an adequate approximation to the practical estimate of secular accelerations due to radiation pressure, at least for a fair variety of orbits. First, as will be shown in the next section, the effect of sunlight on

TABLE 2.—*Values of* V(K, β) *for use with equations (19)*

K	$\beta=0°$	15°	30°	45°	60°	75°	90°
1.05	0.00	1.78	3.44	4.87	5.96	6.65	6.89
1.10	0.00	1.37	2.64	3.73	4.57	5.10	5.28
1.15	0.00	1.21	2.33	3.29	4.03	4.50	4.66
1.20	0.00	1.12	2.17	3.07	3.76	4.19	4.34
1.30	0.00	1.05	2.03	2.88	3.52	3.93	4.07
1.40	0.00	1.04	2.00	2.83	3.46	3.86	4.00
1.50	0.00	1.04	2.01	2.85	3.49	3.89	4.02

$\Delta P/P$ is swamped by the effect of drag if $K<1.12$ approximately, and it is therefore unnecessary in practice to be concerned about the nature of the solution when K is very close to unity. Second, whenever $K>1.12$ the contribution of the second term of equation (17) is moderately small if e is not too large. Presumably the higher-order terms converge rapidly. Although an extension of the power series beyond $0(e^2)$ would be useful for more eccentric orbits, it has not been attempted in the present work.

(*h*) *The nearly circular orbit, $i'=90°$, $K=1$.*—When perigee is at or very near the earth's surface, the approximation leading to equation (17) breaks down. Geometrically, when $K=1$, we have $\phi_{01}=90°$ and $\phi_{02}=270°$, and even when the eccentricity is small the angles u_1 and u_2 are of rather good size, and therefore terms beyond $0(e^2)$ are needed to obtain an adequate approximation. Alternatively, it is straightforward enough in the present special case to solve equation (11) and substitute the results in equation (8) as a power series in e. The appropriate formula, to order 3/2 in e, turns out to be

$$\frac{\Delta P}{P}=-1.40\times10^{-7}D_s W(e,\beta),$$

$$W(e,\beta)=(1+3e/2)\sqrt{2e}\,\{\sqrt{1+\sin\beta}-\sqrt{1-\sin\beta}\}. \tag{20}$$

This expression vanishes for $e=0$ and also for $\beta=0°$ or 180°, as we are entitled to expect from previous illustrations. Table 3 contains $W(e, \beta)$ for a few selected pairs of e and β. The approximate equation (20) with $\beta=90°$ is identical with the exact equation (14) when $K=1$ and the function U is expanded to order 3/2 in e. When $\beta=90°$, equation (20) is good to 1 percent if $e<0.08$, and to 10 percent if $e<0.28$.

The competition of radiation pressure and atmospheric drag

It is well known that the instantaneous tangential acceleration of a satellite moving through a stationary atmosphere is given by

$$T=-(A/m)(C_D/2)\rho v^2, \tag{21}$$

where C_D is the dimensionless drag coefficient, ρ is the atmospheric density at the point in question, and v the speed of the satellite there. When the magnitude of this perturbing acceleration is compared with that due to solar-radiation pressure as given by equation (1), the ratio of the two is

$$R=\frac{4\pi c r_\odot^2 C_D \rho v^2}{2L_\odot}, \tag{22}$$

a quantity that is independent of the characteristics of the satellite itself. Setting $C_D=2$, $\rho=J\times10^{-16}$ gm/cm^3, adopting for v the circular velocity at 800 km, and inserting the other constants, we have

$$R\cong1.2J. \tag{23}$$

TABLE 3.—*Values of* W(*e*, *β*) *for use with equations* (*20*)

e	$\beta=0°$	15°	30°	45°	60°	75°	90°
0.00	.000	.000	.000	.000	.000	.000	.000
0.01	.000	.037	.074	.110	.144	.175	.203
0.02	.000	.054	.107	.158	.206	.251	.291
0.03	.000	.067	.133	.196	.256	.312	.362
0.04	.000	.078	.155	.229	.300	.365	.424
0.05	.000	.089	.176	.260	.340	.414	.481

Thus, outside the earth's shadow the two forces are of equal magnitude at a height near 800 km for a mean state of the atmosphere (Nicolet, 1960c). When the sun is active and when it is close to midday at the perigee of a satellite, the high atmosphere is distended and the level of equal magnitudes is above 800 km.

In equation (23), J decreases more or less exponentially with height. Therefore, atmospheric drag is all-important for low satellites and less so for high ones. For example, Vanguard I (1958 $\beta 2$), with $D_s=0.21$, should by equation (14) and table 1 show a maximum secular acceleration due to radiation pressure of $\pm 0.25\times 10^{-7}$. Referring to equation (8), the quantity sin i' passes through a maximum on the average every 45 days, which is the time taken on the average for $(\alpha_N-\alpha_\odot)$ to regress through 180°; the semi-amplitude of this fluctuation is about 0.1×10^{-7}. A second periodic variation is that of the angle β, which passes through a complete cycle every 2.4 years. This interval is the length of the "day" at perigee, the average time taken for $(\alpha_Q-\alpha_\odot)$ to advance by 360°. The semi-amplitude of this long-run variation is about 0.25×10^{-7}. When the anticipated effect of radiation pressure is compared with the observed accelerations of Vanguard I (Jacchia, 1959d; Briggs, 1959), it appears that the period changes can confidently be attributed to drag. The effect of radiation pressure is small, and about equal to the precision with which the accelerations can be determined; it is less than the effect of drag by a factor ranging from about 5 when perigee occurs at night to about 50 when it occurs nearly under the sun. Thus for satellites as low as Vanguard I radiation effects are to be found by analyzing such elements as perigee height (Musen, Bryant, and Bailie, 1960; Musen, 1960) rather than orbital period. The latter may be employed to deduce the structure of the thermosphere.

At greater heights the situation is more delicate. During its first two weeks aloft, Echo I (1960 $\iota 1$) had a perigee height near 1500 km, several scale heights above the reference level of 800 km. For example, if the scale height in this layer averages about 110 km, corresponding to $T=2000°$ K and a composition of atomic oxygen, equation (23) then gives $R<1.2e^{-6}<0.01$, so that the relative magnitude of the drag force is small.

Echo I of course spends some of its time in sunshine all around the orbit. As shown in case (b) of the previous section, the effect of radiation pressure on period changes is then zero within the framework of our assumptions. On such occasions the characteristics of the thermosphere can be studied without accounting for the complications of solar radiation. There is, however, the limitation that at these times $i'\cong 0°$ and we are therefore confined to examining the twilight zone of the high atmosphere. If the diurnal sunward bulge persists at these great heights, its properties can only be deduced when Echo I has the sun near its zenith in part of its orbit and thus is in darkness half a period later.

When a very high satellite periodically transits the earth's shadow, radiation pressure then has the upper hand. The preliminary mean value of $\Delta P/P$ for Echo I during the first twelve weeks of passage through the umbra was near -4×10^{-6}. The sign accords with expectation because the angle β was in the first and second quadrants during this interval, and the amount is roughly consistent with prediction. The open circles of figure 5 give weekly predicted accelerations and the filled circles the observed accelerations. The first seven observed points are weekly means of the day-to-day values computed under the direction of P. E. Zadunaisky; the last five observed points are relatively rough graphical accelerations by the author and are preliminary only. In order to obtain the best vertical fit of predicted and observed points we must adopt $D_s\cong 270$ in equation (17), whereas a diameter of 100 feet and a mass of 60 kilograms gives $D_s\cong 120$. Apart from this, the two curves are in reasonable agreement.

The factor of 2 or 3 by which the observed period changes exceed the predicted ones could arise from several effects. First, an error in the announced value of D_s could either aggravate or reduce the discrepancy. Second, Echo I during this time may have been passing more or less centrally through a diurnal atmospheric bulge, which would reduce the discrepancy. A third possibility is nonspecular reflection from the balloon surface; complete back reflection will double the magnitude of the perturbing acceleration of equation (1), whereas isotropic reflection by

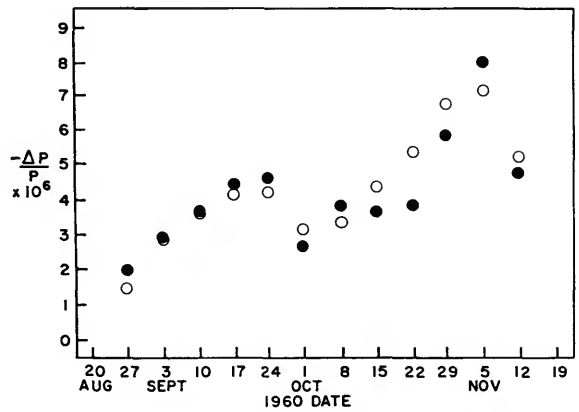

FIGURE 5.—Comparison of observation and theory. The filled circles are preliminary observed secular accelerations of Echo I during its first three months of transiting the earth's shadow; open circles are the predicted values due to solar radiation pressure.

each surface element into its outward hemisphere will increase equation (1) by a factor of 4/3. One definite reason why the observed negative accelerations during these three months should be greater than the predicted values is the effect of terrestrial re-radiation. Reflected sunlight was acting during these weeks to amplify the negative secular acceleration. In addition, if the infrared radiation from the surface and atmosphere is nonisotropic in the sense of being stronger on the daylit hemisphere, this component was also acting during September and October of 1960 in the same fashion. We can, of course, unscramble some of these effects more easily when Echo I has been aloft for a longer time. Perhaps it is not too much to hope that the radiation effects can be assessed well enough so that residuals may then permit deductions on the structure of the highest atmosphere even when Echo I is encountering the earth's shadow.

Remarks and conclusions

Studies of the atmosphere above about 800 km are made difficult because extraneous effects rival that of drag on the period changes of satellites. The competing effect of solar-radiation pressure can be evaluated and eliminated by the use of equations (16) and (17), provided the orbital eccentricity is not too large, that D_s is well known, and that it is possible to estimate a factor by which the satellite deviates from a specular reflector. The effect of terrestrial re-radiation has not been taken into account quantitatively in this study, although its role relative to direct solar pressure may be appreciable. Two further investigations are therefore suggested: (a) extension of the power series of equation (17) for more accurate assessment of the effect of direct solar-radiation pressure; and (b) calculations on the influence of re-radiation from the earth on the orbit of a satellite.

I am grateful to Dr. F. L. Whipple, Director, for the opportunity to work at the Smithsonian Astrophysical Observatory during the summer of 1960, when this study was first conceived; to Dr. L. G. Jacchia of Smithsonian, whose comments helped get the study started; to Mr. P. E. Zadunaisky of Smithsonian, whose acceleration data helped complete it; and to Dr. P. Musen of the National Aeronautics and Space Administration and Drs. H. M. Jones and I. I. Shapiro of Massachusetts Institute of Technology, Lincoln Laboratory, for furnishing me information on the work being done at these institutions on radiation pressure effects.

Abstract

Satellite accelerations play a crucial role in determining the structure of the high atmosphere, and it is therefore important to assess and eliminate the effect of perturbing forces that compete with air drag and that may therefore confuse our picture of the thermosphere. In particular, this study evaluates the effect of solar-radiation pressure on the secular acceleration of earth satellites. For perigee heights less than about 800 km the period changes due to radiation pressure are minor compared with those due to atmospheric drag. At greater heights and lower air densities, radiation pressure becomes increasingly important. When a satellite is in sunshine all around its orbit,

the period change arising from the pressure of sunlight is zero. But during the weeks or months it is penetrating the earth's shadow and is therefore exposed to a photon wind only part of each circuit, the secular acceleration may attain substantial values, positive or negative depending on the orientation of the orbit relative to the sun. Several special cases of orientation are discussed, and a general formula for computing secular accelerations due to radiation pressure is derived as far as terms in the square of the eccentricity.

Experimental and Theoretical Results on the Orbit of Echo I

By Pedro E. Zadunaisky, Irwin I. Shapiro, and Harrison M. Jones

In this paper we compare experimental and theoretical determinations of the orbital elements of the Satellite 1960 ι 1 (Echo I) for every day from August 13, 1960 (one day after launching), through March 1, 1961. This comparison shows that the strikingly large variations of the eccentricity and geocentric perigee distance can be attributed almost wholly to the effects of sunlight pressure on the balloon, in accordance with our theoretical predictions (Parkinson, Jones, and Shapiro, 1960; Shapiro and Jones, 1960, 1961).

We have also inferred preliminary atmospheric densities for the altitude range (about 950 to 1500 km above the International Ellipsoid) traversed by the perigee of Echo. In this calculation it is necessary to consider the energy gain (or loss) of the satellite from the solar-radiation field. After subtracting the variations of the rate of change of period owing to this latter effect, we find that the remaining fluctuations correlate with those of the solar flux at 10.7-cm and 20.0-cm wavelength and can be attributed almost entirely to air drag. In addition, the air drag shows a large increase during the major solar flare of November, 1960.

From the time variation of eccentricity we deduced approximate values for the rates of gas leakage from the balloon. Our conclusions are only tentative because many other imprecisely known quantities (such as the reflection characteristics and shape of Echo as a function of time) influence our results.

Our present (highly speculative) estimate of the lifetime of Echo I is that, barring a substantial change in its shape, it will perish in the spring of 1964.

Description of experimental orbit computation

From observed positions of the satellite we have derived the mean orbital elements by a process of successive differential corrections. That process has been described in detail elsewhere (Zadunaisky, 1960), and we shall therefore give only the main features of the present computations.

The observations used came mainly from the Smithsonian Baker-Nunn photographic tracking stations. Some radio measurements from the Minitrack stations of Goddard Space Flight Center were included for the time during which the satellite's beacon was operating. In addition, we included a very large number of excellent optical observations sent from the Observatory of Paris at Meudon, France.

The word "mean" in reference to the orbital elements must be understood here in two senses. First, it indicates that the first-order short-period perturbations due to the second harmonic of the earth's gravitational potential have been computed analytically and then subtracted from the observations before the differential correction of the elements was performed. Second, the elements are mean in the sense that each set represents observations distributed along a two-day arc, which corresponds to approximately 25 revolutions of the satellite.

A quadratic polynomial in time was used to represent each element, except the inclination; for the latter we found that a linear expression was accurate enough. Then by a process of successive differential corrections we improved only the constant term of each polynomial to obtain a best least-squares fit of the orbit to

the observations made during the two days, one before and one after the epoch of the elements. In the polynomial representing the mean anomaly we always corrected all three coefficients in order to take into account the rapid and unpredictable changes due to atmospheric drag. The coefficients of the linear and quadratic terms of the other polynomials were kept constant for periods of several weeks and were then readjusted. As elements were determined for each day, the observations used in two successive determinations overlapped for one day; we were thus assured of a better continuity in our results.

Description of theoretical orbit computation

Our theoretical orbit computation is based on the well-known first-order differential equations relating the rate of change of the orbital elements to the perturbing accelerations (Moulton, 1914, chap. 10). We solve for the time dependence of the elements by first integrating these equations over an orbital period—keeping the elements constant during the integration. The integration can be carried out analytically in closed form for all perturbing accelerations except that due to air drag. The new values for the elements are then used in determining the changes in the elements during the next orbital period, and so forth. This iteration procedure is carried out on an IBM–7090 digital computer. The initial values used for the elements are those determined from the observations of the satellite; all future values are calculated by the iteration method. This method yields a very accurate estimate of the long-period and secular contributions to the changes in the elements. However, the contributions of the short-period terms are averaged out.

At present, our computer program includes perturbations due to the following phenomena:

(a) direct solar-radiation pressure, including the effects of the earth's shadow;

(b) neutral atmospheric drag.[1] The atmospheric density is assumed to be spherically symmetric and constant in time, but this all-too-simple model is now being generalized;

(c) the second through the fifth harmonics of the earth's gravitational field;

(d) Solar and lunar gravitational fields.

[1] Charge drag is quite small for Echo I and has been neglected.

(e) Solar radiation reflected from the earth.[2] Our model for the reflection characteristics of the earth involves an arbitrary, but uniform, mixture of diffuse and specular reflection. However, only specular reflection is now included in our program.

It is clear that (aside from the approximate nature of our physical model and the errors accompanying observations) our theoretical elements and our experimental elements differ even in principle. Our comparison of the two sets of elements is based on the assumption that the differences that arise purely from the differing principles of element definition are small and can be neglected in this analysis.

Comparison of experimental and theoretical results

In calculating a theoretical orbit for Echo I in order to compare it with results derived from the observations, we must first consider the physical characteristics of the balloon. Soon after launch, the satellite closely approximated a sphere 100 ± 1 ft in diameter. It was constructed from half-mil Mylar, externally coated with an aluminum layer approximately 0.2μ thick. Its initial weight was 156.995 lb, including 33.34 lb of sublimating powders. The powders were of two kinds: the first (weighing 10 lb) was highly evaporative, while the second had a much lower vapor pressure.

The magnitude of the acceleration due to the pressure of sunlight is $K(A/M)\ (I/c)$, where (A/M) is the cross-sectional area-to-mass ratio of the satellite (initally 102 cm^2/gm); I is the solar energy flux; c is the velocity of light; and K is a scattering constant $(0 \leq K \leq 2)$ whose value depends on the reflection characteristics of the surface. The constant c is known very accurately. For the solar constant we have used the value 2.00 cal/cm^2 min, which is quoted in the American Institute of Physics Handbook with a probable error of 2 percent. The ratio A/M, on the other hand, is not accurately known. Small holes that were introduced

[2] The infrared radiation from the earth, if it were uniform, would only have the effect of changing the earth's mass by an entirely negligible amount, provided that the satellite always presented the same cross-sectional area towards the earth. (This last requirement is satisfied for the case of the spherical Echo I.) Preliminary investigations of the infrared radiation from the earth (Intermountain Weather, Inc., Final Report under Contract AF 19 (604) 2418) indicate that at 1000 km this radiation is within ± 10 percent of uniformity. Since the re-radiated power at 1000 km is only a small fraction of that of direct radiation, the effect of the former on the orbit is probably quite small.

before launching and meteoric punctures will permit gas to escape at a rate almost impossible to predict accurately. Hence, since 21 percent of the initial satellite mass was in the form of sublimating powders, it is difficult to determine purely theoretically the accurate time dependence of the satellite mass. The value of K is also uncertain: for specular reflection from a perfect sphere, $K=1$; however, small irregularities in the shape or any diffuseness in the reflection of sunlight will tend to increase K. In view of these difficulties, we have considered $K(A/M)$ (I/c) to be a (partially unknown) parameter and have allowed it to vary in a reasonable manner so as to obtain the best agreement between the theoretical and observed variations in the orbital elements.

In figure 1, we have plotted the residuals of the eccentricity e from a polynomial expression obtained by the method of least squares. The experimentally deduced values are indicated by points, and the theoretical values by open circles. The rather close agreement between the two sets was obtained by assuming that $K=1$ and that the total mass of the satellite decreased at the rate of 0.64 lb/day for the first 13 days, and then decreased at 0.16 lb/day. According to this model, only a negligible amount of the gas remained in the balloon after January 15, 1961. The decrease by a factor of four in the rate of mass loss, in spite of the expected increase in the meteorite holes, may possibly be due to the escape of the more volatile of the two powders.[3] These rates of mass loss are somewhat arbitrary; other rates may lead to equally good or better agreement with observations. However, the uncertainty in our value of $K(A/M)$ (I/c) at any given time is probably not more than a few percent. Further improvement in our estimate of this parameter apparently will require consideration of other physical effects, such as a possible diurnal bulge of the atmosphere (see discussion below of the argument of perigee). Since we infer $K(A/M)(I/c)$, as well as an air-density model, from the data, we may possibly be "covering up" the effects of some neglected physical perturbations.

That the satellite did gradually lose a substantial portion of its mass (or, more precisely, that $K(A/M)$ increased gradually) may be inferred from comparisons of the observed maximum value of the eccentricity ($e_{max}=0.0788$) with the following theoretical calculations:

(a) By assuming that $K(A/M)$ maintains its initial value of 102 cm²/gm, we find $e_{max}=0.0705$.

(b) By assuming that the satellite lost all of its gas soon after launching while K remained unity [$K(A/M)=130$ cm²/gm], we obtain $e_{max}=0.0885$.

We have also plotted in figure 1 the residuals (from a polynomial) of the experimental and theoretical values of the geocentric perigee distance q. The densities used in computing the theoretical curve were obtained by matching approximately a second-degree polynomial in altitude to the logarithm of the experimentally determined densities. The relatively low values of the theoretical perigee distance in the neighborhood of January 1, 1961, are due mainly to the correspondingly high values of the eccentricity. On the other hand, the relatively low theoretical values that persist after the middle of January are related to the "theoretical" density values being somewhat greater than the average "observed" values. This discrepancy could be largely eliminated by a small change in the density values used in the theoretical computation. However, our present air model is independent of time. Hence, for a given altitude, we cannot represent properly both the average air density during November–December and that during January–February when solar activity was relatively much lower (see fig. 3).

The perigee distance reached its first minimum value on December 29, 1960, about two days later than the eccentricity reached its maximum value. This difference is due mainly to the decrease in semimajor axis caused by air drag.

In figure 2, we have plotted the residuals (from polynomials) of the experimental and theoretical values of the argument of perigee ω, the right ascension of the ascending node Ω, and the orbital inclination i.

[3] The slow final rate of mass loss could not be measurably influenced by an accumulation of air molecules penetrating only one surface of the balloon, since it is possible to show that the balloon had so far collided with only about one pound of air. Accretion of mass through collisions with meteoritic dust probably amounted to much less than a pound.

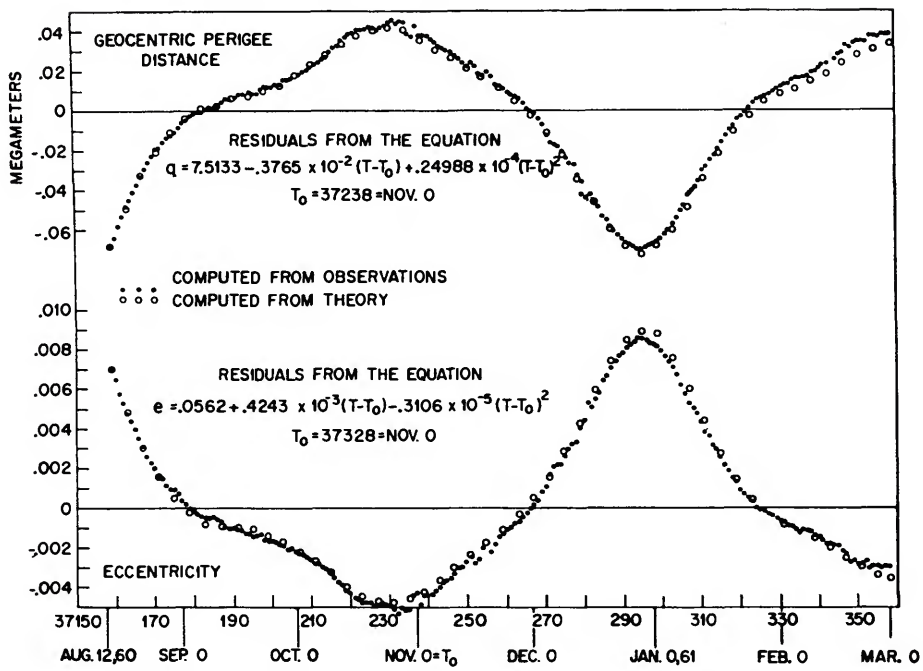

FIGURE 1.—Comparison of experimental and theoretical values for orbital elements of Echo I.

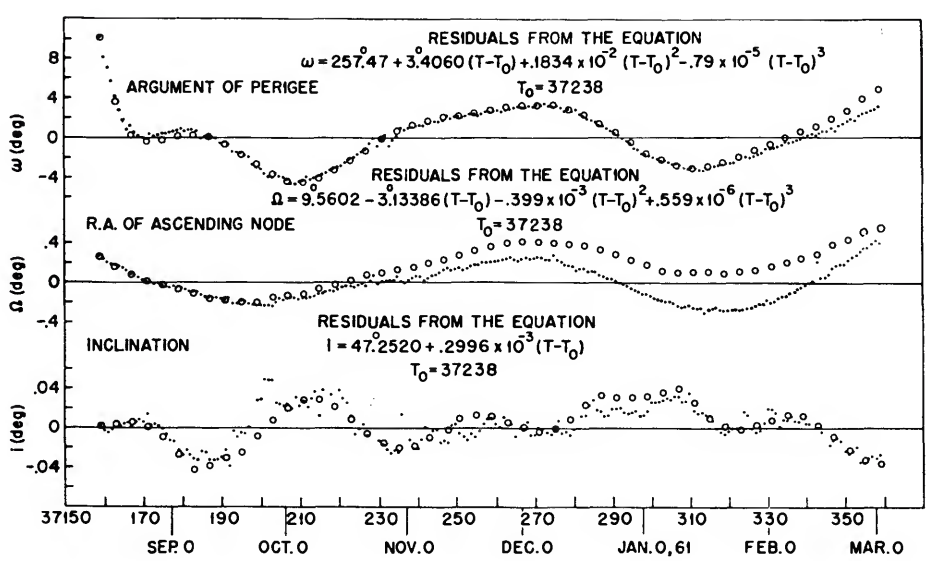

FIGURE 2.—Comparison of experimental and theoretical values for orbital elements of Echo I.

We see that for ω the two curves are generally in good agreement until about February 1, 1961, at which time they start to deviate systematically. Part of this discrepancy would be eliminated by reducing the rate of mass loss of the satellite during the middle of December, 1960, since the contribution to $\dot{\omega}$ due to radiation pressure is positive from 40 days after launch through March 1, 1961.[4] (The combined effect of these changes would reduce the differences between the theoretical and the experimental values of the eccentricity.) We are also investigating the consequences of a possible diurnal bulge in the atmosphere (Jacchia, 1960a). Such a bulge in the equidensity contours will be effective in changing ω when it intersects the orbit plane in a region asymmetrically placed with respect to the apsidal line. To estimate crudely the magnitude of this change in ω, we consider the density to have a δ-function contribution superposed on the otherwise uniform density of the atmosphere along the satellite path. Limited by the average, over-all density deduced from figure 3, we find that ω can change at a maximum rate of approximately 0.1 deg/day.

The theoretical and experimental residuals of Ω are in good agreement until the end of September, 1960. The systematic deviations that occur after that date would be substantially eliminated by correcting the average densities. The relatively low theoretical air density values before January 1, 1961, caused an increase in the residuals, whereas the relatively high subsequent values reduced the residuals. The experimental and theoretical values of i are in close agreement except for a short period near the end of September, 1960.[5] The oscillations in the inclination angle during the first few months after launch are due primarily to effects of sunlight pressure as predicted elsewhere (Shapiro and Jones, 1960).

In figure 3 we have plotted the contributions to the rate of change of period ($\dot{P}$) due to atmospheric drag and to solar-radiation pressure. We computed first the total "observed" dP/dt; then, using the theory outlined in the previous section, we found the rates of change due to radiation pressure ($\dot{P}(R)$). These were then subtracted from dP/dt to obtain the values $\dot{P}(D)$, which we attribute to air drag.[6] As can be seen by comparison with the upper graph in figure 3, the variations in $\dot{P}(D)$ seem to correlate with the variations of the solar flux at the 10.7-cm wavelength. In addition, $-\dot{P}(D)$ exhibits a marked increase at the time of the major solar flare on November 12, 1960 (Jacchia, 1960a). (The wide "scatter" of $\dot{P}(D)$ values in early December, 1960, makes it difficult to discern a correlation with the major flare that occurred during that period.)

We note that radiation pressure can have no effect on the period if the orbit is circular. However, if the orbit is noncircular and is partly in shadow, the satellite can enter and leave the shadow region at different distances from the center of the earth. The resulting net gain or net loss of energy from the radiation field is proportional to the difference of the projections of these distances along the earth-sun line.

From figure 3, we also see that the radiation-pressure contribution to dP/dt is, in general, of the same order of magnitude as that of air drag at these altitudes. Paradoxically, when perigee height is near its minimum value, the change in energy induced by radiation pressure is still comparable to that caused by air drag, despite the increased air density. This fact can be understood in a qualitative way from the following argument. If the air density depends only on height, then as a function of eccentricity, the energy change in one revolution owing to air drag is represented by a constant term plus terms in even powers of the eccentricity. On the other hand, when the qualifications given above are satisfied, the energy change per revolution caused by radiation pressure is represented by a linear

[4] Except for the first week after launch, the change in ω due to radiation pressure is negligibly small until early October, 1960. However, we note that sunlight pressure contributes about 15 percent of the 3.4 deg/day mean rate of change of ω.

[5] The change in i due to a rigid rotation of the atmosphere was not included in our theoretical computations. Its cumulative value on March 1, 1961, would be about −0.01 degree. A more refined analysis will be necessary to establish the presence of this effect on the orbit of Echo.

[6] A portion of this drag may be attributed to a possible dust belt around the earth. However, if one assumes that the air density is correlated with the 10.7-cm wavelength solar flux and that the density of the dust belt is not so correlated, then it appears that at most a small fraction of $\dot{P}(D)$ is due to dust drag.

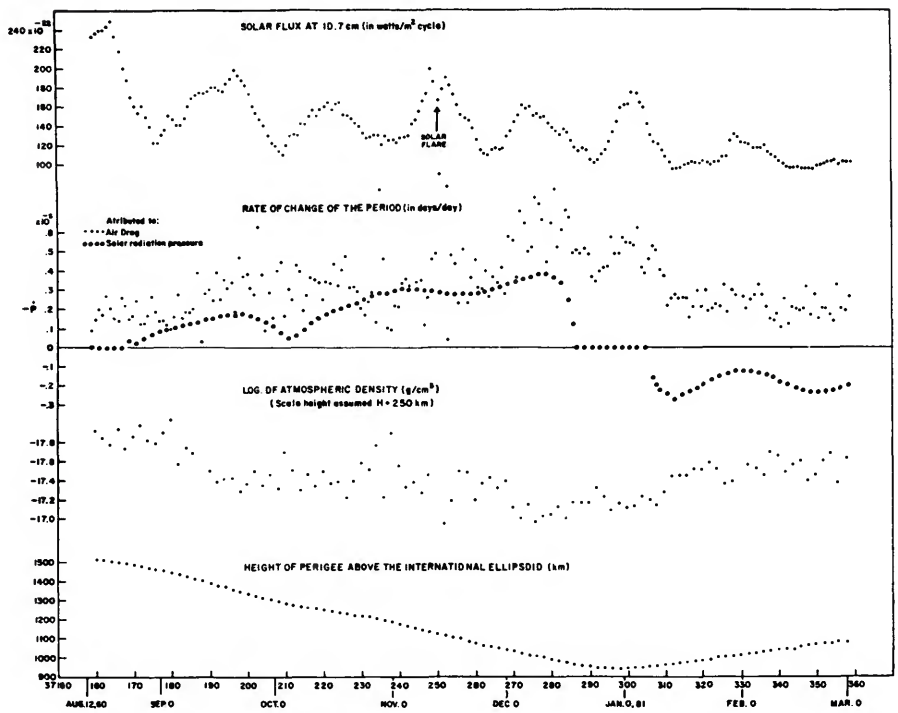

FIGURE 3.—Effects of solar activity on the motion of Echo I.

term plus higher powers in the eccentricity. Hence, the energy change owing to radiation pressure can increase more rapidly with increasing eccentricity than can the energy change owing to air drag when the atmospheric scale height is reasonably large.

We note that Echo I lost energy to the solar-radiation field until the end of December, 1960; then the satellite stayed in sunlight throughout its orbit for about two weeks. In January, 1961, the satellite gained energy from the solar radiation, in the manner described above.[7] In fact, during the latter part of January and much of February, 1961, it gained more energy from the solar-radiation field than was lost to air drag. This marked the first time that a passive artificial satellite exhibited an actual increase in period.

Through March 1, 1961, the cumulative loss of orbital energy of Echo I was manifested in a decrease of about 50 km in its semimajor axis. Of this total, approximately 0.1 km can be attributed to the Poynting-Robertson drag effect. Unfortunately, this effect is hopelessly masked by the large and rapid fluctuations in the atmospheric drag.

[7] In general, a satellite will lose energy to the radiation field when sunlight pressure causes its perigee height to fall, and will gain energy when this pressure causes the perigee height to rise.

Computation of atmospheric densities

It is generally assumed that the neutral air drag acceleration is given by $-\frac{1}{2}C_D(A/M)v^2\rho$, where C_D is a dimensionless aerodynamic drag coefficient; v is the velocity of the satellite relative to the atmosphere; and ρ is the atmospheric density. Using this assumption, one obtains a relation between $\dot{P}(D)$ and the air density ρ_p at the height of the perigee of the satellite's orbit. This relation is

$$\dot{P}(D)=-fC_D(A/M)\rho_p, \qquad (1)$$

where f is given by a rather complicated function of the orbital eccentricity, the oblateness of the earth, and the (assumed) velocity of rotation of the atmosphere (Sterne, 1959). In the derivation of this formula it was assumed that the atmospheric density at an altitude

ΔZ above perigee can be expressed by

$$\rho=\rho_p \exp(-\Delta Z/H), \quad (2)$$

where H is the density scale height.

There are several difficulties associated with inferring atmospheric densities from equation (1). First, it is necessary to use the appropriate $\dot{P}$. With the mean anomaly represented by a polynomial like $M=M_0+M_1(t-t_0)+M_2(t-t_0)^2$, where t_0 is the epoch of the elements, it is usual to consider the rate of change of the period to be given by $\dot{P}=-2M_2/M_1^2$. This form, however, leads to difficulty because the mean anomaly is measured from perigee, the angular motion of which is subject to relatively large variations owing to the solar-radiation pressure. On the other hand, equation (1) was derived on the assumption that the perigee position is stationary. Therefore, in order to use an equivalent $\dot{P}$, we corrected M_2 for the contribution due to the mean acceleration of ω. We then calculated $\dot{P}(D)$ by subtracting $\dot{P}(R)$ from the "corrected" values of $\dot{P}$.

Second, it is not clear what value should be used for C_D. The concepts usually employed in calculating C_D may require considerable modifications for the high altitudes traversed by Echo I. If, however, a future analysis indicates that a different (but constant) value of C_D should be used, then it will be quite simple to correct our density determinations.

Third, it is difficult to determine a meaningful value for the scale height since densities at different altitudes have been calculated for different periods of time. Since the density at each altitude suffers large fluctuations in time, comparing densities at different altitudes at different times is inadequate for determining the relation between densities at different altitudes at the same time. From figure 3 it would seem, as has been shown at lower altitudes, that the solar activity must be considered when determining scale heights. A further difficulty is caused by the possible diurnal bulge in the atmosphere which, among other things, can invalidate equation (2). In any case, the rather large fluctuations in our values of $\dot{P}(D)$ seriously limit the accuracy of scale-height calculations.

In our computation we assumed that the ratio (A/M) varied with time (as determined from our theoretical match with the experimental variations in eccentricity), and that C_D maintained the constant value 2.5 (Stirton, 1960). Air densities corresponding to five possible scale-height values (ranging from 50 to 450 km) were then computed. Some of our results are given in table 2 of Smithsonian Special Report No. 61. For illustrative purposes, we present in figure 3 only the densities derived from the assumption of a 250-km scale height. Of course it should be understood that the scale height is probably not constant over this altitude (and time) range.

Because of the uncertainties in our values of the drag coefficient and the scale height, the densities we have inferred from the orbit of Echo I must be considered provisional. Certainly a more refined analysis of the data is needed to improve bad determinations of $\dot{P}(D)$.

Lifetime of Echo I

Because our knowledge of air densities and the variation of drag coefficient with altitude is inadequate, we find it almost impossible to predict accurately the lifetime of Echo I. We do know, however, that the perigee altitude and the eccentricity oscillate with a peak-to-peak period of about 300 days.[8]

In view of the large amplitude oscillation of perigee height, it is most likely that the satellite will perish soon after one of these regular dips of perigee into the atmosphere. Hence, one can estimate the month of "death" almost as accurately as the year. The best estimate we can make, using air-density values determined during the first few months after the launch, is that the balloon will stop orbiting shortly after its fourth dip into the atmosphere in July, 1963, if its shape is not substantially changed before then.[9] However, in view of the decrease in air density to be expected in the next few years (in accordance with the correlation between sunspot activity and upper atmosphere densities),[10] the balloon will probably survive at least until its fifth dip in the spring of 1964. In figure 4 we

[8] More accurately, the period from maximum-to-maximum value of perigee altitude is closer to 310 days, while the minimum-to-minimum period varies.

[9] Cross-section measurements made on Echo I by the M.I.T. Millstone Hill Radar indicate that little change occurred in the shape of the balloon from the first few days after launch until January 11, 1961.

[10] For this and other useful suggestions, we thank Dr. L. G. Jacchia.

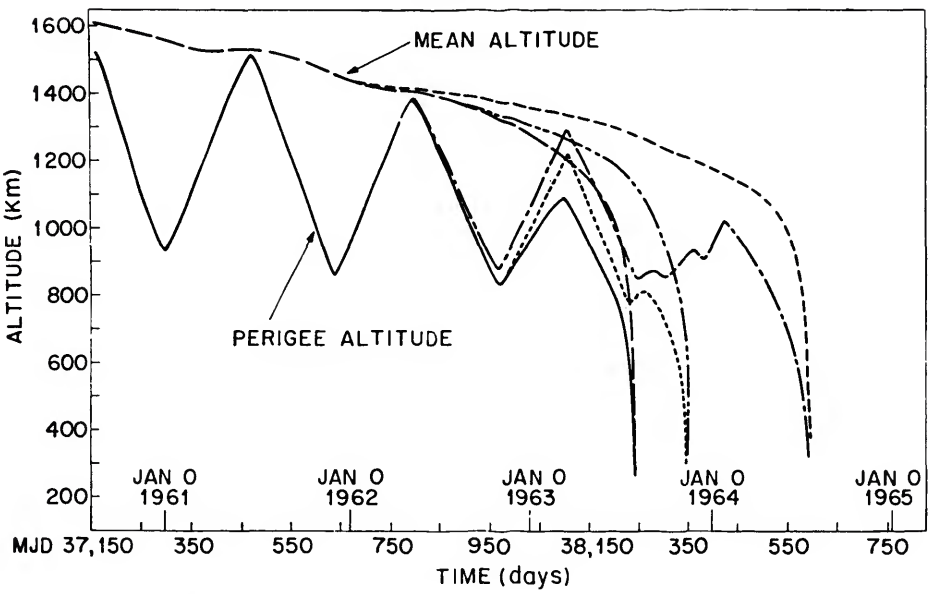

FIGURE 4.—Time variation of perigee altitude and mean altitude of Echo I.

present the time variation of perigee altitude and mean altitude for several different extrapolations of our density model. These curves illustrate various possibilities for the behavior of perigee distance near the end of the balloon's life.

Acknowledgment

We express our gratitude to Mrs. Beatrice Miller for her excellent work in calculating the theoretical and experimental residuals of the orbital elements.

Abstract

In this paper we compare theoretical and experimental determinations of the orbit of Satellite 1960 ι 1 (Echo I). The experimental orbit was deduced from Baker-Nunn photographic data.

The observed variations of the Echo orbit—due primarily to the effects of the pressure of sunlight—are in excellent agreement with our theoretical results. The perigee altitude has an oscillation of large amplitude (approximately 600km) and long period (approximately 300 days), which has a decisive influence on the lifetime of Echo I. Our present best estimate is that the balloon will perish in the spring of 1964.

We have also estimated the rate of escape of gas from the balloon by comparing the observed and the calculated variations in orbit eccentricity.

From the changes in orbital period we have inferred air densities over the altitude range 950 to 1500 km, making corrections for the rather large changes in period that are due to a net loss or net gain of energy from the solar-radiation field. The atmospheric drag is strongly correlated with the flux of the 10-cm and 20-cm solar radiations, as well as with a major solar flare.

The Atmospheric Drag of Artificial Satellites During the October 1960 and November 1960 Events

By Luigi G. Jacchia

Accurate accelerations dP/dt were derived in the interval from November 4 through 24, 1960, for six satellites with perigee heights ranging from 350 to 1121 km.

The accelerations were determined by the following procedure. Using the Differential Orbit Improvement (DOI) program of the Smithsonian Astrophysical Observatory, we computed the orbits at suitable intervals. We then fitted, by means of least squares, empirical time functions to all the elements in the 20-day interval, allowing no systematic residuals except in the mean anomaly M, in which the residuals were permitted to rise to $\pm 10^{-3}$ revolutions in exceptional cases (the error in the major axis resulting from such residuals is smaller than 50 meters). The empirical functions representing the elements were then fed into the DOI program modified to yield residuals in the mean anomaly for individual observations when the orbital elements and their time variations are given. We then plotted these residuals, and added the second time derivative of the resulting curve to the second time derivative of the empirical equation for M; allowance was made for any acceleration resulting from the motion of the perigee. The resulting values of d^2M/dt^2 were then transformed to dP/dt.

The results of these computations are shown in figure 1, in which the acceleration curves are arranged in decreasing order of perigee height z_p. At the bottom we have added the acceleration curve derived by G. V. Groves (1961) for Satellite 1959 $\epsilon 2$. The accelerations of Satellite 1960 $\iota 1$ have been corrected for the effect of radiation pressure, according to the data of Zadunaisky, Shapiro, and Jones (1961).

All these curves are rather faithful images of the geomagnetic-index curves shown in the lower part of the diagram. Since the acceleration curves are drawn in natural rather than in logarithmic scale, the correspondence should be best with the a_p index, of which A_p is a daily mean. The two major magnetic perturbations, with maxima at November 13.4 and November 16.1 (U.T.) are reflected in all the acceleration curves with no appreciable time differential and with relative intensities comparable to those of the peaks in the a_p curve. The beginning and end of the perturbations are essentially coincident with the beginning and end of the magnetic storm, confirming previous results by the author (Jacchia, 1959b). The weaker perturbation of November 21 is clearly visible in the acceleration curve of Echo I (Satellite 1960 $\iota 1$) and can be traced in those of Satellites 1959 $\alpha 1$ and 1960 $\xi 1$.

The figures outside the right margin of figure 1 give the mean value $\overline{A}$ of dP/dt for each satellite before and after the perturbations of November 12 through 17. The plotted points represent the ratio $A/\overline{A}$ of the instantaneous acceleration A to this mean value $\overline{A}$. The relative intensity of the perturbation for each satellite can thus be estimated directly from the amplitude of the individual curves—i.e., by reading the maximum ordinate on the scale on the left. Other pertinent data—the declination of the satellite's perigee δ_p and the geocentric angle ψ between the perigee

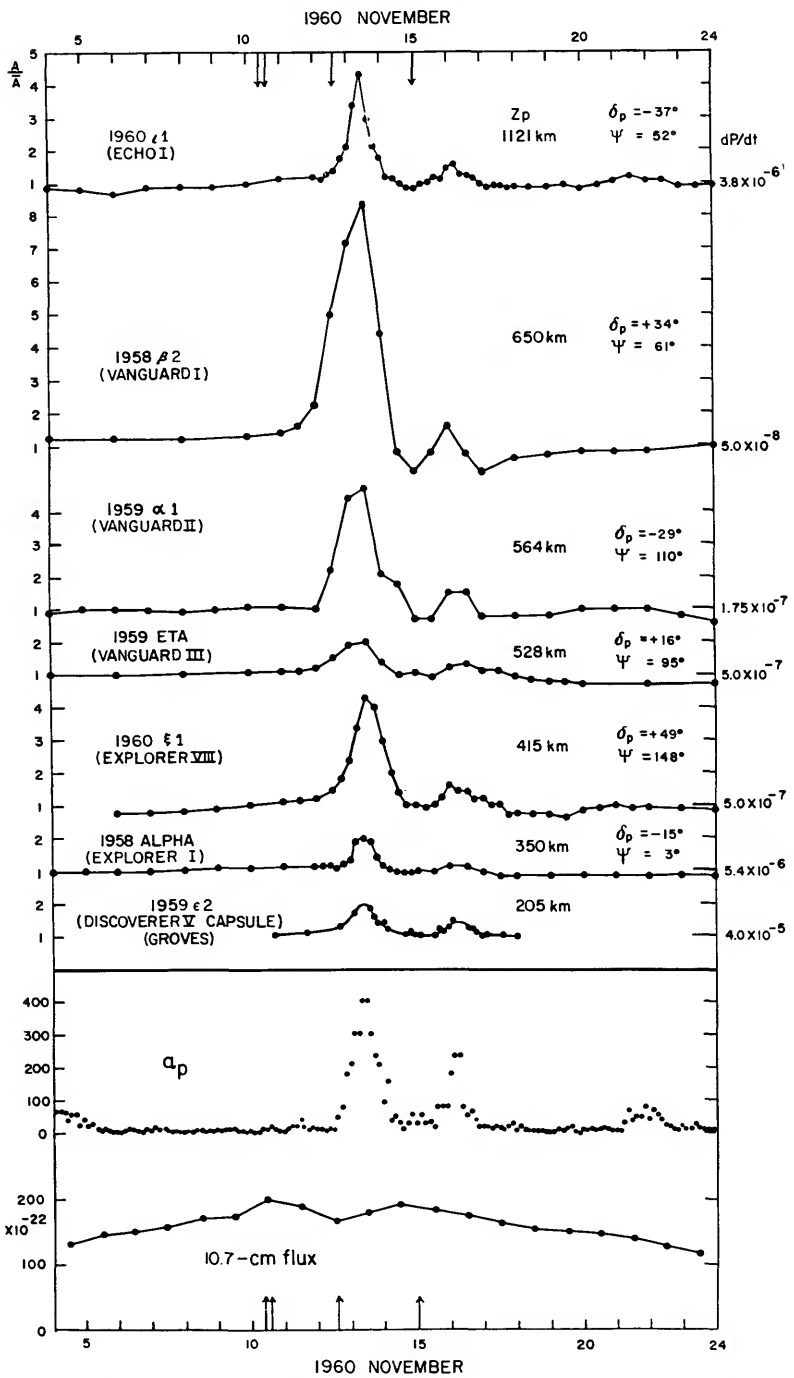

FIGURE 1.—Atmospheric drag of seven artificial satellites during the November 1960 events, compared with the geomagnetic planetary index a_p and the solar flux at 10.7 cm.

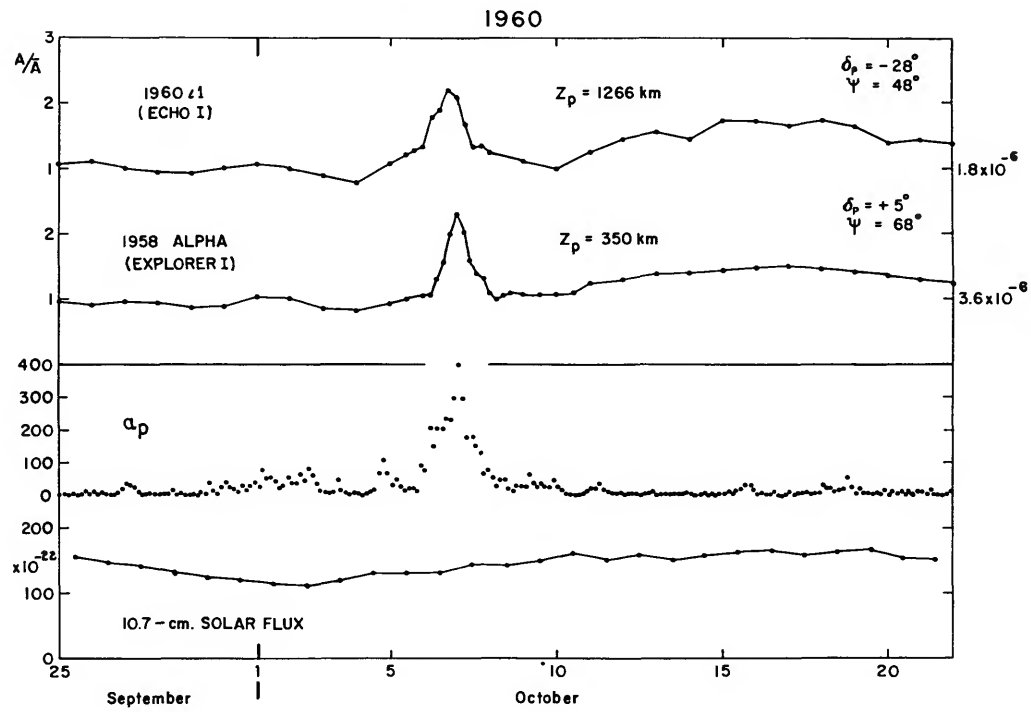

FIGURE 2.—Atmospheric drag of two artificial satellites during the magnetic storm of October 6–7, 1960, compared with the geomagnetic planetary index a_p and the solar flux at 10.7 cm.

and the sun—are given inside the right margin of the diagram. The arrows at the top and at the bottom of the diagram mark the instant corresponding to the appearance of 3^+ flares on the sun.

It should be apparent that the amplitude of the perturbation shows a general tendency to be greater at greater heights, although other factors probably complicate the picture. The two lowest satellites (z_p = 205 and 305 km, respectively) show a jump by a factor of 2 in the drag during the November 13 perturbation, not much greater than the amplitude observed for Satellite 1958 δ1 ($z_p \approx 220$ km) during the magnetic storms of July 9 and September 4, 1958 (Jacchia, 1959b). A correlation of the amplitudes with δ_p and ψ is not immediately apparent. It is true that Satellite 1960 ξ1, with a large amplitude, had its perigee in relatively high latitudes (+49°); on the other hand, Satellite 1958 β2, with the largest amplitude of all, has an inclination of 34°, which keeps the satellite at low latitudes throughout its orbit. The smaller amplitude of the perturbation for the Echo I satellite could be explained by the much greater scale height prevailing at that height.

More clues seem to be necessary to understand the mechanism through which corpuscular radiation interacts with the atmosphere.

As an addendum we present in figure 2 the accelerations of Satellites 1960 ι1 and 1958 Alpha, during the magnetic storm of October 6–7, 1960. The increase of the atmospheric drag amounted to a factor of a little over 2 for both satellites; again the development of the perturbation was simultaneous with that of the magnetic storm.

All satellite accelerations are tabulated in tables 1 and 2.

TABLE 1.—*Accelerations* $\dot{P}$ *of six satellites during the November 1960 events*

($\dot{P}_R$ is the acceleration due to radiation pressure, according to Zadunaisky, Shapiro, and Jones (1960).)

1960 ι1 (Echo I)

Nov. 1960	$10^6\,\dot{P}$	$10^6\,\dot{P}_R$	$10^6(\dot{P}-\dot{P}_R)$
4.0	−6.0	−2.9	−3.1
5.0	−6.0	−3.0	−3.0
6.0	−5.5	−2.9	−2.6
7.0	−6.2	−2.9	−3.3
8.0	−6.2	−2.9	−3.3
9.0	−6.2	−2.9	−3.3
10.0	−6.7	−2.9	−3.8
11.0	−7.3	−2.9	−4.4
11.8	−7.1	−2.9	−4.2
12.0	−7.3	−2.9	−4.4
12.2	−7.1	−2.8	−4.3
12.4	−7.6	−2.8	−4.8
12.6	−8.0	−2.8	−5.2
12.8	−9.4	−2.8	−6.6
13.0	−10.8	−2.8	−8.0
13.2	−15.7	−2.8	−12.9
13.4	−19.2	−2.8	−16.4
13.6	−14.1	−2.8	−11.3
13.8	−11.0	−2.8	−8.2
14.0	−9.6	−2.8	−6.8
14.2	−7.4	−2.8	−4.6
14.4	−7.2	−2.8	−4.4
14.6	−6.6	−2.8	−3.8
14.8	−6.2	−2.8	−3.4
15.0	−6.0	−2.8	−3.2
15.2	−6.5	−2.8	−3.7
15.4	−6.7	−2.8	−3.9
15.6	−7.2	−2.8	−4.4
15.8	−7.2	−2.8	−4.4
16.0	−8.3	−2.8	−5.5
16.2	−8.8	−2.8	−6.0
16.4	−7.6	−2.8	−4.8
16.6	−7.5	−2.8	−4.7
16.8	−7.3	−2.8	−4.5
17.0	−6.6	−2.8	−3.8
17.2	−6.3	−2.8	−3.5
17.4	−6.4	−2.8	−3.6
17.6	−6.4	−2.8	−3.6
17.8	−6.1	−2.8	−3.3
18.0	−6.2	−2.8	−3.4
18.5	−6.3	−2.8	−3.5
19.0	−6.2	−2.8	−3.4
19.5	−6.4	−2.8	−3.6
20.0	−6.0	−2.8	−3.2
20.5	−6.4	−2.8	−3.6
21.0	−6.8	−2.8	−4.0
21.5	−7.4	−2.8	−4.6
22.0	−7.1	−2.9	−4.2
22.5	−7.1	−2.9	−4.2
23.0	−6.4	−2.9	−3.5
23.5	−6.4	−2.9	−3.5
24.0	−6.6	−3.0	−3.6
24.5	−6.6	−3.0	−3.6
25.0	−6.6	−3.0	−3.6

TABLE 1.—*Accelerations* $\dot{P}$ *of six satellites during the November 1960 events*—Continued

1958 β2 (Vanguard I)

Nov. 1960	$10^7\,\dot{P}$
4.0	−0.61
6.0	−0.61
8.0	−0.59
10.0	−0.65
11.0	−0.69
11.5	−0.8
12.0	−1.1
12.5	−2.5
13.0	−3.6
13.5	−4.2
14.0	−2.2
14.5	−0.4
15.0	−0.1
15.5	−0.4
16.0	−0.8
16.5	−0.4
17.0	−0.1
18.0	−0.3
19.0	−0.35
20.0	−0.4
21.0	−0.4
22.0	−0.4
24.0	−0.5
26.0	−0.5

1959 α1 (Vanguard II)

Nov. 1960	$10^7\,\dot{P}$
4.0	−1.5
5.0	−1.8
6.0	−1.7
7.0	−1.7
8.0	−1.6
9.0	−1.8
10.0	−1.9
11.0	−1.9
12.0	−1.7
12.5	−3.8
13.0	−7.7
13.5	−8.3
14.0	−3.7
14.5	−3.1
15.0	−1.3
15.5	−1.2
16.0	−2.7
16.5	−2.7
17.0	−1.4
18.0	−1.4
19.0	−1.4
20.0	−1.8
21.0	−1.7
22.0	−1.7
23.0	−1.4
24.0	−1.1

TABLE 1.—*Accelerations* $\ddot{P}$ *of six satellites during the November 1960 events*—Continued

1959 Eta (Vanguard III)

Nov. 1960	$10^7 \dot{P}$
4.0	−4.9
6.0	−5.0
8.0	−5.1
10.0	−5.4
11.0	−5.6
11.5	−5.6
12.0	−5.9
12.5	−7.6
13.0	−9.5
13.5	−9.9
14.0	−6.9
14.5	−5.0
15.0	−5.3
15.5	−4.7
16.0	−6.0
16.5	−6.7
17.0	−5.7
17.5	−5.7
18.0	−4.7
18.5	−4.1
19.0	−3.7
19.5	−3.7
20.0	−3.4
22.0	−3.5
24.0	−3.6

1960 ξ1 (Explorer VIII)

Nov. 1960	$10^6 \dot{P}$
6.0	−0.37
7.0	−0.39
8.0	−0.41
9.0	−0.45
10.0	−0.50
11.0	−0.56
11.5	−0.58
12.0	−0.61
12.5	−0.75
12.75	−0.92
13.00	−1.2
13.25	−1.7
13.50	−2.15
13.75	−2.0
14.00	−1.5
14.25	−1.0
14.50	−0.7
14.75	−0.5
15.00	−0.5
15.25	−0.45
15.50	−0.5
15.75	−0.6
16.00	−0.8
16.25	−0.7
16.50	−0.7
16.75	−0.6

TABLE 1.—*Accelerations* $\dot{P}$ *of six satellites during the November 1960 events*—Continued

1960 ξ1 (Explorer VIII)

Nov. 1960	$10^6 \dot{P}$
17.00	−0.6
17.25	−0.5
17.50	−0.5
17.75	−0.35
18.0	−0.37
18.5	−0.36
19.0	−0.35
19.5	−0.30
20.0	−0.40
20.5	−0.44
21.0	−0.50
21.5	−0.46
22.0	−0.47
23.0	−0.44
24.0	−0.42

1958 Alpha (Explorer I)

Nov. 1960	$10^6 \dot{P}$
4.0	−5.14
5.0	−5.11
6.0	−5.16
7.0	−5.37
8.0	−5.59
9.0	−5.67
10.0	−5.79
11.0	−6.10
12.0	−5.9
12.2	−6.1
12.4	−6.1
12.6	−5.9
12.8	−6.5
13.0	−7.0
13.2	−10.3
13.4	−10.7
13.6	−10.3
13.8	−7.6
14.0	−6.4
14.2	−5.6
14.4	−5.2
14.6	−5.2
14.8	−5.2
15.0	−5.31
15.5	−5.38
16.0	−6.16
16.5	−5.84
17.0	−5.17
17.5	−4.56
18.0	−4.48
19.0	−4.57
20.0	−4.58
21.0	−4.50
22.0	−4.56
23.0	−4.57
24.0	−4.55

TABLE 2.—*Accelerations $\dot{P}$ of two satellites during the October 1960 events*

($\dot{P}_R$ is the acceleration due to radiation pressure, according to Zadunaisky, Shapiro, and Jones (1960).)

1960 ι1 (Echo I)

Sep. 1960	$10^6\,\dot{P}$	$10^6\,\dot{P}_R$	$10^6\,(\dot{P}-\dot{P}_R)$
25. 0	−3. 55	−1. 63	−1. 9
26. 0	−3. 55	−1. 56	−2. 0
27. 0	−3. 26	−1. 49	−1. 8
28. 0	−3. 07	−1. 36	−1. 7
29. 0	−2. 87	−1. 22	−1. 65
30. 0	−2. 84	−1. 05	−1. 8
Oct. 1. 0	−2. 74	−0. 88	−1. 9
2. 0	−2. 52	−0. 71	−1. 8
3. 0	−2. 11	−0. 56	−1. 6
4. 0	−1. 89	−0. 50	−1. 4
5. 0	−2. 46	−0. 51	−1. 95
5. 50	−2. 8	−0. 56	−2. 2
5. 75	−2. 9	−0. 58	−2. 3
6. 00	−3. 0	−0. 61	−2. 4
6. 25	−3. 8	−0. 64	−3. 2
6. 50	−4. 1	−0. 68	−3. 4
6. 75	−4. 7	−0. 71	−3. 95
7. 00	−4. 5	−0. 75	−3. 8
7. 25	−3. 8	−0. 79	−3. 0
7. 50	−3. 3	−0. 82	−2. 4
7. 75	−3. 3	−0. 86	−2. 4
8. 00	−3. 2	−0. 90	−2. 3
9. 0	−3. 04	−1. 05	−2. 0
10. 0	−2. 97	−1. 19	−1. 8
11. 0	−3. 57	−1. 32	−2. 25
12. 0	−4. 08	−1. 44	−2. 6
13. 0	−4. 22	−1. 45	−2. 8
14. 0	−4. 23	−1. 62	−2. 6
15. 0	−4. 79	−1. 70	−3. 1
16. 0	−4. 87	−1. 78	−3. 1
17. 0	−4. 79	−1. 84	−2. 95
18. 0	−4. 99	−1. 91	−3. 1
19. 0	−4. 95	−2. 00	−2. 95
20. 0	−4. 55	−2. 06	−2. 5
21. 0	−4. 79	−2. 13	−2. 6
22. 0	−4. 71	−2. 21	−2. 5

1958 Alpha (Explorer I)

Sep. 1960	$10^6\,\dot{P}$
25. 0	−3. 5
26. 0	−3. 3
27. 0	−3. 5
28. 0	−3. 5
29. 0	−3. 1
30. 0	−3. 2

TABLE 2.—*Accelerations $\dot{P}$ of two satellites during the October 1960 events*—Continued

1958 (Alpha Explorer I)

Oct. 1960	$10^6\,\dot{P}$
1. 0	−3. 7
2. 0	−3. 6
3. 0	−3. 1
4. 0	−3. 0
5. 0	−3. 4
5. 5	−3. 6
6. 0	−3. 8
6. 2	−3. 8
6. 4	−4. 8
6. 6	−5. 6
6. 8	−7. 2
7. 0	−8. 3
7. 2	−7. 3
7. 4	−5. 8
7. 6	−5. 0
7. 8	−4. 8
8. 0	−3. 9
8. 2	−3. 6
8. 4	−3. 8
8. 6	−3. 8
8. 8	−3. 9
9. 0	−3. 8
9. 5	−3. 9
10. 0	−3. 9
10. 5	−4. 0
11. 0	−4. 5
12. 0	−4. 7
13. 0	−5. 0
14. 0	−5. 0
15. 0	−5. 2
16. 0	−5. 3
17. 0	−5. 4
18. 0	−5. 3
19. 0	−5. 1
20. 0	−4. 8
21. 0	−4. 7
22. 0	−4. 5

Acknowledgment

The assistance of Mr. Jack W. Slowey is gratefully acknowledged.

Effect of the Diurnal Atmospheric Bulge on Satellite Accelerations

By Stanley P. Wyatt

The spherically symmetric isothermal atmosphere

Several authors have derived expressions for the secular acceleration of a satellite moving through the high atmosphere (Sterne, 1958b; Groves, 1958b; King-Hele, Cook, and Walker, 1959). The simplest and most tractable assumptions one can make are that the terrestrial atmosphere is spherically symmetric, stationary, and of constant scale height throughout those strata traveled by the satellite in question. Within the framework of these assumptions, the secular acceleration is given by

$$\frac{\Delta P}{P}=-3C_D\frac{A}{m}\frac{q\rho_q}{(1-e)}\int_0^\pi\frac{(1+e\cos E)^{3/2}}{(1-e\cos E)^{1/2}}\epsilon^{-c(1-\cos E)}dE. \tag{1}$$

Here, $\Delta P/P$ is the dimensionless change of period per period; C_D the drag coefficient; A/m the ratio of the average geometrical cross-section of the satellite to its mass; q the perigee distance and e the eccentricity of the satellite; ρ_q the atmospheric density at the level of perigee; E the eccentric anomaly of the satellite; and ϵ the base of natural logarithms. The dimensionless constant c is defined by $c=qe/H(1-e)$, where H is the scale height of the atmosphere and is assumed to be constant.

Equation (1) can be integrated by two techniques, depending on the magnitude of c and e for the satellite in question. For present-day satellites, the value of q is between approximately 6600 and 8000 km, and of e between 0.00 and 0.25. The scale height of the high atmosphere lies in the approximate range 50 to 100 km. Thus q/H is a large number, between 60 and 160, and the relevant values of c for existing satellites are between 0 and 50. For a satellite orbit of moderate eccentricity, the drag is significant only near perigee. Using the formulas of Sterne (1959), one can change the variable of integration in equation (1) through the substitution $1-\cos E=y^2/c$, making the integrand the product of ϵ^{-y^2} times a power series in y^2/c. The upper limit of integration can be extended to infinity because of the negligibly small air density at large values of y. The secular acceleration for such satellites is given by Sterne's equation (10), with $d=1$. I have confirmed his result; in a spherically symmetric, stationary atmosphere, the secular acceleration of a satellite in an appreciably eccentric orbit is

$$\frac{\Delta P}{P}=-\frac{3\sqrt{\pi}}{\sqrt{2}}C_D\frac{A}{m}\frac{\sqrt{Hq}}{\sqrt{e}}\frac{(1+e)^{3/2}}{(1-e)}\rho_q\left[1+\frac{1}{2}\frac{H}{q}M+\frac{3}{4}\frac{H^2}{q^2}N+\ldots\right], \tag{2}$$

where

$$M=\frac{1-8e+3e^2}{4e(1+e)}, \tag{3a}$$

and

$$N=\frac{3-16e+50e^2+16e^3-5e^4}{32e^2(1+e)^2}. \tag{3b}$$

This formula is accurate to one percent for values of $c\geqq 2.5$ and therefore can be used for all satellites with $e>0.04$.

For small eccentricities, the atmospheric drag is appreciable all around the orbit; consequently, equations (2), (3a), and (3b) are not valid. Instead, equation (1) can be expressed as the product of $\epsilon^{c \cos E}$ times a power series in $e \cos E$. The integral can then be evaluated in terms of Bessel functions of imaginary argument. If n is a positive integer, we have

$$\int_0^{\pi} \epsilon^{c \cos E} \cos nE dE = \pi I_n(c) = \pi \sum_{m=0}^{\infty} \frac{(c/2)^{n+2m}}{m!(n+m)!}. \tag{4}$$

To order e^3, Sterne (1959) finds and I confirm that within the framework of the stated assumptions, the secular acceleration of a satellite is

$$\frac{\Delta P}{P} = -3\pi C_D \frac{A}{m} a \rho_a [\epsilon^{-c} I_0(c) V_0 + e \epsilon^{-c} I_1(c) V_1], \tag{5}$$

where a is the orbital semimajor axis and where

$$V_0 = 1 + \frac{3}{2} e^2 - \frac{e^3}{c}, \tag{6a}$$

and

$$V_1 = 2 - \frac{3}{2} \frac{e}{c} + e^2 \left(1 + \frac{2}{c^2}\right). \tag{6b}$$

Tables of $\epsilon^{-c} I_0(c)$ and $\epsilon^{-c} I_1(c)$ are available in Watson's (1944) treatise on Bessel functions. For a circular orbit, equation (5) reduces to

$$\frac{\Delta P}{P} = -3\pi C_D \frac{A}{m} a \rho_a. \tag{7}$$

Some complicating effects

Modifications of these equations have been derived for several effects. One interesting generalization is the assumption that atmospheric density is a function of height above the oblate-spheroidal earth rather than above a sphere (Groves, 1958; Sterne, 1959). Thus when the perigee of a satellite is located at high latitude, the predicted drag is less than when it is later located near the equator. For a polar satellite, the secular acceleration arising from such an effect would vary approximately 15 percent either side of the mean during rotation of perigee for a scale height of 50 km, and approximately 10 percent for a scale height of 100 km. For low-inclination satellites, the variation would be less. As we shall see later, however, this effect is masked by others for high satellites.

A second modification of the drag equation takes account of the rotation of the atmosphere with the earth (Sterne, 1959). A satellite moving in a direct orbit experiences a "headwind" of smaller magnitude than does one moving in a retrograde orbit. For equatorial orbits, neglect of atmospheric rotation leads to errors of approximately 10 percent in the secular accelerations. For orbits of higher inclination the error is smaller.

A third modification accounts for the increasing scale height of the atmosphere with height above ground (Jacchia, 1960b). From data at heights near 400 km, Jacchia finds that neglect of this variation leads to overestimates of the acceleration by approximately 5 percent in the nighttime atmosphere, and up to 10 percent in the daytime atmosphere. The maximum error occurs near $e=0.02$; of course, the error must be zero for a circular orbit.

The diurnal bulge of the atmosphere

The assumption of a spherically symmetric atmosphere at heights of several hundreds of kilometers has been shown to be untenable by several analyses (Jacchia, 1959c; 1960a; Priester and Martin, 1960; Wyatt, 1959). The high atmosphere bulges toward a point in the sky some 15° to 30° east of the sun. For a fixed index of solar activity, the observed accelerations of Satellite 1958 $\beta 2$ (Vanguard

I) indicate that the air density at 665 km is about 10 times as great when perigee passage occurs an hour or two after noon as when it occurs during the night. It is also clear from observations of several satellites that the scale height of the atmosphere increases with height at all times of day.

Interpreting these results physically, Nicolet (1960a) finds that the density of the high atmosphere is governed largely by the absorption of solar ultraviolet radiation below 200 km. The influx of energy fixes the temperature gradient of the atmosphere between 200 and 300 km and also the temperature of the nearly isothermal atmosphere at greater heights. Because the ultraviolet input at any place depends both on the time of day there and on the general level of solar activity, the high-atmosphere density variations depend on both of these parameters, as observed. Above approximately 300 km the time scale of heat conduction is short and any vertical column of air is isothermal, provided that the injection of heat from the Chapman corona is small. Although T is presumably constant at these levels, the scale height, $H=kT/g\overline{m}$, increases with height. The acceleration of gravity decreases, of course, as the inverse square of the distance from the earth's center, thus contributing to the increase of H. The mean molecular weight $\overline{m}$ also decreases with height, because above approximately 150 km the air is in diffusion equilibrium; each type of molecule is sorted out according to its mass and thus the concentration of N_2 relative to O decreases with height. This factor contributes importantly to the observed increase of scale height with height. It should be added that, although a vertical column above 300 km is spatially isothermal at any one moment, there is a temporal variation of about 500° K between day and night, a variation arising from the varying injection of solar radiant energy at the lower atmospheric levels.

The fundamental drag equation in a bulging atmosphere

Jacchia (1960a) stresses that the diurnal bulge will distort the motions of satellites from the motions they would have if the atmosphere were spherically symmetric. The chief problem addressed in the present paper is the derivation of a fundamental drag equation for a bulging atmosphere in which the scale height increases with height, followed by a comparison with the spherical approximation with H constant. At the expense of some added calculation, the new equation should permit the derivation of more precise atmospheric densities and other parameters of the high atmosphere.

The most tractable assumption is that the atmosphere is axially symmetric, and this assumption is not at odds with observations to date. I shall adopt it here and, with Jacchia (1960a), shall further assume that the atmospheric bulge always points toward the same declination as the sun, but with a lag angle λ. Thus the right ascension of the symmetry axis is $\alpha_\odot+\lambda$. Previous analyses indicate that $15°\leqq\lambda\leqq30°$, so that at any given level of the high atmosphere the peak density occurs between one and two hours after local noon. Jacchia's analysis of the accelerations of Satellites 1958 Alpha, 1958 $\beta 2$, 1958 $\delta 2$, and 1959 $\alpha 1$ shows that between 200 km and 700 km the atmospheric density can be well represented by

$$\rho=\rho_0(z)F_{20}\{1+0.19[\exp(0.0055z)-1.9]\cos^6(\psi'/2)\}, \tag{8}$$

where

$$\log\rho_0(z)=-16.021-0.001985z+6.363\exp(-0.0026z). \tag{9}$$

These equations are in cgs units except that z, the height above ground, is in kilometers. The angle ψ' is the geocentric angle from the axis of the bulge. Equation (9) gives the density as a function of height for the nighttime atmosphere at a moment when the daily-mean 20-cm solar flux of F_{20} (Priester and Martin, 1960) is unity. Unit flux density is defined as $10^{-20}\ Wm^{-2}(c/s)^{-1}$. As can be seen from equation (8), Jacchia finds that the density at a given point is proportional to the first power of the solar flux, other factors being equal. In the brackets of equation (8), the dependence on ψ' indicates the sharpness of the bulge as found empirically and the dependence on z shows that the diurnal effect increases with height. Equation (8) is of such a form that it includes the effect of increasing scale height with height. Jacchia's two formulas are remarkably successful in representing satellite observations to date. Although they are empirical in nature, I propose to adopt them as a basis for computing the drag equation in a bulging atmosphere.

For any satellite in an orbit of moderate eccentricity, the maximum drag occurs not necessarily at perigee passage, but nevertheless fairly near it. For another satellite in a more circular orbit, the maximum drag may occur at any value of the true anomaly. In either case, the height above perigee, $z-z_q$, at which significant drag occurs is never very large. Let us therefore express equations (8) and (9) in terms of $s=z-z_q$. Also, for economy we shall deduce the drag equation for a constant level of solar activity, setting $F_{20}=1$. Equation (9) for the nighttime atmosphere, $\psi'=\pi$, becomes

$$\rho_0(s)\equiv\rho(s,\pi)=\rho(0,\pi)\,\epsilon^{-.004571s-14.651\epsilon^{-.0026z_q}(1-\epsilon^{-.0026s})}$$

$$\cong\rho(0,\pi)\epsilon^{-(.004571+.03809\epsilon^{-.0026z_q})s}(1+.00004952\epsilon^{-.0026z_q}s^2). \tag{10}$$

The approximation here introduced is needed in order for us to integrate the equations. It underestimates the density given in equation (9) by about one percent two scale heights above perigee and by about 20 percent four scale heights above perigee in the range 200 km $\leqq z_q \leqq$ 600 km; thus, it is an adequate representation for any given orbit. Equation (8) becomes, without approximation,

$$\rho\equiv\rho(s,\psi')=\rho(s,\pi)\{1+0.19[\epsilon^{.0055z_q\epsilon^{.0055s}}-1.9]\cos^6(\psi'/2)\}. \tag{11}$$

The general density function we shall employ is obtained by substituting equation (11) in (10) and is

$$\rho(s,\psi')=\rho(0,\pi)\{[1-K\cos^6(\psi'/2)]\epsilon^{-Qs}+L\cos^6(\psi'/2)\epsilon^{-Rs}\}(1+Us^2), \tag{12}$$

where

$$K=.361,$$
$$L=.19\epsilon^{.0055z_q},$$
$$Q=(.03809\epsilon^{-.0026z_q}+.004571)\ \text{km}^{-1},$$
$$R=(.03809\epsilon^{-.0026z_q}-.000929)\ \text{km}^{-1},$$
$$U=.00004952\epsilon^{-.0026z_q}\ \text{km}^{-2}.$$

These quantities are either constant or are functions of perigee height alone and can be tabulated once and for all. We shall consider the physical significance of some of them later.

Having chosen equation (12) for the density function, we find that the secular acceleration of a satellite becomes

$$\frac{\Delta P}{P}=-3C_D\frac{A}{m}\frac{q\rho(0,\pi)}{(1-e)}\int_o^\tau\frac{(1+e\cos E)^{3/2}}{(1-e\cos E)^{1/2}}\{[1-K\cos^6(\psi'/2)]\epsilon^{-Qs}+L\cos^6(\psi'/2)\epsilon^{-Rs}\}(1+Us^2)dE. \tag{13}$$

To progress further, we must express both ψ' and s as functions of E, the eccentric anomaly.

First let us find the relation between ψ', the instantaneous geocentric angle between the bulge-axis and the satellite, and E. Figure 1 shows the geometry, with A the north celestial pole, V the vernal equinox, N the ascending node of the orbit, Q the direction of perigee, P the instantaneous position of the satellite, and B the instantaneous direction of the atmospheric bulge. We wish to evaluate $\psi'\equiv\widehat{BP}$. In triangle ABP we have

$$\cos\psi'=\sin\delta_B\sin\delta_P+\cos\delta_B\cos\delta_P\cos(\alpha_P-\alpha_B), \tag{14}$$

where α_B, δ_B; α_P, δ_P are the right ascension and declination of the bulge and satellite, respectively. By hypothesis $\alpha_B=\alpha_\odot+\lambda$, $\delta_B=\delta_\odot$; and since these coordinates change slowly we shall regard them as effectively fixed over an interval of a few days. Next let us express the equatorial coordinates of the satellite as functions of its slowly varying orbital elements and of its rapidly varying eccentric anomaly. In the spherical triangle NFP, we have $\widehat{NF}=\alpha_P-\alpha_N$, where α_N is the right ascension of the ascending node; $\widehat{FP}=\delta_P$; $\widehat{NP}=\omega+\theta$, where ω is the argument of perigee and θ is the true anomaly; $\angle FNP=i$, the inclination; and $\angle NFP=90°$. With the aid of the relations

$$\sin\delta_P=\sin i\sin(\omega+\theta),$$
$$\cos(\omega+\theta)=\cos\delta_P\cos(\alpha_P-\alpha_N),$$
$$\tan(\alpha_P-\alpha_N)=\cos i\tan(\omega+\theta), \tag{15}$$

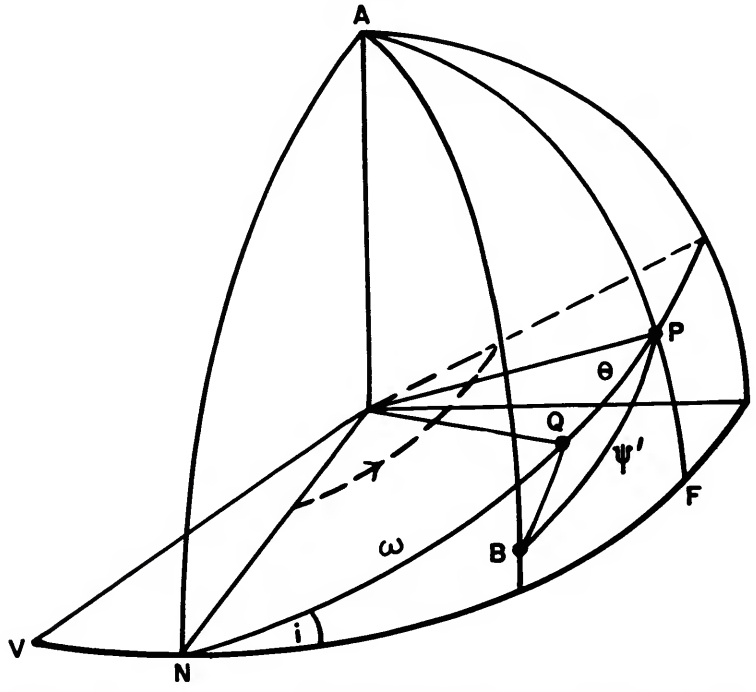

FIGURE 1.—The celestial sphere, showing the interrelationship of the locations of the atmospheric bulge axis B, of satellite perigee point Q, and of the instantaneous satellite position P.

the desired formula comes out to be

$$\begin{aligned}\cos\psi' &= \mu\cos\theta+\nu\sin\theta,\\ \mu &= \sin\delta_B\sin i\sin\omega+\cos\delta_B[\cos(\alpha_N-\alpha_B)\cos\omega-\cos i\sin(\alpha_N-\alpha_B)\sin\omega],\\ \nu &= \sin\delta_B\sin i\cos\omega-\cos\delta_B[\cos(\alpha_N-\alpha_B)\sin\omega+\cos i\sin(\alpha_N-\alpha_B)\cos\omega].\end{aligned}\tag{16}$$

Next, the true anomaly is related to the eccentric anomaly and e, the eccentricity, by the equations

$$\cos\theta=\frac{\cos E-e}{1-e\cos E},$$

$$\sin\theta=\frac{\sqrt{1-e^2}\sin E}{1-e\cos E}.\tag{17}$$

It thus turns out that the required angular separation of the satellite and the bulge axis is

$$\cos\psi'=\frac{\mu(\cos E-e)+\nu\sqrt{1-e^2}\sin E}{1-e\cos E}.\tag{18}$$

An alternative formula for ψ' can be found if we consider in figure 1 the triangle BQP. We have

$$\cos\psi'=\cos\psi'_q\cos\theta+\sin\psi'_q\cos\chi\sin\theta,\tag{19}$$

where $\psi'_q=\widehat{QB}$ is the geocentric angle between perigee and the bulge axis; $\chi=\angle BQP$; and θ again is the true anomaly. Comparison with equations (16) shows that

$$\begin{aligned}\mu &= \cos\psi'_q,\\ \nu &= \sin\psi'_q\cos\chi.\end{aligned}\tag{20}$$

We next wish to obtain s as a function of E. We readily find that

$$s=z-z_q=r-q=a(1-e\cos E)-a(1-e)=\frac{qe(1-\cos E)}{1-e}. \tag{21}$$

Substitution of equations (18) and (21) in equation (13) yields the equation for the secular acceleration of a satellite passing through a Jacchia-type atmosphere, the integrand now being a function of E and of miscellaneous "constants" of the atmosphere and the satellite orbit.

Finally, instead of expressing the acceleration in terms of the nighttime density, $\rho(0,\pi)$, we find it more useful to give it as a function of the density and scale height at the perigee point at the time in question, since the latter quantities are the ones that can be deduced from the observations. From equation (12) we find that

$$\rho(0,\psi'_q)=\rho(0,\pi)\{1+(L-K)\cos^6(\psi'_q/2)\}. \tag{22}$$

Next, we define the density scale height (Jacchia, 1960b) by

$$\frac{1}{H(0,\psi'_q)}\equiv-\frac{1}{\rho}\frac{\partial\rho}{\partial s}\bigg|_{0,\psi'_q}. \tag{23}$$

The density scale height is identical with the ordinary pressure scale height, $kT/g\overline{m}$, if the temperature gradient and molecular-mass gradients are zero separately or if $T/\overline{m}$ is independent of height. Under actual conditions, with $\partial T/\partial s\geqq 0$ and $\partial\overline{m}/\partial s\leqq 0$, the density scale height is somewhat smaller than the ordinary scale height. Differentiating equation (12) and evaluating the right side of equation (23) at $s=0$, $\psi'=\psi'_q$, we obtain

$$H(0,\psi'_q)=\frac{\{1+(L-K)\cos^6(\psi'_q/2)\}}{Q\{1-K\cos^6(\psi'_q/2)+RL\cos^6(\psi'_q/2)\}}. \tag{24}$$

In particular, we may now interpret the constant Q, since equation (24) shows that $H(0,\pi)=Q^{-1}$. Thus Q is the reciprocal of the nighttime scale height at perigee. The perigee scale height on the bulge axis is $H(0,0)=\{1+(L-K)\}\{Q(1-K)+RL\}^{-1}$.

The equation for an eccentric orbit

Let us define a dimensionless variable of integration, y^2, by $y^2\equiv s/H$, where for simplicity in the sequel we shall write $H(0,\psi'_q)\equiv H$. It follows from equation (21) that

$$1-\cos E=\frac{H(1-e)}{qe}y^2. \tag{25}$$

This is the same substitution effected in the first section of this paper, but it should be stressed that we are here concerned with the scale height at a perigee point located at a particular height and at a particular angular distance from the sunward bulge. Our next task is to transform the integrand of equation (13) into a function of y alone. First, the three factors involving s transform very simply, and exactly, by substitution of $s=Hy^2$. Second, the three factors explicitly containing E can be expressed as power series in $(H/q)y^2$. In particular,

$$\frac{(1+e\cos E)^{3/2}}{(1-e\cos E)^{1/2}}=\frac{(1+e)^{3/2}}{(1-e)^{1/2}}\left[1-\frac{H(2-e)}{q(1+e)}y^2+\frac{3H^2}{2q^2(1+e)^2}y^4-\ldots\right], \tag{26}$$

and

$$dE=\sqrt{\frac{2H(1-e)}{qe}}\left[1+\frac{H(1-e)}{4qe}y^2+\frac{3H^2(1-e)^2}{32q^2e^2}y^4+\ldots\right]dy. \tag{27}$$

The product of these factors is

$$\sqrt{\frac{2H}{qe}}\,(1+e)^{3/2}dy\left[1+\frac{H}{q}My^2+\frac{H^2}{q^2}Ny^4+\ldots\right], \tag{28}$$

where M and N, given by equations (3), are functions of e alone. Physically, these terms occur because atmospheric drag exerts a tangential perturbing force; they appear independently of any particular choice of atmospheric model. Third, we need to express ψ' in terms of y. We have $\cos^6(\psi'/2)=\frac{1}{8}(1+\cos\psi')^3$. Substitution of equation (18) then gives us an equation for ψ' as a function of E. With the transformation equation (25) we then obtain ψ' as a power series in $\sqrt{(H/q)}y$. Finally, note that the upper limit of integration of equation (13) becomes $y^2=\dfrac{2qe}{H(1-e)}$. Since we are here dealing with orbits of appreciable eccentricity we may extend the upper limit to infinity without appreciable error. All integrations involving odd powers of y then vanish, and therefore ψ' can be expressed for our purposes as a power series in $(H/q)y^2$. The formula turns out to be

$$\cos^6(\psi'/2)=u-v\frac{H}{q}y^2+w\frac{H^2}{q^2}y^4-\ldots. \tag{29}$$

The coefficients u, v, and w are constants for a given orbit; they are given by

$$u=\frac{1}{8}(1+\mu)^3=\cos^6(\psi_q'/2),$$

$$v=\frac{3(1+e)}{8e}(1+\mu)[\mu(1+\mu)-2\nu^2],$$

$$w=\frac{3(1+e)}{8e^2}[\mu(1+\mu)\{\mu+2e\mu+e\}-\nu^2\{1+3\mu+5e\mu+3e\}]. \tag{30}$$

When we substitute equations (21), (22), (25), (28), and (29) in equation (13), the secular acceleration becomes

$$\frac{\Delta P}{P}=-\frac{3\sqrt{\pi}}{\sqrt{2}}C_D\frac{A}{m}\frac{\sqrt{Hq}}{\sqrt{e}}\frac{(1+e)^{3/2}}{(1-e)}\frac{\rho(0,\psi_q')}{\{1+u(L-K)\}}\int_0^\infty\frac{2}{\sqrt{\pi}}dy[1+(H/q)My^2+(H^2/q^2)Ny^4+\ldots]$$

$$\times[\epsilon^{-QHy^2}\{1-Ku+(H/q)Kvy^2-(H^2/q^2)Kwy^4-\ldots\}$$

$$+\epsilon^{-RHy^2}\{Lu-(H/q)Lvy^2+(H^2/q^2)Lwy^4-\ldots\}][1+UH^2y^4]. \tag{31}$$

Equation (31) can be integrated term by term after multiplication of the several brackets. Note that the three power series in the first two brackets of the integrand have been truncated at $(H^2/q^2)y^4$ in order to keep the calculation manageable. The coefficients of terms of higher order decrease approximately in the ratio H/qe, which is less than about 0.1 provided the eccentricity is not very small. The justification for terminating the final bracket at order y^4 was described in the previous section.

Comparison with the simpler drag formula

Instead of writing down the general result of integrating equation (31), it is simpler to give the ratio of this acceleration to that given by equation (2) for the spherically symmetric atmosphere of constant scale height. One reason, of course, is that the coefficients are nearly identical. A second reason is that the ratio is independent of F_{20}, the solar flux at 20 cm. Let us call this ratio J. To state its meaning more precisely, consider a date on which the perigee of a satellite lies z_q km above

the earth's surface and at a geocentric angle ψ'_q from the bulge. The quantity J is then the secular acceleration of the satellite as it describes one orbit through the Jacchia atmosphere divided by the secular acceleration of the same satellite as it describes the same orbit through a spherically symmetric atmosphere in which the scale height is constant and in which the density and scale height agree with the Jacchia atmosphere at the perigee point (but not necessarily anywhere else along the orbit).

I have integrated equation (31) and computed values of J for perigee heights ranging from 200 km to 600 km, for eccentricities from 0.1 to 0.3, and for four specific orientations of the orbit with respect to the bulge. It turns out that the values of J are never much less than unity and that no term involving either M or N contributes more than 0.007 to the end result. We may thus drop all such terms in both equations (2) and (31) without significant error. The ratio then becomes

$$J=\frac{[1+u(LZ^2-K)]^{1/2}}{[1+u(L-K)]^{3/2}}\left\{1+u(LZ^{-1}-K)-\frac{v}{2qQ}(LZ^{-3}-K)+\frac{3w}{4q^2Q^2}(LZ^{-5}-K)\right.$$
$$\left.+\frac{3U}{4Q^2}+\frac{3Uu}{4Q^2}(LZ^{-5}-K)-\frac{15Uv}{8qQ^3}(LZ^{-7}-K)+\frac{105Uw}{16q^2Q^4}(LZ^{-9}-K)\right\}, \quad (32)$$

where we have set $R\equiv QZ^2$ and where all other quantities have been previously defined.

In table 1 the values of J are computed from equation (32) for several perigee heights, eccentricities, and orientations of the orbit relative to the sunward bulge. The values are given to three decimal places to indicate better the trend of the numbers. Two points should be kept in mind, however, when the entries are examined. First, the final calculations have been much simplified by leaving out all terms in M and N. Second, the convergence of the terms in equation (32) is very rapid in all situations except where the perigee height is large ($z_q\cong 600$ km) and the eccentricity rather small ($e\cong 0.1$). In this extreme situation the atmospheric distortion is a maximum, the scale height is large, and at very low eccentricities the drag may be significant at all points around the orbit. Calculating and integrating the terms in y^6 in equation (31), I find that the true value of J in the most extreme case of table 1 is even more exaggerated than the tabulated entry of 1.52; it is greater by about 3 percent. Truncation of equation (29) at order y^4 affects other entries by smaller amounts.

TABLE 1.—*Values of J for several types of orbit*

	z_q(km)				
	200	300	400	500	600
e					
Perigee coincident with bulge ($\mu=1$, $\nu=0$)					
0.10	1.024	1.016	1.005	0.990	0.977
0.15	1.030	1.028	1.026	1.022	1.018
0.20	1.033	1.035	1.037	1.040	1.044
0.25	1.035	1.039	1.045	1.052	1.060
0.30	1.035	1.041	1.050	1.060	1.072
Semi-latus rectum of orbit coincident with bulge ($\mu=0$, $\nu=\pm1$)					
0.10	1.044	1.076	1.145	1.280	1.520
0.15	1.040	1.067	1.122	1.230	1.435
0.20	1.039	1.062	1.109	1.203	1.382
0.25	1.038	1.059	1.101	1.185	1.346
0.30	1.037	1.057	1.096	1.173	1.322
Orbit normal coincident with bulge ($\mu=0$, $\nu=0$)					
All e	1.032	1.042	1.057	1.084	1.132
Apogee coincident with bulge ($\mu=-1$, $\nu=0$)					
All e	1.030	1.035	1.040	1.045	1.049

Interpretation of the results

Generally, the entries of table 1 show that the secular acceleration in a bulging atmosphere of increasing scale height is greater than in the same orbit when the atmosphere is spherically symmetric

and of constant scale height. This means that use of the simpler formula tends to produce overestimates of the values of $\rho\sqrt{H}$ from the observed accelerations, although not always.

The dominant reason for $J>1$ when either the orbit normal or the apogee coincides with the bulge is the increase of scale height with height. Reference is made, for these and subsequent remarks, to figure 3 of Jacchia's paper (Jacchia, 1960a), which is helpful in visualizing these effects. When the normal to the orbit plane coincides with the bulge axis, the satellite is entirely ignorant of the bulge because it always moves 90° away from it; when apogee coincides with the bulge axis, J is not significantly different from unity because of the $\cos^6(\psi'/2)$ dependence. For both orientations the values of J increase with increasing perigee height because of the gradient of the scale height.

When perigee coincides with the bulge, the gradient of the scale height governs the run of J at low values of z_q; the bulge is not pronounced at these levels. At 500 and 600 km, however, the interplay of the two effects is stronger. At the higher eccentricities a satellite climbs steeply away from perigee, and in the limiting case of an outbound radial orbit it is oblivious of the bulge and the value of J is governed solely by the effects of scale height. At low eccentricities, however, a satellite climbs uphill from perigee rather slowly and encounters equidensity contours that are trending downhill with increasing distance from the bulge axis. The values of J for these cases are slightly less than unity.

Finally, when the semi-latus rectum of the orbit coincides in direction with the bulge axis, the asymmetry is marked, particularly for large perigee heights and low eccentricities. In this case a satellite encounters maximum density at some point displaced 10° or 15° from the perigee point toward the bulge axis; the secular acceleration is therefore significantly greater, up to 50 or 60 percent, than that given by the usual simpler formula.

The equation for a circular orbit

A general formula for the drag in a bulging atmosphere can in principle be derived for orbits of small eccentricity, as before, in terms of Bessel functions of imaginary argument. Tentative work indicates, however, that the resulting expression is of formidable complexity and provides little or no insight into the physical effects. Accordingly, this paper will not be concerned with finding an analytic expression for the acceleration in orbits of very small, but nonzero, eccentricity. Qualitatively, however, it is apparent that the more circular an orbit is, the more indifferent the satellite is to the atmospheric density and scale height at perigee. Maximum drag may occur at any point on the orbit.

In the limiting case of a circular orbit, the greatest drag occurs when ψ' is a minimum. The minimum geocentric angle between satellite and bulge axis, $\psi'_{\min}$, is given by $\psi'_{\min}=\pi/2-i'$, where i' is the angle between the bulge axis and the orbit normal, with $0\leqq i'\leqq \pi/2$. The density function to be employed for a circular orbit is given by equation (12) with $s=0$, and is

$$\rho(0,\psi')=\rho(0,\pi)\{1+(L-K)\cos^6(\psi'/2)\}. \tag{33}$$

In this particular case, moreover, ψ' is given by

$$\cos\psi'=\sin i'\cos E, \tag{34}$$

and the secular acceleration turns out to be

$$\frac{\Delta P}{P}=-3\pi C_D\frac{A}{m}\rho(0,\pi)\left\{1+\frac{(L-K)}{8}\left[1+\frac{3}{2}\sin^2 i'\right]\right\}. \tag{35}$$

Since no satellite passes through the point $\psi'=\pi$ unless $i'=\pi/2$, and since all satellites must pass through $\psi'=\pi/2$, we shall find it more useful to express equation (35) in terms of $\rho(0,\pi/2)$, which can be determined from equation (33). The result is then

$$\frac{\Delta P}{P}=-3\pi C_D\frac{A}{m}\rho(0,\pi/2)\left\{1+\frac{3(L-K)\sin^2 i'}{16+2(L-K)}\right\}. \tag{36}$$

Notice that this result is identical with the simpler equation (7) when $i'=0$. The reason is, of course, that when $i'=0$ and $e=0$ (and under no other conditions) a satellite sees constant density all around the orbit, just as in the spherically symmetric approximation. When $\Delta P/P$ is observed for a satellite moving in a circle with $i'\neq 0$, the atmospheric density deduced from equation (7) will be greater than $\rho(0, \pi/2)$ by a factor equal to the bracket of equation (36). Alternatively interpreted, this factor is the ratio of the secular acceleration at i' to that at $i'=0$. It is greater than unity because of the sharpness of the bulge: density excesses in the daytime hemisphere more than compensate density deficiencies in the dark hemisphere. When $i'=\pi/2$, the satellite passes squarely through the bulge; in this case the bracket is a maximum, ranging from 1.04 at 200 km to 1.22 at 400 km and up to 1.56 at 600 km.

Conclusions

It should be emphasized, with Jacchia, that the density function here employed is not a necessary consequence of high-atmosphere physics, but rather a product of numerical analysis of satellite observations. For this reason it does not seem necessary at this stage to work out the exceedingly complex higher-order approximations to equation (32) or the drag equation for orbits of very small but non-zero eccentricity. The results of table 1 for orbits of moderate eccentricity and of section 8 for circular orbits indicate, without more elaborate calculations, that use of the drag formula for a spherically symmetric atmosphere of constant scale height leads to a somewhat erroneous evaluation of the structure of the high atmosphere.

The formulas developed here should, at the expense of some added calculation, make it possible to improve our picture of the Jacchia-type atmosphere by refining the values of its constants. Qualitatively, the results of table 1 indicate that at heights of 500 km or so the atmospheric density on the bulge axis is a bit greater than given by the usual drag formula, while the density 90° around from the bulge axis is substantially less. We may therefore tentatively conclude that the sunward bulge is even sharper than previously thought.

Acknowledgments

I am happy to thank Dr. F. L. Whipple, Director, for the opportunity to work at the Smithsonian Astrophysical Observatory during the summer of 1960; Dr. L. G. Jacchia, whose comments suggested this work and whose generous interest and advice have been most helpful; and others of the staff for assistance in a variety of ways.

Abstract

Formulas are developed to express the secular acceleration of a satellite on passing through an atmosphere which bulges in the sunward direction and in which the scale height increases with height, these two properties of the high atmosphere having previously been established from satellite observations. Comparison of the new formulas with those for a spherically symmetric atmosphere of constant scale height indicates that deduced atmospheric densities may be systematically incorrect by up to 50 or 60 percent at heights of 500 to 600 km when the earlier and simpler equations are used.

The Motion of Satellite 1958 Epsilon around Its Center of Mass

By G. Colombo

This report presents a preliminary study of the motion of Explorer IV (Satellite 1958 Epsilon) around its center of mass. The body is, to a good approximation, symmetric around its longitudinal axis and, therefore, the tangential motion can be considered a regular precession, at least during one orbital revolution.[1] I shall refer to a precessional velocity ψ, and to an angular velocity around the longitudinal axis, $\dot{\varphi}$, the angular velocity vector ω of the body being the resultant of these two components. Many good observations (Naumann, 1961) of the motion, especially of the variation of $\dot{\varphi}$, were made during the first 60 days after launch, and the variation in the direction of the precessional axis was computed. Although the dererminations are not precise, they definitely indicate an angular displacement of the precessional axis of at least 10° per day in the first 30 days after launch. Also, it is certain that the angular momentum of the body remained almost constant during the whole period under consideration.

I have derived a method for computing the angular perturbation of the angular momentum. Computation of the angular variation of the precessional axis due to the atmospheric drag, using a nutation angle of 84°, yields a maximum value of 5° or 6° per day. For the gravitational torque, the same perturbation has a maximum value of 2° per day. The perturbation due to the action of the earth's magnetic field on an intrinsic magnetic dipole of the satellite amounts to 2° per day if the maximum torque is of the order of 300 dyne-cm, since the effective value of the torque is the value averaged over one precessional period. In addition, an evaluation of a magnetic dipole induced in the ferromagnetic shell of the satellite has been tentatively done. The corresponding theoretical torque would give an important contribution also for a nutation angle of 90°. It seems, however, very difficult to choose a realistic value for the magnetic permeability because (1) the field is very weak and the experimental determinations are made only for stronger fields, and (2) the actual value of the permeability is related to components of the field which are changing sinusoidally. In any case, we give the formula needed to compute the total perturbation per revolution, which depends on the velocity vector of the center of mass at perigee, the position of the earth's magnetic dipole with respect to the orbital plane, and, naturally, on the orbital elements.

This study also treats the problem of the rapid decrease in $\dot{\varphi}$ during the first 30 days after launch. The decrease in the spinning of the satellite is not easily explained by the hypothesis that it is caused by the action of an external torque, since the modulus of the angular momentum remains almost constant. The most probable cause of this decrease is an internal vibrational motion that causes the transfer of angular momentum from the axis of symmetry to a transverse axis. The observed variations are in good qualitative agreement with the law for the decrease in $\dot{\varphi}$.

The question does not seem to be closed, since I definitely think that the problem of the motion of a ferromagnetic body of any shape in a varying weak magnetic field has yet to be solved. With torques as weak as those with which we are working, any effects neglected and perhaps undetectable in the usual experimentations may have a significant influence on a satellite.

[1] Some information (Lundquist, Naumann, and Fields, 1961) about the physical structure of the body of Explorer IV was received just after I completed this report.

1. Coordinate systems

Let us associate the satellite S with three coordinate systems: first, with a moving coordinate system (i, j, k) whose axes lie along the principal axes of inertia of the satellite and whose origin is the center of mass G of the satellite ($\mathbf{k}$ is the unit vector of the gyroscopic axis oriented toward the satellite's nose); second, a coordinate system (c_1, c_2, Ω) with Ω oriented along the precessional axis; and third, a coordinate system (X, Y, Z) with origin at the perigee of the orbit of G; the X-axis is oriented toward $\mathbf{v}_G^*$ (the velocity of G at perigee), the Y-axis is normal to the orbital plane, and the Z-axis is oriented toward the radius vector of the orbit at perigee. Let ψ, φ and δ denote the Eulerian angles of the system (i, j, k) with respect to the system (c_1, c_2, Ω). Let $\mathbf{K}_G$ denote the angular momentum of S with respect to the center of mass G (note that $\mathbf{K}_G$ is in the same direction as Ω, since the tangential motion is a regular precession). Also let θ denote the angle between Ω and the X-axis; θ_1 the angle between Ω and the Y-axis; λ_1 the angle between the projection of Ω on the XZ-plane and the Z-axis; and λ the angle between the projection of Ω on the YZ-plane and the Z-axis (see figs. 1 and 2).

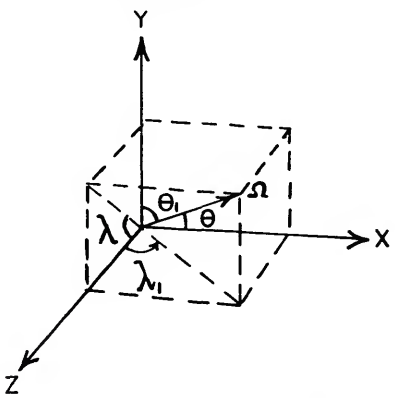

FIGURE 1.—Definition of angles.

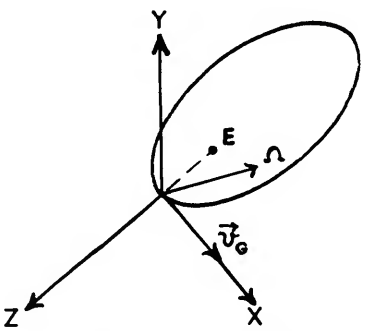

FIGURE 2.—Reference systems.

2. Perturbation of the precessional motion

The elements that characterize the regular precessional motion may suffer perturbations due to the torques exerted by the following: (a) atmospheric drag, (b) gravitational field of the earth acting on the nonspherical shape of S, (c) interaction of the earth's magnetic field with an intrinsic dipole of S, (d) interaction of the earth's magnetic field with an induced dipole of S, (e) energy dissipation due to internal vibrational motion. Let P_a, P_b, P_c, P_d, and P_e denote the perturbations due to a, b, c d, and e, respectively. Assume, as usual, that the total perturbation of the tangential motion is the sum of the perturbations P_a, P_b, P_c, P_d, and P_e evaluated over the unperturbed motion.

To begin, we note that the average torques of P_a, P_b, P_c, P_d, and P_e that affect the motion in one revolution are always perpendicular to $\mathbf{K}_G$ and that for perturbation P_e the external torque is zero. Therefore, the modulus of the angular momentum of S during the motion may be considered constant. The second-order effect of the drag is not considered since it is insignificant. In the motion of Explorer IV (Satellite 1958 Epsilon), this property of the angular momentum was well maintained during the first 30 days after launch. Only for this period do we have good observations.

2.1. Perturbation P_a.—First, the torque due to the atmospheric drag is computed. The instantaneous torque $\mathbf{M}_G$ can be described by the expression

$$\mathbf{M}_G = c^* \rho(G) |v_G| \mathbf{v}_G \times \mathbf{k} = (C_0 - C_2 \cos^2 \gamma + C_3 \cos^3 \gamma) \rho(G) |v_G| \mathbf{v}_G \times \mathbf{k}, \tag{1}$$

where γ is the angle $\mathbf{k}$ makes with $\mathbf{v}_G$; $\rho(G)$ is the atmospheric density at G; $\mathbf{v}_G$ is the velocity of G; and C_0, C_2, and C_3 are the coefficients that characterize the shape of S.[2] We arrive at this expres-

[2] More exactly, the coefficient c^* should be expressed as $c^* = C_0 + C_1 \cos \gamma - C_2 \cos^2 \gamma + C_3 \cos^3 \gamma - C_4 \cos^4 \gamma$, as we will see later, but the second and fifth terms of this expression play the same role as the fourth and third terms respectively. Therefore, we will have a good approximation if we consider only equation (1). We shall return to this argument in section 3.1.

sion by assuming that the center of pressure G' is always along the gyroscopic axis of the satellite and that this center can vary in its position with a change in γ. The computation of C_0, C_2, and C_3 in the case of Explorer IV will be made in section 3.1. Finally, we assume that the velocity of the atmosphere relative to the orbit, compared to the velocity of G over the orbit, is small.

Next, the average value of $\mathbf{M}_G$ in one precessional period is computed. Let v_x, v_y, and v_z denote the components of $\mathbf{v}_G$ with respect to the system (c_1, c_2, Ω). Thus,

$$|v_G| \cos \gamma = \mathbf{v}_G \cdot \mathbf{k} = (v_x \sin \psi - v_y \cos \psi) \sin \delta + v_z \cos \delta,$$

$$\mathbf{k} = (\mathbf{c}_1 \sin \psi - \mathbf{c}_2 \cos \psi) \sin \delta + \Omega \cos \delta. \tag{2}$$

Averaging over ψ from 0 to 2π, we obtain

$$\widetilde{\mathbf{k}} = \cos \delta \boldsymbol{\Omega},$$

$$\widetilde{\cos^2 \gamma \mathbf{k}} = \cos \delta \left[\sin^2 \delta + \frac{v_z^2}{v_G^2} (2 - 5 \sin^2 \delta) \right] \boldsymbol{\Omega},$$

$$\widetilde{\cos^3 \gamma \mathbf{k}} = \left[\frac{v_z^3}{|v_G|^3} \left(\frac{3}{8} \sin^4 \delta + \cos^4 \delta \right) - \frac{3}{8} \frac{v_z}{|v_G|} \sin^2 \delta (\sin^2 \delta - 4 \cos^2 \delta) \right] \boldsymbol{\Omega}. \tag{3}$$

Finally, the average value of $\mathbf{M}_G$ in one revolution is computed. Let

$$\rho^* v_G^{*2} \mathbf{I}_0 = \frac{1}{T} \int_0^T \mathbf{v}_G |v_G| \rho(G) dt,$$

$$\rho^* v_G^{*2} \mathbf{I}_2 = \frac{1}{T} \int_0^T \mathbf{v}_G \frac{v_z^2}{|v_G|} \rho(G) dt,$$

$$\rho^* v_G^{*2} \mathbf{I}_3' = \frac{1}{T} \int_0^T v_z \mathbf{v}_G \rho(G) dt,$$

$$\rho^* v_G^{*2} \mathbf{I}_3'' = \frac{1}{T} \int_0^T \mathbf{v}_G \frac{v_z^3}{v_G^2} \rho(G) dt, \tag{4}$$

where T is the orbital period. Hence,

$$\frac{d\mathbf{K}_G}{dt} = -\rho^* v_G^{*2} \left\{ \cos \delta \left(C_0 - C_2 \frac{\sin^2 \delta}{2} \right) \mathbf{I}_0 - C_2 \cos \delta \left(1 - \frac{5}{2} \sin^2 \delta \right) \mathbf{I}_2 + C_3 \left(\frac{3}{8} \sin^4 \delta + \cos^4 \delta \right) \mathbf{I}_3'' - \frac{3}{8} C_3 \sin^2 \delta (\sin^2 \delta - 4 \cos^2 \delta) \mathbf{I}_3' \right\} \times \boldsymbol{\Omega}; \tag{5}$$

thus, the modulus of $\mathbf{K}_G$ will remain constant for this perturbation ($\mathbf{M}_G$ is perpendicular to $\mathbf{K}_G$) and also for the other perturbations, as we shall see in sections 2.2 and 2.3.

If the moment of inertia around the gyroscopic axis is designated by C, and the initial velocity around this axis by r_0 (assuming that the initial motion is approximately a rotation around the gyroscopic axis only), then $\mathbf{K}_G = C r_0 \boldsymbol{\Omega}$. Therefore, equation (5) becomes

$$\frac{d\boldsymbol{\Omega}}{dt} = -\frac{\rho^* v_G^{*2}}{C r_0} \left\{ \cos \delta \left(C_0 - C_2 \frac{\sin^2 \delta}{2} \right) \mathbf{I}_0 - C_2 \cos \delta \left(1 - \frac{5}{2} \sin^2 \delta \right) \mathbf{I}_2 + C_3 \left(\frac{3}{8} \sin^4 \delta + \cos^4 \delta \right) \mathbf{I}_3'' - \frac{3}{8} C_3 \sin^2 \delta (\sin^2 \delta - 4 \cos^2 \delta) \mathbf{I}_3' \right\} \times \boldsymbol{\Omega}. \tag{6}$$

Equation (6) differs from the analogous form used by Beletsky (1960) for two reasons. First, Beletsky does not consider the possibility of the displacement of the center of pressures along the gyroscopic axis. This displacement is certainly true for Explorer IV, which is very asymmetric with respect to the plane normal to the gyroscopic axis passing through G. Second, the Beletsky equation contains a factor $\cos^2 \delta$, which can be misleading. Actually, there should be a factor of $\cos \delta$ only. In a quasi-tumbling motion, the factor $\cos \delta$ is very small, and, as we shall see, it plays an important role in the discussion. Therefore, in one revolution, the atmospheric drag causes a rotation of the precessional axis around a well-determined axis. This axis is dependent on the vector given by equation (4) and, naturally, on the nutation angle. Also, it is important to note that the terms in $\mathbf{I}_3'$ and $\mathbf{I}_3''$ are not zero if $\cos \delta$ is zero.

Note that the rotation axis of Ω varies from one revolution to another since it depends on the orbital elements of G, of which the most important are the secular variation of the argument of perigee (the motion of perigee) and the right ascension of the ascending node (the regression of the node).

2.2. Perturbation P_b.—To compute the torque corresponding to P_b, we refer to the article by Beletsky (1960). We can write the expression

$$\frac{d\mathbf{K}_G}{dt}=\frac{3}{2}\tilde{\omega}^2(A-C)\cos\theta_1\left(1-\frac{3}{2}\sin^2\delta\right)\mathbf{N}\times\boldsymbol{\Omega}, \tag{7}$$

where $\mathbf{N}$ is the unit vector normal to the orbital plane and parallel to the Y-axis, and A is the moment of inertia with respect to an axis normal to the axis of symmetry through G. Moreover,

$$\tilde{\omega}^2=\frac{h}{T}\int_0^T\frac{dt}{r^3}, \tag{8}$$

where h is the characteristic constant of the earth's gravitational attraction, and r is the geocentric distance of G. If, as before, $\mathbf{K}_G=Cr_0\boldsymbol{\Omega}$, then

$$\frac{d\boldsymbol{\Omega}}{dt}=\frac{3}{2}\frac{\tilde{\omega}^2}{Cr_0}(A-C)\cos\theta_1\left(1-\frac{3}{2}\sin^2\delta\right)\mathbf{N}\times\boldsymbol{\Omega}. \tag{9}$$

Therefore, the gravitational torque causes a rotation of Ω around an axis normal to the orbital plane. This axis of rotation can be considered constant during one revolution. Also, the angular displacement of Ω due to perturbation P_b in one revolution can be computed by use of equation (9).

2.3. Perturbation P_c.—The intrinsic magnetic moment of S can be expressed as

$$\boldsymbol{\mu}=\mu_1\mathbf{i}+\mu_3\mathbf{k}, \tag{10}$$

and the earth's magnetic field as

$$H=H_x\mathbf{c}_1+H_y\mathbf{c}_2+H_z\boldsymbol{\Omega}. \tag{11}$$

Thus, the corresponding torque acting on the body is

$$\mathbf{M}_G^{(m)}=\boldsymbol{\mu}\times\mathbf{H}. \tag{12}$$

Assume that, to a good approximation,

$$\varphi=\frac{2\pi}{m\tau}t, \qquad \psi=\frac{2\pi}{n\tau}t+\psi_0, \tag{13}$$

where $m\neq n$ and $n\tau$ is the period of precession. If $\dot{\varphi}$ is much greater than $\dot{\psi}$, equation (13) can be written with a value of m that is not so large.[3] Also suppose that $\mathbf{H}$ remains constant along the arc of the orbit covered by G in the period $mn\tau$. In this way,

$$\tilde{\mathbf{M}}_G^{(m)}=\mu_3\cos\delta\boldsymbol{\Omega}\times\mathbf{H}. \tag{14}$$

[3] The assumption is not necessary if $\mu_1=0$.

If $m=n$, the average value of $\mathbf{M}_G^{(m)}$ over one precessional period is

$$\tilde{\mathbf{M}}_G^{(m)}=\frac{1}{2}\mu_1(1-\cos\delta)\mathbf{H}\times\mathbf{c}_1+\mu_3\cos\delta\boldsymbol{\Omega}\times\mathbf{H}. \tag{15}$$

The last case will be excluded for the present, but we shall return to it in section 4.1, at the end of this paper. Therefore, equation (14) is retained.

We should average $\mathbf{M}_G^{(m)}$ over one orbital period. To compute this average, we assume that the earth's magnetic field is, in the usual form,

$$\mathbf{H}=\frac{\mu_E}{r^3}[\mathbf{u}-3(\mathbf{u}\cdot\mathbf{r})\mathbf{r}], \tag{16}$$

where $\mathbf{u}$ is the unit vector of the earth's dipole; $\mathbf{r}$ is the unit vector of the direction from the earth's center to G; and μ_E is the magnetic moment of the earth's dipole. The mean value of $\mathbf{M}_G$ is

$$\tilde{\mathbf{M}}_G^{(m)}=\frac{1}{T}\int_0^{2\pi}\mu_3\cos\delta\boldsymbol{\Omega}\times\mathbf{H}\frac{dt}{dv}dv, \tag{17}$$

where v is the true anomaly of G over the orbit. Since

$$\frac{dv}{dt}=\frac{2\pi a^2}{Tr^2}\sqrt{1-e^2},\qquad r=\frac{a(1-e^2)}{1+e\cos(v-\omega)}, \tag{18}$$

we obtain with the usual notation

$$\tilde{\mathbf{M}}_G^{(m)}=\frac{\mu_3\cos\delta}{2\pi a^2\sqrt{1-e^2}}\int_0^{2\pi}r^2\boldsymbol{\Omega}\times\mathbf{H}dv, \tag{19}$$

where $\mathbf{H}$ should be expressed as a function of v. For this perturbation, we should remember that the earth's dipole makes one rotation around the polar axis in one day. Since the angular displacement of $\mathbf{u}$ is about 9° during one revolution, we cannot consider $\mathbf{u}$ constant when integrating equation (19).

We must write $\mathbf{u}=0.95\mathbf{u}_1+0.29[\mathbf{n}\cos T_d(M+\alpha_0-Q)+\mathbf{u}_1\times\mathbf{n}\sin T_d(M+\alpha_0-Q)]$, where $\mathbf{u}_1$ is the unit vector of the earth's polar axis; $\mathbf{n}$ is the unit vector of the ascending node of the orbit; T_d is the orbital period in days; M is the mean anomaly of G; α_0 is the right ascension of $\mathbf{u}$ at the time of perigee passage of G; and Q is the right ascension of the ascending node. The computation of this perturbation is not easy; it would be preferable to postpone it until we have exact information about the internal circuitry and the eventual permanent magnets in the payload.

Let i_m denote the inclination of the orbit over the equatorial plane, π_m, of the earth's magnetic dipole, and $\mathbf{n}_m$ the radius vector of the ascending node of the orbit in this plane. To obtain an idea of the magnitude of this perturbation, we consider $\mathbf{n}_m$ and $\mathbf{u}$ as constant during one revolution.[4] Thus, from equation (19), we have

$$\tilde{\mathbf{M}}_G^{(m)}=\frac{\mu_3\mu_E\cos\delta}{a^3(1-e^2)^{3/2}}\boldsymbol{\Omega}\times\left[\left(1-\frac{3}{2}\sin^2 i_m\right)\mathbf{u}+\frac{3}{2}\sin i_m\cos i_m\mathbf{n}_m\times\mathbf{u}\right]; \tag{20}$$

and finally,

$$\frac{d\boldsymbol{\Omega}}{dt}=\frac{\mu_3\mu_E\cos\delta}{Cr_0a^3(1-e^2)^{3/2}}\boldsymbol{\Omega}\times\left[\left(1-\frac{3}{2}\sin^2 i_m\right)\mathbf{u}+\frac{3}{2}\sin i_m\cos i_m\mathbf{n}_m\times\mathbf{u}\right]. \tag{21}$$

From equation (21), the rotation of Ω due to perturbation P_c can be determined. Therefore, in one revolution Ω rotates around an axis that depends on i_m and $\mathbf{n}_m$.

In each of the three perturbations just discussed, we have found that $\mathbf{K}_G\cdot\frac{d\mathbf{K}_G}{dt}=0$, which means that the modulus of $\mathbf{K}_G$ is not affected by these perturbations, at least if $\mu_1=0$.

[4] This assumption is justified, since the small change in the orientation of $\vec{H}$ along the orbit due to the variation of $\vec{u}$ is negligible when the angle between $\vec{\Omega}$ and $\vec{H}$ is large. When the angle $\vec{\Omega}\vec{H}$ is small, the variation in the direction of $\vec{\Omega}$ is also small.

2.4. Perturbation P_d.—Let us consider the perturbation of the angular momentum due to the interaction between the earth's magnetic field (Fischell, 1961) and the ferromagnetic components of the satellite. To give a possible explanation of the angular rotation of Ω, and also for an angle δ very near to 90°, we suppose that the satellite has a ferromagnetic component in the shape of an elongated cylinder as the shell of the satellite. For such a component, the magnetization vector is almost always oriented as is the axis of the cylinder. Thus,

$$\mathbf{I}=(\mu-1)(\mathbf{H}\cdot\mathbf{m})\mathbf{m}, \tag{22}$$

where $\mathbf{m}$ is the unit vector of the axis of the ferromagnetic component (with $\mathbf{m}=m_1\mathbf{i}+m_3\mathbf{k}$), and μ is its magnetic permeability. If we neglect the small hysteresis effect, the torque acting on the body can be written in the following form:

$$\mathbf{M}_G^{(m')}=(\mu-1)\frac{V}{4\pi}(\mathbf{m}\cdot\mathbf{H})\mathbf{m}\times\mathbf{H}=(\mathbf{m}\cdot\mathbf{H})\mathbf{m}\times\mu^*\mathbf{H}, \tag{23}$$

where V is the volume of the ferromagnetic component. Averaging as in the computation of perturbation P_c, and assuming (if $m_1\neq 0$) that $\dot{\varphi}>>\psi$, we obtain

$$\mathbf{M}_G^{(m')}=\mu^*\left[\frac{m_1^2}{4}(1-3\cos^2\delta)+\frac{m_3^2}{2}(2-3\sin^2\delta)\right]\Omega\times(\mathbf{H}\cdot\Omega)\mathbf{H}. \tag{24}$$

We suppose, as before, that $\mathbf{u}$ and $\mathbf{u}_m$ are constant during one revolution. Then, averaging over one orbital period and neglecting any small terms in e^2, we find that

$$\begin{aligned}\tilde{\mathbf{M}}_G^{(m')}=\frac{\mu^*\mu_E^2}{a^6(1-e^2)^{9/2}}\Omega\times\Big\{&\mathbf{u}\Big[\Big(1-3\sin^2 i_m+\frac{27}{8}\sin^4 i_m\Big)\mathbf{u}\cdot\Omega\\&+\frac{3}{2}\cos i_m\sin i_m\Big(\frac{9}{4}\sin^2 i_m-1\Big)\mathbf{u}\times\mathbf{n}_m\cdot\Omega\Big]+\frac{9}{8}\sin^2 i_m(\mathbf{n}_m\cdot\Omega)\mathbf{n}_m\\&+\Big[\frac{27}{8}\sin^2 i_m\cos i_m(\mathbf{u}\cdot\mathbf{n}_m\times\Omega\cos i_m+\mathbf{u}\cdot\Omega\sin i_m)\\&-\frac{3}{2}\mathbf{u}\cdot\Omega\sin i_m\cos i_m\Big]\mathbf{u}\times\mathbf{n}_m\Big\}\cdot\Big[\frac{m_1}{\mathrm{n}}(1-3\cos^2\delta)+\frac{m_3^2}{2}(2-3\sin^2\delta)\Big].\end{aligned} \tag{25}$$

For an approximate computation, let us suppose that $\sin i_m=\cos i_m=\frac{\sqrt{2}}{2}$, with $\cos\delta=0$ and $\sin\delta=1$. Hence

$$\begin{aligned}\tilde{\mathbf{M}}_G^{(m')}=\frac{(\mu-1)}{4\pi}\frac{\mu_E^2}{a^5(1-e^2)^{9/2}}\Omega\times\Big[\frac{m_1^2}{4}-\frac{m_3^2}{2}\Big]\Big\{&\Big(\frac{11}{32}\mathbf{u}\cdot\Omega+\frac{3}{32}\mathbf{u}\times\mathbf{n}_m\cdot\Omega\Big)\mathbf{u}\\&+\frac{9}{16}(\mathbf{n}_m\cdot\Omega)\mathbf{n}_m+\Big[\frac{27}{32}\mathbf{u}\times\mathbf{n}_m\cdot\Omega+\frac{3}{32}\mathbf{u}\cdot\Omega\Big]\mathbf{u}\times\mathbf{n}_m\Big\}.\end{aligned} \tag{26}$$

This torque is zero if $\mathbf{u}$, Ω, and $\mathbf{n}_m$ are coplanar and if $\mathbf{n}_m$ and Ω are parallel, or if $m_1^2=2m_3^2$, and, therefore, these are all exceptional cases.

2.5. Perturbation P_e.—The observations of Explorer IV definitely indicate that the angular momentum maintains a quasi-constant modulus during the first 30 days after launch. In this period, a diminution of the order of 0.1 of the initial value occurs. Thus, the great diminution of the kinetic energy (the final value is about 1/80 of the initial value) cannot be ascribed to external torques, and therefore must be ascribed to internal dissipation. In this section, we shall study the possibility of a transfer of angular momentum from the motion about the axis of symmetry to the motion about the precessional axis, resulting from internal dissipative vibrational motion sustained by the precessional rigid body motion around the center of mass. Note

that the aerodynamic torque (without the second-order effect) and the gravitational torque are, *a priori*, coplanar with the gyroscopic axis, and, therefore, cannot be responsible for the observed variation of $\varkappa$. Not even the torque due to the second-order effect of the aerodynamic drag can completely explain such diminution. Indeed, the perturbation due to the aerodynamic torque will also cause an equal damping of the precessional component of the angular velocity (Notni and Oleak, 1959; 1960). We should also examine the possibility that this dissipative action, which does not change the modulus of the angular momentum, can result from the interaction between the earth's magnetic field and the satellite. A simple computation of the average work done by the magnetic field acting on the intrinsic magnetic moment gives a value of zero, if $\dot{\varphi} \neq \dot{\psi}$

In the usual notation, the expression for the kinetic energy of S is

$$\mathscr{T} = \frac{1}{2}\left[A(\dot{\delta}^2 + \dot{\psi}^2 \sin^2 \delta) + C(\dot{\varphi} + \dot{\psi} \cos \delta)^2\right]. \tag{27}$$

Moreover, in any instant t of the precessional motion

$$\dot{\psi} = \frac{C(\dot{\varphi} + \dot{\psi} \cos \delta)}{A \cos \delta}. \tag{28}$$

Suppose that initially the motion is a quasi-rotation about the axis of symmetry of the body with velocity r_0. Let P denote a point mass with a very small moment of inertia relative to the inertial characteristics of S. Let P_0 denote the equilibrium position of P when the body is at rest, where $(x_0, 0, z_0)$ are the coordinates of P_0 with respect to (i, j, k). Assume that, if P is not at P_0, then both an elastic force with center at P_0 and a dissipative force acting in the same direction as the velocity of P relative to (i, j, k) and proportional to the velocity act on P. If S has a component with small mass elastically connected to the rigid body, the dissipation can be due to elastic hysteresis. The motion of P with respect to the moving frame (G, i, j, k) is governed by the equation

$$m \frac{dv}{dt} = \mathbf{E} + \mathbf{D} + \mathbf{F}_c + \mathbf{F}_{\mathscr{C}} + \mathbf{R}, \tag{29}$$

where $\mathbf{E}$ is the elastic force; $\mathbf{D}$ is the dissipative force; $\mathbf{F}_c$ is the centrifugal force; $\mathbf{F}_{\mathscr{C}}$ is the Coriolis force; and finally $\mathbf{R}$ is the linkage force. Since we assume that the displacement of P is very small, the centrifugal force that acts on P_0 can always be substituted for the centrifugal force that acts on P. A simple computation gives us the centrifugal force as the sum of two forces. The first of these two forces is almost constant with respect to (i, j, k):

$$\mathbf{F}_c' = -m\left\{(2\dot{\varphi}\dot{\psi} \cos \delta + \ddot{\varphi}^2) z_0 \mathbf{k} - (\dot{\varphi}\mathbf{k} + \dot{\psi}\Omega)^2 (x_0 \mathbf{i} + z_0 \mathbf{k}) + \dot{\psi}^2 \left(\frac{x_0}{2} \sin^2 \delta + z_0 \cos^2 \delta\right) \mathbf{k}\right\}; \tag{30}$$

the second is pulsating:

$$\mathbf{F}_c'' = -m\left\{\left[2\dot{\varphi}\dot{\psi} x_0 \sin \varphi \sin \delta + \dot{\psi}^2 \frac{x_0}{2} \sin 2\delta \sin \varphi\right] \mathbf{k} + \dot{\psi}^2 \left[-\frac{x_0}{2} \sin^2 \delta \cos 2\varphi + \frac{1}{2} z_0 \sin 2\delta \sin \varphi\right] \mathbf{i} + \dot{\psi}^2 \left[\frac{1}{2} x_0 \sin^2 \delta \sin 2\varphi + \frac{1}{2} z_0 \sin 2\delta \cos \varphi\right] \mathbf{j}\right\}. \tag{31}$$

The Coriolis force is not computed since we assume that the point P moves in only one direction, with direction cosines $\alpha_1, \alpha_2, \alpha_3$ relative to (i, j, k). The equation of motion of P is

$$\ddot{s} + 2D\dot{s} + \sigma^2(s - s_0) = -\left[\left(2x_0\dot{\varphi}\dot{\psi} \sin \varphi \sin \delta + \dot{\psi}^2 \frac{x_0}{2} \sin 2\delta \sin \varphi\right) \alpha_3 + \dot{\psi}^2 \left(-\frac{x_0}{2} \sin^2 \delta \cos 2\varphi + \frac{1}{2} z_0 \sin 2\delta \sin \varphi\right) \alpha_1 + \dot{\psi}^2 \left(\frac{1}{2} x_0 \sin^2 \delta \sin^2 \varphi + \frac{1}{2} z_0 \sin 2\delta \cos \varphi\right) \alpha_2\right], \tag{32}$$

where s is the distance from P to P_0 along the direction of motion, and s_0 is the coordinate of the new equilibrium position after the addition of the centrifugal force to the elastic force. Naturally, s_0, x_0, and z_0 depend on δ, $\dot{\varphi}$, and $\dot{\psi}$; however, in order to make a simple, approximate computation, we assume that s_0 is so small that the evaluation of the right-hand side of equation (32) is exact enough. In the specific case of Explorer IV, the constant force involved is so small that this approximation is fully justified. We definitely can write that the equation of motion of P relative to S is, with the above approximation, in the form

$$\ddot{s}+2D\dot{s}+\sigma^2 s=-2a_1\dot{\varphi}\dot{\psi}\sin\varphi\sin\delta-\dot{\psi}^2a_2\sin 2\delta\sin(\varphi-\varphi_1)-\dot{\psi}^2a_3\sin^2\delta\cos(2\varphi-\varphi_2). \tag{33}$$

For this perturbation, the motion of S is characterized by the equations

$$|\mathbf{K}_G|=\text{constant}, \tag{34}$$

and

$$\dot{\varphi}\frac{\Delta\mathscr{T}}{2\pi}=-E_c, \tag{35}$$

where E_c is the total amount of the energy dissipated in one period of rotation of the body around the axis of symmetry. To evaluate E_c, we assume that φ can be considered constant during one rotation of the body around the axis of symmetry. Also, $\varphi=\dot{\varphi}t$. Equation (34) can be written

$$C^2(\dot{\varphi}+\dot{\psi}\cos\delta)^2+A^2\dot{\psi}^2\sin^2\delta=C^2r_0^2. \tag{36}$$

Therefore, from equations (28) and (36), we have

$$\dot{\varphi}+\dot{\psi}\cos\delta=r_0\cos\delta,\qquad \dot{\psi}=\frac{Cr_0}{A}, \tag{37}$$

and finally,

$$\dot{\varphi}=\nu=\frac{A-C}{A}r_0\cos\delta. \tag{38}$$

Thus, equation (33) can be written in the following form:

$$\ddot{s}+2D\dot{s}+\sigma^2 s=A_0\sin 2\delta\sin(\nu t-\varphi_1)+A_1\sin^2\delta\sin(2\nu-\varphi_2). \tag{39}$$

The energy necessary to sustain a forced vibration of the oscillator P is

$$E_c=\frac{DA_0^2\sin^2 2\delta\cdot\nu^2}{\Delta_1^2}+\frac{4DA_2^2\sin^4\delta\cdot\nu^2}{\Delta_2^2}, \tag{40}$$

where

$$\Delta_1^2=(\sigma^2-\nu^2)+4D^2\nu^2,\qquad \Delta_2^2=(\sigma^2-\nu^2)^2+16D^2\nu^2. \tag{41}$$

It is natural for us to assume at this point that $\sigma^2>>\nu^2$, and also that $\sigma^2>>16D^2\nu^2$ (these assumptions exclude the presence of free masses in the interior of the satellite, which is a possibility if any breakage occurs during the launching of the satellite). Hence, the energy dissipated for one cycle is

$$E_c=E_1^2\sin^2 2\delta\cos^2\delta+E_2^2\sin^4\delta\cos^2\delta, \tag{42}$$

and the energy dissipated per second is

$$E_m=E_1^2\sin^2 2\delta\cos^3\delta+E_2^2\sin^4\delta\cos^3\delta. \tag{43}$$

Now, if the modulus of the angular momentum is assumed constant during the motion, then $\mathscr{T}$ depends on δ only. Then,

$$\mathscr{T}=\frac{1}{2}Cr_0^2\frac{A-C}{A}\cos^2\delta+\frac{1}{2}\frac{C^2r_0^2}{A}. \tag{44}$$

If

$$p=\frac{r_0}{\dot{\varphi}+\dot{\psi}\cos\delta}$$

we have

$$\cos\delta=\frac{1}{p},$$

and the equation

$$\frac{d\mathcal{J}}{dm}=-E_m \tag{45}$$

becomes

$$\frac{dp}{dt}=E_1^{*2}\frac{1}{p^2}\left(1-\frac{1}{p^2}\right)+E_2^{*2}\left(1-\frac{1}{p^2}\right)^2, \tag{46}$$

if $(A-C)>0$. Let us consider the solution of equation (46) corresponding to the initial conditions $p(0)=1+\epsilon$, with $t>0$ and arbitrarily, $\epsilon>0$. Since $\frac{dp}{dt}>0$, p is an increasing function of t for any one value of the parameters E_1^{*2}. The sign of d^2p/dt^2 is, for $t>0$, the same as that of $(2E_2^{*2}-E_1^{*2})$ $p^2+2(E_1^{*2}-E_2^{*2})$, which is positive for

$$1\leq p^2\leq\frac{2(E_1^{*2}-E_2^{*2})}{E_1^{*2}-2E_2^{*2}}=\frac{E_1^{*2}}{E_1^{*2}-2E_2^{*2}}+1. \tag{47}$$

The curve in figure 3 shows the trend of the function $p(t)$ if $E_1^{*2}>2E_2^{*2}$, where

$$p^{*2}=\frac{2(E_1^{*2}-E_2^{*2})}{E_1^{*2}-2E_2^{*2}}. \tag{48}$$

This deduction is based on the hypothesis that D/σ^4 remains constant while δ, $\dot{\varphi}$, and $\dot{\psi}$ vary during the motion. Since, however, the characteristics of the oscillator change during the motion, they are functions of δ. If, for example, we assume that $\frac{D}{\sigma^4}=\lambda^2\nu^{-d}$, equation (46) becomes

$$\frac{dp}{dt}=E_1^{*2}\frac{p^d}{p^2}\left(1-\frac{1}{p^2}\right)+E_1^{*2}p^d\left(1-\frac{1}{p^2}\right)^2. \tag{49}$$

Also, the trend of the function $p(t)$ can change since there are two points of inflection. The curve in figure 4 shows the trend of the function $p(t)$ if $0<d<1$ and $E_1^{*2}>2E_2^{*2}$.

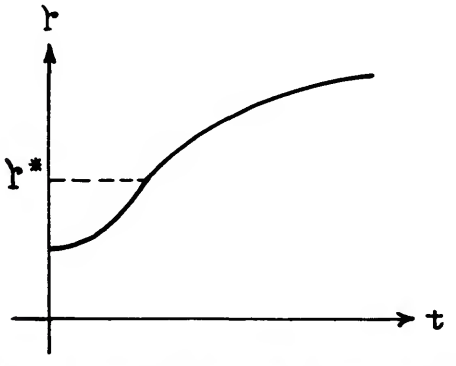

FIGURE 3.—Variation of the precessional period with time (Case I).

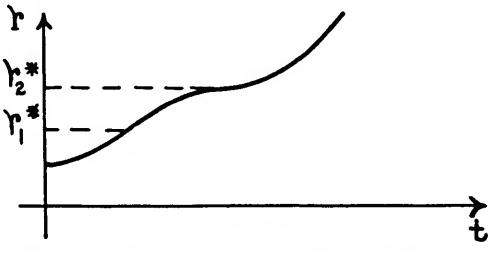

FIGURE 4.—Variation of the precessional period with time (Case II).

3. Body motion of Explorer IV

In this section, we shall compute the extent to which the phenomena considered above can explain the observed motion of Explorer IV during the first 30 days after launch.

3.1. Torque due to the atmospheric drag.—We shall now evaluate for the specific case of this satellite the coefficients introduced above. To begin, we note that the variation of the modulus of the angular momentum during the first 30 days is, to a very good approximation, not more than 3 percent of the initial value. The external forces acting on the body cause a first-order variation in the direction of the momentum, and a small second-order variation in the magnitude of the momentum. The ratio of the magnitude of the total variation of the momentum to the variation of modulus of the angular momentum is only a few percent. An exact computation of the aerodynamic torque would be very time-consuming. Assume that the satellite moves in free molecular flow and that the re-emission of the molecules from the body is completely diffuse.

Since we need only a good approximation of the function $C_0-C_2\cos^2\gamma-C_3\cos^3\gamma$ in order to have equation (1) represent the terms of the atmospheric drag in the best manner, only the coefficients C_0, C_2, and C_3 will be evaluated now. First, we compute the modulus of the momentum for $\gamma=\pi/2$. The total force of the atmospheric drag acts in the direction opposite to that of $\mathbf{v}_G$, while the resultant of the reactions due to the re-emitted molecules is in the same direction as $\mathbf{v}_G$. The drag is $\mathscr{C}\frac{\rho}{2}v_G^2\Sigma$, where Σ is the maximum projected area, and $\mathscr{C}$ is equal to 2.2 for the hypothesis of free molecular flow and diffuse re-emission. The point of application of the resultant drag is on the axis of symmetry at a point G' where $G\mathrm{G}'=-\ell_0\mathbf{k}$, and $\ell_0>0$.

Next, let us consider the situation for $\gamma\neq\pi/2$. The computation is now more complicated since the moments due to the impinging molecules should be distinguished from the moments due to the diffusely re-emitted molecules. If we substitute for the satellite's body an equivalent cylinder with plane bases normal to the axis of symmetry, the resultant force of the impinging molecules is $\mathscr{C}_i\rho(\Sigma_0|\cos\gamma|+\Sigma|\sin\gamma|)\frac{v_G^2}{2}$, where Σ is the same as above; $\mathscr{C}_i=2$; and Σ_0 is the transverse area. The center of pressure, G', is independent of γ and is the same as above. The moment, with respect to G, of the atmospheric drag due to the impinging molecules is

$$\mathbf{M}_G^{(i)}=\frac{\mathscr{C}_i\rho}{2}\ (\Sigma_0|\cos\gamma|+\Sigma_0|\sin\gamma|)\ell_0\mathbf{k}\times\mathbf{v}_G|v_G|. \tag{50}$$

Now we evaluate the component of the torque due to the diffusely re-emitted molecules. As computed by Cook (1959),[5] the total force acting on the lateral surface of the cylinder is perpendicular to the axis of symmetry in the plane parallel to $\mathbf{v}_G$, and the modulus of the total force is

$$\frac{\pi\sqrt{\pi}}{4s_r}\rho\frac{v_G^2}{2}\Sigma_1|\sin\gamma|,$$

where s_r is the "molecular speed ratio of re-emission."[6] Since the center of pressure of the total force is also the same as before, and since the force is perpendicular to the axis of symmetry, then

$$\mathbf{M}_G^{(r)}=\frac{\pi\sqrt{\pi}}{4s_r}\frac{\rho}{2}\Sigma_1\mathbf{k}\ell_0\times\mathbf{v}_G|v_G|. \tag{51}$$

---

[5] On page 26 of his paper, Cook evaluates only the component of the total drag due to re-emission, in the direction of $\mathbf{v}_G$.

[6] $s_r=s\sqrt{\frac{T}{T_r}}$, where $s=\frac{\text{speed of satellite}}{\text{most probable molecular speed}}$, T=absolute temperature of the atmosphere, and T_r=absolute temperature of the gas re-emitted from the surface of the satellite.

We note that the torque due to re-emission from the bases of the cylinder is an order of magnitude smaller than the aerodynamic torque and that if the bases are plane, or if the cylinder is open, this torque is zero. Therefore, for any one γ we obtain, with good approximation,

$$\mathbf{M}_G=\frac{\rho}{2}[2(\Sigma_0|\cos\gamma|+\Sigma_1|\sin\gamma|)+0.2\Sigma_1]\mathbf{k}\ell_0\times\mathbf{v}_G|v_G|. \tag{52}$$

We must now compute the influence of the asymmetry of the body with respect to a plane normal to the axis through the center of pressure. Let us suppose that the momentum of the re-emitted molecules of the nose of the satellite, not computed for the equivalent cylinder with plane bases, is at least one order of magnitude smaller than the total momentum for very small values of γ. We will evaluate the asymmetry of the body by substituting $\ell_0+\ell_1\cos^3\gamma$ for ℓ_0, where $0\leq\ell_1\leq\ell_0$. This assumption is very approximate, but we shall see later that a more exact evaluation is not worth the effort required. The relation $\ell_1>0$ depends only on the fact that none of the molecules impinging on the exhaust nozzle is diffused out of the body. Thus

$$\mathbf{M}_G=\frac{\rho}{2}[2(\Sigma_0|\cos\gamma|+\Sigma_1|\sin\gamma|)+0.2\Sigma_1](\ell_0-\ell_1\cos^3\gamma)\mathbf{k}\times\mathbf{v}_G|v_G|, \tag{53}$$

where $\Sigma_0=200$ cm^2, $\Sigma_1=3000$ cm^2, $\ell_0=14$ cm, and $\ell_1=7$ cm.

We made the approximate evaluation of ℓ_1 by considering position I of the satellite corresponding to the angle $\gamma\cong\pi/6$, and position II corresponding to the angle $\gamma\cong5\pi/6$; these positions are diagrammed in figure 5. The momentum of the impinging molecules is the same for the two positions, but the momentum of the diffusely re-emitted molecules is not the same. If only a small fraction of the $(\rho\Sigma_0 v_G\cos\gamma)$ molecules impinging on the exhaust nozzle are re-emitted from the body in position II, then these molecules are diffusely re-emitted with a momentum equal to $0.2\rho\Sigma_0 v_G^2\frac{\sqrt{3}}{2}L$ in position I, where L (the distance from the nozzle to G) is about 100 cm. This value for the momentum is the difference in the momentums corresponding to the two positions. If we evaluate this difference by using equation (53), then $\ell_1=7$ cm.

Finally, we evaluate the coefficients C_0, C_2, and C_3 by identifying the value of $\mathbf{M}_G$ from equation (53) with the value of $\mathbf{M}_G$ from equation (1) for the same value of $\gamma(\gamma=\pi/2,\ 0,\ \pi)$. We obtain

$$C_0=4.2\times10^4\text{ cm}^3,\qquad C_2=3.5\times10^4\text{ cm}^3,\qquad C_3=2\times10^3\text{ cm}^3.$$

To finish, we must evaluate for Explorer IV the vectors defined in equation (4). In figure 6 the ratio $(\rho v_G^2)/(\rho^* v_G^{*2})$ has been plotted against the true anomaly of G over the orbit, where ρ^* is the density and $\mathbf{v}_G^*$ is the velocity at perigee. We assume that the scale height is about 40 km. The vectors in equation (4) can be evaluated from the graph in figure 6. If we consider only the contribution of the drag in the interval $(-15°,\ 15°)$ around perigee, and if $\mathbf{v}_G$ is assumed constant and equal to $\mathbf{v}_G^*$, then

$$\mathbf{I}_0=\frac{1}{12}\frac{\mathbf{v}_G}{|v_G|},\qquad \mathbf{I}_2=\frac{\cos^2\theta}{12}\frac{\mathbf{v}_G}{|v_G|},\qquad \mathbf{I}_3'=\frac{\cos\theta}{12}\frac{\mathbf{v}_G}{|v_G|},\qquad \mathbf{I}_3''=\frac{\cos^3\theta}{12}\frac{\mathbf{v}_G}{|v_G|}. \tag{54}$$

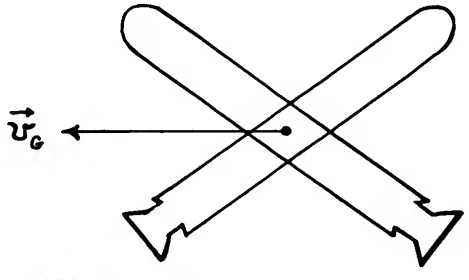

FIGURE 5.—Asymmetric property of the satellite.

Substituting C_0, C_2, C_3, $\mathbf{I}_0$, $\mathbf{I}_2$, $\mathbf{I}_3'$ and $\mathbf{I}_3''$ in equation (6), we obtain this differential equation:

$$\frac{d\Omega}{dt}=-\frac{p^*v^{*2}}{Cr_0}\left\{\frac{\cos\delta}{12}\left(4.2\times10^5-3.5\times10^4\,\frac{\sin^2\delta}{2}\right)-3.5\times10^4\,\frac{\cos\delta}{12}\cos^2\theta\left(1-\frac{5}{2}\sin^2\delta\right)\right.$$
$$\left.+2\,\frac{\cos^3\theta}{12}\cdot10^3\left(\frac{3}{8}\sin^4\delta+\cos^4\delta\right)-10^3\cdot\frac{3}{8}\cdot\cos\theta\sin^2\delta(\sin^2\delta-4\cos^2\delta)\right\}\frac{\mathbf{v}_G^*}{|\mathbf{v}_G^*|}\times\Omega. \qquad (55)$$

Thus, the direction of the angular momentum rotates around $\mathbf{v}_G^*$. Using equation (55) with $\delta=84°$, $\theta=45°$, $v^*=8$ km/sec, $\rho=1.8\times10^{-13}$ grams/cm^3, $r_0=2\pi/12$ sec^{-1}, $C=4.7\times10^7$ grams/cm^2, we obtain $\frac{\Delta\Omega}{\text{rev}}\cong0.^\circ45$. Note that the motion of the satellite is a quasi-tumbling motion corresponding to a roll period of 1 second.

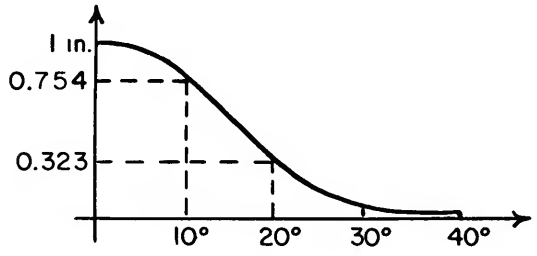

FIGURE 6.—Relative atmospheric density versus true anomaly along the orbit.

We observe also that the value of ρ^* was taken from tables from Jacchia (1960a). This is a representative value, close to the mean for the epoch. Since, according to the same source, erratic fluctuations in ρ^* by a factor of 2 are in order, we can expect that the variations of Ω due to the atmospheric drag were similarly affected.

3.2. Gravitational torque.—In this section, we shall compute the magnitude of the perturbation due to the gravitational torque, P_b. Using the orbital elements of Explorer IV, we find that equation (8) becomes $\tilde{\omega}^2=10^{-6}$ rad^2/sec^2, and equation (9) becomes $\frac{d\Omega}{dt}=1.62\times10^{-6}\cos\theta_1\left(1-\frac{3}{2}\sin^2\delta\right)\mathbf{N}\times\Omega$. Hence, $\frac{|\Delta\Omega|}{\text{rev}}=0.^\circ61\cos\theta_1\sin\theta_1\left(1-\frac{3}{2}\sin^2\delta\right)$.

3.3. Magnetic torque.—To compute the perturbation due to the magnetic torque, P_c, we assume that the earth's magnetic dipole is $\mu_E=8.1\times10^{25}$ emu; thus, $\frac{\mu_E}{a^3(1-e^2)^{3/2}}\cong0.25$ gauss. Let us put $i_m=50°$, $\frac{\Delta\Omega}{\text{rev}}=1.4\times10^3\frac{\mu_3}{Cr_0}\cos\delta\left(-\frac{1}{4}\mu+\frac{3}{4}\mathbf{n}_m\times\mathbf{u}\right)\times\Omega$. For example, we notice that if the intrinsic magnetic moment has, parallel to the axis of the body, a component of the order of 0.5 amp-m^2 (corresponding, for example, to a solenoid parallel to the axis of symmetry, with 10,000 turns and 1 cm in diameter, in which there is a current of 0.5 amp), then $\frac{|\Delta\Omega|}{\text{rev}}=0.^\circ01$. This action corresponds to a maximum torque of 12.5 dyne-cm.

Measurements carried out by the Radio Corporation of America (private communication) on Tiros I (Satellite 1960 $\beta2$) showed the presence of a disturbing magnetic torque of about 200 dyne-cm owing, probably, to interaction between the earth's magnetic field and the component of the intrinsic magnetic dipole parallel to the spin axis. Perhaps 70 percent of the torque comes from the residual magnetism of the high permeability components in the satellite; the remaining 30 percent comes from current loops in the electrical circuitry of the satellite's instrumentation.

Grumman (private communication) has estimated the disturbing magnetic torque expected for the Orbiting Astronomical Observatory proposed for launch in 1963. The major part of the torque expected in this satellite will result from its permeable structure; the contribution of the

internal complex circuitry will be minimized by proper electrical design. The amount of torque predicted is many hundred dyne-cm. Since we do not know if this minimization has been done for Explorer IV, the value 17.5 may be too small.

Finally, let us make a crude evaluation of the torque, averaged over one precessional period, due to the induced magnetic dipole that we obtained in section 2.4.

If we assume that $m_1=0$, $m_3=1$ and $\Omega=\mathbf{u}\frac{\sqrt{2}}{2}-\mathbf{n}_m\frac{\sqrt{2}}{2}$,

then

$$\mathbf{M}_G^{(m')}=+\mathbf{u}\times\mathbf{n}_m\frac{(\mu-1)V\mu_E^2}{16\pi a^6(1-e^2)^{9/2}}. \tag{56}$$

Finally,

$$\tilde{\mathbf{M}}_G^{(m')}=+7\times10^{-4}(\mu-1)V\mathbf{u}\times\mathbf{n}_m \text{ dyne-cm}. \tag{57}$$

The shell of the body of Explorer IV and the casing of the last-stage rocket left attached as part of the satellite were both made of 410 stainless steel, whose initial permeability is 110. If we assume that there is no premagnetization [7] to be considered, then equation (57) becomes (using $V=2000$ cm^3 and $\mu=110$)

$$\tilde{\mathbf{M}}_G^{(m')}=+154\mathbf{u}\times\mathbf{n}_m \text{ dyne-cm},$$

which corresponds to a variation of 1°.3 per revolution. The chosen value of γ may be far from the actual value for the reasons given in the introduction. This amount is quite sufficient to explain the variation of Ω during the motion, and even during the period of tumbling motion.

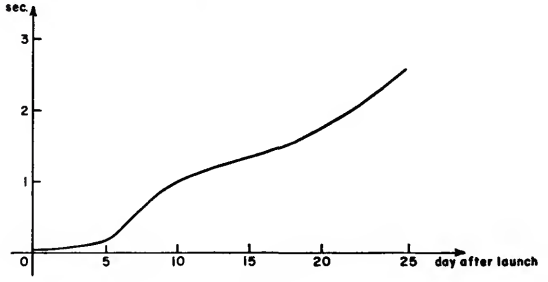

FIGURE 7.—Observed variation of the precessional period.

4. Results and conclusions

4.1. The period of rotation around the gyroscopic axis.—The history of the period of rotation around the gyroscopic axis is traced in figure 7. Fields (Lundquist, Naumann, and Fields, 1961) determined the period from the modulation of the counting rate of the directional counter. The observations seem to have been made very carefully. Thus, the observed curve can be compared with the theoretical one [8] that was obtained from the energy transfer due to the internal vibrational motion (see figs. 3 and 4). The existence of the first point of inflection is evident. The explanation given earlier of the definite second point of inflection, which corresponds to the 23rd day after launch, may seem artificial. However, this second point of inflection can be explained in another way. Perhaps the decrease in the probably significant torque due to the interaction between the earth's magnetic field and the ferromagnetic components of the satellite plays an important role.

The rapid increase in the period on the 31st day after launch corresponds to the first time in the history of the satellite that $\dot{\varphi}=\dot{\psi}$. Perturbation P_d may also be the explanation of this phenomenon. Note that this particular case has been excluded for reasons of simplicity.

[7] If there is any important premagnetization (Lundquist, Naumann, and Fields, 1961), this may become a predominant factor with respect to the induced magnetization, and therefore must also be considered in the perturbation P_e.

[8] We observe that $\dot{\varphi}+\dot{\psi}\cos\delta\cong\dot{\varphi}$ and also that $p\cong r_0/\dot{\varphi}$ during the whole period of motion.

The rapid decrease in the period on the 33rd day after launch is very striking. Several causes sufficient to explain such a phenomenon can be found quite easily. The necessary torque is so small, 10 dyne-cm in comparison to the 200 dyne-cm which are needed to explain the decrease in the first 5 days, that any electromagnetic phenomenon may be responsible for this exceptional decrease. Consequently, we would need to know the internal ferromagnetic components to evaluate their interaction with the earth's magnetic field. This torque can at least partially explain the decrease in $\dot{\varphi}$ due to energy leakage by magnetic hysteresis in the ferromagnetic components. Because of the shape of the body, we prefer to consider this action more than the influence of the eddy currents. While we exclude the possibility that the initial decrease of $\dot{\varphi}$ can be explained only by the eddy currents, the action of these currents and the magnetic hysteresis in the ferromagnetic components consistent with the variation of the earth's magnetic field along the orbit can contribute to the decrease during the whole period of motion.

4.2. Possibility of the determination a priori *of the body motion.*—There are two phenomena of first-order magnitude in the body motion of Explorer IV: the decrease of $\dot{\varphi}$ and the rotation of Ω, with the modulus of the angular momentum assumed to be constant in the first-order approximation. The first phenomenon was explained in section 4.1. In this section, the change in the direction of Ω will be discussed.

If we exclude the possibility of handling the global problem of the motion of G and of the motion of S around G, then we should know the function $\delta(t)$ and the dependence of the orbital elements of G on time. From equations (6) and (9), and from the equation attained by averaging exactly equation (19), we can write the global perturbation equation

$$\frac{d\Omega}{dt}=\mathbf{R}(\delta,\theta,\theta_1,\gamma,\lambda_1,\lambda_2)\times\Omega, \tag{58}$$

which has the first integral $\Omega^2=1$. If we project this equation over the inertial frame of reference, taking into account the variability with time of the X, Y, Z axes, we obtain the equations

$$\frac{d\Omega_1}{dt}=f_1(\Omega_1,\Omega_2,t), \qquad \frac{d\Omega_2}{dt}=f_2(\Omega_1,\Omega_2,t), \tag{59}$$

where Ω_1 is the right ascension and Ω_2 is the declination of Ω. In this way, if exact observations of the variation of Ω and also of $d\Omega/dt$ are available, we can compute the additional torque that is necessary to explain the total variation of Ω. The experimental determination of the axis of tumble is not so exact as the determination of the angular velocity $\dot{\varphi}$. Therefore, such a computation cannot give exact enough information about this additional torque. Indeed, the determination of the axis of tumble has a possible error of 10°, an error that is very much greater than we can tolerate in a complicated computation, considering the work involved.

4.3. The displacement of Ω *during one revolution.*—The only numerical computation which can be made easily is that of the average diurnal variation of Ω. The variation observed in the first 30 days after launch was evaluated as more than 10° per day. Of this amount, 5° or 6° can be explained as a consequence of the perturbations P_a, P_b, and P_c. That is, 60 percent of the variation which was evaluated from the recorded signal strength observations correlated with the satellite's antenna radiation pattern (Naumann, 1961), from the variation of the angle of the axis of tumble with v_G^* (Zadunaisky, 1961), and from the recorded variation of the temperature of the body correlated with the position of the sun.

The rapid change in the direction of Ω during the first day after launch is easily explained if we assume that the factor $\cos\delta$ is very important for the perturbations P_a and P_c and that the atmospheric drag can cause a variation of 10° or more per day. We compute the angular variation of Ω for $\delta=84°$ in order to obtain an idea of the order of magnitude of the perturbations P_a, P_b, and P_c in the period of quasi-tumbling motion.

The gravitational torque may be responsible for a variation of 0°.1 per revolution around the orbital plane, the drag torque for an average variation of 0°.4 per revolution, and the magnetic torque for an average variation of 0°.2 per revolution, if we assume that the satellite has an intrinsic magnetic moment corresponding to a maximum torque of 300 dyne-cm, as has been provided for the other satellites. If we take into account the fact that the axes of the rotations due to P_a, P_b, and P_c are not parallel, we can compute the average variation. The result is not much more than 0°.45 per revolution, or 6° per day, which is the maximum amount.[9]

We note, finally, that the perturbation P_d due to the interaction between the earth's magnetic field and the ferromagnetic components of the satellite is not easily computed, because of three chief problems: the direction of the induced magnetic moment, the evaluation of the permeability, and the hysteresis phenomenon.

Acknowledgment

I express my appreciation to Dr. Mario D. Grossi, Mr. Imre G. Izsak, Dr. Luigi G. Jacchia, Dr. Charles A. Whitney, and Mr. Pedro Zadunaisky for their help in the preparation of this paper.

[9] It is easy to show that the total amount of the angular variation of $\vec{\Omega}$ in one day is less than the sum of the variations per revolution, because of the variation of the orbital elements caused mostly by gravitational effects and by air drag, and because of the variation in the orientation of the earth's magnetic dipole.

On the Accuracy of Measurements Made Upon Films Photographed by Baker-Nunn Satellite Tracking Cameras

By Karoly Lassovszky

At present the Smithsonian Astrophysical Observatory operates twelve Baker-Nunn satellite tracking cameras throughout the world. The photographs taken by these cameras are reduced at the photoreduction division of the Observatory's headquarters in Cambridge, Massachusetts.

The introduction to the first catalog of precise satellite positions (Lassovszky, 1960) mentioned that we had earlier begun an investigation to determine the accuracy of the measurements of the satellite positions on Baker-Nunn films. These studies included consideration of personal measuring errors and similar problems. Some preliminary results appeared in the first catalog. In the present paper, we give further details.

Personal measuring errors

The focal length of the Baker-Nunn camera is 50 cm. Although the exposure time is usually very short, varying from 0.2 to 3.2 when the camera is stationary, a fast-moving satellite produces on the film a trail that may be several centimeters long. If the exposure is made near the equator, we do not obtain perfect point images even of the stars. Plate 1 shows a typical exposure. Since a rotating barrel shutter interrupts the exposure five times, the photographic trail of the satellite is chopped into six segments divided by short breaks. (The star images are too short to show breaks.) The length of each break corresponds to the time interval during during which the shutter was closed. The interval may be as much as 0.16; and the length, several millimeters. At the instant the third (the central) break is made, the time of the exposure is photographed on the film. To determine the position of the satellite at this time, we measure the center of the central break and the centers of the reference-star images.

Generally, the satellites are so faint that, in order to obtain measurable images, we must have the camera move to track the satellite. If the tracking rate is precisely the same as the rate of satellite motion, we obtain a point image of the satellite with star trails in the background (see plate 1). We then measure the point image of the satellite and the central breaks of the reference stars.

Even if we obtain a point image of the satellite on some frames, we do not generally find such images on all frames of the same film, since the angular velocity of the satellite is not the same at different altitudes. The image may be more or less elongated, or even appear as a short trail. If the image has an oblong shape, we measure its center. If the image is actually a trail, we obtain the position of the center by measuring both ends of the trail.

If the camera tracking rate differs substantially from that of the satellite, the satellite trail may be so long that shutter breaks become visible in it as well as in the star trails. In that case, the central breaks in the trails of both the satellite and the stars are measured.

The accuracy of the measurements on trails or on breaks is, of course, less than that of the measurements made on point images, and we may expect that the greater the length of the trail or break, the less the accuracy of the

measurement. We shall discuss now some personal errors that may affect the accuracy of the measurements.

Settings at different orientation angles.—During the measurement, the filmholder is rotated until the north-south direction on the film is parallel to the Y-axis of the measuring machine. (All the measurements discussed here were made on Mann two-screw comparators.) Since the camera may track in any direction on the sky, the trails or breaks can form various angles with the X- or Y-axis of the comparator. We might expect that the accuracy of the setting of the image on the reticle lines would be affected by the angle. To answer this question, we measured two different breaks at different orientation angles.

In one case, the length of the break was 100μ. The film was rotated through ten degrees in orientation angle between each set of 30 independent settings made on both the X- and Y-reticle lines. The standard error of all the settings made on the X-reticle line was 3.31μ, and the standard error of all the settings made on the Y-reticle line was 3.33μ. Since the standard errors were almost the same, we conclude that the accuracy of the measurements on the average is the same whether the measurer makes the settings on the horizontal (X) or on the vertical (Y) line. The standard errors of the 30 measurements on each reticle line made separately at different orientation angles varied between 2.6 and 4.0μ on the X-line and between 2.5 and 4.8μ on the Y-line. Neither of these values, however, shows any systematic change with the orientation angle, in either the X-axis or the Y-axis. Thus, we believe that the accuracy of the measurements is not a function of the orientation angle.

A second set of measurements carried out by another person supports this conclusion. In this case, the length of the break was 41μ; the film was rotated five degrees between each set of measurements; and 12 independent settings were made on both the X- and Y-reticle lines at each orientation angle. Figure 1 shows the standard errors of the X-measurements obtained at each angle. This figure and three others not given here indicate that the standard errors have a random distribution and show no sign of dependence on the orientation angle.

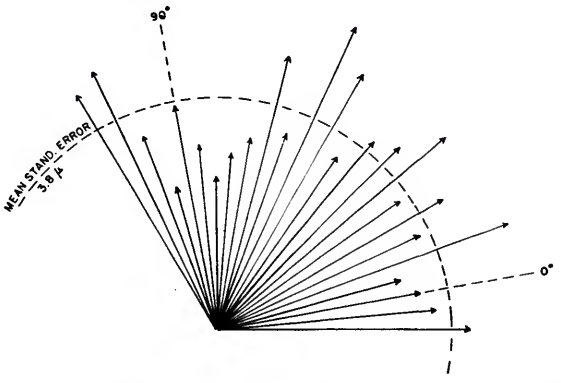

FIGURE 1.—Standard errors of the measurements of a break at different orientation angles.

Since the accuracy of the measurement seems to be independent of the orientation angle, we restricted our other investigations of personal errors to a single angle. We chose $0°$; that is, we placed the film in the comparator in such a position that the trails or breaks were parallel to the horizontal reticle line (X-axis), and the settings were made on the vertical line (Y-axis).

Frequency distribution of settings.—Seventeen measurers made settings on trails and on breaks of different lengths, turning the screw of the measuring machine until the reticle line, according to the measurer's estimate, was centered on the image. Each such series contained about two dozen settings. Since some persons measured more than one trail or break, the total number of measurement series was 34.

We find great variety in the frequency distribution of the settings made by the different measurers. Of course the distribution also depends strongly on the length of the image. Moreover, we might expect that the distribution depends also on whether the measurements were made on trails or on breaks.

Of the 34 series of images, 28 were trails and 6 were breaks. The trails varied in length from 0.052 to 3.955 mm; and the breaks from 0.031 to 0.410 mm. The frequency distributions of the settings vary greatly with the persons measuring and with the image length; also, not many settings were made on a single image. Therefore, in order more easily to compare the results obtained on trails and

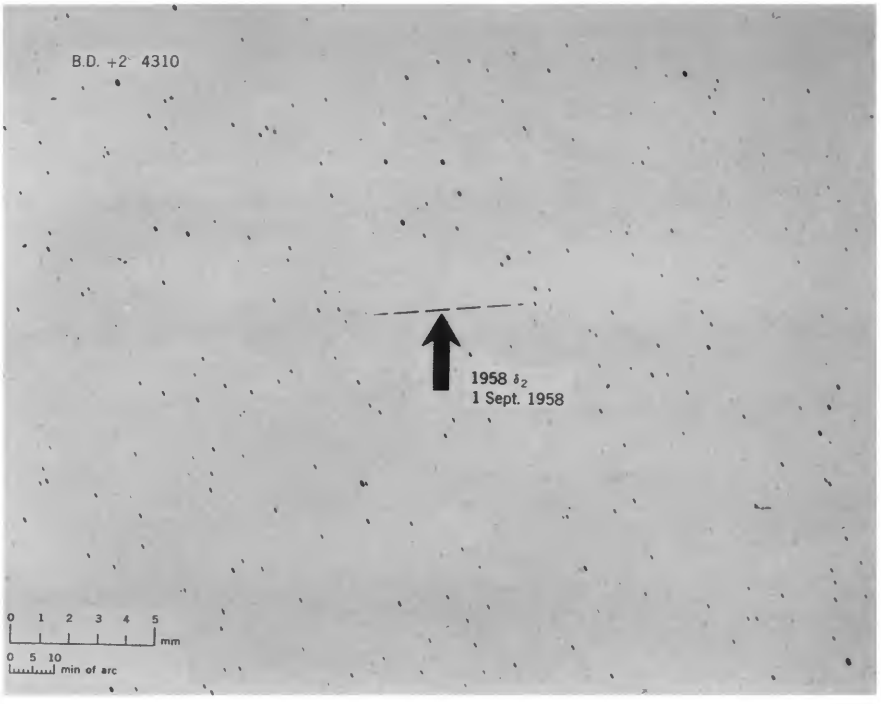

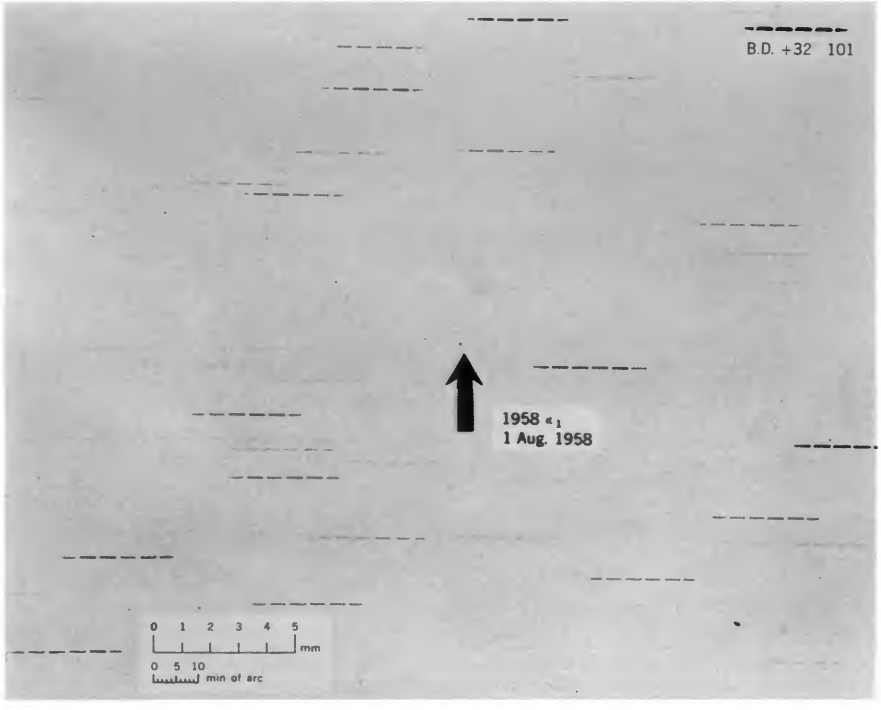

Photographs of satellites. *Top*, when camera is stationary; *bottom*, when camera is tracking.

on breaks, we determined the frequency distribution from all the settings made on the six breaks and independently determined the distribution from all the settings made on the six shortest trails. The mean length of the breaks was 0.151 mm, and that of the trails was 0.154 mm; that is, they were practically equal. The two frequency distributions are given in figure 2; the length of each vertical line indicates in percent the number of settings made at different distances (expressed in microns) from the zero point, which is the mean of all the settings. (Because of the "magnitude error," to be discussed later in the paper, this point is not necessarily the center of the break or the trail.)

Although the scattering of the settings on the breaks seems to be slightly smaller, considering the inhomogeneous and scanty material, we cannot definitely state that there is any substantial difference between the two distributions. On the contrary, from their similarity we can draw the conclusion, at least on the basis of the material at hand, that the accuracy of the measurements is not essentially affected by whether the measurement was made on a break or on a trail. Therefore, in the following discussion, we shall disregard whether the image was a break or a trail and use all the data together. In any case, the measurements made on breaks were too few in number to be discussed separately.

The lengths of the images varied from 0.031 to 3.955 mm. If we arrange the observation series according to the increasing length of the image, we notice a progressive flattening of the frequency distribution curves. However, continuity is strongly disturbed because of the different accuracies of the measurements made by different persons; this personal effect fades out if we combine the material into several groupings. From the groups formed in this way, we show in figure 3 the frequency distribution curve of the group having an average image length of 0.080 mm, and that of the group having an average image length of 2.886 mm. If we add to these curves those obtained for an intermediate image length (shown in figure 2), we can see by comparison that the frequency distribution curves flatten progressively as the length of the image increases.

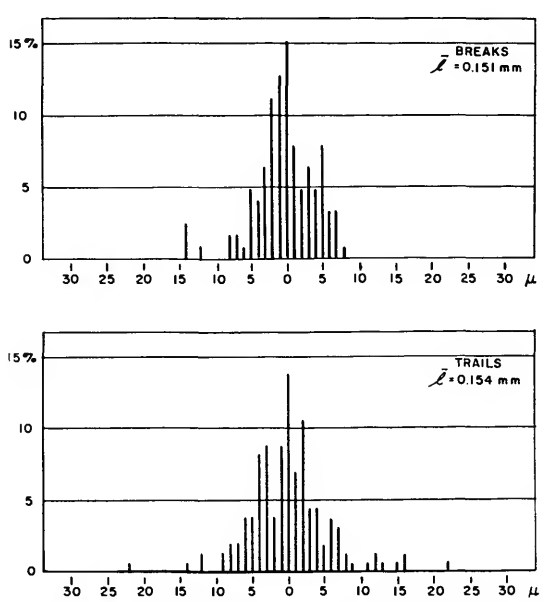

FIGURE 2.—Mean frequency distributions of settings made on breaks and trails.

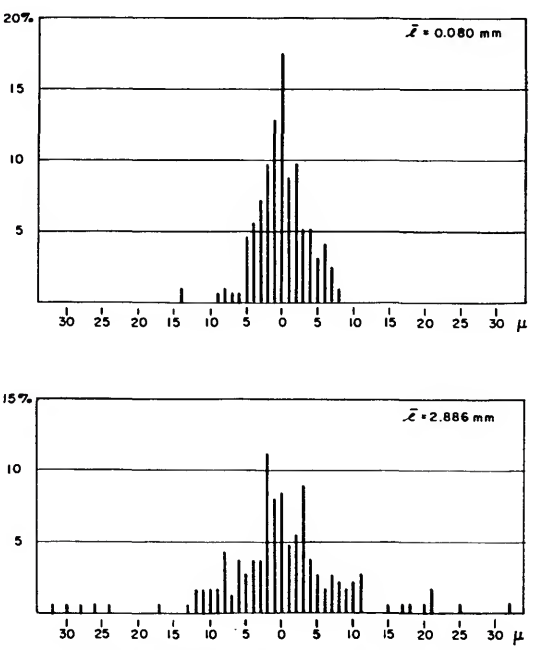

FIGURE 3.—Frequency distributions of settings made on images of different lengths.

The "magnitude error."—In measuring, we set the reticle line at the point that, in our judgment, is the center of the break or the trail. In the frequency distribution curves, the zero point represents the mean of these settings. This does not mean, however, that the zero point is really the center of the image, for two reasons. Besides the scattering of the observation errors, an effect that may be lessened by increasing the number of observations and taking the mean, our procedure involves a systematic error whose effect cannot be reduced even by increasing the number of observations; it is well known that we usually do not measure the center of the image exactly even if it is a perfect disk since, for physiological reasons, we do not stop turning the screw at the exact instant when the reticle line is centered on the image. This systematic error differs for different observers; futhermore, it varies even for the same observer according to the size of the image disk, which in turn depends upon the brightness of the star. For this reason, it is often called the "magnitude error." We usually eliminate this error by first making a direct measurement of an image and then, after rotating the film or plate through 180°, making a reverse measurement of it.

When we measure breaks or trails instead of disks, a similar error may occur which depends upon the width of the break or the length of the trail, as well as upon the person who makes the measurement.

To determine the magnitude error, we made settings not only at the point that the observer estimated to be the center of the image but also at both ends of the oblong image. The difference between the settings at the two ends gives the length of the image, and their mean gives the center of the image. We can assume that the values for the center and the lengths computed by this method may also be affected by systematic error for some physiological reason, since we may perhaps make these settings differently when the end of the image is on the left side or on the right side, or when it is above or below. The results of our statistical investigations, however, indicate that this systematic error is insignificant compared to the "magnitude error."

The Mann comparators we use are provided with a projection system. When the X-screw is moved clockwise, the X-readings increase, and the image projected on the screen passes through the vertical cross line from left to right. Of the 34 observation series discussed here, in 21 cases the mean values of the estimated centers were less than the values of the centers computed from the settings made on the two ends of the images; in 11 cases they were more, and in 2 cases the centers coincided.

Of the 17 observers who made the measurements, on the average 9 stopped turning the screw only after the center of the image passed the reticle line, 7 stopped before it passed the line, and one did it both ways. It must be emphasized that this statement is valid only for the means of the settings. In fact, the scattering of the accidental errors is so great that many accidental errors are larger than the magnitude error. Perhaps the best way of stating this is that a given person systematically makes more settings on one side of the center than on the other side.

The magnitude errors, that is, the differences between the estimated and the computed centers obtained for the images, varied from -39μ to $+65\mu$. Arranging all the magnitude errors in order of increasing absolute value and indicating for each error the corresponding length of image, we can expect to find a relationship between the two quantities. The magnitude errors are, of course, greatly influenced by the systematic personal effects, but, since our data are scarce, we are obliged to use all of these heterogeneous data. Plotting the magnitude errors against the image lengths, we find that although there is a great scattering, the expected relationship is certainly apparent. Forming 8 groups from the material, we get the relationship represented in figure 4. The scattering of the individual values is conspicuous only at the longer lengths, but these long images were measured only for the purpose of this study. In practice, the trails are usually less than 0.2 mm and the breaks smaller than 0.1 mm.

The effect of the distances of the reference stars on the accuracy

For the determination of the satellite positions, we used the linear plate-constant method. For

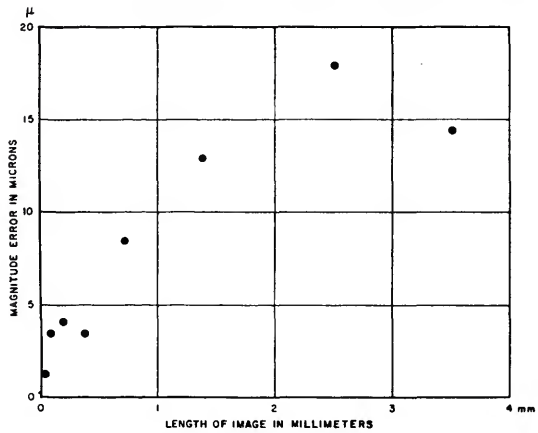

FIGURE 4.—The relationship between the length of image and the "magnitude error."

the computation of the six plate constants, three reference stars would theoretically be sufficient. However, we have persisted in using six stars, employing the least-squares method to compute the six constants from twelve equations. When there were large residuals, one or two reference stars were sometimes omitted. If large residuals still remained, we repeated the measurements, never using fewer than four reference stars.

We further decided that the reference stars should lie not farther from the satellite image than 20 mm on the film, a distance corresponding to 2°.3 in the sky, and that the reference stars should be symmetrical about the satellite image, so that the image will always lie within the configuration even if some of the reference stars must later be omitted.

Among the different sources of error that influence the accuracy of the reduced position, distortion of the emulsion may cause serious problems. Another source of error may be the optical distortion of the field of the camera. When we began to use the linear plate-constant method, we assumed that, within the admissible maximum area of configuration of the reference stars, the distortion did not appreciably influence the accuracy. We were aware, however, that this assumption needs proof since, if it were not valid, our method would not be wholly reliable.

To find out how the position obtained is affected by use of reference stars at different distances, we chose various star groups, each containing six stars, around the object whose position was to be determined. The average distances of the groups differed, but, in a given group, the distances of the stars were nearly the same. On a chart of the area surrounding the object, rings were constructed around the central image; stars were chosen so that the reference stars of a given group were all inside the ring and properly distributed. Since the width of the frame was only 54 mm, the exterior radius of a complete ring cannot be larger than 27 mm even when the center object was exactly in the middle. However, we could go even farther from the center object by choosing three reference stars in the left part and three in the right part of an incomplete ring with an exterior radius larger than 27 mm.

We chose three stars on a frame and determined their positions by using reference stars at different distances. One of the stars was approximately in the center (II) of the frame; of the other two, one was in the center of the left (I) half and one was in the center of the right (III) half of the frame. In field I, four groups of reference stars were available around the chosen center star; in field II, seven groups; and in field III, six groups. The greatest dis-

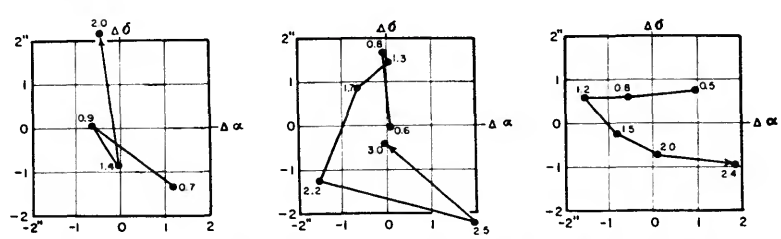

FIGURE 5.—The shifts of the positions of three different stars on the same frame when reference stars at different distances from the center star are used. The numbers at the positions give the mean distances of the reference stars in centimeters.

tance of the groups in field I was approximately 2 cm; in field II, 3 cm; and in field III, 2.5 cm. The position of each center star was determined separately from each of the groups around it; then the mean position of each center star was computed from all the stars in its field. Choosing the mean position as origin, we can see in figure 5 how the position of the center star changes when different groups are used for the reduction. For every position of the central star, the chart indicates the mean distance of the group of reference stars used to determine that position. No relationship seems to exist between the position and the distance, at least in the area examined. This result may be regarded as favorable since the scattering of the mean positions is not very much greater than that to be expected even if these positions had been obtained from the reiteration of the measurements using the same reference stars.

We also tried to find out, from another graphic representation of these results, how the distances of the reference stars influence the computed positions. Combining the results obtained for the three centers we took the mean of the positions obtained from the groups that were nearer to the center star than 1.4 cm, then took separately the mean of the positions from groups that were farther than 1.4 cm from the center star. The distributions of the individual positions around the two mean positions are illustrated in figure 6. Although the number of observations is not very large, one notices at first glance that the scattering of the positions derived from the groups of reference stars nearer to the center star than 1.4 cm is undoubtedly smaller than the scattering at distances larger than 1.4 cm. However, even

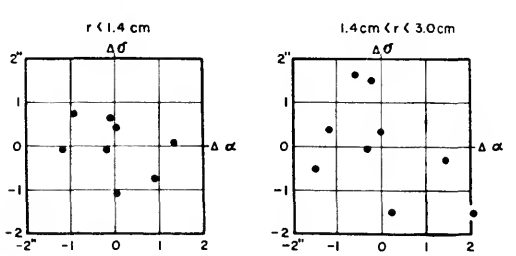

FIGURE 6.—The scattering of the positions obtained when reference stars at different mean distances are used.

in the latter case, all the positions are in a 4″ x 4″ square; that is, they are in an area not larger than we can expect from the measurements made with the Mann comparators on the Baker-Nunn films.

In practice, we of course choose reference stars that are as near as possible to the satellite image, even though sometimes, in areas poor in stars, we are obliged to use reference stars that are farther than 1.4 cm from the satellite image. On the basis of our investigation, however, we seem justified in using the linear plate-constant method, at least in an area with a diameter of 5 cm (5°.8).

The accuracy of the measurements

We may regard the figures given in the preceding section as a graphical illustration of the accuracy that we obtain in the reduction of Baker-Nunn films. Making use of the numerical values of the measurements, we can also express this accuracy numerically; that is, we can compute the standard error of a position determined on a Baker-Nunn film.

Before we made the investigations discussed in the preceding section, we had already obtained some information about the relative accuracy of the measurements made with both the Van Biesbroeck goniometers and the Mann comparators.

In SAO Special Report No. 41, we described the methods used to measure the position of a satellite, and recounted the sources of errors that we could expect. The accidental personal errors cannot be avoided, but we can lessen their influence by using a greater number of reference stars, or by increasing the number of settings on them, or by repeating the whole measurement. We assume that the so-called magnitude error is eliminated (or at least lessened) when both direct and reverse measurements are made.

At the beginning of the photoreduction project at the Smithsonian, two Van Biesbroeck goniometers were chiefly used. The goniometer, which in fact consists of two independent instruments, a theodolite and a filmholder, may itself be a source of errors. Since the two parts of the machine are not stably connected, changes may occur, in time, so that the axis of the film holder may not pass exactly through the center of the theodolite, and the vertical axis of the

theodolite may not be perpendicular to the axis of the filmholder. The smallest readable unit on the Van Biesbroeck goniometer is 1″.

On a screw comparator, there are two chief sources of errors: the periodic and the secular screw errors. The smallest readable unit of the Mann comparators is 1μ, corresponding to 0″.4 on the Baker-Nunn films. According to the manufacturer, the periodic error of the Mann machines is less than 1μ, and the secular error within the measuring area of the reference stars is less than 0.5μ. We can regard both values as satisfactorily low.

In the photoreduction division, each computer from time to time measures the same image twice to check his own consistency. (Averages of the differences obtained from a large number of such double measurements give characteristic information of the efficiency of the measurers.) Figure 7 shows the results of 54 such double measurements made with the Van Biesbroeck goniometers, and of 90 double measurements made with the Mann comparators. The coordinates of each dot give the differences in α and in δ of the two positions obtained by the double measurement in question. The distance D of the dot from the origin represents the angular separation of the two positions. The much smaller scattering of the dots shows at a glance that the measurements made with the comparators are of higher accuracy than those made with the goniometers.

From all the double measurements, the following standard errors have been derived for a single determination of position:

Number of double measurements made with		Standard errors μ_α	μ_δ	μ_D
Van Biesbroeck goniometer:	54	3″.99	3″.21	5″.72
Mann comparator:	90	1. 10	1. 12	1. 82

These values show that the accuracy obtainable with the Mann comparators is more than three times greater. These results differ only slightly from those given in Special Report No. 41 (p. 8), which was based upon fewer observations.

The positions obtained from the measurements made with goniometers seem to have on the average a larger error in α than in δ. The difference is small, however, and after the omission of a few double measurements in which the agreement between the two positions is poorest, the difference becomes insignificant. On the other hand, the positions obtained with the Mann comparators showed the same standard error in both α and δ. As we shall see, the same conclusion was reached from other measurements made later. This result does not seem to confirm earlier conclusions that the error in right ascension is generally larger. (This larger error in right ascension was explained by the fact that most of the satellites whose positions were measured at that time were traveling in a west-to-east direction, and errors in the direction of motion are somewhat greater than errors perpendicular to the line of motion.)

We must not forget that for each double measurement the same reference stars were used; therefore, the effect of any catalog errors is the same in both measurements. Thus, the catalog errors are not reflected in the position errors of the satellite. To examine the effect of catalog errors, we made special measurements. We determined the positions of seven satellites when they were passing through areas rich in stars. Thus we could determine the position of each satellite using four, and in one case even five, independent configurations of reference stars. The configurations used for each satellite were chosen so that their mean distances from the satellite were approximately the same. (This was done in order to eliminate the occasional effect of the distance of the star from the satellite image.) The measurements were made by five different persons. The agreement between the positions obtained from different configurations was satisfactory. From the 29 independent positions, the following standard errors were derived for one position:

n	μ_α	μ_δ	μ_D
29	1″.00	1″.01	1″.50

These values differ only slightly from those determined by the double measurements (11″.0, 1″.12, 1″.82). Although we might have expected to obtain larger values when different reference stars were used, in fact the values are slightly smaller. We can conclude that the catalog errors have practically no effect on the accuracy that can be obtained with the Mann comparator on the Baker-Nunn films.

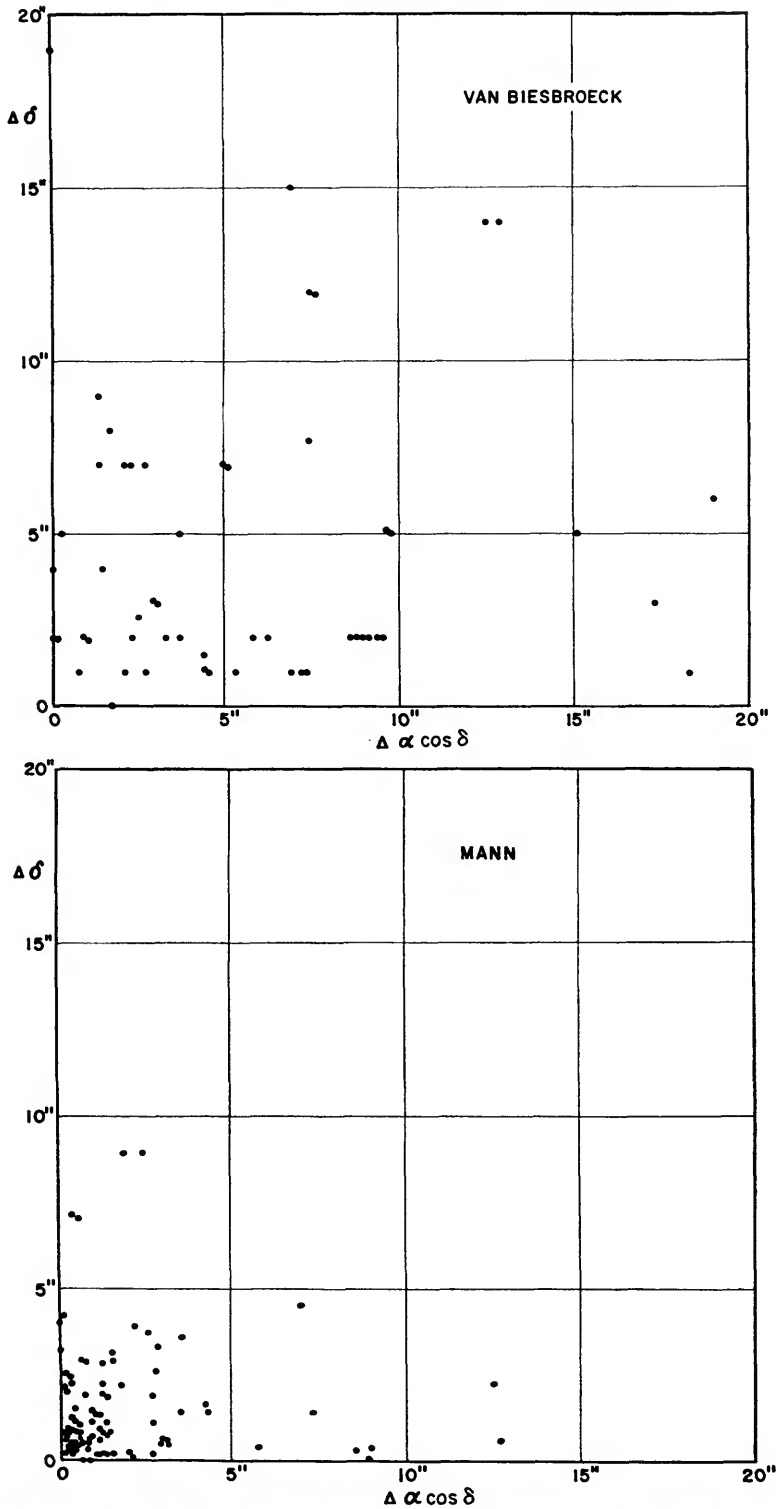

FIGURE 7.—Differences in α and δ of double meaurements made with Van Biesbroeck goniometers and with Mann comparators.

In addition, we have some other measurements that can be used for the determination of accuracy. As mentioned in the first paragraph of this section, we can also use to determine the accuracy the measurements made to find out how the distance of the reference stars from the satellite image influences the determination of the satellite's position. We made two groups of positions, one group derived from the reference star configurations that were nearer to the center star than 1.4 cm, and the other group where the distances varied between 1.4 and 3.0 cm. From these two groups, the following standard errors were found for one position:

r	n	μ_α	μ_δ	μ_D
$r<1.4$	8	0".83	0".66	1".03
$1.4<r<3.0$	9	1.4	1.12	1.60

The standard errors obtained from the first group are, of course, smaller. The standard errors obtained from the second group are approximately the same as those from the many previous measurements. This fact may seem unexpected since the average distances of the reference star configurations are generally smaller for the usual measurements than they were in the second group of these special measurements. This favorable result can perhaps be explained by the facts that for these special measurements a better film was used, and the center object was not a satellite but a star image.

If we combine all the results discussed here but discard the eight positions obtained from the measurements of the reference star configurations nearer to the center star than 1.4 cm, we get as the final result:

μ_α	μ_δ	μ_D
1".09	1".11	1".77

If restricted to one decimal, we can say that the standard error of a position determined from the measurements made with Mann comparators on Baker-Nunn films is $\pm 1".1$, both in right ascension and in declination.

Acknowledgment

I express thanks to Mr. G. Kirklin for helping with some of the reduction work.

Density of the Heterosphere Related to Temperature

By Marcel Nicolet

An analysis of the behavior of the heterosphere, i.e., of the terrestrial atmosphere where the mean molecular mass cannot be taken as a constant parameter, requires a theoretical study to supplement observational results from which it is not yet possible to obtain all the parameters needed for a complete picture of the physical conditions.

If a general consistent picture of the vertical distribution of density in the heterosphere at heights between 200 km and 1500 km is obtained from acceleration data derived from earth-satellite orbits, the analysis leads sometimes to unjustified conclusions concerning the physical conditions. The sharp increase of molecular mass, the gradient of temperature increasing with height, the inflection of density curves, and the correlation of density with unusual indices of solar activity are among other physical anomalies that are introduced into this analysis.

In this paper, an improved method for calculating physical parameters of the heterosphere is applied, in which the temperature is selected as the essential parameter, and diffusion and heat conduction are introduced.

Formulas for density

The vertical distribution of the upper atmosphere density deduced from the rate of change of the period of the motion of a satellite in its orbit is generally represented by the formula

$$\rho=\rho_0 \exp\ (-z/H_\rho), \tag{1}$$

in which ρ denotes density at height z, and ρ_0 at $z=0$; and H_ρ is a parameter of the vertical distribution of density, which must be defined by

$$\frac{1}{\rho}\frac{d\rho}{dz}=-\frac{1}{H_\rho}, \tag{2}$$

with the condition

$$dH_\rho/dz=0. \tag{3}$$

These formulas cannot lead to correct conclusions concerning the temperature or the mean molecular mass in the heterosphere.

To provide a basis for an analysis of the vertical distribution of the temperature and mean molecular mass, we must use at least the general formula representing conditions of a perfect gas and of hydrostatic distribution.

The general form to be used is (Nicolet, 1954)

$$\frac{dp}{p}=\frac{dn}{n}+\frac{dT}{T}=-\frac{dz}{H}, \tag{4}$$

where p is the total pressure; n is the total molecular concentration; T is the absolute temperature; and H is the local atmospheric scale height. The atmospheric scale height H is defined by

$$H\equiv\frac{kT}{mg}, \tag{5}$$

where m is the mean molecular mass; g is the acceleration of gravity; and k is Boltzmann's constant. The variation is, therefore, related to the variation of T, m and g; that is,

$$\frac{dH}{H}=\frac{dT}{T}-\frac{dm}{m}-\frac{dg}{g}. \tag{6}$$

By using equation (6), and introducing the gradient of the atmospheric scale height

$$\beta\equiv dH/dz, \tag{7}$$

we find that the general equation (4) leads to

$$\frac{1}{p}\frac{dp}{dz}=-\frac{1}{H}, \tag{8}$$

and

$$\frac{1}{\rho}\frac{d\rho}{dz}=-\frac{1+\beta}{H}. \tag{9}$$

Thus, from equations (2) and (9), the relation between the local atmospheric scale height H and the density parameter H_ρ is

$$H=(1+\beta)H_\rho. \tag{10}$$

The values of H_ρ, which are deduced from the slope of the density-versus-altitude curve, cannot represent real atmospheric conditions. The use of H_ρ may lead to wrong conclusions about the structure of the thermosphere, especially where the gradient of the atmospheric scale height is large.

If the height interval is small enough, β can be assumed constant for calculation purposes. If equations (8) and (9) are written in the form

$$\frac{dp}{p}=-\frac{1}{\beta}\frac{dH}{H}, \tag{11}$$

and

$$\frac{d\rho g}{\rho g}=-\frac{1+\beta}{\beta}\frac{dH}{H}, \tag{12}$$

the integration with β=constant leads to

$$\frac{p}{p_0}=\left(\frac{H}{H_0}\right)^{-1/\beta}, \tag{13}$$

and

$$\frac{\rho g}{\rho_0 g_0}=\left(\frac{H}{H_0}\right)^{-(1+\beta)/\beta}. \tag{14}$$

The expansion of equations (13) and (14) gives

$$\frac{p}{p_0}=\exp\left\{-\frac{z}{\frac{1}{2}(H+H_0)}\left[1+\frac{1}{3}\left(\frac{H-H_0}{H+H_0}\right)^2+\frac{1}{5}\left(\frac{H-H_0}{H+H_0}\right)^4+\ldots\right]\right\} \tag{15}$$

$$\frac{\rho g}{\rho_0 g_0}=\exp\left\{-\frac{(1+\beta)z}{\frac{1}{2}(H+H_0)}\left[1+\frac{1}{3}\left(\frac{H-H_0}{H+H_0}\right)^2+\frac{1}{5}\left(\frac{H-H_0}{H+H_0}\right)^4+\ldots\right]\right\} \tag{16}$$

The second term in brackets is less than 0.01 at $z=H_0$ if $\beta\leq 0.42$ and at $z=\frac{1}{2}H_0$ if $\beta\leq 0.84$. Neglecting terms less than 0.01 before unity, we can reduce equation (16) to

$$\frac{\rho g}{\rho_0 g_0}=\exp\left(-\frac{(1+\beta)z}{\frac{1}{2}(H+H_0)}\right), \tag{17}$$

which is sufficiently accurate when an analysis is made in a height interval less than one scale height.

With a constant gradient of the scale height, equation (10) leads to

$$\beta_\rho=\frac{\beta}{1+\beta}, \tag{18}$$

and equation (12) becomes

$$\frac{d\rho g}{\rho g}=-\frac{1}{\beta_\rho}\frac{dH_\rho}{H_\rho}. \tag{19}$$

If the same terms are neglected as were for expression (16), equation (19) becomes after integration,

$$\frac{\rho g}{\rho_0 g_0}=\exp\left(-\frac{z}{\frac{1}{2}(H_\rho+H_{0\rho})}\right). \tag{20}$$

Equation (15) must be compared with expressions (1) and (20). Since an analysis of the physical conditions of the heterosphere cannot be made without allowing for the effect of the gradient of the scale height, it is useful to have available a variety of atmospheric models for which computations have been carried out for combinations of the scale-height gradients associated with the variations of temperature and of mean molecular mass.

It will be noticed that the difference between the parameter of density H_ρ with its gradient β_ρ and the local atmospheric scale height H with its gradient β increases with increasing values of β.

Method of determining atmospheric models

Inspection of density values at 200 km obtained by calculation reveals that the scale-height gradient below 150 km plays the leading role in determining the density at higher altitudes (Nicolet, 1960b). In other words, if boundary conditions are assumed in the neighborhood of 120 km, the atmospheric density between 200 km and 250 km is fixed by the scale-height gradient between 120 km and 150 km but is not much affected by the values of the scale-

height gradient above 150 km. The net result is that the vertical distribution of density at high altitudes depends on the temperature at the level of the thermopause, and the variation of the scale-height gradient above the thermopause is due essentially to the decrease of molecular mass. Thus, the atmospheric conditions are defined by a diffusion distribution and related to the time of conduction (Nicolet, 1960c).

From an analysis using various boundary conditions and scale-height gradients, it appears that the temperature must be considered the most important parameter in deducing the vertical distribution of atmospheric density. Consequenlty, the vertical distribution of temperature is related to the conditions of heat conduction, and the heterosphere can be assumed to be in diffusion equilibrium. Average conditions lead, therefore, to consistent atmospheric models in which the temperature and its vertical gradient can be determined when diffusion equilibrium is assumed.

The diurnal variation of the density is represented by a change of the temperature and a variation of its vertical gradient. In the same way, the effects of solar activity can be interpreted by a variation of the ultraviolet radiation that affects the temperature gradient and leads to variations of the temperature of the isothermal layer. In fact, it should be possible to predict how the density must vary during a solar cycle when the boundary conditions are known.

Finally, the magnetic storm effects can also be included since Jacchia (1961) has shown that the atmospheric-drag perturbations during geomagnetic disturbances have a worldwide distribution. The interpretation must be that a general heating occurs, corresponding to an increase of the temperature at all latitudes.

It is certain that atmospheric conditions change in the E layer and involve a variation of temperature that is an important parameter to determine boundary conditions for atmospheric models of the heterosphere. We cannot present here all the possibilities, and average conditions have been adopted in order to lead to a density of the order of 4×10^{-12} gm/cm^3 at 200 km. It must be noticed that for the same gradient of temperature, a variation of $\pm50°$ K at 120 km leads to a variation of ±50 percent of the density at 200 km.

The average conditions adopted here are as follows:

Density	$\rho(120\text{ km})=3.5\times10^{-11}$ gm/cm^3
Temperature	$T(120\text{ km})=325°$ K
Concentration	$n(0)=7.6\times10^{10}$ oxygen atoms/cm^3
Concentration	$n(O_2)=1.2\times10^{11}$ oxygen molecules/cm^3
Concentration	$n(N_2)=5.8\times10^{11}$ nitrogen molecules/cm^3
Scale height	$H=10.37$ km

Atmospheric conditions from 150 km to 650 km

The vertical distribution of density between 120 km and 150 km is practically unaffected by the form of the variation with height of the scale-height gradient, and the density in the region of 150 to 160 km is almost a constant for the same boundary conditions at 120 km. The values of density to be expected at 150 km for temperatures varying from 877° K to 642° K are given in table 1. Such a range of temperatures corresponds to equal intervals of times ($t=0$, $t=10$) for a cooling by conduction of the whole heterosphere considered as a plane-parallel atmosphere subject to diffusion. The 12 models of table 1 correspond to the following temperatures at 150 km and their associated gradients between 150 km and 160 km:

Model no.	T(°K)	$\left(\frac{dT}{dz}\right)_{\text{km}}$
0	877	18
1	873	15
1.5	863	14
2	852	13
3	829	11
4	803	10
5	777	9
6	751	8
7	726	7
8	699	6
9	671	5
10	642	4

In tables 1 to 10, T refers to temperature in °K; H, the atmospheric scale height in km; β, the gradient of H for the height interval indicated in the table; $H\rho$, the density parameter deduced from formula (10); ρ, the density in gm/cm^3 with (–12) for 10^{-12}; p, the pressure in mm Hg with (–6) for 10^{-6}; M, the mean

molecular mass with the mass of atomic oxygen $M=16$; n, the total concentration in cm^{-3} with $(+10)$ for (10^{10}).

The essential character of the data of table 1 is that the parameters $H\rho$ and M are almost constant, while the atmospheric scale height and its gradient vary. The density is almost constant, $(2.5\pm0.1)\times10^{-12}$ gm/cm^3 for temperatures higher than 700°K. Below 700°K, boundary conditions at 120 km are affected.

Since $H\rho=(20\pm1)$ km for the whole range of temperatures, it is clear that density data deduced from satellite air-drag may lead to wrong conclusions about the atmospheric structure. For example, a constant scale height is sometimes deduced from an analysis of satellite data even though there is in fact a strong gradient of the atmospheric scale height. When an association was made between the apparent scale height and the temperature, the wrong conclusion was reached that the atmosphere was almost isothermal.

Consequently, table 1 reveals that the variation of the atmospheric scale height and its gradient can be very important, while other parameters, and particularly the density parameter $H\rho$, show no practical variation. Such a variation of the atmospheric scale height must lead to the variation of all physical parameters at higher altitudes.

TABLE 1.—*Physical parameters at 150 km*

No.	T	H	$\beta_{150\text{-}160}$	H_ρ	ρ	p	M	N
0	877	29.8	0.67	20.0	2.41(−12)	5.0(−6)	26.2	5.6(+10)
1	873	29.6	0.56	20.7	2.43	5.0	26.2	5.6
1.5	863	29.3	0.53	20.9	2.45	5.0	26.2	5.6
2	852	28.9	0.48	21.0	2.48	5.0	26.2	5.7
3	829	28.1	0.44	21.0	2.54	5.0	26.1	5.8
4	803	27.3	0.38	21.0	2.59	5.0	26.1	6.0
5	777	26.4	0.35	21.1	2.62	4.9	26.1	6.0
6	751	25.6	0.31	20.8	2.65	4.8	26.1	6.1
7	726	24.7	0.28	20.4	2.61	4.5	26.1	6.0
8	699	23.8	0.28	20.1	2.35	3.9	26.1	5.4
9	671	22.9	0.25	19.8	2.14	3.4	26.0	4.9
10	642	21.2	0.20	19.2	1.97(−12)	3.0(−6)	26.0	4.8(+10)

TABLE 2.—*Atmospheric conditions at 200 km*

No.	T	H	$\beta_{200\text{-}210}$	H_ρ	ρ	p	M	N
0	1540	56.0	0.32	42.7	4.07(−13)	1.6(−6)	24.8	9.9(+9)
1	1414	51.8	0.27	41.3	4.14	1.5	24.7	1.0(+10)
1.5	1358	49.6	0.25	40.1	4.17	1.4	24.7	1.0
2	1305	47.8	0.23	39.6	4.17	1.4	24.6	1.0
3	1210	44.3	0.20	38.1	4.16	1.3	24.5	1.0
4	1126	41.6	0.18	36.2	4.10	1.2	24.4	1.0(+10)
5	1051	39.0	0.15	34.5	3.98	1.1(−6)	24.3	9.9(+9)
6	985	36.8	0.13	32.0	3.84	9.8(−7)	24.1	9.6
7	925	34.8	0.13	31.3	3.59	8.6	24.0	9.0
8	867	32.8	0.12	30.4	3.03	6.9(−7)	23.8	7.7(+9)

TABLE 3.—*Atmospheric conditions at 240 km*

No.	T	H	$\beta_{240\text{-}260}$	H_ρ	ρ	p	M	N
0	1791	68.4	0.25	58.8	1.77(−13)	8.3(−7)	23.9	4.5(+9)
1	1613	62.2	0.21	54.2	1.72	7.3	23.7	4.4
1.5	1532	59.3	0.19	52.3	1.70	6.9	23.6	4.3
2	1458	56.7	0.18	49.7	1.66	6.4	23.5	4.2
3	1327	52.0	0.16	49.0	1.58	5.6	23.3	4.1
4	1215	48.2	0.14	44.2	1.47	4.8	23.0	3.8
5	1120	44.9	0.13	41.8	1.35	4.2	22.8	3.6
6	1037	42.1	0.12	39.4	1.23	3.5	22.5	3.3
7	965	39.7	0.11	37.0	1.09(−13)	2.9	22.2	2.9
8	896	37.4	0.10	35.1	8.64(−14)	2.2(−7)	21.9	2.4(+9)

At 200 km (see table 2), the gradient of the atmospheric scale height is about 50 percent of its value at 150 km; even for a range of 500° K in the temperature, the density remains practically constant; $\rho=(4.1\pm0.1)\times10^{-13}$ gm/cm^3 for $1050°\,K\leq T\leq1550°\,K$. This shows again how important are the boundary conditions that are chosen in the E layer; what is needed is a very small gradient to reduce the 200-km density by an appreciable percentage. However, the variation is more apparent in the pressure, which decreases with decreasing temperature.

Between 250 km and 650 km, the gradient of the atmospheric scale height is generally between $\beta=0.2$ and 0.1, as can be seen from an inspection of the figures in tables 3 to 8. Since the gradient is relatively small, the difference between the atmospheric scale height H and the density parameter $H\rho$ becomes less important, i.e., 20 percent to 10 percent. Nevertheless, the effect of small values of β between 0.1 and 0.2 cannot be neglected since it corresponds to the decrease of the molecular mass in the isothermal layer.

Inspection of figures of physical parameters from 200 km to 650 km shows how their amplitude increases with altitude. For example, at 400 km (see table 6), the density varies by a factor of 10, and the pressure by a factor of 20, and the mean molecular mass decreases from $M=20.6$ to $M=16.6$ when the

TABLE 4.—*Atmospheric conditions at 300 km*

No.	T	H	$\beta_{300-320}$	H_ρ	ρ	p	M	N
0	1975	81.3	0.18	73.7	6.86(−14)	3.7(−7)	22.6	1.8(+9)
1	1752	73.3	0.16	65.9	6.15	3.0	22.2	1.7
1.5	1650	69.6	0.15	63.3	5.80	2.7	22.0	1.6
2	1556	66.3	0.14	60.6	5.44	2.4	21.8	1.5
3	1393	60.5	0.12	55.5	4.76	1.9	21.4	1.3
4	1261	55.8	0.12	51.7	4.08	1.5	21.0	1.2
5	1150	52.0	0.11	48.8	3.45	1.2(−7)	20.4	1.0(+9)
6	1057	48.7	0.10	46.1	2.89	9.4(−8)	20.2	8.6(+8)
7	978–I(*)	46.0	0.10	43.3	2.35	7.2	19.8	7.2
8	903–I	43.3	0.09	41.0	1.71(−14)	5.0(−8)	19.4	5.3(+8)

*The symbol *I* means the temperature at the thermopause.

TABLE 5.—*Atmospheric conditions at 340 km*

No.	T	H	$\beta_{340-360}$	H_ρ	ρ	p	M	N
0	2036	88.0	0.16	80.0	4.00(−14)	2.3(−7)	21.8	1.1(+9)
1	1796	79.4	0.14	72.4	3.40	1.8	21.3	9.6(+8)
1.5	1683	75.3	0.13	68.6	3.13	1.6	21.0	8.9
2	1583	71.6	0.12	65.8	2.86	1.4	20.8	8.3
3	1408	65.2	0.12	61.0	2.36	1.0(−7)	20.3	7.0
4	1271	60.3	0.11	57.2	1.92	7.7(−8)	19.8	5.8
5	1155–I	56.1	0.10	53.6	1.54	5.7	19.4	4.8
6	1059–I	52.6	0.09	49.8	1.23(−14)	4.3	18.9	3.9
7	978–I	49.7	0.08	47.3	9.55(−15)	3.1	18.3	3.1
8	903–I	46.8	0.09	44.8	6.61(−15)	2.0(−8)	18.1	2.2

TABLE 6.—*Atmospheric conditions at 400 km*

No.	T	H	$\beta_{400-420}$	H_ρ	ρ	p	M	N
0	2086	96.9	0.14	41.2	1.93(−14)	1.2(−7)	20.6	5.6(+8)
1	1826	87.3	0.13	82.3	1.53	8.7(−8)	20.0	4.6
1.5	1707	82.8	0.12	74.6	1.36	7.3	19.7	4.1
2	1597	78.6	0.11	73.6	1.19	6.1	19.4	3.7
3	1412–I	71.6	0.10	67.7	9.11(−15)	4.2	18.9	2.9
4	1272–I	66.2	0.09	62.7	6.89	3.0	18.4	2.2
5	1155–I	61.5	0.08	59.2	5.16	2.1	18.0	1.7
6	1059–I	57.6	0.07	55.4	3.86	1.4(−8)	17.6	1.3(+8)
7	978–I	54.2	0.08	52.6	2.81	9.9(−9)	17.3	9.8(+7)
8	903–I	52.1	0.09	50.4	1.82(−15)	6.0(−9)	16.6	6.4(+7)

temperature range is between 2100°K and 900° K, corresponding to a variation of H from 97 km to 52 km. Such a general result shows that an arbitrary choice of the mean molecular mass cannot be made as it was for the COSPAR International Reference Atmosphere (1961). It is unwise to attempt to specify atmospheric conditions with an arbitrary molecular mass, since it may lead to inconsistent information relative to the thermal or diffusive equilibrium of the upper atmosphere. Wrong conclusions indicating a decrease of temperature between 400 km and 500 km, such as obtained by Lundback (1961), reveal that the analysis of observational data is not correct since the atmosphere at these altitudes is at least isothermal. It should also be borne in mind that diffusion must adapt the molecular weight mg to the temperature conditions prevailing in the isothermal region, and there is no reason, therefore, to expect some sharp decrease of molecular mass at a particular altitude.

When the molecular mass is more than 14, the gas is presumed to consist essentially of nitrogen and oxygen, and it should be remembered that molecular nitrogen behaves almost in the same way, both for mixing and for diffusion conditions. Its mass $M=28$ does not differ very much from the mean molecular mass of the air, $M=29$. Thus, the vertical distribution of molecular nitrogen is closely related to the vertical distribution of tempera-

TABLE 7.—*Atmospheric conditions at 520 km*

No.	T	H	$\beta_{520-540}$	H_ρ	ρ	p	M	N
0	2123	113.4	0.13	104.0	5.45(−15)	3.9(−8)	18.6	1.8(+8)
1	1837–I	101.6	0.12	95.2	3.85	2.15	17.9	1.3
1.5	1711–I	96.4	0.11	90.9	3.19	1.9	17.6	1.1(+8)
2	1598–I	91.6	0.10	86.5	2.62	1.5(−8)	17.3	9.1(+7)
3	1412–I	83.6	0.09	79.4	1.75	9.2(−9)	16.8	6.3
4	1272–I	77.6	0.08	74.1	1.17(−15)	5.7	16.3	4.3
5	1155–I	72.3	0.09	68.6	7.76(−16)	3.5	15.8	3.0
6	1059–I	68.1	0.10	64.2	5.15	2.2	15.4	2.0
7	978–I	65.0	0.11	60.6	3.35	1.4(−9)	14.9	1.4(+7)
8	903–I	63.6	0.15	58.0	1.92(−16)	7.7(−10)	14.1	8.2(+6)

TABLE 8.—*Atmospheric conditions at 560 km*

No.	T	H	$\beta_{560-580}$	H_ρ	ρ	p	M	N
0	2128	118.3	0.12	104.2	3.72(−15)	2.7(−8)	18.0	1.2(+8)
1	1837–I	105.9	0.11	100.2	2.54	1.7	17.4	8.8(+7)
1.5	1711–I	100.4	0.10	95.2	2.06	1.3(−8)	17.1	7.3
2	1598–I	95.4	0.10	90.1	1.66	9.8(−9)	16.8	5.9
3	1412–I	87.1	0.09	83.3	1.06(−15)	5.7	16.3	3.9
4	1272–I	80.9	0.10	76.9	6.85(−16)	3.4	15.8	2.6
5	1155–I	75.8	0.10	70.9	4.36	2.0	15.3	1.7
6	1059–I	72.0	0.12	66.7	2.78	1.2(−9)	14.8	1.1(+7)
7	978–I	69.7	0.16	63.5	1.74(−16)	7.6(−10)	14.1	7.4(+6)
8	903–I	70.2	0.22	60.4	9.65(−17)	4.2(−10)	12.9	4.5(+6)

TABLE 9.—*Atmospheric conditions at 650 km*

No.	T	H	$\beta_{650-700}$	H_ρ	ρ	p	M	N
0	2131–I	128.8	0.10	124.2	1.66(−15)	1.3(−8)	17.1	5.9(+7)
1	1837–I	114.8	0.10	109.9	1.07(−15)	7.4(−9)	16.5	3.9
1.5	1711–I	109.0	0.10	104.8	8.25(−16)	5.4	16.2	3.1
2	1598–I	103.8	0.10	99.3	6.32	4.0	15.9	2.4
3	1412–I	95.5	0.11	90.6	3.70	2.1	15.2	1.5(+7)
4	1272–I	90.1	0.12	84.3	2.19	1.2(−9)	14.6	9.1(+6)
5	1155–I	86.8	0.19	78.2	1.28(−16)	6.7(−10)	13.7	5.6
6	1059–I	86.0	0.26	74.5	7.55(−17)	3.9	12.7	3.6
7	978–I	88.3	0.36	72.6	4.42	2.4	11.4	2.3
8	903–I	97.6	0.70	74.9	2.36	1.4(−10)	9.5	1.5(+6)

ture in the homosphere and heterosphere. Its concentration at 400 km varies according to temperature conditions defined by table 6 from 2×10^8 molecules/cm^3 to 5×10^6 molecules/cm^3, i.e., a factor of the order of 40 when its concentration at 150 km remains constant,

TABLE 10.—*Atmospheric conditions at 900 km*

No.	T	H	$\beta_{900-1000}$	H_ρ	ρ	p	M	N
0	2133–I	156.5	0.14	147.6	2.52(−16)	2.2(−9)	15.1	1.0(+7)
1	1837–I	144.2	0.20	133.0	1.29	1.0(−9)	14.1	5.5(+6)
1.5	1711–I	140.8	0.24	126.9	8.86(−17)	7.0(−10)	13.4	4.0
2	1598–I	140.1	0.30	122.5	6.06	4.8	12.6	2.9
3	1412–I	145.3	0.44	118.6	2.88	2.4	10.7	1.6
4	1272–I	159.6	0.58	122.8	1.47(−17)	1.3(−10)	8.8	1.0(+6)
5	1155–I	180.6	0.61	135.0	7.93(−18)	8.1(−11)	7.1	6.8(+5)
6	1059–I	201.2	0.53	154.8	4.73	5.4	5.8	4.9
7	978–I	216.6	0.39	179.2	3.11	3.8	5.0	3.8
8	903–I	224.9	0.23	205.3	2.18(−18)	2.8(−11)	4.4	3.0(+5)

TABLE 11.—*Atmospheric data between 1000 km and 2000 km*

No.	T	z	H	ρ(total)	ρ(He)	p	M	N(total)	N(He)
0	2133	1000	171	1.28(−16)	6.2(−18)	1.2(−9)	14.2	5.4(+6)	9.3(+5)
		1250	232	2.82(−17)	4.1(−18)	3.4(−10)	11.2	1.5(+6)	6.2(+5)
		1500	352	8.20(−18)	2.8(−18)	1.4(−10)	7.9	6.3(+5)	4.3(+5)
		2000	666	1.79(−18)	1.4(−18)	5.1(−11)	4.2	2.3(+5)	2.1(+5)
1	1837	1000	164	6.08(−17)	5.3(−18)	5.5(−10)	12.7	2.9(+6)	8.0(+5)
		1250	257	1.19(−17)	3.4(−18)	1.6(−10)	8.7	8.3(+5)	5.0(+5)
		1500	412	3.68(−18)	2.2(−18)	7.3(−11)	5.8	3.8(+5)	3.3(+5)
		2000	642	1.05(−18)	9.9(−19)	2.9(−11)	4.2	1.5(+5)	1.5(+5)
1.5	1711	1000	165	4.03(−17)	4.8(−18)	3.6(−10)	11.8	2.0(+6)	7.3(+5)
		1250	278	7.73(−18)	2.9(−18)	1.1(−10)	7.5	6.2(+5)	4.4(+5)
		1500	434	2.59(−18)	1.9(−18)	5.4(−11)	5.1	3.0(+5)	2.8(+5)
		2000	612	8.14(−19)	7.9(−19)	2.1(−11)	4.1	1.2(+5)	1.2(+5)
2	1598	1000	170	2.68(−17)	4.5(−18)	2.5(−10)	10.7	1.5(+6)	6.7(+5)
		1250	303	5.24(−18)	2.6(−18)	8.1(−11)	6.4	4.9(+5)	3.9(+5)
		1500	446	1.94(−18)	1.6(−18)	4.2(−11)	4.6	2.5(+5)	2.4(+5)
		2000	579	6.49(−19)	6.4(−19)	1.6(−11)	4.0	9.7(+4)	9.6(+4)
3	1412	1000	189	1.24(−17)	3.7(−18)	1.3(−10)	8.5	8.8(+5)	5.5(+5)
		1250	339	2.79(−18)	2.0(−18)	4.8(−11)	5.1	3.3(+5)	3.0(+5)
		1500	435	1.22(−18)	1.1(−18)	2.6(−11)	4.2	1.8(+5)	1.7(+5)
		2000	516	4.10(−19)	4.1(−19)	9.0(−12)	4.0	6.1(+4)	6.1(+4)
4	1273	1000	216	6.51(−18)	3.0(−18)	7.7(−11)	6.7	5.9(+5)	4.6(+5)
		1250	347	1.79(−18)	1.6(−18)	3.2(−11)	4.4	2.4(+5)	2.3(+5)
		1500	405	8.48(−19)	8.2(−19)	1.6(−11)	4.1	1.2(+5)	1.2(+5)
		2000	466	2.64(−19)	2.6(−19)	5.2(−12)	4.0	4.0(+4)	4.0(+5)
5	1155	1000	241	3.78(−18)	2.5(−18)	5.0(−11)	5.4	4.2(+5)	3.7(+5)
		1250	336	1.24(−18)	1.2(−18)	2.1(−11)	4.2	1.8(+5)	1.8(+5)
		1500	371	5.93(−19)	5.9(−19)	1.1(−11)	4.0	8.9(+4)	8.9(+4)
		2000	423	1.67(−19)	1.7(−19)	3.0(−12)	4.0	2.5(+4)	2.5(+4)
6	1059	1000	254	2.48(−18)	2.0(−18)	3.5(−11)	4.7	3.2(+5)	3.0(+5)
		1250	316	9.04(−19)	8.8(−19)	1.5(−11)	4.1	1.3(+5)	1.3(+5)
		1500	342	4.17(−19)	4.2(−19)	6.8(−12)	4.0	6.2(+4)	6.2(+4)
		2000	387	1.05(−19)	1.1(−19)	1.7(−12)	4.0	1.6(+4)	1.6(+4)
7	978	1000	255	1.78(−18)	1.6(−18)	2.5(−11)	4.4	2.5(+5)	2.4(+5)
		1250	294	6.71(−19)	6.7(−19)	1.0(−11)	4.0	1.0(+5)	1.0(+5)
		1500	316	2.94(−19)	2.9(−19)	4.5(−12)	4.0	4.4(+4)	4.4(+4)
		2000	358	6.65(−20)	6.7(−20)	1.0(−12)	4.0	1.0(+4)	1.0(+4)
8	903	1000	247	1.34(−18)	1.3(−18)	1.8(−11)	4.1	1.9(+5)	1.9(+5)
		1250	273	4.99(−19)	5.0(−19)	7.0(−12)	4.0	7.5(+4)	7.5(+4)
		1500	292	2.06(−19)	2.1(−19)	2.9(−12)	4.0	3.1(+4)	3.1(+4)
		2000	330	4.11(−20)	4.1(−20)	5.8(−13)	4.0	6.2(+3)	6.2(+4)

namely 4×10^{10} molecules/cm^3. Such a large variation affects the mean molecular mass since the corresponding variation in density is the order of a factor of 10.

Presence of helium

It should be noticed from the figures of tables 7 and 8 that the mean molecular mass becomes less than $M=16$. This is due to the introduction of helium. Diffusion leads to an important concentration of helium atoms at the upper levels (Nicolet, 1961a). Physical conditions such as that represented by the already analyzed models lead to an almost constant value of n(He) at 500 km. The values of helium concentration do not vary by more than ±30 percent from an average value for temperatures between 2100° K and 750° K. The absolute value is, however, related to the level of the beginning of diffusion.

Starting from the normal mixing ratio $n(\mathrm{He})/n(\mathrm{N_2})$, the concentration of atomic helium at 105 km is

$$n(\mathrm{He})_{105\mathrm{km}}=3.0\times10^7 \text{ atoms/cm}^3. \quad (21)$$

If diffusion begins at that level, the concentration at 500 km is

$$n(\mathrm{He})_{500\mathrm{km}}=(1.8\pm0.5)\times10^6 \text{ atoms/cm}^3, \quad (22)$$

when the temperature at 500 km varies from 2133° K (model no. 0) to 733° K (model no. 10). If, instead of beginning at 105 km, the diffusion starts at 110 km or 115 km, the concentration given by equation (22) must be decreased by a factor of 2 or 4. A difference of about 5 km of the altitude of the diffusion level corresponds to a difference of a factor of 2 in the concentration of helium.

In the present calculation, we have adopted 105 km as the level where diffusion of helium begins; a correction is easily introduced if diffusion is considered to start at other altitudes.

Table 9, which gives the atmospheric conditions at 650 km, shows how the effect of helium may be important at such altitudes when the temperature is sufficiently low. For example, if $T\leq1000°$ K, corresponding to nighttime conditions at the beginning of 1961,

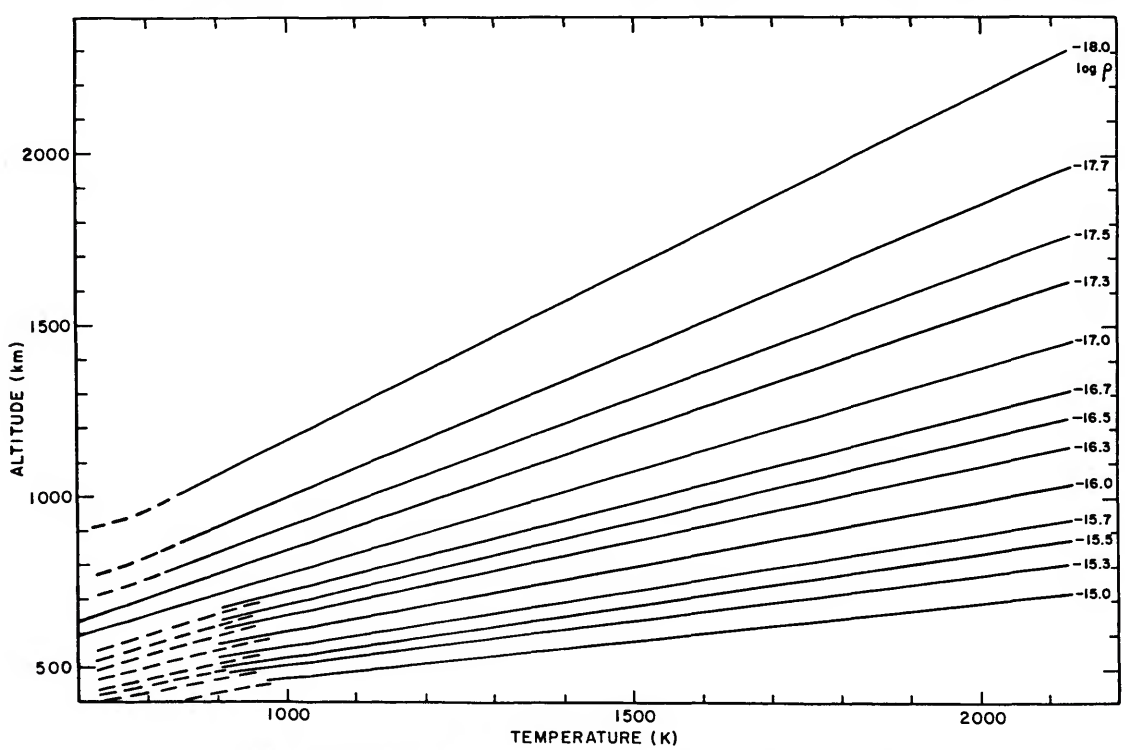

FIGURE 1.—Altitudes of surfaces of equal density as a function of the temperature.

the total density decreases to less than 5×10^{-17} gm/cm^3, while the density of helium reaches about 5×10^{-18} gm/cm^3. The presence of helium leads to a molecular mass less than 12. The effect of helium has also an important consequence. The atmospheric scale height never decreases below 85 km even if the temperature at 650 km varies by about 1000° K.

The effect of helium is particularly apparent at 900 km, where there is a large variation of the mean molecular mass (see table 10). The mean molecular mass, which is still of the order of 15 near 2000° K, may reach such a low value as 5 for temperatures less than 1000° K.

Since the perigee heights of Satellite 1960 ι 1 (Echo I) are in the range of 900 to 1600 km, a set of atmospheric data is given in table 11 for altitudes between 1000 km and 2000 km. The density and concentration of helium are included in the table to allow a comparison with the total density and concentration. A change in the level of diffusion of helium can easily be introduced by an adequate correction.

From an analysis of data on the orbit of Echo I, Zadunaisky, Shapiro and Jones (1961) and Römer (1961) have deduced densities that cannot be explained by an atomic oxygen atmosphere or atomic hydrogen atmosphere, but are in accordance with an effect of helium.

An atomic mass $M=16$ would require a temperature too high to fit observational data between 500 km and 700 km. An effect of atomic hydrogen on the mean molecular mass would lead to too high concentrations. The atmospheric-drag perturbations as observed by Jacchia (1961) during geomagnetic disturbances show that the drag of the neutral constituents of the atmosphere has still the most important effect even at altitudes above 1000 km. The figures of table 11 show how helium can be introduced in the analysis of Zadunaisky, Shapiro and Jones (1961) with scale heights greater than 300 km at 1500 km, and then 150 km at 900 km. The presence of helium is unavoidable above 1000 km.

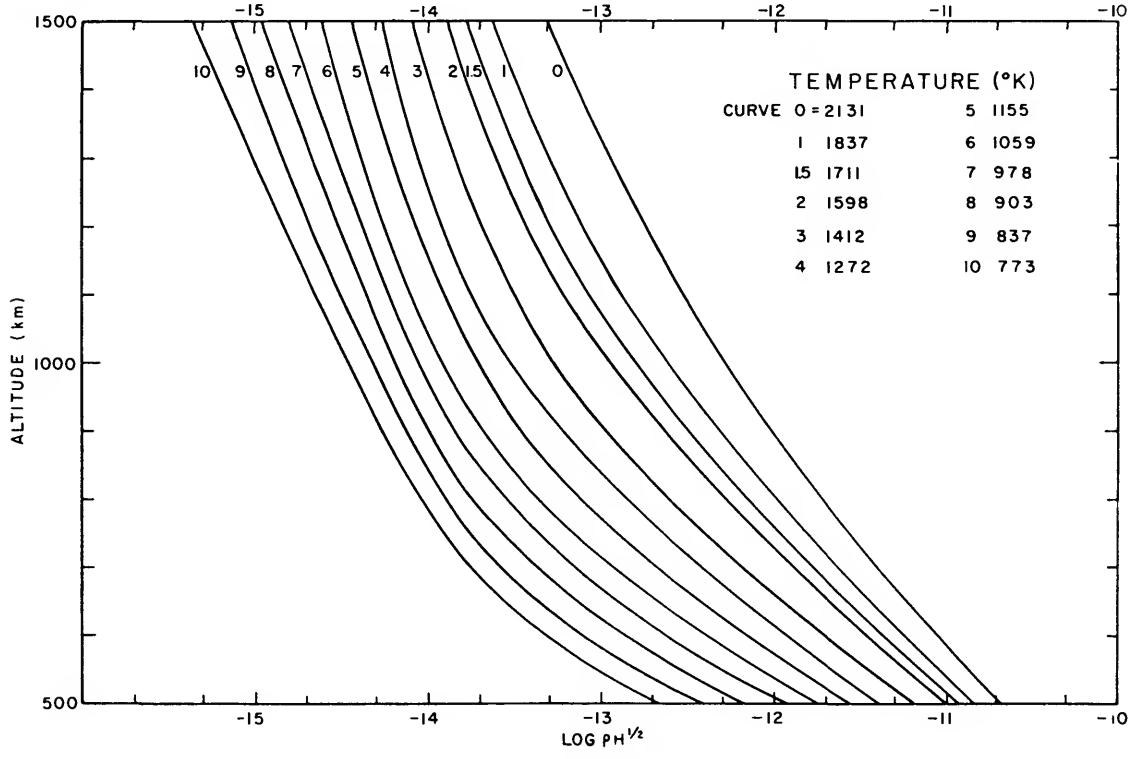

FIGURE 2.—Vertical distribution of log $\rho H^{1/2}$ as a function of temperature.

General tables of ρ, $\rho H^{1/2}$, and H

Table 12 summarizes the vertical distribution of density deduced according to the physical conditions described in the preceding sections and, therefore, the results obtained for the various models already analyzed by their various parameters in tables 1 to 11. It can be noticed that the levels of constant density increase regularly with increasing temperature. A picture of constant density levels between 500 km and 2000 km is provided in figure 1. There is a linear relation between the altitude and the temperature, and the various slopes for curves of constant density show the increasing effect of the temperature when the absolute value of the density decreases. Such relations between temperature and variation of density with height must be related to the diurnal bulge described by Jacchia (1960a) and must be also associated with the results of his (1961) accurate analysis of the atmospheric-drag perturbations.

From comparison of the density data of table 12 with published data on densities deduced from satellite air-drag, a picture of the temperature variation during the years 1958 to 1961 can be provided (Nicolet, 1961b). The maximum density obtained in October 1958 corresponds to a temperature between 2000° and 2100° K, while the average value from September 1958 to January 1959 may correspond to a temperature between 1700° and 1800° K. The two density distributions given by Martin *et al.* (1961) correspond to about 1750° K and 1150° K. As far as the density distributions given by King-Hele and Walker (1961) are concerned, they represent average conditions showing the variation from 1958 to 1960, namely 1750° K to 1350° K for late-1958 and late-1960 daytime values, and 1050° K to 950° K for late-1959 and late-1960 nighttime values. Even if a systematic error is involved in such a determination, the variation of the temperature shows the general trend of the diurnal variation and the solar activity effect (Nicolet, 1960c).

In order to make available a consistent table of parameters more closely associated with data deduced from satellite observations, table 13 gives the values of $\rho H^{1/2}$ and H from 150 to 2000 km. The value of $H^{1/2}$ is not subject to variation at 150 km for a range of temperatures of about 125° K with defined boundary conditions at 120 km, and a small variation is apparent near 200 km. The maximum variation occurs in the region of 600 to 700 km. At 1000 km (see fig. 2), the variation for $750 \leq T \leq 1850$° K corresponds to the variation obtained at 500 km. It should be noticed that $\rho H^{1/2}$ and H do not necessarily vary in the same way, and, therefore, ρ and $\rho H^{1/2}$ may have different variations in the region where different constituents are involved.

TABLE 12.—*Computed atmospheric densities*

Height z (km)	Model number and temperature											
	No. 0 T_∞ 2133° K	1 1837	1.5 1711	2 1598	3 1412	4 1272	5 1155	6 1059	7 978	8 903	9 837	10 773
150	−11.618	−11.614	−11.611	−11.606	−11.595	−11.587	−11.582	−11.577	−11.583	−11.629	−11.690	−11.706
160	−11.836	−11.824	−11.818	−11.813	−11.801	−11.793	−11.788	−11.785	−11.796	−11.845	−11.889	−11.932
170	−12.009	−11.996	−11.987	−11.983	−11.971	−11.967	−11.967	−11.967	−11.979	−12.033	−12.086	−12.134
180	−12.154	−12.139	−12.134	−12.130	−12.123	−12.120	−12.123	−12.128	−12.146	−12.206	−12.205	−12.322
190	−12.280	−12.268	−12.264	−12.261	−12.257	−12.259	−12.266	−12.277	−12.301	−12.367	−12.433	−12.498
200	−12.390	−12.383	−12.380	−12.380	−12.381	−12.387	−12.400	−12.416	−12.445	−12.519	−12.592	−12.666
210	−12.492	−12.488	−12.488	−12.490	−12.495	−12.507	−12.526	−12.548	−12.583	−12.662	−12.745	−12.824
220	−12.583	−12.585	−12.588	−12.592	−12.602	−12.622	−12.644	−12.674	−12.714	−12.801	−12.889	−12.979
240	−12.752	−12.765	−12.770	−12.780	−12.801	−12.833	−12.870	−12.910	−12.963	−13.064	−13.168	−13.274
260	−12.900	−12.925	−12.900	−12.955	−12.987	−13.029	−13.078	−13.131	−13.197	−13.311	−13.430	−13.550
280	−13.036	−13.072	−13.096	−13.113	−13.159	−13.214	−13.275	−13.340	−13.419	−13.545	−13.676	−13.810
300	−13.164	−13.211	−13.237	−13.264	−13.322	−13.389	−13.462	−13.539	−13.629	−13.767	−13.910	−14.057
320	−13.284	−13.343	−13.374	−13.408	−13.479	−13.558	−13.640	−13.728	−13.830	−13.979	−14.133	−14.292
340	−13.298	−13.469	−13.505	−13.544	−13.627	−13.717	−13.813	−13.910	−14.020	−14.180	−14.345	−14.514
360	−13.507	−13.588	−13.631	−13.676	−13.770	−13.873	−13.975	−14.085	−14.203	−14.374	−14.548	−14.728
380	−13.613	−13.703	−13.752	−13.801	−13.907	−14.020	−14.134	−14.252	−14.381	−14.561	−14.745	−14.936
400	−13.714	−13.815	−13.867	−13.925	−14.041	−14.162	−14.287	−14.413	−14.551	−14.740	−14.936	−15.138
420	−13.810	−13.921	−13.983	−14.042	−14.169	−14.300	−14.434	−14.570	−14.717	−14.910	−15.111	−15.322
440	−13.907	−14.026	−14.090	−14.157	−14.294	−14.434	−14.578	−14.724	−14.876	−15.079	−15.289	−15.511
460	−14.000	−14.127	−14.196	−14.268	−14.416	−14.564	−14.717	−14.870	−15.034	−15.244	−15.462	−15.695
480	−14.089	−14.266	−14.299	−14.376	−14.533	−14.690	−14.854	−15.016	−15.188	−15.405	−15.635	−15.873
500	−14.178	−14.321	−14.398	−14.480	−14.646	−14.813	−14.983	−15.151	−15.330	−15.552	−15.799	−16.047
520	−14.264	−14.415	−14.496	−14.582	−14.757	−14.932	−15.110	−15.290	−15.475	−15.717	−15.959	−16.215
540	−14.347	−14.506	−14.592	−14.682	−14.867	−15.049	−15.237	−15.423	−15.618	−15.867	−16.118	−16.377
560	−14.430	−14.595	−14.686	−14.780	−14.975	−15.164	−15.361	−15.556	−15.760	−16.016	−16.270	−16.532
580	−14.513	−14.682	−14.777	−14.876	−15.079	−15.277	−15.483	−15.686	−15.896	−16.159	−16.418	−16.678
600	−14.592	−14.765	−14.867	−14.971	−15.182	−15.388	−15.602	−15.813	−16.032	−16.299	−16.559	−16.815
650	−14.780	−14.971	−15.084	−15.199	−15.432	−15.660	−15.893	−16.122	−16.355	−16.627	−16.879	−17.113
700	−14.955	−15.168	−15.291	−15.418	−15.672	−15.917	−16.170	−16.413	−16.654	−16.917	−17.148	−17.347
750	−15.126	−15.358	−15.492	−15.629	−15.903	−16.166	−16.433	−16.684	−16.921	−17.165	−17.363	−17.401
800	−15.289	−15.541	−15.684	−15.833	−16.126	−16.403	−16.678	−16.928	−17.154	−17.367	−17.532	−17.674
850	−15.446	−15.719	−15.873	−16.029	−16.338	−16.625	−16.900	−17.143	−17.348	−17.529	−17.670	−17.796
900	−15.599	−15.889	−16.053	−16.218	−16.541	−16.833	−17.101	−17.325	−17.507	−17.662	−17.788	−17.910
1000	−15.893	−16.216	−16.395	−16.572	−16.907	−17.186	−17.423	−17.606	−17.750	−17.873	−17.991	−18.119
1250	−16.550	−16.925	−17.112	−17.281	−17.554	−17.747	−17.889	−18.044	−18.173	−18.302	−18.441	−18.600
1500	−17.086	−17.434	−17.587	−17.712	−17.914	−18.072	−18.227	−18.380	−18.532	−18.686	−18.854	−19.048
2000	−17.747	−17.979	−18.089	−18.188	−18.387	−18.578	−18.777	−18.979	−19.177	−19.386	−19.609	−19.867

TABLE 13.—*Values for log* $\rho H^{1/3}$ *and* H

z (km)	Model number and temperature											
	No. 0 $T_7$2133° K	1 1837	1.5 1711	2 1598	3 1412	4 1272	5 1155	6 1059	7 978	8 943	9 837	10 773
150	−8.38	−8.38	−8.38	−8.38	−8.38	−8.37	−8.37	−8.38	−8.39	−8.44	−8.49	−8.54
	29.8	29.6	29.3	28.9	28.1	27.3	26.4	25.6	24.7	23.8	22.9	21.3
160	−8.55	−8.55	−8.55	−8.55	−8.55	−8.55	−8.55	−8.55	−8.57	−8.64	−8.70	−8.74
	36.5	35.2	34.6	33.8	32.5	31.1	29.9	28.7	27.5	26.3	25.1	23.9
170	−8.70	−8.70	−8.70	−8.70	−8.70	−8.70	−8.70	−8.72	−8.74	−8.80	−8.89	−8.92
	42.4	40.1	39.1	38.1	36.2	34.4	32.7	31.2	29.8	28.4	26.9	25.5
180	−8.82	−8.82	−8.82	−8.82	−8.82	−8.82	−8.85	−8.85	−8.89	−8.96	−9.04	−9.11
	47.4	44.4	43.0	41.7	39.3	37.1	35.1	33.3	31.7	30.1	28.4	26.8
190	−8.92	−8.92	−8.92	−8.92	−8.46	−8.46	−9.00	−9.00	−9.04	−9.12	−9.19	−9.28
	52.0	48.2	46.5	44.9	42.0	39.5	37.2	35.2	33.3	31.5	29.7	28.0
200	−9.02	−9.03	−9.03	−9.04	−9.06	−9.08	−9.10	−9.13	−9.17	−9.26	−9.35	−9.43
	56.0	51.6	49.6	47.8	44.5	41.6	39.0	36.8	34.8	32.8	30.9	29.1
210	−9.10	−9.12	−9.13	−9.14	−9.16	−9.19	−9.22	−9.26	−9.30	−9.40	−9.49	−9.59
	59.6	54.6	52.4	50.3	46.6	43.4	40.7	38.3	36.1	34.0	32.1	30.2
220	−9.19	−9.21	−9.22	−9.23	−9.26	−9.29	−9.34	−9.38	−9.43	−9.52	−9.64	−9.74
	62.8	57.3	54.9	52.6	48.6	45.2	42.2	39.6	37.4	35.2	33.2	31.2
240	−9.34	−9.37	−9.39	−9.41	−9.44	−9.49	−9.54	−9.60	−9.66	−9.77	−9.89	−10.01
	68.4	62.1	59.3	56.7	52.0	48.2	44.9	42.1	39.7	37.4	35.2	33.2
260	−9.47	−9.51	−9.54	−9.57	−9.62	−9.68	−9.74	−9.80	−9.89	−10.01	−10.14	−10.28
	73.3	66.3	63.1	60.2	55.1	50.9	47.4	44.4	41.9	39.4	37.3	35.2
280	−9.59	−9.66	−9.68	−9.72	−9.77	−9.85	−9.92	−10.00	−10.10	−10.24	−10.38	−10.52
	77.5	70.0	66.5	63.4	57.9	53.4	49.7	46.6	44.0	41.4	39.2	37.0
300	−9.70	−9.77	−9.82	−9.85	−9.92	−10.02	−10.10	−10.19	−10.30	−10.44	−10.60	−10.77
	81.3	73.3	69.6	66.3	60.5	55.8	52.0	48.7	46.0	43.3	41.1	38.8
320	−9.82	−9.92	−9.96	−10.00	−10.08	−10.17	−10.28	−10.38	−10.49	−10.66	−10.82	−11.00
	84.8	76.4	72.6	69.0	62.9	58.1	54.1	50.7	47.9	45.2	42.8	40.4
340	−9.92	−10.02	−10.07	−10.12	−10.22	−10.33	−10.44	−10.55	−10.68	−10.85	−11.02	−11.21
	88.0	79.4	75.3	71.6	65.2	60.3	56.1	52.6	49.7	46.8	44.4	42.0
360	−10.03	−10.13	−10.19	−10.24	−10.36	−10.47	−10.60	−10.72	−10.85	−11.03	11.22	−11.41
	91.1	82.1	77.9	74.0	67.5	62.4	58.0	54.4	51.3	48.8	46.0	43.8
380	−10.12	−10.24	−10.30	−10.36	−10.48	−10.62	−10.74	−10.89	−11.02	−11.21	−11.41	−11.62
	94.1	84.8	80.4	76.4	69.6	64.4	59.8	56.1	52.8	50.6	48.0	45.7
400	−10.22	−10.35	−10.42	−10.48	−10.62	−10.74	−10.89	−11.04	−11.19	−11.39	−11.60	−11.82
	96.9	87.3	82.8	78.6	71.6	66.2	61.5	57.6	54.2	52.1	49.5	47.4
420	−10.31	−10.44	−10.52	−10.59	−10.74	−10.89	−11.04	−11.19	−11.35	−11.55	−11.74	−12.00
	99.6	89.7	85.1	80.0	73.5	68.0	63.1	59.0	55.7	53.9	51.5	49.3

440	−10.40	−10.55	−10.62	−10.70	−10.85	−11.01	−11.17	−11.34	−11.49	−11.70	−11.92	−12.16
	102	92.0	87.2	82.8	75.3	69.6	64.5	60.7	57.4	55.4	53.4	51.5
460	−10.49	−10.64	−10.72	−10.80	−10.96	−11.14	−11.31	−11.48	−11.66	−11.85	−12.09	−12.33
	105	94.3	89.3	84.7	77.3	71.1	66.6	62.5	59.2	57.1	55.2	54.0
480	−10.57	−10.74	−10.82	−10.92	−11.09	−11.26	−11.44	−11.62	−11.80	−12.02	−12.25	−12.49
	107	96.8	91.7	87.1	79.6	73.4	68.2	64.5	61.1	59.0	57.5	57.2
500	−10.66	−10.82	−10.92	−11.00	−11.19	−11.38	−11.55	−11.74	−11.92	−12.17	−12.41	−12.66
	111	99.5	94.4	89.7	81.8	75.9	70.6	66.4	63.2	61.1	60.4	61.3
520	−10.74	−10.92	−11.00	−11.10	−11.30	−11.49	−11.68	−11.89	−12.07	−12.32	−12.55	−12.80
	113	102	96.4	91.6	83.6	77.6	72.3	68.1	65.0	63.6	63.9	66.3
540	−10.82	−11.00	−11.10	−11.19	−11.40	−11.60	−11.80	−12.00	−12.21	−12.46	−12.70	−12.96
	116	104	98.4	93.6	85.4	79.2	74.0	70.0	67.2	66.7	68.2	72.5
560	−10.89	−11.08	−11.19	−11.29	−11.51	−11.72	−11.92	−12.18	−12.34	−12.59	−12.85	−13.08
	118	106	100	95.4	87.1	80.9	75.8	72.0	69.7	70.2	73.4	80.0
580	−10.96	−11.16	−11.28	−11.39	−11.60	−11.82	−12.04	−12.25	−12.47	−12.72	−12.96	−13.21
	121	108	102	97.3	88.8	82.7	77.8	74.3	72.8	74.6	79.8	88.8
600	−11.05	−11.24	−11.36	−11.47	−11.70	−11.92	−12.15	−12.37	−12.59	−12.85	−13.09	−13.32
	123	110	104	99.2	90.6	84.6	80.0	77.1	76.2	79.9	87.3	99.1
650	−11.22	−11.44	−11.57	−11.70	−11.96	−12.18	−12.42	−12.66	−12.89	−13.13	−13.36	−13.55
	129	115	109	104	95.5	90.1	86.8	86.0	88.3	97.6	111	128
700	−11.40	−11.64	−11.77	−11.89	−12.17	−12.42	−12.68	−12.92	−13.14	−13.38	−13.57	−13.74
	134	120	114	109	101	97.3	96.3	98.9	106	122	141	156
750	−11.55	−11.80	−11.96	−12.10	−12.39	−12.66	−12.92	−13.15	−13.37	−13.57	−13.74	−13.92
	139	125	119	114	108	107	110	117	130	152	170	179
800	−11.70	−12.00	−12.14	−12.29	−12.59	−12.85	−13.12	−13.36	−13.55	−13.74	−13.89	−14.03
	145	131	125	121	118	120	128	142	159	181	193	194
850	−11.85	−12.15	−12.31	−12.47	−12.80	−13.06	−13.31	−13.52	−13.70	−13.89	−14.01	−14.14
	150	137	132	130	130	137	152	171	189	206	210	203
900	−12.00	−12.31	−12.48	−12.64	−12.96	−13.23	−13.47	−13.68	−13.85	−14.00	−14.11	−14.25
	156	144	141	140	145	160	181	201	217	225	221	210
1000	−12.28	−12.62	−12.80	−12.96	−13.27	−13.52	−13.72	−13.92	−14.05	−14.18	−14.31	−14.44
	171	164	165	170	189	216	241	254	255	248	234	218
1250	−12.85	−13.22	−13.39	−13.54	−13.80	−14.00	−14.14	−14.29	−14.44	−14.59	−14.74	−14.92
	232	257	278	303	339	347	336	316	294	273	254	234
1500	−13.31	−13.62	−13.77	−13.89	−14.09	−14.27	−14.44	−14.62	−14.80	−14.96	−15.14	−15.35
	352	412	435	446	435	405	371	342	316	292	271	250
2000	−13.85	−13.08	−14.19	−14.31	−14.54	−14.74	−14.96	−15.18	−15.40	−15.62	−15.85	−16.14
	666	642	611	579	516	466	423	388	358	330	306	283

Effects of the Earth's Ionosphere on HF Radio Astronomy from Artificial Satellites

By M. D. Grossi, K. M. Strom, and S. E. Strom

Ground-based radio telescopes are known to be able to conduct reliable observations only within the band roughly defined by 10 mc/s and 10,000 mc/s. The lower limit is established by ionospheric refraction effects, and the upper limit by atmospheric behavior.

Airborne and balloon-borne radio telescopes can extend the upper limit above 10,000 mc/s with high-altitude observations. For the frequency band below 10 mc/s, a satellite-borne radio telescope appears a suitable means of observation.

Recent literature (Haddock, 1960) has pointed out the desirability and the feasibility of a satellite-borne HF [1] radio telescope orbiting outside the ionospheric layer of maximum electron density. Among others, the Harvard College Observatory is presently involved in the design of such a satellite (Space Radio Project). The satellite will be able to perform observations not affected by the limitations imposed by the ionosphere.

Many relevant experiments can be performed by such orbiting telescopes. Among these are (Haddock, 1960; Burke and Franklin, 1955; Davies, 1954; Piddington, 1951; Herbstreit and Johler, 1948): (a) measurement of integrated radio flux from our galaxy at frequencies below the F2 layer cutoff; (b) measurement of the dynamic spectra of solar bursts well below 30 mc/s; (c) measurement of the dynamic spectra of planetary radio bursts well below 30 mc/s.

General

The purpose of the present report is to present an analysis of some effects of the ionosphere on HF observations from satellite-borne radio telescopes. We deal primarily with a search for focusing effects of the ionosphere on incoming cosmic noise in the HF band. The analysis covers a variety of cases of interest for satellites in various orbital altitudes and with a wide range of observation frequencies.

In this preliminary analysis, we have considered the ionosphere to be a nonhomogeneous, nonisotropic, magnetoionic medium. The electron-density profile used in the calculations is illustrated in figure 1. We assume the earth's magnetic field to be dipole in nature. We have taken into account ionospheric irregularities and discontinuities only for cases in which these disturbances are much larger in size than are the wavelengths considered.

We compute the effects of the ionosphere on incoming radiation by employing a Hamiltonian optics approach. We discuss the necessary numerical procedures involved in the ray-tracing in relation to a program suitable for use in an IBM–7090 computer.

Rays are computed and plotted for sources located at infinity and for frequencies in the band 1–30 mc/s.

We basically consider refraction, reflection, and resultant focusing effects of the ionosphere for frequencies higher and lower than critical, and for satellites in conjunction and in opposition with respect to the source and the earth. In cases of special interest, we compute the equivalent aperture of the ionosphere, considering the ionosphere to be analogous at radio frequencies to a spherical shell lens, with the observing satellites located at the focal region.

[1] Considered as the frequency range 1–10 mc/s.

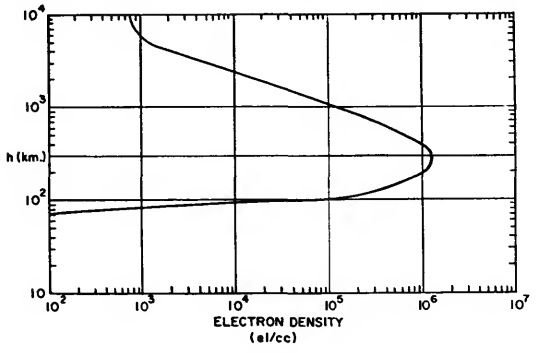

FIGURE 1.—Electron-density profile derived from averages of IGY data.

Hamiltonian ray-tracing in the earth's ionosphere

In this section, we consider plane waves incident on the ionosphere from a radio source effectively at infinity. We disregard the specific nature and position of the source, and the effect of the interplanetary medium.

The effect of absorption in the earth's ionosphere is not included in the equations as written, although the inclusion of this effect would involve the addition of only one equation to the system. It is reasonable to neglect absorption because the collision frequencies encountered in most cases considered here are extremely small. However, the Hamiltonian ray-tracing method is suitable for use in quite general cases of propagation in a magnetoionic medium.

The method of ray-tracing follows from the application of the principles of Hamiltonian optics. Mathematically, this ray-tracing problem reduces to solving simultaneously the following six differential equations (Haselgrove, 1955; Wong, 1960).

$$\dot{r}=\frac{1}{\mu^2}\left[y_1-\mu\frac{\partial\mu}{\partial y_1}\right]; \tag{1}$$

$$\dot{\theta}=\frac{1}{\mu^2 r}\left[y_2-\mu\frac{\partial\mu}{\partial y_2}\right]; \tag{2}$$

$$\dot{\Phi}=\frac{1}{\mu^2 r\sin\theta}\left[y_3-\mu\frac{\partial\mu}{\partial y_3}\right]; \tag{3}$$

$$\dot{y}=\frac{1}{\mu}\frac{\partial\mu}{\partial r}+\dot{\theta}y_2+\dot{\Phi}y_3\sin\theta; \tag{4}$$

$$\dot{y}_2=\frac{1}{r}\left[\frac{1}{\mu}\frac{\partial\mu}{\partial\theta}-\dot{r}y_2+\dot{\Phi}y_3 r\cos\theta\right]; \tag{5}$$

$$\dot{y}_3=\frac{1}{r\sin\theta}\left[\frac{1}{\mu}\frac{\partial\mu}{\partial\Phi}-\dot{r}y_3\sin\theta-\dot{\theta}y_3 r\cos\theta\right]. \tag{6}$$

These are the Hamiltonian equations for a ray path in a general magnetoionic medium. They are analogous to the Hamiltonian equations in classical mechanics. The ray is described in terms of the associated wave normal.

The quantities in equations (1) through (6) are defined as follows: r, θ, Φ are the spherical coordinates of a point in the earth's ionosphere; y_1, y_2, y_3 represent the components of the wave normal with respect to a Cartesian system whose origin is placed at r, θ, Φ. This system is illustrated in figure 2. The y_1 direction is along r; y_2 along θ; and y_3 along Φ. The system is chosen to be right-handed and orthogonal; $\dot{r}$, $\dot{\theta}$, etc., are the derivatives of these variables with respect to time.

The phase refractive index μ is given explicitly by a form of the Appleton-Hartree formula (where collisions between electrons and air molecules or positive ions are neglected):

$$\mu^2=1-\frac{\dfrac{N(r,\theta,\Phi)}{1.24\times10^4 f^2}}{1-M\pm\sqrt{M^2+\dfrac{f_H^2}{f^2}\cos^2\psi}} \tag{7}$$

where f=frequency of radiation in mc/s; $N(r,\theta,\Phi)$ is number of electrons/cm^3 (the electron density, which is, in general, dependent upon the position in the ionosphere as well as the height of the point under consideration); $f_H(r,\theta,\Phi)$=the gyrofrequency in mc/s; and M is given by

$$M=\frac{\dfrac{1}{2}\left[\dfrac{f_H}{f}\sin\psi\right]^2}{1-\dfrac{N(r,\theta,\Phi)}{1.24\times10^4 f^2}}, \tag{8}$$

(ψ=the angle between the wave normal and the earth's magnetic field). If this field is taken to be dipole in nature, and if the polar axis of the spherical coordinate system coincides with the dipole axis, then:

$$\cos\psi=\frac{y_1\cos\theta+\dfrac{1}{2}y_2\sin\theta}{\{y_1^2+y_2^2+y_3^2\}^{1/2}\left\{\cos^2\theta+\dfrac{1}{4}\sin^2\theta\right\}^{1/2}}. \tag{9}$$

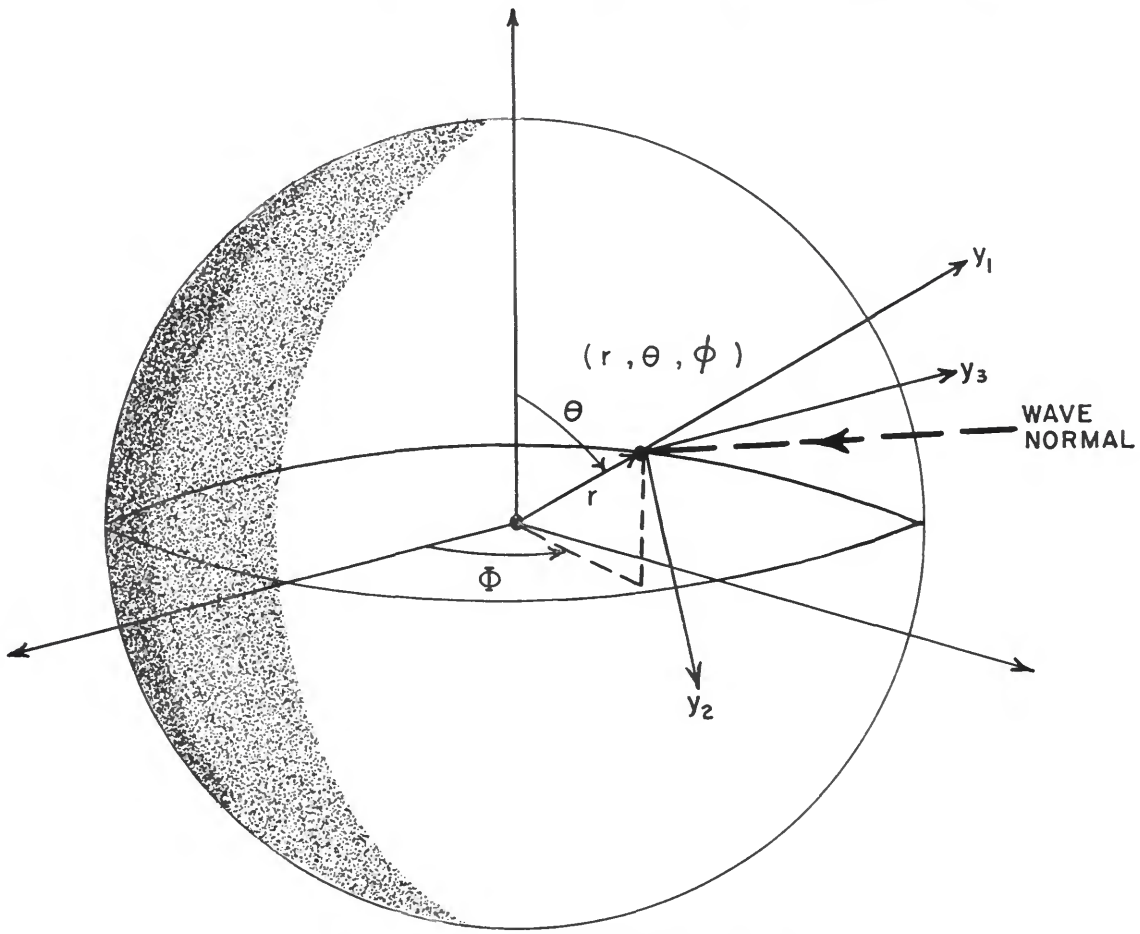

FIGURE 2.—Spherical coordinate system used in ray tracing.

Note that in a general magnetoionic medium the direction of the wave normal is not coincident with the direction of the ray. We must therefore make the distinction between these two directions when considering a magnetoionic medium (such as the earth's ionosphere) that is nonisotropic. The electromagnetic energy is propagated along the ray direction. However, there are two distinct phase velocities, one along the ray and the other along the associated wave normal. Equations (1) through (6) are written for a nonisotropic medium; thus we need to include the wave normal components, y_1, y_2, y_3, and their derivatives.

Note also that an electromagnetic wave incident in a magnetoionic medium splits into two characteristic modes of propagation called the extraordinary rays and the ordinary rays, which are generally distinct entities. In equation (7), the positive sign corresponds to the ordinary ray, and the negative to the extraordinary ray.

For our case of a radio source effectively at infinity, we consider the incoming rays as parallel. These rays are incident on the ionosphere. The boundary of the ionosphere is chosen to be at about 8,000 km from the earth's surface, where the electron density reaches the assumed interplanetary value of 600/cm^3. The initial conditions for the ray-trace are easily assigned by examination of the geometry of the situation. The geometry is illustrated in figure 3, where r_0 is chosen as 14,378 km; θ_0 and Φ_0 vary for the individual ray trace; and y_1, y_2, and y_3 are then

636-014—63——14

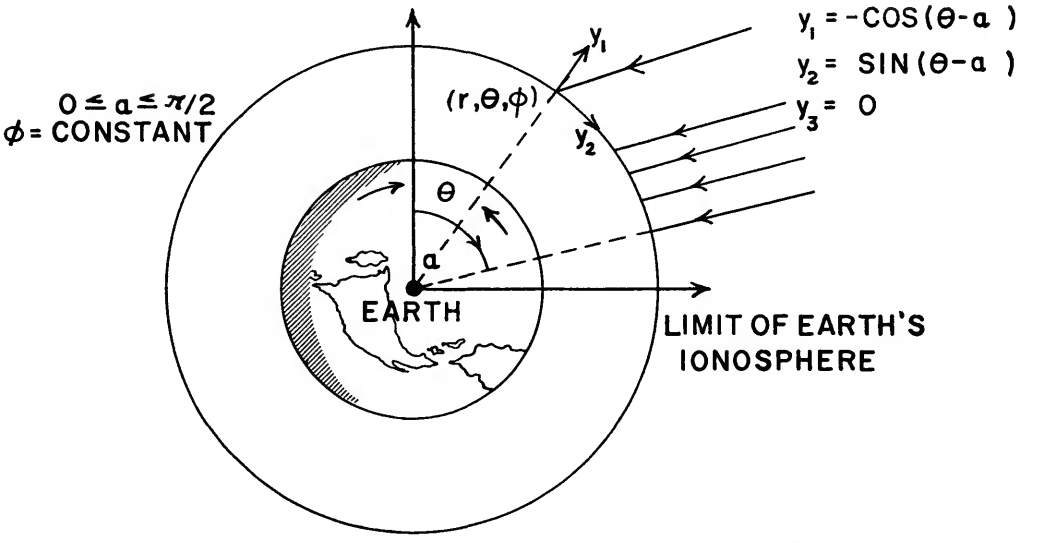

FIGURE 3.—Geometry for assigning initial conditions for ray-tracing.

assigned according to the convention in figure 4.

If we want, we can set y_3=constant for each ray trace. Then y_3 can be varied for each set of ray traces. For our computations, we found this to be the most systematic way of assigning initial conditions. For simplicity, in the cases considered here, we assumed $y_3=0$. After the initial conditions are assigned, the rays are automatically traced by the computer. The results of these computations are illustrated in figures 5, 6, 7, 8.

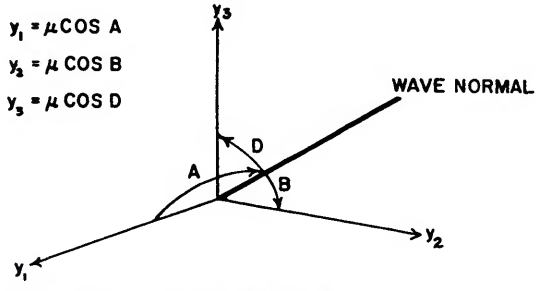

FIGURE 4.—Convention for assigning wave normal components.

The method chosen for numerical integration of equations (1) through (6) is the fourth-order Runge-Kutta method. The advantage of this method lies in the fact that we need only to know the values of the variables r, θ, Φ, y_1, y_2, y_3 at $t=t_0$. In other words, only one set of initial conditions is needed with which to begin the integration. It is possible to estimate the truncation error per step of integration (Hildebrand, 1956). But in practice it is extremely difficult (for the present functions) to approximate the total rounding-off error for this method; therefore, there is an uncertain factor in the solution. However, for nearby paths, the errors are systematic. A detailed analysis of the method can be found in Hildebrand (1956), Bennett, Milne, and Bateman (1956), and Ralston and Wilf (1960).

The boundary conditions are the initial values of r, θ, Φ, y_1, y_2, y_3, with

$$\begin{aligned} y_1 &= \mu \cos A, \\ y_2 &= \mu \cos B, \\ y_3 &= \mu \cos C, \end{aligned} \tag{10}$$

in accordance with the notation shown in figure 4.

We assign the position, and we assume the direction of the ray and the wave normal initially coincident. The program for solution of the differential equations (1) through (6) is written in FORTRAN (Graham, Grossi, Strom, and Strom, 1960).

Numerical solutions of the equations follow from an application of the Runge-Kutta method. The initial conditions and the frequency are read into the machine. Subroutines

for electron-density profiles and the necessary derivatives are interchangeable for various ionospheric models, including different electron-density profiles and discontinuities. Both ordinary and extraordinary ray paths are then computed. At each integration step, the present calculated values of r, θ, and Φ are printed out. Calculation time for ray-path length 10^4 km is approximately 15 seconds on the IBM–7090 computer. One can see that, at 0 and $\theta=180°$ (i.e., at the magnetic poles), there are discontinuities in equations (1) through (6). These discontinuities do not significantly affect the computation of the ray paths, provided that the path is a straight line over the magnetic poles. However, if the ray is undergoing a change in direction (refraction or reflection) in the vicinity of the pole, the integration errors increase. In fact, the certainty to which focal points may be predicted is greatly reduced. Significant errors are also introduced when the ray enters a region in which the gradient of electron density is great, i.e., at about 300 km of altitude (see fig. 1). These errors can be reduced by use of smaller integration steps.

The illustrated ray paths avoid these discontinuities so that the total errors are small.

The search for focal regions

The method outlined in the previous section has been applied to the cases of 5, 10, 12, 18, and 22 mc/s sources at infinity. For simplicity, we restricted the analysis to cases in which the rays remained in the (r, θ) plane. Thus, $y_3=0$ for all cases considered.

In figures 5, 6, 7, and 8, we provide an example of the plotting performed for the 5, 10, 12 mc/s cases. The incident rays are initially equidistant and parallel. Owing to the close proximity of these rays on the scale of figures 6, 7, and 8, we have illustrated the incident rays by thick black lines. The rays are then plotted separately after the point of significant divergence.

We notice there are extended focal regions along the line containing the center of the earth and the source in opposition. Haselgrove, Haselgrove, and Jennison (1961) postulated the presence of focal regions in a situation of conjunction. Figure 5 illustrates our tracings for this case. The source here is considered extended. Figures 6, 7, and 8 illustrate our calculations for the situation of opposition and contradict the common belief that the ionosphere would create a shadow in situations of opposition with respect to a source at infinity. The rays illustrated in these figures are ordinary rays.

It is important to note, however, that a satellite-borne radio telescope located at a point of the focal region will not experience a continuous intensified reception of the cosmic radio background. Owing to the multipath structure of the ionospheric propagation, alternate maxima and minima of the intensity received should be observed.

Calculation of the geometric gain for the ionosphere

With the data obtained, we are able now to calculate the geometrical gain of the ionosphere. We again assume the ionosphere to be analogous to a spherical shell lens. The gain as computed is A_1/A_2, where areas A_1 and A_2 are illustrated in plate 1; A_1 is the area intercepted by the incident rays at the boundary of the ionosphere, and A_2 is the area of the circle of least confusion, where the observing satellite is placed.

Taking advantage of the symmetry of the earth's magnetic field, we have $A_1=2\pi r^2 \sin\theta d\theta$, where r and θ obey the convention in figure 2.

The value of A_2 follows directly from the determination of the radius of the circle of least confusion. For the case illustrated in figure 6, the value of the geometrical gain lies between 3 and 10, depending on the rays chosen for calculation. Figures 7 and 8 illustrate cases in which the value of the gain lies between 5 and 20.

The results obtained are based on idealized assumptions concerning the electron density and magnetic field. However, the focal properties of the actual ionosphere are affected by irregularities and discontinuities of various causes; consequently, the focusing behavior can be predicted only in statistical terms.

To obtain a preliminary idea of the magnitude of these effects, we have considered a nonspherically symmetric distribution of electron density. We retained the $N(r)$ curve as illustrated in figure 1, but we imposed the simple

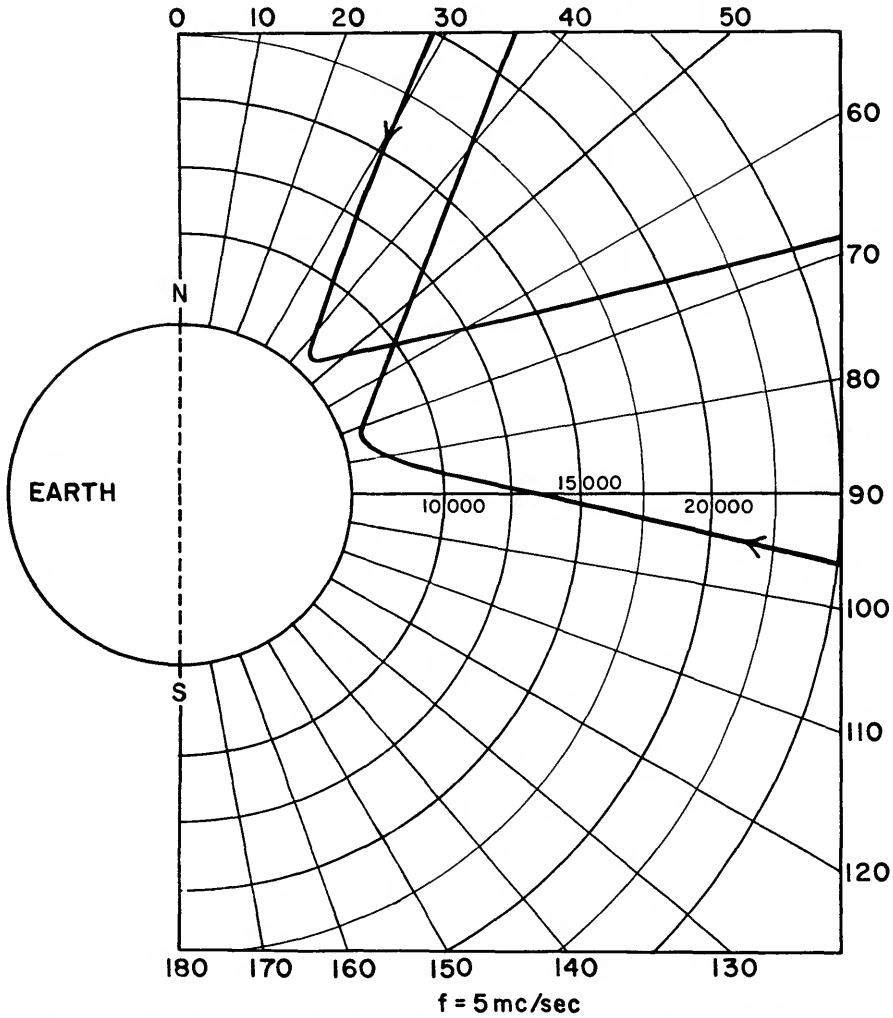

FIGURE 5.—Ray-tracing for a situation of conjunction with $f=5$ mc/s (distances are measured from the center of the earth).

model of day-to-night variation shown in figure 9. The minimum value of electron density corresponds to the center of the night side of the earth. Computations show that the effect of this model of day-to-night variation on the geometrical size of the focal region is negligible.

Extension of the method and further search for interesting focal regions

We plan to refine our analysis by adopting a fully three-dimensional model of the ionosphere and by including various realistic models of irregularities and discontinuities that are large with respect to the wavelength.

These models will include electron clouds, ionospheric winds, seasonal variations, solar bursts, and magnetic storms..

Absorption, when not negligible, will also be computed.

With our refined analysis, we will study the effect of the ionosphere on the incoming cosmic

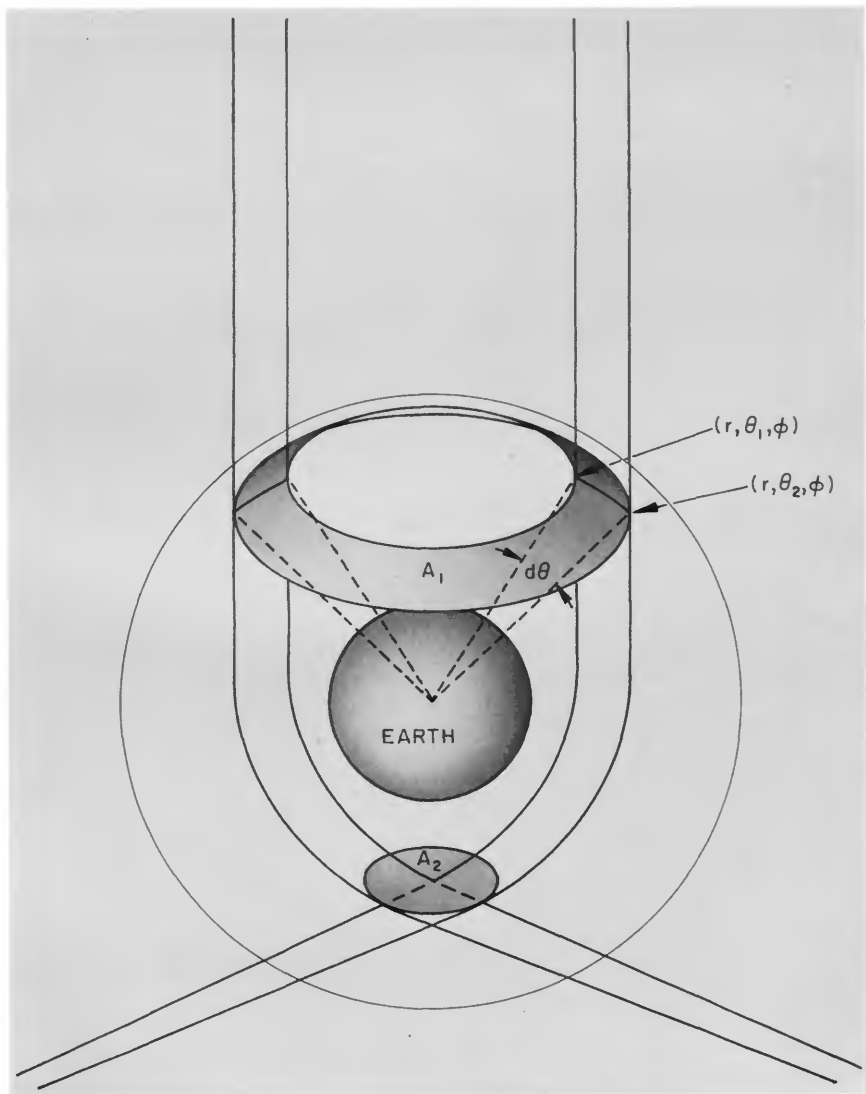

Geometry for computing the geometrical gain.

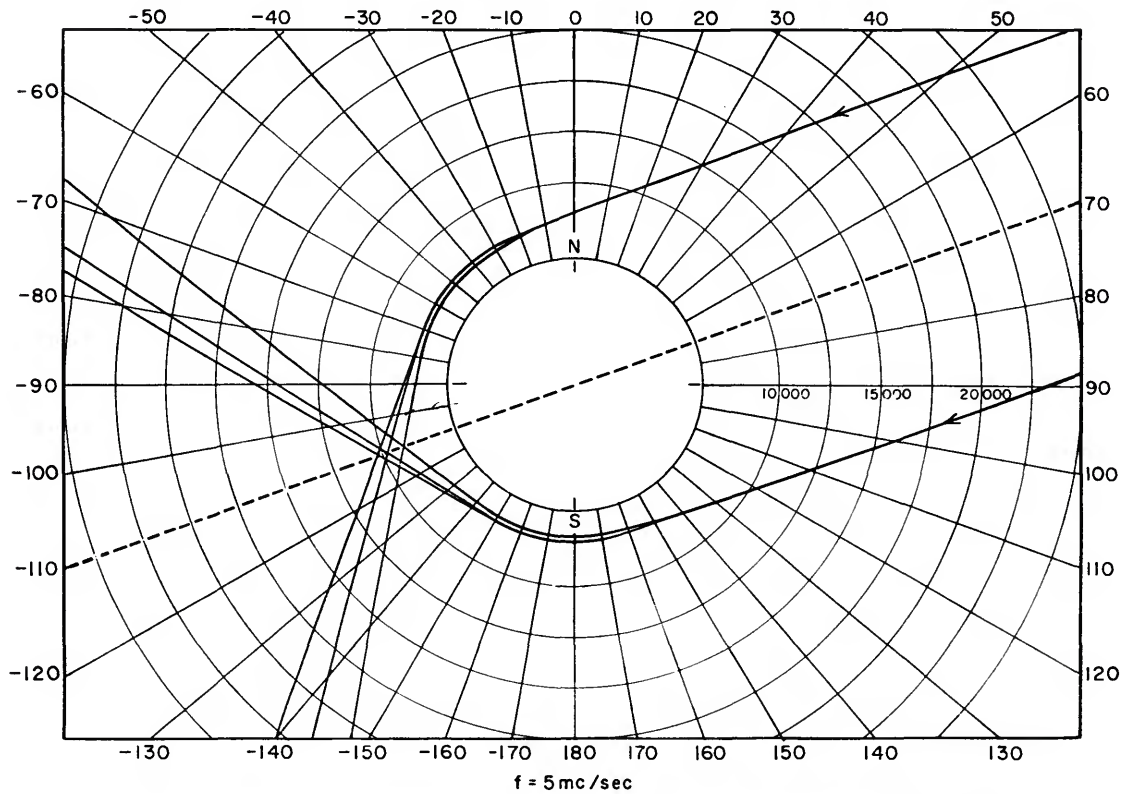

FIGURE 6.—Ray-tracing for a situation of opposition with $f=5$ mc/s (distances are measured from the center of the earth).

noise, taking into account known radio sources, both concentrated and diffused. We will plot cosmic noise distributions on spheres that are concentric with the earth and that have various radii.

In the search for interesting focal regions, we will investigate the focusing properties of the ionosphere for frequencies higher than the critical frequency of the F_2 layer.

For these frequencies, the optical behavior of the ionosphere below the F_2 layer will also be examined by using a Luneberg lens model (Luneberg, 1944), with the source at infinity and the focal region on the boundary of the spherical refractor.

The search for the existence of a possible focal region of the earth's ionosphere on the surface of the moon is also planned. Data will be collected to determine the feasibility of a moon-based HF radio telescope exploiting the focusing properties of the earth's ionosphere.

Acknowledgments

We wish to thank Dr. R. J. Davis for his encouragement, his sustaining interest, and guidance in performing this research; and Dr. A. E. Lilley for his valuable criticisms and suggestions.

The computer program was developed, in part, at Raytheon Missile and Space Division in conjunction with Independent Research Program 71–1587–010. Computations relevant to the radio astronomical cases were performed on the IBM–7090 of the Smithsonian Astrophysical Observatory's computation and analysis division.

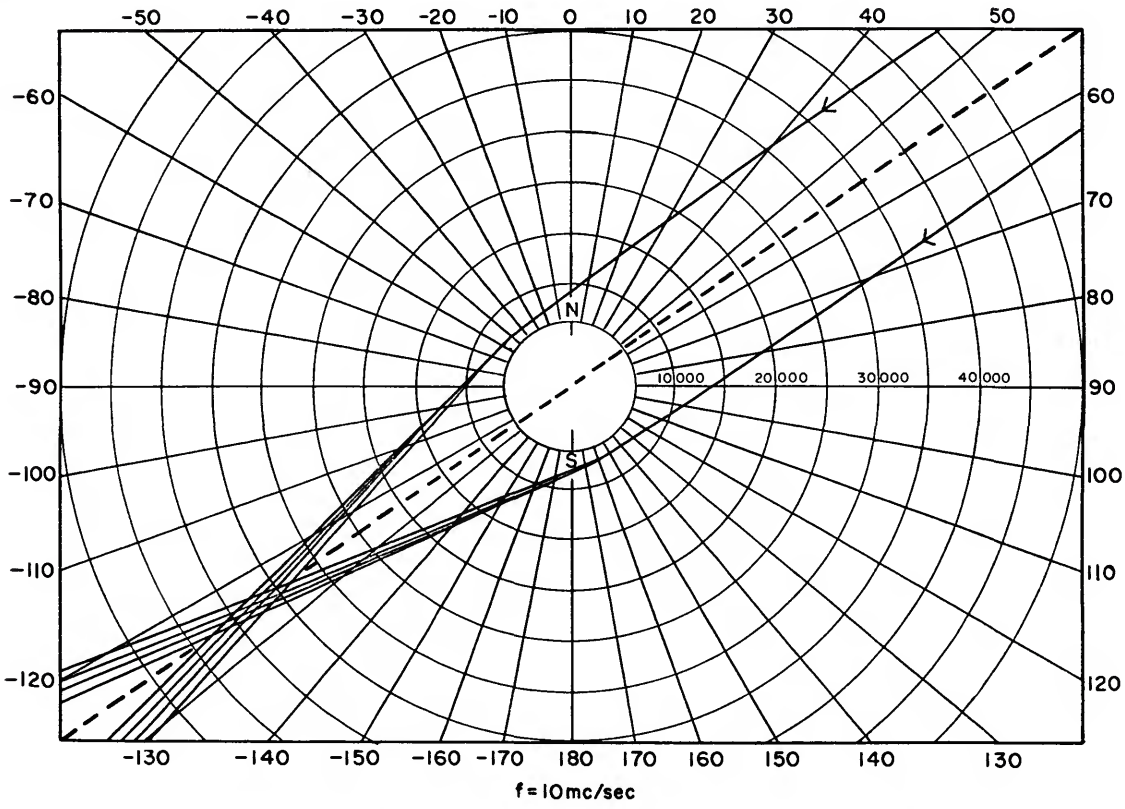

FIGURE 7.—Ray-tracing for a situation of opposition with $f=10$ mc/s (distances are measured from the center of the earth).

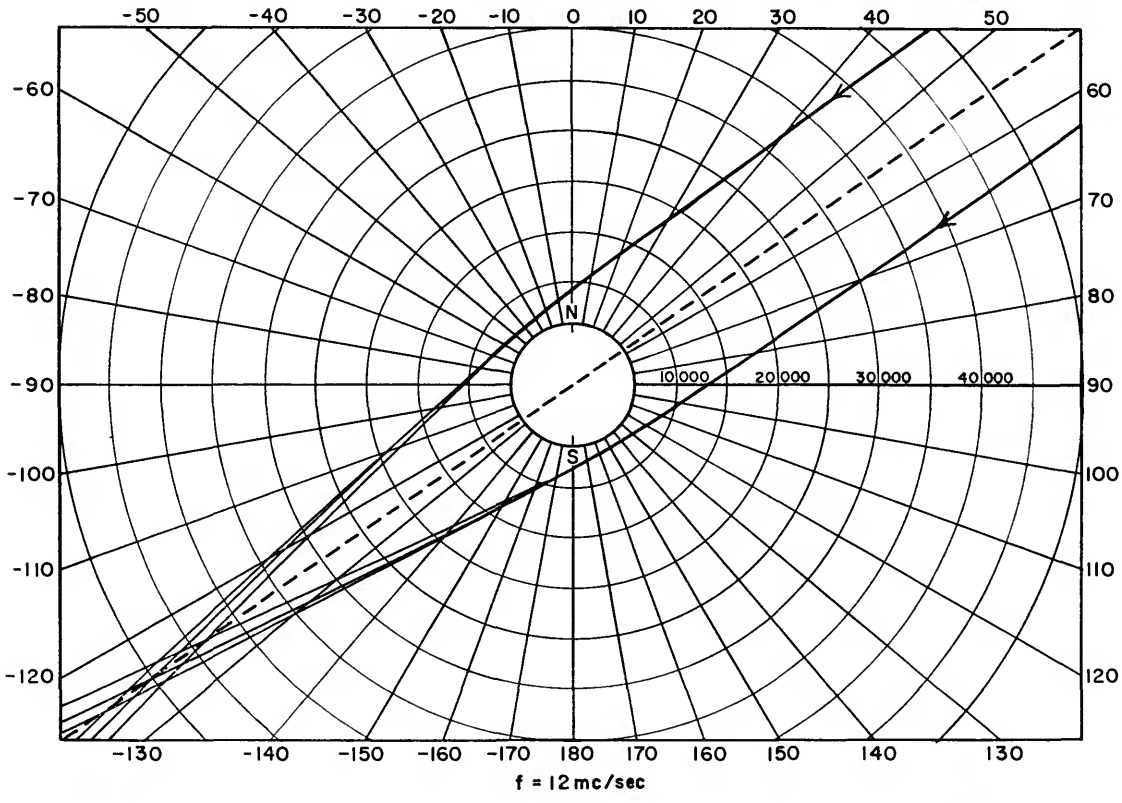

FIGURE 8.—Ray-tracing for a situation of opposition with $f=12$ mc/s (distances are measured from the center of the earth).

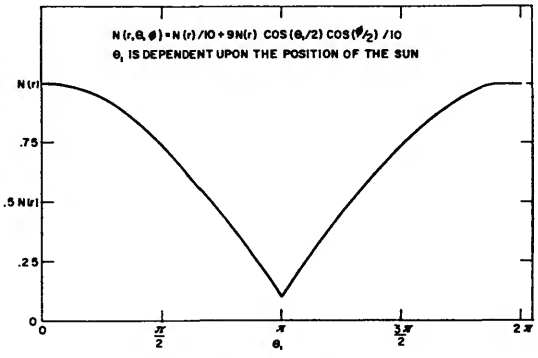

FIGURE 9.—Day-to-night variation of electron density.

Short-Periodic Oscillations in the Drag of Satellite 1958 Alpha

By Luigi G. Jacchia and Jack W. Slowey

The authors have derived accurate orbital accelerations over extensive time intervals for several artificial earth satellites; they are now in the process of converting the accelerations to atmospheric densities and then analyzing them. The procedure for deriving the accelerations, which has been briefly described by Jacchia (1961), involves the plotting of residuals in mean anomaly for all individual satellite observations. A survey of such plots for Satellite 1958 Alpha (Explorer I) from January 1958 to April 1961 has revealed the existence of persistent, periodic drag oscillations that can easily be recognized over intervals of several weeks when the observations are sufficiently numerous and well distributed. The usable observational material for this satellite consists almost exclusively of field-reduced positions from photographs taken with the Baker-Nunn cameras; unfortunately, the time intervals during which the number and distribution of observations were favorable to the detection of the oscillations are not very numerous. Whenever the oscillations could be detected, they had a period of about 3.5 days, except toward the end (March 1961), when the period increased to 4.2 days.

Table 1 gives values of the orbital accelerations $\frac{dP}{dt}$ during four time intervals during which oscillations were rather obvious; these values are plotted in figure 1. Although most of the observed oscillations are tightly grouped in a few such intervals, scattered oscillations with an unmistakable periodicity of 3.5 days can be recognized here and there, providing, we think, sufficient continuity for the numbering of the individual cycles over the whole time interval here considered. The time in the tables and diagrams is expressed in Modified Julian Days (MJD), i.e., in Julian Days minus 2 400 000.5.

Table 2 gives a list of all observed times of maximum of the short-periodic drag oscillations, together with their residuals from a linear reference equation: max=MJD 36280.0+3.52n, where n is the serial number of the maximum. The data of table 2 are plotted in figure 2.

Instantaneous periods, derived from the data of table 2, are given in table 3 and plotted in figure 3.

The drag oscillations we have described must be interpreted as due to a systematic variation of the effective presentation area of the satellite, caused by the precession of the angular-momentum vector of the satellite body in its tumbling motion.

If the satellite is a cylinder of length L and base radius $r=\epsilon L$, its total area A is given by $A=2\pi\epsilon L^2(1+\epsilon)$. Let α be the angle that the angular-momentum vector makes with the direction of motion. The mean presentation area S will be a function of α; let us call S_0 the value that S assumes when $\alpha=0$, and S_1 the value when $\alpha=90°$. We shall have

$$S_0=\frac{A}{\pi(1+\epsilon)}, \qquad (\alpha=0°)$$

$$S_1=\frac{2}{\pi}\frac{A}{1+\epsilon}\left(\frac{\epsilon}{2}+\frac{1}{\pi}\right); \qquad (\alpha=90°)$$

and, always,

$$S_0 \geq S \geq S_1.$$

The ratio $\frac{S_1}{S_0}=\frac{2}{\pi}+\epsilon$ represents the maximum factor by which the satellite drag can vary owing to change in α, provided the period of the tumbling is very small compared to the orbital

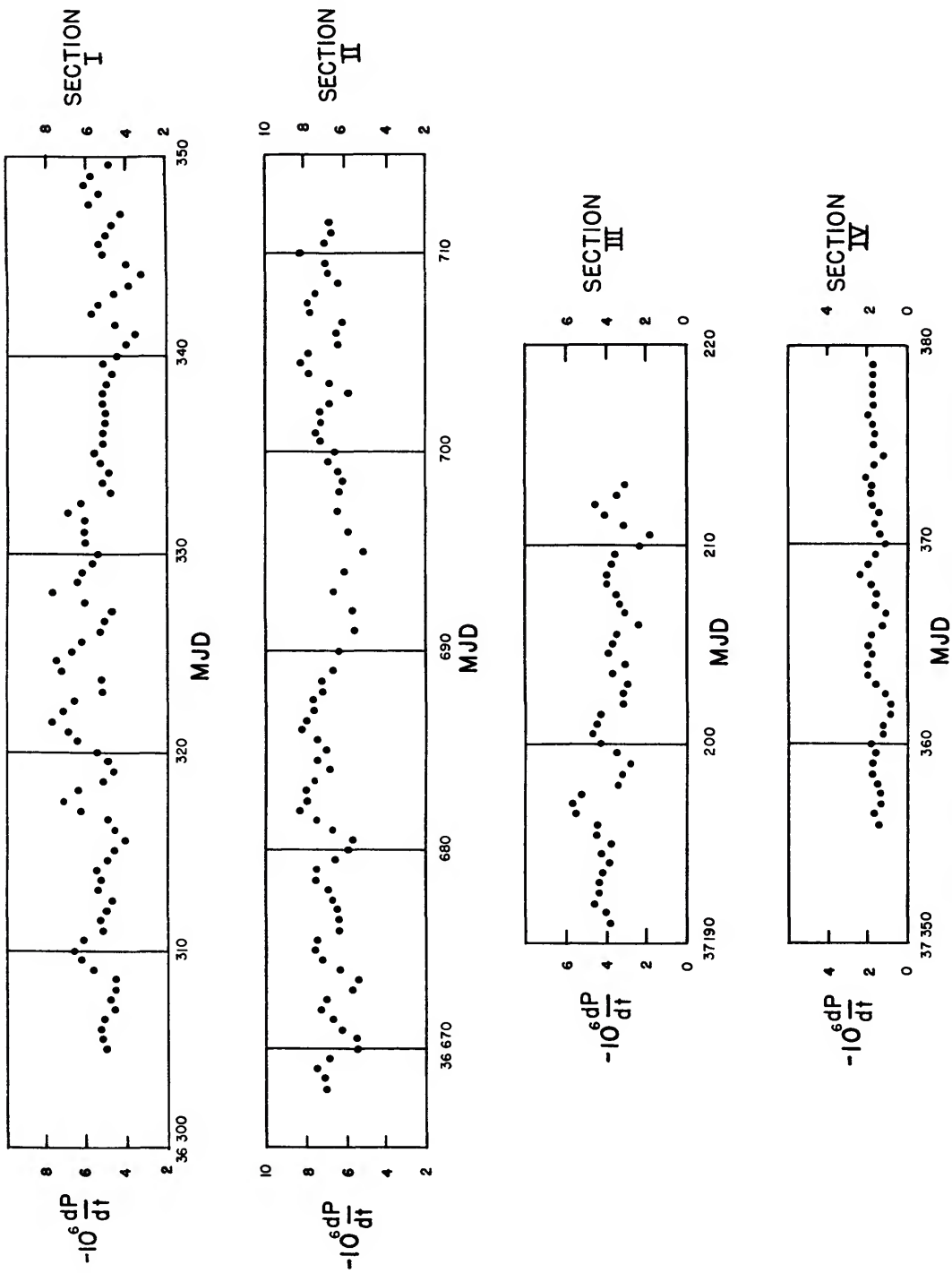

FIGURE 1.—Accelerations of 1958 Alpha during four selected time intervals.

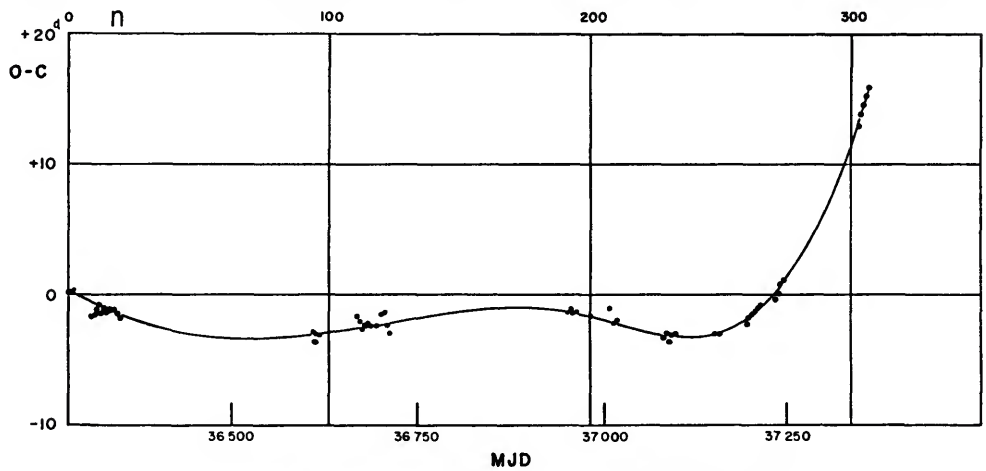

FIGURE 2.—Residuals from the equation Max=36280.0+3.52n.

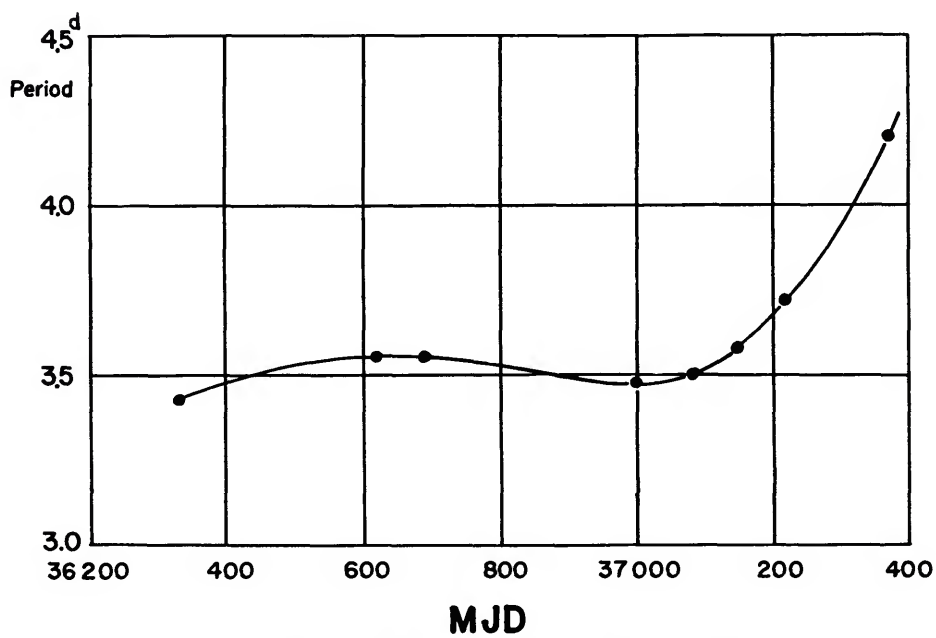

FIGURE 3.—Period of the short-periodic drag oscillations in 1958 Alpha.

TABLE 1.—*Accelerations* $\frac{dP}{dt}$ *of Satellite 1958 Alpha in selected sections*

MJD	$-10^6\frac{dP}{dt}$
SECTION I (MJD 36305–36349)	
36305.0	5.0
05.5	5.1
06.0	5.2
06.5	5.0
07.0	4.6
07.5	4.7
08.0	4.5
08.5	4.5
09.0	5.6
09.5	6.2
10.0	6.5
10.5	6.1
11.0	5.1
11.5	5.2
12.0	5.0
12.5	4.7
13.0	5.3
13.5	5.2
14.0	5.4
14.5	4.9
15.0	4.5
15.5	4.0
16.0	4.5
16.5	4.8
17.0	6.3
17.5	7.1
18.0	6.4
18.5	5.1
19.0	4.6
19.5	4.9
20.0	5.4
20.5	6.4
21.0	6.9
21.5	7.7
22.0	7.2
22.5	6.5
23.0	5.2
23.5	5.2
24.0	7.2
24.5	7.5
25.0	6.7
25.5	6.2
26.0	5.2
26.5	5.0
27.0	4.7
27.5	6.0
28.0	7.7
28.5	6.4
29.0	6.2
29.5	5.6
30.0	5.3
30.5	6.0
31.0	6.0
31.5	6.0
36332.0	6.9
32.5	6.2
33.0	4.8
33.5	5.1
34.0	4.8
34.5	5.2
35.0	5.5
35.5	5.1
36.0	5.1
36.5	5.0
37.0	5.0
37.5	5.1
38.0	5.1
38.5	5.0
39.0	4.7
39.5	5.1
40.0	4.4
40.5	4.0
41.0	3.5
41.5	4.5
42.0	5.7
42.5	5.4
43.0	4.7
43.5	3.9
44.0	3.3
44.5	4.0
45.0	5.2
45.5	5.3
46.0	5.0
46.5	4.7
47.0	4.2
47.5	4.8
48.0	5.4
48.5	6.0
49.0	5.7
49.5	4.8
SECTION II (MJD 36668–36711)	
36668.0	6.9
68.5	7.0
69.0	7.4
69.5	6.8
70.0	5.4
70.5	5.4
71.0	6.1
71.5	6.6
72.0	7.1
72.5	6.9
73.0	5.6
73.5	5.4
74.0	6.2
74.5	7.1
75.0	7.4
75.5	7.4
76.0	6.2
36676.5	6.3
77.0	6.3
77.5	6.6
78.0	6.8
78.5	7.4
79.0	7.4
79.5	6.5
80.0	5.8
80.5	5.6
81.0	6.6
81.5	7.4
82.0	8.3
82.5	7.9
83.0	7.9
83.5	7.5
84.0	6.8
84.5	7.3
85.0	6.9
85.5	7.4
86.0	8.1
86.5	7.9
87.0	7.5
87.5	7.5
88.0	7.1
88.5	7.1
89.0	6.6
90.0	6.3
91.0	5.5
92.0	5.6
93.0	6.5
94.0	6.0
95.0	5.1
96.0	5.8
97.0	6.3
98.0	6.2
98.5	6.1
99.0	6.3
99.5	6.8
36700.0	6.5
00.5	7.2
01.0	7.4
01.5	7.2
02.0	7.2
02.5	6.7
03.0	5.7
03.5	6.7
04.0	7.8
04.5	8.1
05.0	7.8
05.5	6.4
06.0	6.4
06.5	6.1
07.0	7.8
07.5	7.8
08.0	7.5
08.5	6.3
09.0	6.8
09.5	6.9
10.0	8.2
36710.5	7.0
11.0	7.0
11.5	6.7
SECTION III (MJD 37191–37213)	
37191.0	3.8
91.5	4.0
92.0	4.5
92.5	4.3
93.0	4.3
93.5	4.1
94.0	3.9
94.5	4.2
95.0	3.7
95.5	4.4
96.0	4.4
96.5	5.4
97.0	5.6
97.5	5.2
98.0	3.4
98.5	3.2
99.0	2.8
99.5	3.4
37200.0	4.1
00.5	4.6
01.0	4.4
01.5	4.2
02.0	3.1
02.5	3.1
03.0	2.9
03.5	3.6
04.0	3.1
04.5	3.8
05.0	3.6
05.5	3.4
06.0	2.3
06.5	3.0
07.0	3.2
07.5	3.5
08.0	3.9
08.5	4.0
09.0	3.7
09.5	3.5
10.0	2.2
10.5	1.8
11.0	3.1
11.5	4.0
12.0	4.5
12.5	3.4
13.0	3.0
SECTION IV (MJD 37356–37379)	
37356.0	1.5
56.5	1.6
57.0	1.4
57.5	1.4
58.0	1.6
58.5	1.8

TABLE 1.—*Accelerations* $\frac{dP}{dt}$ *of Satellite 1958 Alpha in selected sections*—Continued

MJD	$-10^6\frac{dP}{dt}$	MJD	$-10^6\frac{dP}{dt}$
37359.0	1.8	37369.5	1.6
59.5	1.6	70.0	1.1
60.0	1.8	70.5	1.4
60.5	1.3	71.0	1.6
61.0	1.3	71.5	1.4
61.5	0.9	72.0	1.8
62.0	0.9	72.5	1.8
62.5	1.1	73.0	1.8
63.0	1.5	73.5	2.1
63.5	2.0	74.0	1.6
64.0	2.0	74.5	1.2
64.5	1.8	75.0	1.6
65.0	2.0	75.5	1.6
65.5	1.8	76.0	1.7
66.0	1.3	76.5	1.9
66.5	1.1	77.0	1.7
67.0	1.6	77.5	1.7
67.5	1.6	78.0	1.7
68.0	1.8	78.5	1.7
68.5	2.4	79.0	1.7
69.0	2.0		

TABLE 2.—*Satellite (1958 Alpha: Observed drag maxima expressed in MJD and residuals from the equation Max=36280.0+3.52n*

n	*t*	*o–c*
0	36280.2	+0.2
1	283.7	+0.2
2	287.3	+0.3
9	310.0	−1.7
10	313.6	−1.6
11	317.5	−1.2
12	321.4	−0.8
13	324.4	−1.4
14	328.2	−1.1
15	331.6	−1.2
16	(335.1)	(−1.2)
17	338.6	−1.2
18	342.2	−1.2
19	345.4	−1.5
20	(348.5)	(−1.9)
94	608.1	−2.8
95	611.4	−3.0
96	614.8	−3.1
103	640.0	−2.6
104	643.3	−2.8
111	669.0	−1.7
112	672.1	−2.1
113	36675.2	−2.6
114	678.7	−2.6
115	682.5	−2.3
116	686.1	−2.2
118	(693.0)	(−2.4)
120	700.9	−1.5
121	704.5	−1.4
122	707.0	−2.4
123	(710.0)	(−3.0)
191	951.0	−1.3
192	954.6	−1.2
193	958.0	−1.4
195	965.0	−1.4
200	36982.3	−1.7
207	(37007.5)	(−1.1)
209	013.5	−2.2
210	(017.2)	(−2.0)
228	079.4	−3.2
229	083.0:	−3.0:
230	086.0	−3.6
231	090.0:	−3.1:
232	093.6	−3.0
248	37150.0	−3.0
249	153.5	−3.0
260	193.0	−2.2
261	197.0	−1.7
262	200.7	−1.5
263	204.5	−1.3
264	208.3	−1.0
265	212.0	−0.8
271	233.5	−0.4
272	(237.5)	(+0.1)
273	241.8	+0.8
274	245.6	+1.1
303	(359.6)	+13.0
304	364.0	+13.9
305	368.2	+14.6
306	372.4	+15.3
307	376.5	+15.9

TABLE 3.—*Periods of the short-periodic drag oscillations observed in Satellite 1958 Alpha, deduced from the data in table 2*

MJD	Period
36330	3.43 days
620	3.55
690	3.55
37000	3.47
090	3.50
150	3.58
220	3.72
370	4.2

period (if not, the departure from the statistical mean involved in the computation of S_1 could become important).

For Satellite 1958 Alpha we have $\epsilon=0.0375$, which gives $S_0/S_1=1.48$. Although most of the observed oscillations appear to fall within this amplitude, a few cycles seem to exceed it, reaching in the amplitude a factor of nearly 2. If we consider that the plotted accelerations are the second derivatives of a curve that is often determined by only a few points, we would not, at this stage, attribute much significance to these large amplitudes but rather consider the over-all distribution of amplitudes as falling reasonably well within the computed limits.

A variation of the drag by the maximum factor S_0/S_1 would imply a variation of α close to 90° in half the precessional period of $3^d.5$, i.e., values of $\frac{d\alpha}{dt}$ of the order of 40° to 50° per day. Colombo (1961) found that the interaction of the earth's magnetic field and the ferromagnetic components of Satellite 1958 Epsilon (Explorer IV) can easily explain precessional perturbations of the angular momentum of 17° per day for that satellite, while the gravitational torque and the drag torque cannot account for more than 6° per day. It may be necessary to invoke similar magnetic interactions to explain the much larger precessional motion in Satellite 1958 Alpha.

The data of table 3 need to be corrected if they are to be interpreted as periods of the precessional motion of the angular-velocity vector referred to a fixed coordinate system. The period is obviously referred to the perigee of the satellite's orbit, which had an average daily precessional motion of $+2^\circ.1$ in 1958 and $+2^\circ.4$ in 1961. This would result in corrections of $\pm 0^d.07$ to $\pm 0^d.10$; unfortunately, it is impossible to specify the sign of the correction, unless the direction of the precessional motion of the angular-velocity vector is known.

In a forthcoming paper we shall give a complete listing of the accelerations of Satellite 1958 Alpha, together with those of the other satellites involved in the atmospheric investigations. This preliminary note is intended primarily to call to the attention of atmospheric investigators the errors that can arise when drag data of nonspherical satellites are used.

The Analysis of Gravity

By Harold Jeffreys

Properties of gravity

Gravity over the surface of the earth is a continuous function of latitude and longitude. A little more can be said, because it is an integral based on the distribution of density, which at worst has only finite discontinuities. We can form an idea of the rate of convergence of an expansion in spherical harmonics as follows. In one variable, if f, a function of bounded variation in $(0, 2\pi)$, is analyzed in a Fourier series, the coefficients must decrease like $1/n$ and their contributions to $\int f^2 dx$ like $1/n^2$. For the integral of such a function the decreases will be like n^{-2} and n^{-4}. Over a sphere we should expect the sums of contributions to $\iint f^2 dS$ from all harmonics of degree n to decrease similarly, and if all harmonics were normalized to make $\iint S_{nm}^2 dS = 4\pi a^2$ the expectations of the coefficients of S_{nm} would decrease like $n^{-5/2}$. As the derivation of gravity from the potential introduces a factor $n-1$, the coefficients in the potential should decrease like $n^{-7/2}$. Then a rough calculation shows that if the major variations are for $n=0$, 1, 2, we should expect the contributions to $\iint f^2 dS$ from $n=4$ to be about ¼ of those for $n=3$, and those for $n>4$ to be about ⅛ of those for $n=3$. For a smoother function than the integral of a function arising from simple discontinuities in density the decrease would be more rapid. We should note also that if we simply assume $\iint f^2 dS$ to exist, it is necessary that the double sum of the squares of the coefficients a_{nm}, b_{nm} shall converge. Hence

$$\sum_{m=0}^{n} (a_{nm}^2 + b_{nm}^2)$$

must decrease faster than $1/n$. If it decreases like $1/n^2$ the coefficients will on the whole decrease like $n^{-3/2}$. This tolerates greater irregularity in f than we have just considered. But in the series

$$\sum_{1}^{\infty} n^{-2} = \frac{1}{6}\pi^2,$$

the first few terms are 1, 0.25, 0.11, 0.06, and 2/3 of the excess over 1 is already taken into account. So it is worth while, even for the study of gravity alone, to proceed by examining the coefficients of spherical harmonics for $n=0$, then for $n=0$ and 2 (those in $n=1$ being theoretically absent), then for $n=0$, 2, 3, then for $n=0$, 2, 3, 4, and so on. This consideration is even more striking for the external potential on account of the extra factor $\frac{1}{n-1}$, and also because there is a factor $(a/r)^{n+1}$ in the potential, which falls off rapidly as we recede from the Earth's surface.

There is one apparent objection to this analysis, that there are special narrow regions, especially mountains and ocean deeps, where the height of the rock surface above sea level is anomalous for a region of the order of 100 km in width. This is the distance such that a spherical harmonic of degree 200 or so keeps the same sign, and in a harmonic representation such regions would require many harmonics of such orders to represent them, the terms adding up in the anomalous regions but nearly canceling outside. Then the rapid decrease of the coefficients might not start until $n=200$ or so. However, such regions, on account of their limited area, cannot contribute much to $\iint g^2 dS$. The essential point of the spherical harmonic analysis is to consider a classification of gravity anomalies into widespread ones, keeping the same sign over distances comparable with the radius of the Earth, and local ones that

change sign within much smaller distances. The analysis can investigate the former. The local anomalies will need special treatment, but the best treatment must have a standard of comparison, and the best standard would be a function that best fits the Earth as a whole, that is, one based on the lower harmonics.

If only we knew gravity everywhere, the problem would be easy. If

$$g=\sum\sum(A_{ns}\cos n\lambda+B_{ns}\sin n\lambda)P_n^s(\sin\phi), \quad (1)$$

then on account of the orthogonality of the spherical harmonics

$$\iint g\cos\phi(\cos n\lambda,\sin n\lambda)P_n^s d\phi d\lambda=\iint (P_n^s)^2 (A_{ns}\cos^2 n\lambda, B_{ns}\sin^2 n\lambda)\cos\phi d\lambda, \quad (2)$$

taken over the surface. Thus the determination of all A_{ns}, B_{ns} would be reduced to simple integration. For conveniently spaced values of g the formulas could be replaced by numerical summation. However, this does not work. Gravity is observed only at isolated points and must be interpolated before we have the data for the integrals. In some attempts linear interpolation has been used right across major oceans, and this is certainly invalid. What we have to do is to choose the coefficients to fit the observed values as well as possible; any interpolation will introduce errors.

The harmonic analysis of a continuous function, such as the separation of a periodic term from random noise, is a difficult statistical problem, which has not been satisfactorily solved even for one variable. The ordinary method of least-squares depends entirely on the errors of separate observations being independent, and this is nearly true for errors of measurement. For gravity the errors of measurement, judged by different observations at the same place, are nowadays not more than 1 mgal; even early in the 19th century most of them were not much over 10 mgal. But differences between stations within 1° or 2° of each other are normally 20 mgal or so, and cannot be errors of observation. In fact the observations depart from any smooth representation of gravity by a short-range variation, which is mainly genuine; and such a variation of gravity must be a continuous function of position. But the correlation between neighboring values of such a function tends to +1 when the separation tends to 0, and the basis of the method of least-squares breaks down.

Can we arrange the analysis so as to retain the advantages of the method of least-squares? For some separation the correlation must become negative, and hence there is a separation such that it is zero. Then there is no point in using a lot of observations very close together—they all say the same thing. If we can find a distance such that the correlation is small and can form summaries for observations covering such a range of distance, there is some hope of an approach to independence.

Analysis of gravity observations

I should say at this point that the external field is completely determined if we know free-air gravity defined by $g_f=g\left(1+\frac{2h}{a}\right)$, where g is gravity at height h above sea level (Jeffreys, 1959). A formula correct to orders h^2 and eh is available. All I have to say really concerns free-air gravity, which is constant on a vertical ascent; the correction $2g/a$ is 308 mgal/km. Our problem is to estimate the low harmonics in g_f. The five harmonics P_1, P_1^1 (cos λ, sin λ), P_2^1 (cos λ, sin λ) are theoretically absent from g_f.

Some principles that can guide us are as follows. First, it is known that heavy grouping of data can give a very accurate determination. If we have observations of a periodic function of x uniformly spaced from 0 to 2π, then comparison of the means over the ranges $-\frac{1}{4}\pi$ to $\frac{1}{4}\pi$, and $\frac{3}{4}\pi$ to $\frac{5}{4}\pi$, determines the coefficient of cos x with a standard error only 1.1 times that obtained by using the whole of the observations; and similarly for the coefficient of sin x. Now a harmonic containing cos 3λ keeps the same sign over a range of 60° in longitude. If we used only the central half of such ranges we should get a good determination for cos 3λ, and the end halves would give sin 3λ. Further, whether higher terms are present or not, there will be little correlation between the errors produced in the means. Thus least-squares would be expected to give a good approximation if the data are summarized for ranges of 30° in

latitude and longitude. The problem is to fill in the gap between individual stations and 30° squares.

In my analysis (Jeffreys, 1941, 1943), I saw no advantage, and some disadvantages, in trying to use more than one observation in a 1° square. I took the most northerly observation in whatever list I was using. The 1° squares were then combined into 10° squares. It was found that the free-air anomaly (the departure from the International Gravity Formula of Cassinis, which was used as the standard) regularly showed an increase with height over land, and a decrease with depth of the sea bottom over sea. This is a consequence of any form of compensation, but study of compensation and its imperfections was not the object at this stage. The important thing was that here was a clearly systematic effect, and if the result for a 10° square was to be representative of the square it must be evaluated for the mean height of the square. Thus to the data in a 10° square I fitted a formula $a+bh$ by least-squares and reduced to mean height by evaluating $a+b\bar{h}$, where $\bar{h}$ is the mean height interpolated from Prey's calculation. Similar methods were used for sea squares and squares that were partly land and partly sea (the values of b for sea squares were generally less than for land squares). The standard errors τ_0 of the estimates for the mean height were evaluated as usual.

The next question was, how much would the 10° means be expected to differ from the 30° means? We have no information other than the gravity data themselves; and harmonics in a range about $n=18$ would produce a fluctuation in the 10° means and largely cancel in the 30° means. I grouped the 10° squares into 30° squares, so that a 30° square might have nine 10° squares in it. There was a scatter larger than the apparent uncertainty of the 10° means (treated as having independent errors) could explain, and this implied a variation that could keep the same sign for 10°, with an additional uncertainty which I expressed by a standard error τ_1 of 20 mgal. This, it must be understood, is not the uncertainty of the 10° means themselves, but of the probable departure of the true means over 10° squares from a smooth formula that would fit the 30° squares. It was the latter that I was trying to find.

Combining the uncertainty τ_1 with the crude uncertainty τ_0 I derived means and standard errors for the 30° squares. Again the actual variation was greater than the uncertainties taken into account so far would explain, and I introduced a further variation with root mean square $\tau_2=12$ mgal to take this into account; τ_2 would include contributions from all harmonics of degree ≤ 6. Then I formed the normal equations, neglecting all nondiagonal terms, to see what harmonics might have coefficients substantially more than their standard errors. Apart from the constant and P_2 terms, whose existence was not in doubt, three showed up, namely $P_3^1 \cos \lambda$, $P_2^2 \cos 2\lambda$, and $P_3^2 \cos 2\lambda$. Normal equations were then formed fully for coefficients of P_0, P_2, and these three terms, and solved. As the τ_2 variation would include these variations, their mean square was subtracted from τ_2^2 and the result was used to estimate uncertainties. Residuals were formed and reanalyzed, and a term in $P_3^3 \sin 3\lambda$ was detected. (Two slight departures were made from this treatment, but they need not delay us here.)

If I were doing the work again I should make two modifications. In the first approximation, τ_2 included the variation I was trying to estimate, and this was removed in the second. A more usual practice would have been to analyze from the 10° squares directly and look for outstanding correlations between the residuals at different separations, increasing the uncertainties correspondingly if any showed up. Also, the analysis was carried out piecemeal, groups of harmonics whose values were likely to influence estimates of one another being taken together. Now that electronic calculators are available, it would be easy to do the direct analysis for all possible harmonics to degree 3. I should not, however, expect either change to affect the results greatly.

Zhongolovitch's analysis

After my work an analysis resembling it in many respects was made by I. D. Zhongolovitch (1952). He determines systematic corrections for some of the older observers very much as I

did, and also some corrections to base station values for more recent ones. My 10° "squares" were of course not square except near the equator, the range of distance in longitude being less than in latitude. So long as the uncertainties were evaluated I do not think that this could make much difference. Zhongolovitch used regions more nearly square. Each extended over 10° of latitude, but the numbers along each zone of latitude were chosen so that the areas would be approximately the same as for equatorial squares. Thus they dropped from 36 in the equatorial zone to 3 in each polar zone. The advantage of this is, I think, more than compensated by the fact that it is no longer possible to group nine 10° squares into one 30° square and get an estimate of the τ_1 variation at an early stage in the analysis.

He estimates b and b' as I did, but gives two sets of solutions, one (first variant) using the simple mean for the stations in each square, the other (second variant) reducing to the mean heights of the squares as I did. As the second variant corrects for an obvious systematic error, I think the first needed no consideration. In my work I considered the possibility that for forms $a+bh$, $a'+b'h'$ applied to the squares that were partly land and partly sea, the values of a, a' for the land and sea portions might be different. I took all the 18 squares where a and a' were well determined and found $a'>a$ in 9 cases, $a'<a$ in 7, and $a'=a$ in 2, and decided that there was no systematic difference. Zhongolovitch, however, used 46 squares and finds a mean $a'-a=19$ mgal and allows for it. The respective numbers are $a'>a$, 32 cases, and $a'<a$, 14 cases. As his total number of squares is not very much different from mine, I think that the difference between 18 and 46 cases must be due to his having retained squares where I should not have considered a and a' well determined.

My comparison was with the International Gravity Formula, which can be written $979770 + 3446.0\ P_2\ (\sin\phi) + 5.3\ P_4\ (\sin\phi)$. Zhongolovitch's is with Helmert's formula $978.030\ (1+0.5302\sin^2\phi - 0.000007\sin^2 2\phi) = 979754.85 + 3454.40\ P_2 + 6.26\ P_4$.

However, his solutions take no account whatever of either τ_0 or τ_1. The first, τ_0, will be arge if there are few observations or if their values vary irregularly within a square. But he forms normal equations for the coefficients of the harmonics using the data for the separate squares as independent estimates, treating all as of equal weight. This is clear from his table 6; if any allowance had been made for the uncertainty of the reduction to the mean height of the region, the diagonal coefficients would be less for the second variant than for the first, but in fact they are the same. Thus excessive weight has been given to squares with scanty or irregular data. Standard errors are derived from the scatter of the data, but they may be too low on account of correlation between adjacent errors due to the presence of harmonics of degrees about 6; and as the values for squares near the poles have especially large uncertainties τ_0, if there is any systematic error in them it will have biased some of the estimates, especially those of the coefficients of P_2 and P_3.

In table 7 Zhongolovitch (1952) gives 15 different solutions from his data for each variant. Here A_{nm}, B_{nm} are departures from the coefficients in Helmert's formula. The normal equations are for coefficients up to A_{44}, B_{44}, with certain multipliers, but in the solutions some coefficients are either taken as zero or given values taken as not subject to error. I state the coefficients estimated.

Column 1. A_{00}, A_{20} only.
2. A_{00}, A_{20} (A_{40} taken equal to difference between Helmert's and the International value).
3. A_{00}, A_{20}, A_{30}.
4. A_{00}, A_{20}, A_{40} (A_{40} treated as initially unknown).
5. A_{00}, A_{20}, A_{30}, A_{40}.
6. A_{00}, A_{20}, A_{22}, B_{22}.
7. A_{00}, A_{20}, A_{22}, A_{31}, A_{32}, B_{33}.
8. All to B_{33}.
9. All to B_{44}.
10, 11, 12. A_{30}, A_{40} re-estimated as for 3, 4, 5 with values of A_{00} and A_{20} from column 1.
13. All to B_{33}; coefficients up to B_{22} taken from column 6.
14. All to B_{44}; coefficients up to B_{33} taken from column 13.

It is column 14 that Zhongolovitch quotes in a later paper (1957). It practically halves

A_{30} and A_{31} in comparison with column 9. Column 15 is based on the hypothesis that the same gravity formula holds in the unoccupied squares as in the occupied ones. This is reasonable, but is applied as follows. Values for the unoccupied squares are calculated from column 13; then the whole of the coefficients up to B_{88} are calculated by numerical integration over the whole surface. Naturally this makes only slight changes in the coefficients up to B_{33}. No uncertainties are given, and in fact the nearest approaches to estimates with valid uncertainties are given by columns 8 and 9. Column 15 fits the observed squares with standard deviation 18 mgal, the unobserved ones with standard deviation 5 mgal. This of course is too good to be true. We really have no idea how the contributions from intermediate harmonics vary in the unobserved regions; even if a range of 180° in longitude is available, it cannot adequately separate a harmonic of degree n from one of degree $n + 1$.

It appears that if harmonics above the second degree are considered at all, only columns 8 and 9 are genuine least-squares solutions and all the others must underestimate the uncertainties. As indicated above, even columns 8 and 9 are doubtful on account of correlation of errors and of treatment of all squares as equally well determined. Nevertheless the comparison is of some interest. Column 7 estimates the same harmonics as I found, and should agree with mine if the method is free from bias.

Comparison of the solutions is made easier in terms of the mean squares of the contributions of the various harmonics to gravity. The mean squares of P_{nm} (cos $m\lambda$, sin $m\lambda$) are as follows:

n	m	Mean square
0	0	1
1	0	1/3
	1	1/3
2	0	1/5
	1	3/5
	2	12/5
3	0	1/7
	1	6/7
	2	60/7
	3	360/7
4	0	1/9
	1	10/9
	2	20
	3	280
	4	2240

From column 9, for each entry of the form $a \pm \sigma$ we take a^2, σ^2 times the mean square of P_{nm} (cos $m\lambda$, sin $m\lambda$). An extra figure was kept in the calculation. (See table 1.)

A_{40} is not included in the summation because some departure from the international formula in this coefficient is to be expected on any hypothesis concerning the earth's internal state.

TABLE 1.

	Estimate	Mean square from estimate	Mean square from uncertainty
A_{30}	$+15.42 \pm 6.05$	34.0	5.2
A_{31}	$+8.23 \pm 3.14$	58.0	8.5
B_{31}	$+0.32 \pm 2.35$	0.9	4.7
A_{32}	$+0.23 \pm 0.80$	0.4	5.5
B_{32}	-1.93 ± 0.68	31.9	3.9
A_{33}	$+0.57 \pm 0.32$	16.7	5.2
B_{33}	$+0.47 \pm 0.31$	11.4	4.8
		153.3	38.1
A_{40}	$+2.27 \pm 6.28$		
A_{41}	-4.96 ± 2.46	27.3	6.7
B_{41}	-2.74 ± 1.93	8.3	4.1
A_{42}	-0.07 ± 0.43	0.1	3.7
B_{42}	$+0.65 \pm 0.46$	8.4	4.2
A_{43}	$+0.21 \pm 0.12$	12.3	4.0
B_{43}	$+0.09 \pm 0.12$	2.3	4.0
A_{44}	$+0.033 \pm 0.041$	2.4	3.8
B_{44}	$+0.061 \pm 0.042$	8.3	3.9
		69.5	34.6

TABLE 2.

	Column 8	Column 9	Column 7	H.J. (1943)
A_{00}	$+22.32\pm1.79$	$+22.80\pm1.83$	22.33 ± 1.83	$+2.47\pm1.93$
A_{20}	-15.80 ± 4.86	-17.53 ± 5.24	-11.87 ± 4.37	$-6.1\ \pm5.0$
A_{22}	$+3.54\pm1.30$	$+5.27\pm1.52$	$+4.43\pm1.22$	$+4.01\pm1.42$
B_{22}	$+0.06\pm1.29$	$+0.46\pm1.39$		
A_{30}	$+12.37\pm5.24$	$+15.42\pm6.05$		
A_{31}	$+4.25\pm2.16$	$+8.23\pm3.14$	$+4.32\pm2.24$	$+4.24\pm2.43$
B_{31}	-0.96 ± 1.95	$+0.32\pm2.35$		
A_{32}	$+1.08\pm0.66$	$+0.23\pm0.80$	$+1.07\pm0.68$	$+1.30\pm0.68$
B_{32}	-1.32 ± 0.60	-1.93 ± 0.68		
A_{33}	$+0.95\pm0.25$	$+0.57\pm0.32$		
B_{33}	$+0.65\pm0.25$	$+0.47\pm0.31$	$+0.62\pm0.25$	$+0.46\pm0.26$
$1/\alpha$	$296.0\ \pm0.6$	$295.8\ \pm0.7$	$296.6\ \pm0.6$	$296.2\ \pm0.7$

Taking the mean-square contributions from the uncertainties as estimates of the probable contributions to the mean squares of the estimates from the outstanding variation, we have from the third harmonics 5.4, and from the fourth 4.3. The value for χ^2 would be 28.1 on 7 degrees of freedom for the third harmonics, 16.4 on 8 degrees of freedom for the fourth. Both would be highly significant if the estimates were independent, but this is doubtful, and nearly half of the sum 69.5 for the fourth harmonics comes from A_{41}, which is just over twice its standard error. In my preliminary analysis A_{41} was $+1.4\pm2.0$.

If we subtract the contributions from the random errors, we are left with 115.2 mgal^2 from the third harmonics and 34.9 mgal^2 from the fourth. From our rough preliminary consideration these are in about the ratio that we should expect, although it is rather surprising that so much of the contribution comes from one harmonic. Also the decrease cannot continue at the rate suggested, since it would imply $\tau_1^2+\tau_2^2<1/8$ of the contribution from $n=3$; actually it is about ten times that contribution.

In my solution the mean-square contribution from 7 third harmonics was 46 mgal^2, of which 27 mgal^2 was accounted for by random errors; thus my terms are substantially less than Zhongolovitch's.

On the face of it the third harmonic coefficients that can be determined without serious doubt as to their signs are A_{30}, A_{31}, B_{32}, and possibly A_{33}. Those that I found were A_{31}, A_{32}, and B_{33}, thus agreeing only for A_{31}.

Comparing column 9 with column 8, in which the fourth harmonics were not estimated, we find the following (table 2). I also give my solutions and Zhongolovitch's column 7.

Three of the changes exceed the standard errors in column 9, and five exceed those in column 8. The most striking is for A_{31}. The changes are surprising, seeing that only one coefficient of a fourth harmonic in column 9 exceeds twice its apparent standard error. The difference between his A_{00}, A_{20} and mine is mostly due to the fact that he has compared his data with Helmert's formula, whereas I used the International formula. The estimates of α (the ellipticity) are comparable. For the harmonics that I found worth estimating the agreement between my results and column 8 is quite good. However, I found no indication of a significant A_{30}, which is striking in both column 8 and column 9; and my A_{32} is in good agreement with column 8 but not with column 9, and I failed to find B_{32} or A_{33}.

Comparison with results from artificial satellites

Comparison with results from artificial satellites shows further anomalies. The zonal harmonics in the field are well determined because they produce effects that accumulate secularly or over long periods. If the potential is taken in the form

$$U=\frac{\mu}{r}\left[1+\sum_{n=2}^{\infty}\sum_{m=0}^{n}\left(\frac{a}{r}\right)^n P_n^m(C_{nm}\cos s\lambda + S_{nm}\sin s\lambda)\right]$$

determinations for $m=0$, $n=0$ to 5 have been found. Terms with $m\neq0$ give effects that accumulate for much shorter times, and hence are more difficult to evaluate. The coefficient in g is nearly $n-1$ times the corresponding one in U. Then we have, chiefly from the work of Kozai (1961b,c):

$1/\alpha$	298.20 ± 0.03		
$10^6 C_{22}$	$+0.60 \pm 0.28$	A_{22}	$+0.60 \pm 0.28$
$10^6 S_{22}$	-2.24 ± 0.28	B_{22}	-2.24 ± 0.28
$10^6 C_{30}$	$+2.29 \pm 0.02$	A_{30}	$+4.58 \pm 0.04$
$10^6 C_{31}$	$+2.99 \pm 0.36$	A_{31}	$+5.98 \pm 0.72$
$10^6 S_{31}$	$+1.18 \pm 0.31$	B_{31}	$+2.36 \pm 0.62$
$10^6 C_{32}$	$+0.20 \pm 0.20$	A_{32}	$+0.40 \pm 0.40$
$10^6 S_{32}$	$+0.36 \pm 0.20$	B_{32}	$+0.72 \pm 0.40$
$10^6 C_{33}$	-1.71 ± 0.29	A_{33}	-3.42 ± 0.58
$10^6 S_{33}$	$+0.84 \pm 0.27$	B_{33}	$+1.68 \pm 0.54$
$10^6 C_{40}$	$+2.12 \pm 0.041$	A_{40}	$+6.36 \pm 0.12$
$10^6 C_{50}$	$+0.232 \pm 0.021$	A_{50}	$+0.93 \pm 0.08$

Comparing with the values from gravity (allowing for the $n-1$ factor), we see that the best established term from artificial satellites, C_{20}, leads to a value of the ellipticity α differing from the gravity value by about three times the standard error. Again C_{30} would correspond to $A_{30}=+4.6\pm0.04$. As my value (1943) was $+1.6\pm5.0$ (Table VI, p. 63), it is consistent; but Zhongolovitch's values deviate by about 1.5 and 1.7 times their apparent standard errors. With regard to these terms I am sure that the artificial satellite values are right. Helmert's formula, used by Zhongolovitch for comparison, corresponds closely to the artificial satellite value of α. The sum of his A_{20} and A_{30} is small, and P_{20} and P_{30} keep the same sign through most of the northern hemisphere. It looks as if the separation of these harmonics must depend mostly on the scanty observations in latitudes south of $-30°$, and the difference between his solution and mine for A_{30} is due to his having given too much weight to them. I am inclined to think that the error in my A_{20} is due to errors in the comparison of base stations. As many of these have now been improved, and there are now many more observations in the North Pacific and in the southern hemisphere, it should now be possible to make a much better determination.

For $m=0$, A_{31} is reasonably consistent with my value and with Zhongolovitch's column 8, and A_{32}, B_{33} might be consistent. But A_{22}, B_{22}, B_{31}, B_{32}, A_{33} are in serious disagreement. Here it seems to me that the values from gravity and from satellites are both under suspicion. The error in A_{20} indicates at least that there is some systematic error in gravity, which may have affected the estimates of the other coefficients. Kozai (1961c, p. 10), on the other hand, remarks that the true standard errors of his values are much larger than those quoted; if I understand him, nonorthogonality in the normal equations had not been allowed for.

Possibilities of improvement

I think that in the long run gravity should give much better determinations for $m\neq0$ than the artificial satellites. The number of 10° squares would be 542 if all were occupied; the polar circles of radii 10° are each treated as one square. A full gravity survey would not eliminate τ_1, which will contribute a mean square departure in the neighborhood of 400 mgal^2. The error of representation, the departure of the true mean over the square from the estimated mean, would be about the same, but would be divided by about 3 if we had one observation for every 5° square. Thus, if we had an observation in every 5° square, the mean square contribution to any harmonic arising from the uncertainties could be brought down to about 1 mgal^2. This is to be compared with about 5 mgal^2 from the present gravity data. Kozai's results as they stand give less than 1 mgal^2 up to B_{31}, 1.4 mgal^2 for A_{32} and B_{32}, 15 mgal^2 for A_{33} and B_{33}. He also gives values for coefficients up to B_{44}, some of which have greater uncertainties still. Since his uncertainties are said to be probably too low, it seems that even if artificial satellites may give the better values for $m=1$ and possibly $m=2$, gravity survey will still be needed for higher m.

It may appear that Zhongolovitch's work would have used many more observations than mine, but this does not seem to be the case. He has 410 squares altogether, of which 204 contain observations. I had 542, of which 217 had observations. For the 30° squares I had 49 occupied out of a possible 62, but if we take only those where the standard error is ≤15 mgal the number sinks to 33, which do not include any centered on latitudes $+90°$, $-60°$, and $-90°$. Zhongolovitch also comments on the extreme asymmetry of the distribution with regard to the equator.

Acknowledgments

This work was done while I was acting as a consultant at the Smithsonian Astrophysical Observatory. The translation of the relevant parts of Zhongolovitch's work was done by my wife, to whom my thanks are due.

Abstract

Methods of analysis of gravity to estimate the low harmonics are discussed. The work of Zhongolovitch is described in some detail, as it does not appear to have been translated and is the most extensive analysis made so far. There are serious inconsistencies between his results, mine, and those derived from artificial satellites, and suggestions are made for future work in the hope that these may be reconciled.

The Stabilization of an Artificial Satellite at the Inferior Conjunction Point of the Earth-Moon System

By G. Colombo

It is obviously important to be able to keep an artificial satellite stable at the inferior conjunction point (L_1) of the earth-moon system, while using the minimum amount of momentum. The fact that the inferior conjunction point is an exact solution of the four-body problem (earth-moon-sun-satellite) (Colombo, 1960; Klemperer and Benedikt, 1958, p. 25), if we neglect only high-order perturbations, is an advantage of this solution that makes it preferable in some ways to the triangular Lagrangian solution (L_4) of the restricted three-body problem. On the other hand, the larger degree of instability of position L_1 compared to that of L_4 is a disadvantage. It is, however, necessary to note that the perturbing action of the sun on L_4 is of the same order of magnitude as that of the moon.

In the discussion that follows, we shall first compare the order of approximation of the solutions L_1 and L_4 to indicate their characteristics. Second, we shall study some devices to stabilize a satellite in a region around L_1 without using momentum. The devices considered are a solar sail of relatively small dimensions, and a mechanical autonomous device. It is also possible to obtain this stabilization with a jet system that uses a minimum momentum.

Each stabilization system needs a built-in position-detection device of high precision, which may become possible in the next few years. But the final goal of this paper is to indicate the smallness of the acceleration needed to keep a satellite in a region of 50 km around L_1, and to examine the possible stabilization systems, assuming that the position-sensors could detect displacements of the order of 2 km. This discussion, even though theoretical at present, may be useful in the future for designing a device to stabilize a satellite at the inferior conjunction point.

1. Collinear solution

The symbols used are defined as follows:

E, center of the earth;
M, center of the moon;
S, center of the sun;
τ^*, inertial reference system;
τ_E, reference system centered at E and oriented as τ^*;
$\mathbf{a}(Q)$, acceleration of a moving point Q with respect to τ_E
$\mathbf{A}(Q)$, acceleration of a moving point Q with respect to τ^*
$\mathbf{A}_S(Q)$, acceleration due to the action of all the perturbing bodies S, V, M, J
$\mathbf{A}_E(Q)$, acceleration due to the action of the earth
$\mathbf{A}_M(Q)$, acceleration due to the action of the moon
m_1, mass of the earth
m_2, mass of the moon
m_3, mass of the sun

$\mathbf{F}$, force on E due to M

$\mathbf{v}_M$, velocity of the moon with respect to τ_E

The fundamental hypothesis may be stated as follows: $\mathbf{A}_S(Q)$ is a linear function of Q, at any time t, in a spherical region around E. With this hypothesis we shall neglect small terms, which we will evaluate at the end of this section. (We shall also neglect the perturbations due to the oblateness of the earth and to the possible oblateness of the moon.)

Let us define P with the following equation:

$$\mathbf{EP}=\rho\mathbf{EM}. \tag{1}$$

Thus, for the above hypothesis we can write

$$\mathbf{A}_S(P)=(1-\rho)\mathbf{A}_S(E)+\rho\mathbf{A}_S(M). \tag{2}$$

Next, we write the equations of motion of M and P with respect to τ_E, and the equation of motion of E with respect to τ^*:

$$\left.\begin{aligned}\mathbf{a}(P)&=-\mathbf{A}^*(E)+\mathbf{A}_E(P)+\mathbf{A}_M(P)+\mathbf{A}_S(P),\\ \mathbf{a}(M)&=-\mathbf{A}^*(E)-\frac{\mathbf{F}}{m_2}+\mathbf{A}_S(M),\\ \mathbf{A}^*(E)&=\frac{\mathbf{F}}{m_1}+\mathbf{A}_S(E).\end{aligned}\right\} \tag{3}$$

Consequently,

$$\left.\begin{aligned}\mathbf{a}(M)&=-\mathbf{F}\,\frac{m_1+m_2}{m_1m_2}+\mathbf{A}_S(M)-\mathbf{A}_S(E),\\ \mathbf{a}(P)&=-\frac{\mathbf{F}}{m_1}+\mathbf{A}_E(P)+\mathbf{A}_M(P)+\mathbf{A}_S(P)-\mathbf{A}_S(E).\end{aligned}\right\} \tag{4}$$

Finally,

$$\mathbf{a}(P)=-\frac{\mathbf{F}}{m_1}+\mathbf{A}_E(P)+\mathbf{A}_M(P)+\rho[\mathbf{A}_S(M)-\mathbf{A}_S(E)]. \tag{5}$$

The accelerations $\mathbf{A}_E(P)$ and $\mathbf{A}_M(P)$ and the force $\mathbf{F}$ are parallel; therefore, we can solve the equation in ρ:

$$\mathbf{A}_E(P)+\mathbf{A}_M(P)=\frac{m_2(1-\rho)-\rho m_1}{m_1m_2}\,\mathbf{F}. \tag{6}$$

If we take, for example, the solution ρ_1, satisfying the conditions $0<\rho_1<1$, we will have

$$\mathbf{a}(P)=\rho_1\mathbf{a}(M). \tag{7}$$

This solution corresponds to the inferior conjunction point L_1. If we put a satellite at point L_1 with an initial velocity $\mathbf{v}(P)$ equal to $\rho_1\mathbf{v}_M$, the satellite will always satisfy the equation

$$\mathbf{EP}=\rho_1\mathbf{EM}. \tag{8}$$

The motion of P will be homotetic to the motion of M with respect to E.

To obtain a rough estimate of the degree of approximation, let us consider the most unfavorable condition for the perturbation. Assume that the moon and sun are in conjunction and, for simplicity, neglect the smaller action of the other perturbing bodies. We have for any Q of $\mathbf{EM}$, under these conditions, the equation

$$\mathbf{A}_S(Q)-\mathbf{A}_S(E)=\frac{\mathbf{EM}}{|EM|}\,\frac{k^2m_3}{|ES|^2}\left\{\frac{2|EQ|}{|ES|}+\frac{3|EQ|^2}{|ES|^2}\right\}. \tag{9}$$

We showed that the linear term does not cause relative perturbations, which can never come from the total quadratic term, but only from the difference,

$$\rho_1 \mathbf{A}_S(M) - \mathbf{A}_S(L_1) = -\frac{\mathbf{EM}}{|EM|}\, 1.5\times 10^{-8} \text{ cm/sec}^2. \tag{10}$$

This perturbation is of the same order of magnitude as the solar pressure for a body with an area-to-mass ratio of 10^{-4} cm^2/gram.

2. Triangular position

The difficulty of defining exactly a triangular solution for the real earth-moon system is well known. We choose to define the point L_4 with the equation

$$\mathbf{EL}_4 = \frac{1}{2}\,\mathbf{EM} + \frac{\sqrt{3}}{2}\,\mathbf{n}\times\mathbf{EM}, \tag{11}$$

where

$$\mathbf{n} = \frac{\mathbf{EM}\times\mathbf{v}_m}{|\mathbf{EM}\times\mathbf{v}_m|}. \tag{12}$$

I think this is the most natural definition of the libration point L_4, but it is not an exact solution of the real earth-moon-sun-satellite problem, even if we neglect the parallactic term as we did in the previous section.

We shall now evaluate the acceleration needed to keep a satellite at L_4, taking into account only the sun's action. Let us put, as in the fundamental hypothesis given above,

$$\mathbf{A}_S(P) = \mathbf{A}_S(E) - \alpha\mathbf{EP} + 3\alpha\,\frac{\mathbf{ES}\cdot\mathbf{EP}}{|ES|^2}\,\mathbf{ES}, \tag{13}$$

where

$$\alpha = \frac{k^2 m_3}{|ES|^3}. \tag{14}$$

From equation (3), taking into account equation (13), we obtain the following equations of motion for P and M:

$$\left.\begin{aligned} \mathbf{a}(P) &= \mathbf{A}_E(P) + \mathbf{A}_M(P) - \mathbf{A}_M(E) - \alpha\mathbf{EP} + 3\alpha\,\frac{\mathbf{ES}\cdot\mathbf{EP}}{|ES|^2}\,\mathbf{ES}, \\ \mathbf{a}(M) &= \mathbf{A}_E(M) - \mathbf{A}_M(E) - \alpha\mathbf{EM} + 3\alpha\,\frac{\mathbf{ES}\cdot\mathbf{EM}}{|ES|^2}\,\mathbf{ES}. \end{aligned}\right\} \tag{15}$$

Now, if we define the operator,

$$e^{t\theta}\mathbf{a} = \mathbf{a}\cos\theta + \mathbf{n}\times\mathbf{a}\sin\theta, \tag{16}$$

we will have for L_4:

$$\left.\begin{aligned} \mathbf{A}_E(P) + \mathbf{A}_M(P) - \mathbf{A}_M(E) &= e^{i\pi/3}[\mathbf{A}_E(M) - \mathbf{A}_M(E)] \\ \mathbf{EL}_4 &= e^{i\pi/3}\mathbf{EM}. \end{aligned}\right\} \tag{17}$$

The acceleration needed to keep P at L_4 is:

$$\mathbf{A}^{(e)} = \frac{3\alpha\sqrt{3}}{2|ES|^2}\,\{(\mathbf{ES}\cdot\mathbf{EM})\mathbf{n}\times\mathbf{ES} - (\mathbf{ES}\cdot\mathbf{n}\times\mathbf{EM})\mathbf{ES}\} + \frac{\sqrt{3}}{2}\,\frac{d\mathbf{n}}{dt}\times\mathbf{v}_M + \frac{\sqrt{3}}{2}\,\frac{d^2\mathbf{n}}{dt^2}\times\mathbf{EM}. \tag{18}$$

The intensity of the acceleration (18) is of the order of 10^{-3} cm/sec^2. Note that in this position the acceleration due to the action of the moon is of the same order of magnitude, that is to say, 3×10^{-3} cm/sec^2. Therefore, the question is: since the triangular Lagrangian solution is a solution of a schematic model of the real problem, made by neglecting a force of the same order of magnitude as

the force that we do consider, what information will we gain from this model about the real motion of a satellite in a region around the point L_4?

The perturbing acceleration (18) may be considered an almost-periodic perturbation. We denote by n_m and n_s the mean motions of moon and sun respectively. The quasi-period of $\mathbf{A}^{(e)}$ is $\frac{2\pi}{2(n_m-n_s)}$. This acceleration may cause a forced oscillation, but it is necessary to observe that if we take into account all the terms of the same order of magnitude, we have to work with a nonlinear, nonautonomous system. Moreover, this system seems to be very close to a harmonic or subharmonic resonance condition. In fact, it is very easy to write the vectorial equation for the motion of P in a small region around L_4. We put $\mathbf{EP}=\mathbf{EL}_4+\mathbf{L}_4\mathbf{P}=\mathbf{EL}_4+\mathbf{x}$, and we obtain as a first approximation:

$$\ddot{\mathbf{x}}+\frac{k^2}{|EM|^3}\left\{m_E\left[1-3\frac{\mathbf{EL}_4\cdot\mathbf{x}}{|EL_4|^2}\right]+m_M\right\}\mathbf{x}$$
$$-3\frac{k^2}{|EM|^5}\left\{m_E\left[\mathbf{EL}_4\cdot\mathbf{x}+\frac{1}{2}\mathbf{x}^2-\frac{5}{2}\left|\frac{\mathbf{EL}_4\cdot\mathbf{x}}{EL_4}\right|^2\right]\mathbf{EL}_4+m_M[\mathbf{ML}_4\cdot\mathbf{x}]\mathbf{ML}_4\right\}$$
$$-\alpha\left\{\mathbf{x}-3\frac{\mathbf{ES}\cdot\mathbf{x}}{|ES|^2}\mathbf{ES}-\frac{3}{|ES|^2}[(\mathbf{EL}_4\cdot\mathbf{ES})\mathbf{EL}_4-(\mathbf{EM}\cdot\mathbf{ES})\mathbf{EM}]\right\}+\mathbf{A}^{(e)}=0. \quad (18')$$

A preliminary crude analysis of equation (18) makes the opinion stated above almost certain. We will not waste time by indicating the difficulties of the problem of the secular stability of the motion around L_4. We will only refer the reader to the work of Brown and Shook (1933) on the Trojan group, and observe that the case we are studying is more complicated than the Trojan case for the following reason: the earth-to-moon mass ratio is much smaller, and the effects of the perturbing acceleration due to the sun are very much greater than are those due to Saturn in the case of the Trojan group.

If the problem were only to study the short-period stability, it would be enough to perform a numerical integration. I think, however, it is necessary to begin with a solution defined precisely as we have defined it. Starting as we suggested above, we can evaluate carefully all the forces of the same order of magnitude acting on the satellite.

3. Inequalities for the acceleration in a region around L_1

To study the possibility of stabilizing a satellite in position L_1, we must first study carefully the gravitational acceleration of a point P in a region around L_1. Taking into account only the action of the sun and neglecting the other celestial bodies, we have from equation (3):

$$\mathbf{a}(P)=\mathbf{A}_S(P)-\mathbf{A}_S(E)+\mathbf{A}_E(P)+\mathbf{A}_M(P)-\frac{\mathbf{F}}{m_1}$$
$$=-\alpha\mathbf{EP}+3\alpha\frac{\mathbf{ES}\cdot\mathbf{EP}}{|ES|^2}\mathbf{ES}+\mathbf{A}_E(P)+\mathbf{A}_M(P)-\frac{\mathbf{F}}{m_1}. \quad (19)$$

We know that

$$\mathbf{EP}^*=\mathbf{EL}_1=\rho_1\mathbf{EM} \quad (20)$$

is an exact solution of equation (19). Now we put

$$\mathbf{EP}=\mathbf{EP}^*+\mathbf{P}^*\mathbf{P} \quad (21)$$

and we obtain the equation

$$\frac{d^2\mathbf{P}^*\mathbf{P}}{dt^2}=\left(\frac{\partial\mathbf{A}_E(P)}{\partial P}\right)_{P^*}\cdot\mathbf{P}^*\mathbf{P}+\left(\frac{\partial\mathbf{A}_M(P)}{\partial P}\right)_{P^*}\cdot\mathbf{P}^*\mathbf{P}+O_2(\mathbf{P}^*\mathbf{P}), \quad (22)$$

denoting by $O_2(\mathbf{P^*P})$ terms of two orders of magnitude less than the other terms, in a spherical region R around L_1 of radius 150 km. We will write equation (22) in the following form:

$$\left.\begin{aligned} \frac{d^2\mathbf{P^*P}}{dt^2} &= -(\alpha_1+\alpha_2)\mathbf{P^*P}+3(\alpha_1+\alpha_2)\frac{\mathbf{P^*P}\cdot\mathbf{EM}}{|EM|^2}\mathbf{EM}+O_2(\mathbf{P^*P}), \\ \alpha_1 &= \frac{hm_1}{|EP^*|^3}, \\ \alpha_2 &= \frac{hm_2}{|MP^*|^3}. \end{aligned}\right\} \tag{23}$$

Now we consider the reference system $\bar{\tau}$, centered at P^* with the Z-axis normal to the ecliptic, and the X-axis directed toward the point Υ. We define a fictitious moon M^* and a fictitious earth E^*, in the following manner: M^* and E^* move in circular orbits centered at P^* in the XY-plane with radii $(1-\rho_1)a$ and $\rho_1 a$, where a is the semimajor axis of the real moon. The true longitude of M^* is the mean longitude of the real moon, and E^* is always in the opposite direction to M^* with respect to P^*. We note that it is possible to choose the initial position of M^* in such a way that the angle between the directions P^*M and P^*M^* is never greater than 8°. Now we write equation (23) in the form:

$$\left.\begin{aligned} \frac{d^2\mathbf{P^*P}}{dt^2} &= -(\alpha_1^*+\alpha_2^*)\mathbf{P^*P}+3(\alpha_1^*+\alpha_2^*)\frac{\mathbf{P^*P}\cdot\mathbf{E^*M^*}}{|E^*M^*|^2}\mathbf{E^*M^*}+\Delta\mathbf{a}+O_2(\mathbf{P^*P}), \\ \alpha_1^* &= \frac{hm_1}{|E^*P^*|^3}, \\ \alpha_2^* &= \frac{hm_2}{|M^*P^*|^3}. \end{aligned}\right\} \tag{24}$$

We will evaluate $\Delta\mathbf{a}$ when P moves in the rotating orbit we shall define soon. We take a reference system $\bar{\tau}_{(r)}(x, y, z)$ centered at P^*, the z-axis coincident with the Z-axis, and the x-axis directed always toward M^*. We suppose P moves in an ellipse ϵ with respect to $\bar{\tau}_{(r)}$, with principal diameters in the x and y directions and semidiameters p and q, respectively. The components of the explicit part of the acceleration at the right-hand side of equation (24) are

$$2(\alpha_1^*+\alpha_2^*)x,\ -(\alpha_1^*+\alpha_2^*)y,\ 0. \tag{25}$$

If we take an auxiliary reference system $\tau'_{(r)}$ centered at P^*, ξ-axis directed toward M, ζ-axis normal to the osculating plane of the moon's orbit, the components of the explicit part of the acceleration, we have at the right-hand side of equation (23) are

$$2(\alpha_1+\alpha_2)\xi,\ -(\alpha_1+\alpha_2)\eta,\ -(\alpha_1+\alpha_2)\zeta. \tag{26}$$

Now we put

$$\lambda = \frac{\alpha_1+\alpha_2}{\alpha_1^*+\alpha_2^*}, \tag{27}$$

and we obtain

$$|\Delta a| = (\alpha_1^*+\alpha_2^*)\{4(\lambda\xi-x)^2+(\lambda\eta-y)^2+\lambda^2\zeta^2\}^{1/2}. \tag{28}$$

Let us denote by $i^*>0$ the maximum of the angles $\widehat{x\xi}$, $\widehat{y\eta}$, $\widehat{z\zeta}$. On the arc of the ellipse ϵ where $x>0$, $y>0$, we have

$$\left.\begin{aligned} 0 &\le \xi \le x\cos i^*+y\sin i^*, \\ 0 &\le \eta \le x\sin i^*+y\cos i^*, \\ 0 &\le \zeta \le (x^2+y^2)^{1/2}\sin i^*. \end{aligned}\right\} \tag{29}$$

Let λ^* be the maximum value of the function $\lambda(t)$ we defined in equation (27). If we put $x=p\cos\theta$, $y=q\sin\theta$, $0\leq\theta\leq\pi/2$, we will find:

$$|\Delta a|\leq(\alpha_1^*+\alpha_2^*)\{\cos^2\theta[3p^2(\lambda^*\cos i^*-1)^2+p^2(\lambda^*+1)^2-2\lambda^*p^2\cos i^*]+\sin^2\theta[3p^2\sin^2 i^* +q^2(\lambda^{*2}+1)-2\lambda^*q^2\cos i^*]+2\sin\theta\cos\theta[3pq(\lambda^*\cos i^*-1)\sin i^*-2\lambda^*pq\sin i^*]\}^{1/2}. \quad (30)$$

Or if we take into account that i^* is less than 8° and $0°\leq\theta\leq 90°$, $\lambda^*<3$, we obtain

$$|\Delta a|<(\alpha_1^*+\alpha_2^*)\{p^2\cos^2\theta[4(\lambda^*-1)^2+\sin^2 i^*]+q^2\sin^2\theta[(3+\lambda^*)\sin^2 i^*+(\lambda^*-1)^2]\}^{1/2}. \quad (31)$$

Let us put $q=8p$; then we have finally,

$$|\Delta a|<8p(\alpha_1^*+\alpha_2^*)\{(\lambda^*-1)^2+(3+\lambda^*)\sin^2 i^*\}^{1/2}. \quad (32)$$

4. A forced orbit around L_1

Now let us consider a particle P moving with the fictitious acceleration with respect to $\bar{\tau}$,

$$-(\alpha_1^*+\alpha_2^*)\mathbf{P}^*\mathbf{P}+3(\alpha_1^*+\alpha_2^*)\frac{\mathbf{P}^*\mathbf{P}\cdot\mathbf{E}^*\mathbf{M}^*}{|E^*M^*|^2}\mathbf{E}^*\mathbf{M}^*+\mathbf{S}\frac{\mathbf{S}^*\mathbf{E}^*}{|S^*E^*|}, \quad (33)$$

where $\mathbf{S}>0$ is constant, and S^* is the mean sun. Let us choose the unit value of time in such a way that the mean motion of the moon is 1 and the unit value of length is a. We write the equation of motion of P with respect to $\bar{\tau}_{(r)}$, and we find:

$$\left.\begin{aligned}\frac{d^2x}{dt^2}-2\frac{dy}{dt}&=(1+2A)x-|S|\cos(1-n)t,\\ \frac{d^2y}{dt^2}+2\frac{dx}{dt}&=(1-A)y+|S|\sin(1-n)t,\\ \frac{d^2z}{dt^2}&=-Az,\end{aligned}\right\} \quad (34)$$

where n is the mean motion of the sun ($n\cong 1/13$ for the unit value we chose) and

$$A=\frac{1-m_2/m_1}{\rho_1^3}+\frac{m_2/m_1}{(1-\rho_1)^3}. \quad (35)$$

We note also that for the unit value we chose $A\cong 6$. This system has a periodic solution in the form

$$\left.\begin{aligned}x&=p\cos(1-n)t,\\ y&=q\sin(1-n)t,\\ z&=0.\end{aligned}\right\} \quad (36)$$

For our purpose we need only a crude evaluation of the solution. We have approximately

$$p\cong\frac{1}{30}S,\qquad q\cong\frac{8}{30}S. \quad (37)$$

If we take $p\cong 20$ km we need a constant acceleration $|S|=4.2\times10^{-4}$ cm/sec.^{2}

5. Stabilization on the forced orbit

Now we go back to equation (23) and project it onto the reference system $\bar{\tau}_{(r)}$, taking the same unit value of time and length we used in the preceding section. We will have

$$\left.\begin{aligned}\ddot{x}-2\dot{y}&=[1+2A+a_{11}(t)]x+a_{12}(t)y+a_{13}(t)z-|S|\cos(1-n)t+X-\varphi_1(t),\\ \ddot{y}+2\dot{x}&=[1-A+a_{22}(t)]y+a_{21}(t)x+a_{23}(t)z+|S|\sin(1-n)t+Y-\varphi_2(t),\\ \ddot{z}&=[-A+a_{33}(t)]z+a_{31}(t)x+a_{32}(t)y+Z-\varphi_3(t).\end{aligned}\right\} \quad (34')$$

We added three distinct accelerations to the right-hand side. The first is the constant acceleration S we introduced in the previous section. The second is the result of a stabilizing control device; we suppose that this control device supplies the following acceleration:

$$\left.\begin{aligned} X&=-(1+2A+\delta_2^2)[x-p\cos(1-n)t]-\delta_1^2[\dot{x}+(1-n)p\sin(1-n)t],\\ Y&=-\beta_1^2[\dot{y}-(1-n)q\cos(1-n)t],\\ Z&=-\gamma_1^2\dot{z}. \end{aligned}\right\} \tag{38}$$

The coefficients are related to the intensity of the answer and the sensitivity of the instrumentation for detecting deviations from the prescribed motions. The third acceleration (φ_1, φ_2, φ_3) is the acceleration we need to ensure that equation (34′) still has the exact solution of equation (36). For this purpose the component must be

$$\varphi_i=a_{i1}(t)x+a_{i2}(t)y+a_{i3}(t)z+O_2^{(i)}(\mathbf{P^*P}), \tag{39}$$

where $O_2^{(i)}(\mathbf{P^*P})$ are the components of the accelerations that are two orders of magnitude smaller than those we put in $O_2(\mathbf{P^*P})$ in equation (23). We have

$$\{\sum\varphi_i^{(i)2}\}^{1/2}\leq|\Delta a|+O_2(\mathbf{P^*P}). \tag{40}$$

If we take into account equation (32) and we observe that in our case $i^*\leq 8°$, $\lambda^*\leq 1+3e$ (e is the eccentricity of the moon's orbit), we will have

$$|\Delta a|\leq 0.5|S|, \tag{41}$$

when the point P moves in the proposed orbit around L_1 in equation (36). No doubt, if we are able to achieve the accelerations in equations (34) and (35) to be added to the constant acceleration **S**, the satellite will be stable in the orbit in equation (36). The degree of stability is related to the coefficients δ_1, δ_2, β_1, γ_1 entering into the components X, Y, Z. We can use as much as 0.2 $|S|$ for the purpose of stabilization; this means (if $p=20$ km) 1×10^{-4} cm/sec^2. If we want to have a damping factor of 1 or more, we need a device capable of detecting a variation of 2 km/hr in the velocity—that is, a high-sensitivity device. In any event, we need to be able to detect a variation of 2 km in position to have a sufficiently good stabilization. Figure 1 gives a diagram of the acceleration needed to keep the satellite stable in the orbit in equation (36). The needed acceleration vectors have their origin at the point O; their ends are in the shaded region. The maximum angle between the direction mean sun-satellite and the required orientation is less than arc sin 7/10 or 45°. Therefore, it would be possible to obtain the acceleration we need from the solar pressure over a system of sails or flat orientable balloons that are linked to each other and to the satellite in such a way that the configuration can be altered from within the satellite.

To obtain a crude evaluation of the maximum extent of the surface needed to provide the required external force we shall proceed as follows. We suppose the satellite to be at the geometric center of a plane, orientable, reflecting surface. The maximum extent of the surface will be computed in such a way that the corresponding acceleration of the complex satellite-sail, due to the radiation pressure, is $1.8\cdot|S|$, when the normal **N** to the plane is parallel to the direction **SP**. If the orientation of the sail is changed so that **N** makes an angle $\theta\left(<\frac{\pi}{2}\right)$ with the direction **SP**, the acceleration will have the direction of **N** and its intensity will be $1.8\cdot|\mathbf{S}|\cdot\cos^2\theta$. Thus diminishing the extent of the surface and varying the orientation, we will be able to supply to the complex all the acceleration vectors with the ends inside the region bounded by the closed curve $OQRQ'O$ and therefore all the acceleration vectors with the ends inside the shadowed region. We can now evaluate the ratio A/m from the equation (Garwin, 1958; Sohn, 1959) $1.8|S|=0.8\times10^{-4}A/m$ in the c.g.s. system. If we assume, as before, that $p=20$ km we will find $A/m=9.5$. This means that for

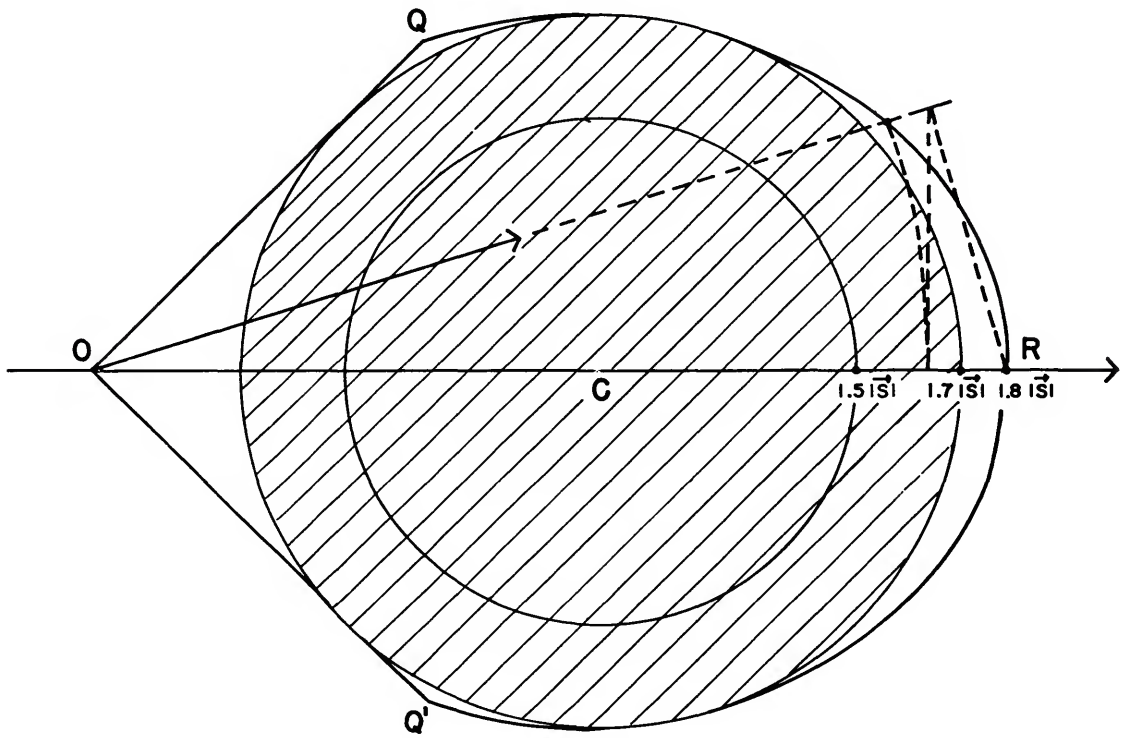

FIGURE 1.—Diagram of the accelerations.

a 200-kg satellite we need a maximum reflecting area of 19×10^5 cm^2 or 190 m^2. I think we are not very far from the actual possibility of achieving an automatic control device (including directional and positional sensors, computer, and servomechanism) that can arrange at any time the required configuration of the system of sails or flat balloons; the solar pressure over the complex will provide both the external force and the external torque needed for the adjustment of both the position and the direction of the complex.

We shall not discuss the technical questions involved, since this is not the purpose of the present study. Nor shall we discuss in detail the possibility of providing the same stabilization with very small rockets. The preceding sections make it clear that it would be possible to program the action of such rockets so that they could act from time to time for a short period, when the control device detects some variation in position and velocity, in such a way that the amount of consumed momentum is a minimum. However, to make this computation we need first a careful analysis of the gravitational motion of a nonsailed satellite around the libration point and, second, an exact evaluation of the sensitivity of the instrumentation.

6. Autonomous stabilization of a system of two points

Since we are considering only the theoretical possibilities, at least for the present, we should like to discuss one other method for stabilizing a satellite at the inferior conjunction point without consuming momentum. For simplicity, we shall deal with the classical restricted three-body problem; and to stay close to the problem of the preceding sections we shall use the same reference systems and the same unit values for the dimensions as in section 4. Let us consider the motion of two points $P_1(x_1, y_1, z_1)$ and $P_2(x_2, y_2, z_2)$ of equal mass, and suppose that P_1 and P_2 are constrained by the following holonomic constraint:

$$\mathbf{P_1P_2^2}=[a-b(x_1+x_2)^2]^2, \tag{42}$$

where (x_1+x_2) is the x coordinate of the center of mass G of the two bodies. To build this constraint we need only a position sensor and an internal device to change the distances between the points as necessary. We can change the exterior force that acts on the system by changing only (with the interior force) the distance P_1P_2. We will need only energy without loss of mass for the system.

Now we write the Lagrangian equations of motion of the system:

$$\left.\begin{aligned}
&\ddot{x}_1-2\dot{y}_1=(1+2A)x_1+\lambda(x_1-x_2)-4\lambda b(x_1+x_2)\{a-b(x_1+x_2)^2\}\\
&\ddot{x}_1-2\dot{y}_2=(1+2A)x_1+\lambda(x_2-x_1)-4\lambda b(x_1+x_2)\{a-b(x_1+x_2)^2\}\\
&\ddot{y}_1+2\dot{x}_1=(1-A)y_1+\lambda(y_1-y_2)\\
&\ddot{y}_1+2\dot{x}_2=(1-A)y_2+\lambda(y_2-y_1)\\
&\ddot{z}_1+A\dot{z}_1=\lambda(z_1-z_2)\\
&\ddot{z}_1+A\dot{z}_2=\lambda(z_2-z_1).
\end{aligned}\right\} \tag{43}$$

Let us consider the static solution,

$$\left.\begin{aligned}
&y_1=y_2=0,\\
&z_1=z_2=0,\\
&x_1=-x_2=\frac{a}{2},\\
&\lambda=-\frac{1+2A}{2}=\lambda^*,
\end{aligned}\right\} \tag{44}$$

and study the linear stability of the solution. We put

$$\left.\begin{aligned}
&x_1=\frac{a}{2}+\xi_1,\\
&x_2=-\frac{a}{2}+\xi_2,\\
&\lambda=\lambda^*+\lambda_1,
\end{aligned}\right\} \tag{45}$$

and we will obtain from equations (42) and (43) the following system:

$$\left.\begin{aligned}
&\xi_1-\xi_2=0,\\
&\ddot{\xi}_1-2\dot{y}_1=(1+2A)\xi_1-\frac{(1+2A)}{2}(\xi_1-\xi_2)+4\lambda^*ba(\xi_1+\xi_2),\\
&\ddot{\xi}_2-2\dot{y}_2=(1+2A)\xi_2-\frac{(1+2A)}{2}(\xi_2-\xi_1)+4\lambda^*ba(\xi_1+\xi_2),\\
&\ddot{y}_1+2\dot{\xi}_1=(1-A)y_1-\frac{(1+2A)}{2}(y_1-y_2),\\
&\ddot{y}_2+2\dot{\xi}_1=(1-A)y_2-\frac{(1+2A)}{2}(y_2-y_1),\\
&\ddot{z}_1+Az_1=-\frac{(1+2A)}{2}(z_1-z_2),\\
&\ddot{z}_1+Az_2=-\frac{(1+2A)}{2}(z_2-z_1).
\end{aligned}\right\} \tag{46}$$

It is very easy to see that if

$$4ab > 1, \tag{47}$$

we have linear stability.

It would be possible to study some nonholonomic constraint of the form $|P_1P_2| = f(P_1, P_2, \dot{P}_1, \dot{P}_2, t)$, which can give a more realistic and reliable stabilization device, by taking into account the actual possibility of detecting deviations in position and velocity as well as the time lag between the detection of the deviations and the suitable variation of the distance computed and accomplished by the interior mechanisms. To gain an idea of the reliability of the stabilization complex, we will suppose $a = 10$ km. This means $a = 10/380000$ and, from equation (47), we need $b > 9500$. If we choose $b = 19000$, for a displacement of G in the x-direction of 1 km we need to vary the distance P_1P_2 from 10 km to 9.5 km. Obviously, we need a highly sensitive control complex. It is interesting to note that it is possible, in principle, to change the exterior gravitational force acting on the complex by using only an interior force and information from outside.

References

In this bibliography are to be found references to all the literature cited in the various papers of this volume.

ALLEN, C. W.
1957. Astrophysical quantities. Athlone Press, New York.

BATES, D. R.
1951. The temperature of the upper atmosphere. Proc. Phys. Soc., London, ser. B, vol. 64, pp. 805–821.

BELETSKY, V. V.
1960. Motion of an artificial earth satellite about its center of mass. *In* L. V. Kurnosova, ed., Artificial earth satellites, vol. 1, Plenum Press, New York, pp. 30–54.

BENNETT, A. A.; MILNE, W. E.; AND BATEMAN, H.
1956. Numerical integration of differential equations. Dover Publications, Inc., New York.

BRIGGS, R. E.
1959. A table of the times of perigee passage for Satellite 1958 $\beta 2$. Smithsonian Astrophys. Obs. Spec. Rep. 30, pp. 9–12.

BROUWER, D.
1959. Solution of the problem of artificial satellite theory without drag. Astron. Journ., vol. 64, pp. 378–397.

BROWN, E. W., AND SHOOK, C. A.
1933. Planetary theory. Cambridge University Press, Cambridge.

BURKE, B. F., AND FRANKLIN, K. L.
1955. Observation of a variable radio source with the planet Jupiter. Journ. Geophys. Res., vol. 60, pp. 213–217.

CHAPMAN, S.
1957. Notes on the solar corona and terrestrial ionosphere. Smithsonian Contr. Astrophys., vol. 2, pp. 1–12.

CHARLIER, C. V. L.
1927. Die Mechanik des Himmels, 2nd ed. W. de Gruyter Co., Leipzig, vol. 1.

COLOMBO, G.
1960. Sui satelliti del sistema terra-luna. Rendiconti Accad. Naz. Lincei, ser. 8, vol. 28, pp. 169–172.
1961. The motion of Satellite 1958 Epsilon around its center of mass. Smithsonian Astrophys. Obs. Spec. Rep. 70. [Included in the present volume, pp. 149–164.]

COOK, G. E.
1959. Aerodynamic drag of near earth satellites. Royal Aircraft Establishment (Farnborough), Tech. Note No. G.W. 531, 46 pp.

CORNFORD, E. C.
1958. A comparison of orbital theory with observations made in the United Kingdom on the Russian satellites. Royal Aircraft Establishment (Farnborough), 25 pp.

DAVIES, R. D.
1954. An analysis of bursts of solar radio emission and their association with solar and terrestrial phenomena. Monthly Notices Roy. Astron. Soc., London, vol. 114, pp. 74–92.

DAVIS, E. L., and STEIN, J. G.
1960. A description of a near earth satellite orbit computation program using oblate spheroidal coordinates. Interim Tech. Rep. No. 1, Georgia Inst. Technology.

ELWERT, G.
1956. Rontgenstrahlung Koronaler Kondensationen. Zeitschr. Astrophys., vol. 41, pp. 67–83.

FISCHELL, R. E.
1961. Magnetic and gravity attitude stabilization of earth satellites. Proc. COSPAR Space Symposium, Florence, April 1961, North-Holland Publishing Co., Amsterdam, pp. 373–410.

GARFINKEL, B.
1959. The orbit of a satellite of an oblate planet. Astron. Journ., vol. 64, pp. 353–357.

GARWIN, R. L.
1958. Solar sailing—a practical method of propulsion within the solar system. Jet Propulsion, vol. 28, pp. 188–190.

GRAHAM, E. A.; GROSSI, M. D., STROM, K.; and STROM, S.
1960. Final report on propagation of short and medium short e.m. waves above and in the neighborhood of the ionospheric layer of maximum electron density. Satellite Communication Study, BR–1095, Raytheon Co., Missiles Systems Division, Bedford, Mass.

GROVES, G. V.
1958. Effect of the earth's equatorial bulge on the lifetime of artificial satellites and its use in determining atmospheric scale heights. Nature, vol. 181, p. 1055.
1961. Correlation of upper atmosphere air density with geomagnetic activity, November 1960. Space Research II, North-Holland Publishing Co., Amsterdam.

HADDOCK, F. T.
1960. Radio astronomy observation from space. Journ. Amer. Rocket Soc., vol. 30, pp. 598–602.

HASELGROVE, C. B., HASELGROVE, J., and JENNISON, R. C.
1961. Ray paths from a cosmic radio source to a satellite in orbit. Proc. Roy. Soc., London, vol. 261, pp. 423–434.

HASELGROVE, J.
1955. Ray theory and a new method for ray tracing. *In* The physics of the ionosphere, The Physical Society, London, pp. 355–364.

HERBSTREIT, J. W., AND JOHLER, J. R.
1948. Frequency variation of the intensity of cosmic radio noise. Nature, vol. 161, pp. 515–516.

HILDEBRAND, F. B.
1956. Introduction to numerical analysis. McGraw-Hill Book Co., New York.

HOSFELD, R.
1954. Comparisons of stellar scintillation with image motion. Journ. Opt. Soc. Amer., vol. 44, pp. 284–288.

JACCHIA, L. G.
1955. On the numerical integration of functions tabulated in logarithmic form. Mathematical Tables and Other Aids to Computation, vol. 9, pp. 63–65.
1958a. Basic orbital data for Satellite 1957 β1. Smithsonian Astrophys. Obs. Spec. Rep. 9; Smithsonian Contr. Astrophys., vol. 2, pp. 285–286.
1958b. Erratic orbital acceleration of 1957 Beta. Sky and Telescope, vol. 17, p. 278.
1958c. Orbital results for Satellite 1957 β1. Smithsonian Astrophys. Obs. Spec. Rep. 13, pp. 1–8. [Included in the present volume, pp. 1–4.]
1958d. Program for determination of geographic sub-satellite points. Smithsonian Astrophys. Obs. Spec. Rep. 11, pp. 26–27.
1958e. Satellite 1957 Beta. Harvard Coll. Obs., Announcement Cards 1391–1392.
1958f. The secular perturbations and the orbital acceleration of Satellite 1958 β2. Smithsonian Astrophys. Obs. Spec. Rep. 12, pp. 25–28.
1959a. Atmospheric fluctuations of solar origin revealed by satellites. Harvard Coll. Obs., Announcement Card 1423.
1959b. Corpuscular radiation and the acceleration of artificial satellites. Nature, vol. 183, pp. 1662–1663.
1959c. The diurnal effect in the orbital acceleration of Satellite 1957 β1. Smithsonian Astrophys. Obs. Spec. Rep. 20, pp. 5–8.[Included in the present volume, pp. 29–30.]
1959d. Solar effects on the acceleration of artificial satellites. Smithsonian Astrophys. Obs. Spec. Rep. 29, pp. 1–15. [Included in the present volume, pp. 55–66.]
1959e. Two atmospheric effects in the orbital acceleration of artificial satellites. Nature, vol. 183, pp. 526–527.
1960a. A variable atmospheric-density model from satellite accelerations. Smithsonian Astrophys. Obs. Spec. Rep. 39; Journ. Geophys. Res., vol. 65, pp. 2775–2782.
1960b. The effect of a variable scale height on determinations of atmospheric density from satellite accelerations. Smithsonian Astrophys. Obs. Spec. Rep. 46, pp. 1–4. [Included in the present volume, pp. 77–80.]
1961. The atmospheric drag of artificial satellites during the October 1960 and November 1960 events. Smithsonian Astrophys. Obs. Spec. Rep. 62. [Included in the present volume, pp. 133–138.]

JACCHIA, L. G., AND BRIGGS, R. E.
1958. Orbital accelerations of Satellite 1958 β2. Smithsonian Astrophys. Obs. Spec. Rep. 18, pp. 9–12. [Included in the present volume, pp. 13–16.]

JASTROW, R., AND BRYANT, R.
1960. Variations in the orbit of the Echo satellite. Journ. Geophys. Res., vol. 65, pp. 3512–3513.

JEFFREYS, H.
1941. The determination of the Earth's gravitational field. Monthly Notices Roy. Astron. Soc., Geophys. Suppl., vol. 5, pp. 1–22.
1943. The determination of the Earth's gravitational field. Second paper. Monthly Notices Roy. Astron. Soc., Geophys. Suppl., vol. 5, pp. 55–66.
1959. The Earth, 4th ed. Cambridge University Press, Cambridge.

KALLMAN-BIJL, H. K.; BOYD, R. F. L.; LAGOW, H.; POLOSKOV, S. M.; AND PRIESTER, W.
1961. COSPAR International Reference Atmosphere (CIRA, 1961). North-Holland Publishing Co., Amsterdam.

KING-HELE, D. G.
1959. Density of the atmosphere at heights between 200 km and 400 km, from analysis of artificial satellite orbits. Nature, vol. 183, pp. 1224-1227.

KING-HELE, D. G.; COOK, G. E.; AND WALKER, D. M. C.
1959. Contraction of satellite orbits under the influence of air drag, Part 1. Royal Aircraft Establishment (Farnborough), Tech. Note No. G.W. 533.

KING-HELE, D. G., AND WALKER, D.M.C.
1961. Upper-atmosphere density during the years 1957 to 1961 determined from satellite orbits. Proc. COSPAR Space Symposium, Florence, April 1961, North-Holland Publishing Co., Amsterdam, p. 918.

KLEMPERER, W. B., AND BENEDIKT, E. T.
1958. Selenoid satellites. Astron. Acta, vol. 4, pp. 25–30.

KOZAI, Y.
1959a. The earth's gravitational potential derived from the motion of Satellite 1958 $\beta 2$. Smithsonian Astrophys. Obs. Spec. Rep. 22, pp. 1–6. [Included in the present volume, pp. 51–54.]
1959b. The motion of a close earth satellite. Astron. Journ., vol. 64, pp. 367–377.
1959c. On the effects of the sun and the moon upon the motion of a close earth satellite. Smithsonian Astrophys. Obs. Spec. Rep. 22, pp. 7–10. [Included in the present volume, pp. 47–50.]
1961a. Effects of solar radiation pressure on the motion of an artificial satellite. Smithsonian Astrophys. Obs. Spec. Rep. 56, pp. 25–33. [Included in the present volume, pp. 109–112.]
1961b. The gravitational field of the earth derived from the motion of three satellites. Astron. Journ., vol. 66, pp. 8–10.
1961c. Tesseral harmonics of the potential of the earth as derived from satellite motions. Smithsonian Astrophys. Obs. Spec. Rep. 72.
1962. Numerical results from orbits. Smithsonian Astrophys. Obs. Spec. Rep. 101.

KUIPER, G., ED.
1952. The atmospheres of the earth and planets. University of Chicago Press, Chicago.
1954. The earth as a planet. University of Chicago Press, Chicago.

LASSOVSZKY, K.
1960. The catalogue of precise satellite positions. Smithsonian Astrophys. Obs. Spec. Rep. 41.

LUNDBACK, A.
1961. Atmospheric properties up to 500 km concluded from circular satellite orbits. Publikationer fra Det Danske Meteorologiske Institut, Meddelelser No. 14, pp. 1–17.

LUNDQUIST, C. A.; NAUMANN, R. J.; AND FIELDS, S. A.
1961. Recovery of further data from 1958 Epsilon. Proc. COSPAR Space Symposium, Florence, April 1961, North-Holland Publishing Co., Amsterdam, pp. 520–534.

LUNEBERG, R. K.
1944. Mathematical theory of optics. Brown University, Providence.

MARTIN, H. A.; NEVELING, G. W.; PRIESTER, W.; AND ROEMER, M.
1961. Model of the upper atmosphere from 130 through 1600 km, derived from satellite orbits. Proc. COSPAR Space Symposium, Florence, April 1961, North-Holland Publishing Co., Amsterdam, p. 902.

MINZNER, R. A., AND RIPLEY, W. S.
1956. The ARDC model atmosphere, 1956. Air Force Surveys in Geophys., No. 86, Geophys. Res. Dir., AFCRC, ARDC.

MOULTON, F. R.
1914. An introduction to celestial mechanics, 2nd ed. Macmillan Co., New York.

MUSEN, P.
1959. Application of Hansen's theory to the motion of an artificial satellite in the gravitational field of the earth. Journ. Geophys. Res., vol. 64, pp. 2271–2279.
1960. The influence of the solar radiation pressure on the motion of an artificial satellite. Journ. Geophys. Res., vol. 65, pp. 1391–1396.

MUSEN, P.; BRYANT, R.; AND BAILIE, A.
1960. Perturbations in perigee height of Vanguard I. Science, vol. 131, pp. 935–936.

NAUMANN, R. J.
1961. Directional dependence of counting rates from Explorer IV. Paper presented at the Argus Conference, Stanford Research Institute, Menlo Park, Calif., Jan. 17–20.

NICOLET, M.
1954. Dynamic effects in the high atmosphere. *In* G. P. Kuiper, ed., The earth as a planet, University of Chicago Press, Chicago, chap. 13, pp. 644–712.
1958a. Pennyslvania State Univ., Ionosphere Res. Lab., Scientific Rep. No. 102.
1958b. High atmosphere densities. Science, vol. 127, p. 1317.
1960a. Les variations de la densité et du transport de chaleur par conduction dans l'atmosphère supérieure. Centre National de Recherches de l'Espace, Bruxelles, Notes Préliminaires No. 5.
1960b. The properties and constitution of the upper atmosphere. *In* J. A. Ratcliffe, ed., The physics of the upper atmosphere, Academic Press, New York, chap. 2, pp. 17–71.

1960c. Structure of the thermosphere. Ionosphere Res. Lab., Pennsylvania State Univ., Scientific Rep. No. 134; Planetary and Space Sci., vol. 5, 1961, pp. 1–32.

1961a. Helium, an important constituent in the lower exosphere. Journ. Geophys. Res. vol. 66, pp. 2263–2264.

1961b. Les modèles atmosphériques et l'hélium. Proc. COSPAR Space Symposium, Florence, April 1961, North-Holland Publishing Co., Amsterdam, p. 896.

NOTNI, P., AND OLEAK, H.

1959. Die Bewegung eines rotierenden zylinderförmigen Satelliten in der Atmosphäre (Part I). Veröff. Sternw. Babelsberg, vol. 13, no. 3, 30 pp.

1960. Die Bewegung eines rotierenden zylinderförmigen Satelliten in der Atmosphäre (Part II). Veröff. Sternw. Babelsberg, vol. 13, no. 5, 45 pp.

O'KEEFE, J. A., AND ECKELS, A.

1958. Satellite 1958 β2. Harvard Coll. Obs., Announcement Card 1420.

O'KEEFE, J. A.; ECKELS, A.; AND SQUIRES, R. K.

1959. The gravitational field of the earth. Astron. Journ., vol. 64, pp. 245–253.

O'KEEFE, J. A.; HERTZ, H. G.; AND MARCHANT, M.

1958. Oblateness of the earth by artificial satellites. Harvard Coll. Obs., Announcement Card 1408.

PARKINSON, R. W.; JONES, H. M.; AND SHAPIRO, I. I.

1960. Effects of solar radiation pressure on earth satellite orbits. Science, vol. 131, pp. 920–921.

PIDDINGTON, J. H.

1951. The origin of galactic radio-frequency radiation. Monthly Notices Roy. Astron. Soc., vol. 111, pp. 45–63.

PRIESTER, W.

1958. Communication from Univ. Obs., Bonn, Germany, dated Dec. 18.

PRIESTER, W., AND MARTIN, H. A.

1960. Solare und tageszeitliche Effekte in der Hochatmosphäre aus Beobachtungen küntslicher Erdsatelliten. Mitt. Universitäts-Sternwarte Bonn, No. 29, 53 pp.

RALSTON, A., AND WILF, H. S.

1960. Mathematical methods for digital computers. John Wiley and Sons, New York.

RÖMER, M.

1961. Modell der Exosphäre im Höhenbereich 1000–1700 km berechnet aus den Bahnänderungen des Satelliten Echo I. Mitt. Universitäts-Sternwarte Bonn, No. 37, pp. 1–34.

SCHILLING, G. F., AND WHITNEY, C. A.

1958. Atmospheric densities from Explorer IV. Smithsonian Astrophys. Obs. Spec. Rep. 18.

SHAPIRO, I. I., AND JONES, H. M.

1960. Perturbations of the orbit of the Echo balloon. Science, vol. 132, pp. 1484–1486.

1961. Loss of mass in Echo satellite. Science, vol. 133, p. 579.

SIRY, J. W.
1960. Atmospheric densities at altitudes up to 750 kilometers obtained from analysis of satellite observations. Paper presented at the CSAGI meeting, Moscow, July 1958. Ann. IGY, vol. 12, part 1, p. 289.

SMART, W. M.
1953. Celestial mechanics. Longmans, Green and Co., London.

SOHN, R. L.
1959. Attitude stabilization by means of solar radiation pressure. Journ. Amer. Rocket Soc., vol. 29, pp. 371–373.

SPITZER, L.
1952. The terrestrial atmosphere above 300 km. *In* G. Kuiper, ed., The atmospheres of the earth and planets, University of Chicago Press, Chicago, pp. 211–247.

STACKEL, P.
1891. Veber die Integration der Hamilton-Jacobi'schen Differentialgleichung mittels Separation der Variabeln. Habilitationsschrift, Halle.

STERNE, T. E.
1958a. An atmospheric-density model, and some remarks on the inference of density from the orbit of a close earth satellite. Astron. Journ., vol. 63, pp. 81–87.
1958b. Formula for inferring atmospheric density from the motion of artificial earth satellites. Science, vol. 127, p. 1245.
1958c. High altitude atmospheric density. *In* The physics of fluids, vol. 1, p. 165.
1959. Effect of the rotation of a planetary atmosphere upon the orbit of a close satellite. Journ. Amer. Rocket Soc., vol. 29, pp. 777–782. [Abstract *in* Astron. Journ., vol. 64, p. 54.]

STERNE, T. E.; FOLKART, B.M.; AND SCHILLING, G. F.
1957. An interim model atmosphere fitted to preliminary densities inferred from USSR satellites. Smithsonian Astrophys. Obs. Spec. Rep. 7; Smithsonian Contr. Astrophys., vol. 2, pp. 275–279.

STIRTON, R. J.
1960. The upper atmosphere and satellite drag. Smithsonian Contr. Astrophys., vol. 5, pp. 9–15.

STRUBEL, R. A.
1960. The geometry of the orbits of artificial satellites. North Carolina State College, Tech. Memo. ERD 106/4.

VINTI, J. P.
1959. New method of solution for unretarded satellite orbits. Journ. Research Nat. Bur. Standards, vol. 63B, pp. 105–116.

WATSON, G. N.
1944. A treatise on the theory of Bessel functions, 2nd ed. The Macmillan Co., New York, pp. 698–713.

WHITNEY, C. A.
1958. The orbit and variable acceleration of Satellite 1958 Alpha. Smithsonian Astrophys. Obs. Spec. Rep. 11, pp. 14–17.
1959. The structure of the high atmosphere. I. Linear models. Smithsonian Astrophys. Obs. Spec. Rep. 21, pp. 1–12. [Included in the present volume, pp. 35–42.]

WHITTAKER, E. T.
1959. A treatise on the analytical dynamics of particles and rigid bodies, 4th ed. Cambridge University Press, Cambridge.

WHITTAKER, E. T., AND WATSON, G. N.
1958. A course of modern analysis, 4th ed. Cambridge University Press, Cambridge, Chapter XXII, p. 491.

WONG, M. S.
1960. Ionospheric ray tracing with an analogue computer. *In* M. Desirant and J. L. Michiels, ed., Electromagnetic wave propagation, Academic Press, New York, pp. 37–48.

WYATT, S. P.
1959. Solar effects in the motion of Vanguard. Nature, vol. 184, pp. 351–352.

ZADUNAISKY, P. E.
1960. The orbit of Satellite 1958 $\alpha 1$ (Explorer I) during the first 10500 revolutions. Smithsonian Astrophys. Obs. Spec. Rep. 50, 28 pp.
1961. Atmospheric drag on non-spherical artificial satellites. Smithsonian Astrophys. Obs. Spec. Rep. 65.

ZADUNAISKY, P. E.; SHAPIRO, I. I., AND JONES, H. M.
1961. Experimental and theoretical results on the orbit of Echo I. Smithsonian Astrophys. Obs. Spec. Rep. 61, 22 pp. [Included in the present volume, pp. 125–132.]

ZHONGOLOVITCH, I. D.
1952. The external gravitational field of the earth and the fundamental constants connected with it. Trudy Inst. Theor. Astron., Moscow, vol. 3, pp. 1–126. [In Russian.]
1957. Gravitational potential of the earth. Bull. Inst. Theor. Astron., Moscow, vol. 6, pp. 505–523. [In Russian.]

Special Reports of the Smithsonian Astrophysical Observatory

Numbers 1 through 113

No.	*Date*	*Title*	*Author*
1	October 14, 1957 (reissued December 2, 1957)	*Preliminary Orbit Information for USSR Satellites Alpha One and Alpha Two	G. F. Schilling and T. E. Sterne
2	November 5, 1957	*Additional Orbit Information for USSR Satellites 1957 Alpha One and Beta One	J. S. Rinehart and G. F. Schilling
3	November 15, 1957	*Some Preliminary Values of Upper Atmosphere Density from Observations of USSR Satellites	T. E. Sterne and G. F. Schilling
4	November 30, 1957	*Glossary of Astronomical Terms for the Description of Satellite Orbits	J. Ashbrook, G. F. Schilling, and T. E. Sterne
5	December 4, 1957	*Soviet Orbit Predictions and Orbital Information for USSR Satellites 1957 Alpha One, Alpha Two and Beta	G. F. Schilling and E. S. Fergusson
6	December 17, 1957	*Visual Observations of Alpha One Made by Moonwatch Stations During Lifetime of the Object	L. Campbell, Jr. and J. A. Hynek
7	December 31, 1957	*An Interim Model Atmosphere Fitted to Preliminary Densities Inferred from USSR Satellites	T. E. Sterne, B. M. Folkart, and G. F. Schilling
8	January 31, 1958	*Soviet Orbit Information for USSR Satellites 1957 Alpha Two and Beta One	G. F. Schilling
9	February 21, 1958	*Basic Orbital Data for Satellite 1957 Beta One	L. G. Jacchia
10	March 1, 1958	*Processed Observational Data for USSR Satellites 1957 Alpha and 1957 Beta	R. M. Adams, N. McCumber, and M. Brinkman
11	March 31, 1958	Status Reports on Optical Observations of Satellites 1958 Alpha and 1958 Beta	G. F. Schilling, ed.
		Preliminary Results from Optical Tracking of the U.S. Earth Satellites	J. A. Hynek and F. L. Whipple

*Reprinted in Smithsonian Contributions to Astrophysics, vol. 2, no. 10, 1958.

636-014—63——16

No.	Date	Title	Author
11 (cont'd.)		*Optical Satellite Observations*	
		The Network of Precision Photographic Satellite Tracking Stations	K. G. Henize
		Moonwatch Observations of Satellites 1958 Alpha, 1958 Beta and 1958 Gamma	L. Campbell, Jr.
		Scientific Results	
		The Orbit and Variable Acceleration of Satellite 1958 Alpha	C. A. Whitney
		The Density of the Upper Atmosphere	T. E. Sterne
		Life Expectancy of Satellite 1958 Alpha	L. G. Jacchia
		Use and Distribution of Satellite Predictions	R. M. Adams
		Program for Determination of Geographic Sub-Satellite Points	L. G. Jacchia
		Predictions for Crossings of Given Latitude Parallels—APO Ephemeris 5	J. Gaustad
		Predictions for Photographic Satellite Tracking Stations—APO Ephemeris 4	C. H. Moore and D. A. Lautman
		Program of Spot Predictions for Specifying Observing Sites—APO Ephemeris 3	R. Briggs
		Charts of Predicted Satellite Positions	J. B. Fairman and G. Veis
		Harvard Announcement Cards	
12	April 30, 1958 (reissued August 20, 1959)	Miscellaneous Information on the Artificial Earth Satellites	J. A. Hynek and G. F. Schilling, eds.
		The U.S.S.R. Satellites	
		Soviet Orbit Information for Satellite 1957 Beta	J. B. Clarke and D. L. O'Hara
		Moonwatch Observations of the Fall of Satellite 1957 Beta One	E. P. Bullis and L. Campbell, Jr.
		A Precision Measurement of the Brightness of Satellite 1957 Alpha One	G. S. Hawkins
		Note on the Mass-Area Ratios of the U.S.S.R. Satellites	G. F. Schilling and J. S. Rinehart
		The U.S. Satellites	
		Moonwatch Catalogue	E. P. Bullis and L. Campbell, Jr.

No.	*Date*	*Title*	*Author*
12	(cont'd.)	The Acceleration of Satellites 1958 Alpha and Gamma	C. A. Whitney
		The Secular Perturbations and Orbital Acceleration of Satellite 1958 Beta Two	L. G. Jacchia
		Improvements in the Prediction Program for Crossings of Given Latitude Parallels	R. M. Adams
		Satellite Characteristics and Scientific Results	
		Densities of the Upper Atmosphere Derived from Satellite Observations	G. F. Schilling and T. E. Sterne
		Technical Parameters of the Artificial Satellites	G. F. Schilling
13	May 21, 1958 (reissued December 1, 1959)	*Orbital Results for Satellite 1957 Beta One	L. G. Jacchia
14	July 15, 1958	*Reports and Analyses of Satellite Observations*	G. F. Schilling, ed.
		Moonwatch Catalogue—May through June 1958	E. P. Bullis and L. Campbell, Jr.
		Status of the Photographic Satellite Tracking System	K. G. Henize
		Timing Satellite Observations	R. J. Davis
		Preliminary Note on the Mass-Area Ratios of Satellites 1958 $\delta 1$ and 1958 $\delta 2$	G. F. Schilling, C. A. Whitney, and B. M. Folkart
15	July 20, 1958 (reissued March 28, 1960)	*The Descent of Satellite 1957 Beta One	L. G. Jacchia
16	July 25, 1958	Positions of Satellite 1957 Beta One During the First 100 Revolutions	R. M. Adams, R. E. Briggs, and E. K. L. Upton
17	September 5, 1958 (out of print)	Positions of Satellite 1958 Alpha During the First 1400 Revolutions	R. G. Teske
18	October 4, 1958	*Satellite Data and Analyses*	G. F. Schilling, ed.
		Technical Parameters of Satellites 1958 Delta and 1958 Epsilon	J. B. Clarke
		Communications Center of the Optical Satellite Tracking Program	C. M. Peterson
		*Orbital Acceleration of Satellite 1958 Beta Two	L. G. Jacchia and R. E. Briggs
		Atmospheric Densities from Explorer IV	G. F. Schilling and C. A. Whitney
		Moonwatch Catalogue—July and August, 1958	E. P. Bullis and L. Campbell, Jr.

*Reprinted in Smithsonian Contributions to Astrophysics, vol. 6, 1963.

No.	*Date*	*Title*	*Author*
19	December 6, 1958	*The Earth's Gravitational Potential as Derived from Satellites 1957 Beta One and 1958 Beta Two	L. G. Jacchia
		A Satellite Meteor-Trap	G. S. Hawkins
		*A Flashing Satellite for Geodetic Studies	C. A. Whitney and G. Veis
		Operational Information	
20	January 5, 1959	*An Empirical Formula for Satellite Ephemerides Near the End of Their Lifetime	L. G. Jacchia
		*The Diurnal Effect in the Orbital Acceleration of Satellite 1957 Beta One	L. G. Jacchia
		Progress Report on the Planning of an Artificial Satellite Containing an Astronomical Telescope	R. J. Davis
		A Suggested Rocket Experiment for Determination of Atmospheric Densities and Winds at Extreme Heights	R. E. McCrosky
		Operational Information	
		Moonwatch Catalogue—September 1958	E. P. Bullis and L. Campbell, Jr.
21	February 27, 1959	*The Structure of the High Atmosphere—I. Linear Models	C. A. Whitney
		Moonwatch Catalogue—October, November and December, 1958	
		Operational Information	
22	March 20, 1959 (reissued March 3, 1961)	*The Earth's Gravitational Potential Derived from the Motion of Satellite 1958 Beta Two	Y. Kozai
		*On the Effects of the Sun and the Moon upon the Motion of a Close-Earth Satellite	Y. Kozai
23	March 30, 1959	The Orbit of Satellite 1958 Zeta	G. Veis
24	April 9, 1959	Catalogue of Satellite Observations for January and February 1959	R. G. Albert and R. M. Adams
25	April 20, 1959 (reissued May 5, 1961)	*The Structure of the High Atmosphere II. A Conduction Model	C. A. Whitney
26	May 21, 1959	Catalogue of Satellite Observations for March and April 1959	R. G. Albert and R. M. Adams
27	June 30, 1959	An Iterative Method of Orbit Determination from Three Observations of a Nearby Satellite	R. E. Briggs and J. W. Slowey
		Determination of the Orbit of Satellite 1958 Beta One	A. S. Leonard

*Reprinted in Smithsonian Contributions to Astrophysics, vol. 6, 1963.

No.	*Date*	*Title*	*Author*
27	(cont'd.)	Cumulative Table of Contents, Special Report Numbers 11 through 27	
28	September 16, 1959	Catalogue of Satellite Observations for May and June 1959	R. G. Albert
28A	September 23, 1959	Catalogue of Satellite Observations: Addenda and Corrigenda, Station Coordinate Lists	
29	September 21, 1959	*Solar Effects on the Acceleration of Artificial Satellites	L. G. Jacchia
30	November 12, 1959	*Anticipated Orbital Perturbations of Satellite 1959 Delta Two	Y. Kozai and C. A. Whitney
		A Table of the Times of Perigee Passage for Satellite 1959 Beta Two	R. E. Briggs
		*Note on the Secular Motions of the Node and Perigee of an Artificial Satellite	Y. Kozai
31	January 18, 1960	Catalogue of Satellite Observations for July and August 1959	R. G. Albert
		Osculating Elements	Y. Kozai
32	January 29, 1960	Catalogue of Satellite Observations	R. G. Albert
33	February 1, 1960	*On the Effects of Image Motion on the Accuracy of Measurement of a Flashing Satellite	J. A. Hynek
34 (C-8)	February 2, 1960	Catalogue of Observations of Satellite 1958 $\delta 2$ for the Period August 1–22, 1959	R. G. Albert
35 (C-9)	February 5, 1960	Catalogue of Observations of Satellite 1958 $\delta 2$ for the Period August 23–31, 1959	R. G. Albert
36 (C-10)	February 8, 1960	Catalogue of Additional Observations of Satellite 1958 $\delta 2$ for the Period May 1–May 29, 1959	R. G. Albert
37 (C-11)	February 10, 1960	Catalogue of Observations of Satellites 1958 $\delta 2$, 1958 Epsilon, and 1958 Zeta	R. G. Albert
38	January 15, 1960	Orbit Determination from Simultaneous Doppler-Shift Measurements	I. G. Izsak
39	March 30, 1960 (reissued January 30, 1961)	A Variable Atmospheric-Density Model from Satellite Accelerations	L. G. Jacchia
40R	May 24, 1960 (revised June 30, 1960)	Orbital Elements for July and August, 1959	
		Satellite 1958 Alpha	B. Miller
		Satellites 1958 $\beta 1$ and $\beta 2$	C. A. Martin
		Satellite 1958 $\delta 2$	Y. Kozai
		Satellites 1959 $\alpha 1$ and $\alpha 2$	R. C. Nigam
		Satellite 1958 Gamma	I. G. Izsak
		Relative Positions of the Sun and Perigee of an Artificial Earth Satellite	P. E. Zadunaisky

*Reprinted in Smithsonian Contributions to Astrophysics, vol. 6, 1963.

No.	*Date*	*Title*	*Author*
41	May 25, 1960 (out of print)	The Catalogue of Precise Satellite Positions	K. Lassovszky
		Preliminary Time Reduction for the Determination of Precise Satellite Positions	E. Weston
		The Star Chart Project	P. A. Pardue
		Explanation of Codes Used in the Catalogue	E. P. Bullis
		Shutter Correction in Time for the Baker-Nunn Camera	P. E. Zadunaisky
42 (C–12)	May 25, 1960	Catalogue of Satellite Observations	D. V. Mechau
43 (C–13)	May 25, 1960	Catalogue of Satellite Observations	D. V. Mechau
44 (C–14)	May 25, 1960	Catalogue of Satellite Observations	D. V. Mechau
45	July 11, 1960	List of Coordinates of Stations Engaged in the Observation of Artificial Satellites	D. V. Mechau
46	July 11, 1960	*The Effect of a Variable Scale Height on Determinations of Atmospheric Density from Satellite Accelerations	L. G. Jacchia
		Comment on the Paper Entitled "Symmetry of the Earth's Figure"	C. A. Whitney
47 (C–15)	September 9, 1960	Catalogue of Satellite Observations	D. V. Mechau
48 (C–16)	September 9, 1960	Catalogue of Satellite Observations	D. V. Mechau
49 (C–17)	September 9, 1960	Catalogue of Satellite Observations	D. V. Mechau
50	October 3, 1960	The Orbit of Satellite 1958 Alpha (Explorer I) During the First 10,500 Revolutions	P. E. Zadunaisky
51	October 17, 1960	Satellite Orbital Data	D. V. Mechau
		Satellites 1958 β1 and 1958 β2	B. Miller
		Satellites 1958 δ2 and 1959 ι1	Y. Kozai
		On the Orbital Elements of Satellite 1959 ι1	Y. Kozai
52	November 21, 1960	*A Theory of Satellite Motion About an Oblate Planet: I. A Second-Order Solution of Vinti's Dynamical Problem	I. G. Izsak
53	December 5, 1960	The Orbits and the Accelerations of Satellites 1959 α1 and 1959 α2	R. C. Nigam

*Reprinted in Smithsonian Contributions to Astrophysics, vol. 6, 1963.

No.	*Date*	*Title*	*Author*
54 (C–18)	December 19, 1960	Catalogue of Satellite Observations: Satellite 1958 Alpha, 1958 $\beta 1$, 1958 $\beta 2$, 1958 $\delta 2$, 1958 Epsilon, for June 1–Aug. 31, 1960	D. V. Mecahu
55 (C–19)	December 19, 1960	Catalogue of Satellite Observations: Satellites 1959 $\alpha 1$, 1959 $\alpha 2$, 1959 Eta, 1959 $\iota 1$, for June 1–Aug. 31, 1960	D. V. Mechau
56	January 30, 1961	A Method of Analysis for Lens and Mirror Systems	R. J. Davis, S. E. Strom, and K. M. Strom
		A Determination of the Ellipticity of the Earth's Equator From the Motion of Two Satellites	I. G. Izsak
		Effects of Solar Radiation Pressure on the Motion of an Artificial Satellite	Y. Kozai
57 (C–20)	March 3, 1961	Catalogue of Satellite Observations: Satellites 1960 $\beta 1$ (carrier rocket Tiros I), for Apr. 1–June 1, 1960; 1960 $\beta 2$ (Tiros I), for Apr. 2–Aug. 31, 1960; 1960 $\gamma 1$ (carrier rocket, Transit 1B), for Apr. 13–June 3, 1960; 1960 $\gamma 2$ (Transit 1B) for Apr. 14–July 25, 1960	D. V. Mechau
58 (C–21)	March 3, 1961	Catalogue of Satellite Observations: Satellites 1960 $\iota 1$ (Echo I), and 1960 $\iota 2$ (carrier rocket, Echo I), for Aug. 12–Aug. 31, 1960	D. V. Mechau
59	March 3, 1961	The Positions of the Baker-Nunn Camera Stations	G. Veis
60	March 10, 1961	*The Effect of Radiation Pressure on the Secular Acceleration of Satellites	S. P. Wyatt
61	March 20, 1961	*Experimental and Theoretical Results on the Orbit of Echo I	P. E. Zadunaisky, I. I. Shapiro, and H. M. Jones
62	May 26, 1961	*The Atmospheric Drag of Artificial Satellites During the October 1960 and November 1960 Events	L. G. Jacchia
63	May 29, 1961	*Effect of the Diurnal Atmospheric Bulge on Satellite Accelerations	S. P. Wyatt
64	July 7, 1961	The Revised Orbit of Satellite 1958 Zeta	R. C. Nigam
65	July 14, 1961	Atmospheric Drag on Non-Spherical Artificial Satellites	P. E. Zadunaisky

*Reprinted in Smithsonian Contributions to Astropyhsics, vol. 6, 1963.

No.	*Date*	*Title*	*Author*
66 (C–22)	July 17, 1961	Catalogue of Satellite Observations: Satellites 1958 Alpha (Explorer I), 1958 $\beta 1$ (carrier rocket, Vanguard I), 1958 Epsilon (Explorer IV), 1959 $\alpha 1$ (Vanguard II), 1959 $\alpha 2$ (carrier rocket, Vanguard II), 1959 Eta (Vanguard III), and 1959 $\iota 1$ (Explorer VII), for Sept. 1–Dec. 31, 1960	D. V. Mechau
67 (C–23)	July 17, 1961	Catalogue of Satellite Observations: Satellites 1960 $\iota 1$ (Echo I), and 1960 $\iota 2$ (carrier rocket, Echo I), for Sept. 1–Dec. 31, 1960	D. V. Mechau
68 (C–24)	July 17, 1961	Catalogue of Satellite Observations: Satellites 1960 $\beta 1$ (carrier rocket, Tiros I), for Sept. 14–21, 1960; 1960 $\beta 2$ (Tiros I), for Sept. 2–Oct. 15, 1960; 1960 $\gamma 1$ (carrier rocket, Transit 1B), for July 7–27, 1960; 1960 $\gamma 2$ (Transit 1B), for July 26–Nov. 7, 1960; 1960 $\eta 1$ (Transit 2A), for June 26–Dec. 29, 1960; 1960 $\eta 2$ (Greb), for June 22–Dec. 23, 1960; 1960 $\eta 3$ (carrier rocket, Transit 2A, Greb), for June 23–Dec. 31, 1960; 1960 $\xi 1$ (Explorer VIII), for Nov. 4–Dec. 30, 1960; 1960 $\xi 2$ (carrier rocket, Explorer VIII), for Nov. 19–Dec. 24, 1960; 1960 Omicron (Discoverer XVII), for Nov. 13–Dec. 31, 1960; and 1960 Sigma (Discoverer XVIII), for Dec. 8–31, 1960	D. V. Mechau
69	July 17, 1961	List of Coordinates of Stations Engaged in the Observation of Artificial Earth Satellites	D. V. Mechau
70	July 18, 1961	*The Motion of Satellite 1958 Epsilon Around its Center of Mass	G. Colombo
71	July 24, 1961	Elements of the Orbit of the Satellite 1959 Eta (Vanguard III) During the First Year after Launching	P. E. Zadunaisky and B. Miller
72	August 9, 1961	Tesseral Harmonics of the Potential of the Earth as Derived From Satellite Motions	Y. Kozai
73	August 10, 1961	Differential Orbit Improvement with the Use of Rotated Residuals	I. G. Izsak
74	September 18, 1961	*On the Accuracy of Measurements Made Upon Films Photographed by Baker-Nunn Satellite Tracking Cameras	K. Lassovszky

*Reprinted in Smithsonian Contributions to Astrophysics, vol. 6, 1963.

No.	*Date*	*Title*	*Author*
75	September 19, 1961	*Density of the Heterosphere Related to Temperature	M. Nicolet
76	October 2, 1961	*Effects of the Earth's Ionosphere on HF Radio Astronomy From Artificial Satellites	M. D. Grossi, K. M. Strom, and S. E. Strom
77	October 24, 1961	*Short-periodic Oscillations in the Drag of Satellite 1958 Alpha	L. G. Jacchia and J. W. Slowey
78	October 25, 1961	Satellite Orbital Data: Satellites 1958 Alpha, 1958 β1 and 1959 ι1, for May–Dec. 1960	D. V. Mechau B. Miller
79	October 30, 1961	*The Analysis of Gravity	H. Jeffreys
80	November 1, 1961	*The Stabilization of an Artificial Satellite at the Inferior Conjunction Point of the Earth-Moon System	G. Colombo
81	November 24, 1961	The Orbits of the Satellites 1959 α1 and 1959 α2 and the Perturbations on the Perigee Distance of 1959 α1	R. C. Nigam
82 (P–1)	November 30, 1961	Catalog of Precisely Reduced Observations: Satellites 1959 α1, for Feb. 17–June 30, 1959; and 1959 Eta, for Sept. 18–Dec. 31, 1959	G. Veis
83	January 31, 1962	Project Celescope	R. J. Davis and Celescope staff
84	February 9, 1962	Preliminary Analysis of the Atmospheric Drag of the Twelve-Foot Balloon Satellite (1961 δ1)	L. G. Jacchia and J. W. Slowey
85 (P–2)	February 12, 1962	Catalog of Precisely Reduced Observations: Satellites 1959 α1, for July 1–Dec. 31, 1959; 1959 α2, for Mar. 6–May 31, 1959; 1960 ι2, for Sept. 10–Dec. 31, 1960; 1960 Omicron, for Nov. 13–Nov. 16, 1960; and 1960 Sigma, for Dec. 8–Dec. 10, 1960	G. Veis
86	February 21, 1962	Satellite Orbital Data Satellites 1958 Alpha, for Jan. 1–July 1, 1961; 1958 β1, for Jan. 1–July 27, 1961; 1960 ξ1, for Nov. 4, 1960–July 3, 1961; 1961 δ1, for Feb. 16–July 2, 1961; and 1961 υ1, for April 28–Sept. 1, 1961 Satellite 1959 ι1, for Dec. 31, 1960–July 1, 1961	I. G. Izsak B. Miller J. Weingarten

*Reprinted in Smithsonian Contributions to Astrophysics, vol. 6, 1963.

No.	*Date*	*Title*	*Author*
87 (C–25)	February 23, 1962	Catalogue of Satellite Observations: Satellites 1958 Alpha (Explorer I), 1958 β1 (carrier rocket, Vanguard I), 1959 α1 (Vanguard II), 1959 α2 (carrier rocket, Vanguard II), 1959 Eta (Vanguard III), and 1959 ι1 (Explorer VII), for Jan. 1–June 30, 1961	D. V. Mechau
88 (C–26)	February 23, 1962	Catalogue of Satellite Observations: Satellites 1960 ι1 (Echo I) and 1960 ι2 (carrier rocket, Echo I), for Jan. 1–June 30, 1961	D. V. Mechau
89 (C–27)	February 23, 1962	Catalogue of Satellite Observations: Satellites 1960 ξ1 (Explorer VIII), for Nov. 3, 1960–June 30, 1961; 1961 δ1 (Explorer IX), for Feb. 16–June 30, 1961; and 1961 υ1 (Explorer XI), for April 27–June 30, 1961	D. V. Mechau
90	March 14, 1962	On the Critical Inclination in Satellite Theory	I. G. Izsak
91 (P–3)	April 20, 1962	Catalogue of Precisely Reduced Observations: Satellites 1958 δ2, for Dec. 1–17, 1958; 1959 α2, for Jan. 1–Dec. 31, 1960; and 1959 Eta, for Jan. 1–June 30, 1960	
92 (E–1)	April 23, 1962	Satellite Orbital Data	I. G. Izsak
		Satellite 1958 δ2, for Dec. 7–14, 1959	Y. Kozai
		Satellite 1959 α1, for Feb. 21–Dec. 30, 1959	P. Stern and M. Gutierrez
		Satellite 1959 α2, for Mar. 19–May 28, 1959	P. Stern
		Satellite 1959 Eta, for Sept. 23–Dec. 30, 1959	R. Nigam and P. Stern
		Satellite 1960 ι2, for Sept. 11, 1960–Mar. 12, 1961	I. Izsak and J. Weingarten
		Satellite 1960 Omicron, for Nov. 13–15, 1960	J. Weingarten
		Satellite 1960 Sigma, for Dec. 8–10, 1960	J. Weingarten
93	May 4, 1962	Satellite Orbital Data	I. G. Izsak
		Satellite 1958 Alpha, for July 1, 1961–Jan. 1, 1962	B. Miller
		Satellite 1959 ι1, for July 1, 1961–Jan. 1, 1962	M. Gutierrez
		Satellite 1960 ξ1, for July 1, 1961–Jan. 1, 1962	M. Hall
		Satellite 1961 δ1, for July 2, 1961–Jan. 5, 1962	J. Weingarten

No.	*Date*	*Title*	*Author*
94	May 23, 1962	On the Motion of Explorer XI Around its Center of Mass	G. Colombo
95 (P–4)	June 18, 1962	Catalog of Precisely Reduced Observations: Satellites 1959 Eta, for July 1–Dec. 31, 1960; and 1960 $\iota 2$, for Jan. 1–June 30, 1961	K. Haramundanis
96 (C–28)	June 25, 1962	Catalogue of Satellite Observations: Satellites 1958 Alpha (Explorer I), 1959 $\alpha 1$ (Vanguard II), 1959 Eta (Vanguard III), and 1959 $\iota 1$ (Explorer VII), for July 1–Dec. 31, 1961; and 1959 $\alpha 2$ (carrier rocket, Vanguard II), for July 1–27, 1961	B. Miller
97 (C–29)	June 25, 1962	Catalogue of Satellite Observations: Satellites 1960 $\iota 1$ (Echo I) and 1960 $\iota 2$ (carrier rocket, Echo I), for July 1–Dec. 31, 1961	B. Miller
98 (C–30)	June 25, 1962	Catalogue of Satellite Observations: Satellites 1960 $\xi 1$ (Explorer VIII) and 1961 $\delta 1$ (Explorer IX), for July 1–Dec. 31, 1961; 1961 $\nu 1$ (Explorer XI), for July 1–Sept. 28, 1961; and 1961 $o 1$ (Transit 4a) and 1962 $o 2$ (Injun Solar Radiation), for June 29–Dec. 31, 1961	B. Miller
99	July 16, 1962	Chemical Analysis of 643 Particles Collected by High-Altitude Aircraft and Balloons	F. B. Riggs, Jr., F. W. Wright, and P. W. Hodge
100	July 30, 1962	Accurate Drag Determinations for Eight Artificial Satellites; Atmospheric Densities and Temperatures	L. G. Jacchia and J. W. Slowey
101	July 31, 1962	Numerical Results from Orbits	Y. Kozai
102 (P–5)	August 27, 1962	Catalog of Precisely Reduced Observatlons: Satellite 1959 $\alpha 1$ for the Entire Year 1960	J. MacDonald, K. Haramundanis et al.
103	August 28, 1962	Satellite Orbital Data Satellite 1959 Eta (Vanguard III), Sept. 1, 1960–Dec. 31, 1961 Satellite 1960 $\iota 1$ (Echo I), Jan. 1–Dec. 31, 1961	I. G. Izsak B. Miller B. Miller
104 (P–6)	September 10, 1962	Catalog of Precisely Reduced Observations: Satellite 1961 $\delta 1$ from Launch Feb. 16–June 30, 1961	J. MacDonald et al.
105	September 28, 1962	The Trajectory of Tektites	G. S. Hawkins and S. K. Rosenthal
106 (P–7)	November 1, 1962	Catalog of Precisely Reduced Observations: Satellite 1959 $\alpha 1$ From Jan. 1–June 30, 1961; Satellite 1959 $\eta 1$ from Jan. 1–June 30, 1961	P. Stern

No.	*Date*	*Title*	*Author*
107	November 9, 1962	On Some Singular Orbits of an Earth-Moon Satellite with a High Area-Mass Ratio	G. Colombo and D. A. Lautman
108	November 20, 1962	On the Libration Orbits of a Particle Near the Triangular Point in the Semirestricted Three-Body Problem	G. Colombo, D. Lautman, and C. Munford
109	December 21, 1962	Re-Entry and Recovery of Fragments of Satellite 1960 $\epsilon 1$	C. A. Lundquist, R. C. Vanderburgh, W. A. Munn, D. Tilles, E. L. Fireman, and J. DeFelice
110	December 14, 1962	Project Celescope, an Astrophysical Reconnaissance Satellite	R. J. Davis, ed.
111	December 15, 1962	Possible Contributions of Space Experiments to Cometary Physics	P. Swings
112	January 21, 1963	On the Secular Decrease in the Inclination of Artificial Satellites	R. C. Nigam
113	January 23, 1963	Satellite Orbital Data	I. G. Izsak
		Satellite 1958 Alpha, for April 1–July 1, 1962	B. Miller
		Satellite 1959 $\alpha 1$, for March 31–June 30, 1962	M. Gutierrez
		Satellite 1959 Eta, for March 31–June 30, 1962	M. Hall
		Satellite 1959 $\iota 1$, for March 31–June 30, 1962	M. Gutierrez
		Satellite 1960 $\xi 1$, for April 1–July 1, 1962	M. Hall
		Satellite 1961 $\delta 1$, for March 31–June 30, 1962	J. Weingarten

U.S. GOVERNMENT PRINTING OFFICE: 1963